Aerosol Chamber Study of Secondary Organic Aerosol Formation from Mixtures of Anthropogenic and Biogenic Precursors

A thesis submitted to the University of Manchester for the

degree of Doctor of Philosophy

in the Faculty of Science and Engineering

Yunqi Shao

School of Earth and Environmental Sciences

2022

[BLANK PAGE]

Table of Contents

[BLANK PAGE]

Abstract

This thesis reports the use of an aerosol chamber to investigate Secondary Organic Aerosol (SOA) transformation and formation in biogenic and anthropogenic VOC mixtures. Experiments conducted to comprehensively describe and characterise the Manchester aerosol chamber (MAC) are reported. Photo-oxidation chamber experiments were conducted using online and offline mass spectrometric instrumentation, including Gas Chromatography-Mass Spectrometer (GC-MS), Aerosol Mass Spectrometer (AMS), Chemical Ionisation Mass spectrometer (CIMS) and liquid chromatography ultra-high resolution mass spectrometry (UPLC-orbitrap-MS). These were used to explore SOA transformation and formation in anthropogenic (*o*-cresol) and biogenic (α-pinene and isoprene) mixed precursors in the presence of NOx and inorganic seed particles (ammonium sulphate) through investigation of the SOA particle mass yield and characterisation of SOA composition in mixed precursor systems.

The MAC characterisation study highlights the importance of conducting regular characterisation experiments to track the performance of the simulation chamber and emphasises the need to develop a routine set of standardised experiments for chambers, elucidating the particular characteristics of each facility, thus enabling the interpretation of the results.

The study of SOA formation from mixed precursors established a novel chamber experimental design associated with initial "iso-reactivity" of the systems towards the dominant oxidant (OH), achieved by adjustment of the initial concentration of precursors in the mixed system. The SOA particle mass yield exhibited suppression when compared with that of α-pinene when mixed with isoprene, but a minor yield enhancement was tentatively found while adding isoprene to *o*-cresol. The α-pinene/*o*-cresol system exhibited a higher measured SOA particle mass yield than that calculated based on additivity. The measured and predicted yields were comparable in ternary systems. The ambiguity in reference for yield evaluation present challenges to the evaluation of changes in SOA formation when more than one precursor contributed to the SOA mass, as do differences in the prevailing chemical regime.

An automated non-targeted accurate mass analysis of LC-Orbitrap-MS data was used to characterise the particulate products from mixed precursor systems. α-pinene oxidation products

were shown to dominate the binary mixed α-pinene / isoprene system in terms of fractional signal contribution and the number of particle components detected. *o*-cresol oxidation products (methyl-nitrocatechol and methy-nitrophenol) dominated the SOA particle composition in both *o*-cresol / isoprene and *o*-cresol / α-pinene binary systems in negative ionisation mode. This thesis further stressed the significance of unique-to-mixture products formation, which contributes to molecular composition and signal abundance in *o*-cresol-containing binary systems in positive ionisation mode. Compounds uniquely identified in each mixture were identified, with the potential to be used as tracers in SOA source attribution in future ambient studies.

Finally this thesis reports the alteration of average carbon oxidation state of SOA particle components in all systems, by employing HR-TOF-AMS, FIGAERO-CIMS and LC-Orbitrap MS to characterise the SOA composition. The oxidation state of nitrogen (OS_N) for compounds that composed of Carbon (C), Hydrogen (H), Oxygen (O) and Nitrogen (N) element significantly influenced average $\overline{OSc}$ in single α-pinene and o-cresol system in FIGAERO-CIMS and LC-Orbitrap MS measurement. A substantial discrepancy in the estimated $\overline{OSc}$ between the FIGAERO-CIMS and HR-ToF-AMS and LC-Orbitrap MS techniques was found, likely associated with the characteristic of each technique and their limitation. α-pinene driven SOA and o-cresol oxidation products were shown to dominate the average $\overline{OSc}$ of SOA in binary α-pinene/isoprene system and binary o-cresol /isoprene system. In contrast, both α-pinene and o-cresol oxidation products contributed to the alteration of the average $\overline{OSc}$ during SOA formation in the binary α-pinene/o-cresol system. In the ternary precursor system, the $\overline{OSc}$ of SOA is not dominantly controlled by any single precursors but is associated with molecular interaction of the product.

[BLANK PAGE]

Declaration

235

A portion of the work referred to in the thesis (Paper 1 and 2) has joint authorship, which might be included in a thesis submitted by another student to this university or any other university or other institute of learning.

[BLANK PAGE]

Copyright Statement

(i) The author of this thesis (including any appendices and/or schedules to this thesis) owns certain copyright or related rights in it (the "Copyright") and she has given The University of Manchester certain rights to use such Copyright, including for administrative purposes.

(ii) Copies of this thesis, either in full or in extracts and whether in hard or electronic copy, may be made only in accordance with the Copyright, Designs and Patents Act 1988 (as amended) and regulations issued under it or, where appropriate, in accordance with licensing agreements which the University has from time to time. This page must form part of any such copies made.

(iii) The ownership of certain Copyright, patents, designs, trademarks and other intellectual property (the "Intellectual Property") and any reproductions of copyright works in the thesis, for example graphs and tables ("Reproductions"), which may be described in this thesis, may not be owned by the author and may be owned by third parties. Such Intellectual Property and Reproductions cannot and must not be made available for use without the prior written permission of the owner(s) of the relevant Intellectual Property and/or Reproductions.

(iv) Further information on the conditions under which disclosure, publication and commercialisation of this thesis, the Copyright and any Intellectual Property and/or Reproductions described in it may take place is available in the University IP Policy (see http://documents.manchester.ac.uk/DocuInfo.aspx?DocID=24420), in any relevant Thesis restriction declarations deposited in the University Library, The University Library's regulations (see http://www.library.manchester.ac.uk/about/regulations/) and in The University's policy on Presentation of Theses.

[BLANK PAGE]

Acknowledgement

I would like to thank the following people, without whom I would not have been able to complete this research and made it through my PhD degree.

My utmost appreciation goes to the "Chamber Group" at the University of Manchester, my main supervisor, Professor Gordon McFiggans, whose insight, knowledge, and expertise steered me throughout this research. Also, many thanks to my second supervisor, Dr Rami Alfarra, whose support ensured that my experimental work remained on the right track throughout this research. Special thanks to my colleagues and partners, namely Aristeidis, Yu, and Mao, who have supported me in my research work and empowered me into becoming a resilient person to overcome my stressful moments for the past four years of my studies.

I would like to extend my heartfelt thanks to Jacqui, Kelly, Aiden, Jimmy, and Martyn at the University of York. They offered valuable assistance and guidance on specific instruments in the laboratory and data analysis. A massive thanks to the research fellows at the University of Manchester, namely Dr Stephen Boult, Felipe, and Kaki, who have guided and supported me to operate essential instruments. Without their immeasurable support, it would not have been possible to conduct this research.

I would also like to thank Organic Tracers and Aerosol Constituents - Calibration Centre (OGTAC-CC) for funding that letting me attend the offline mass spectrometry training in TROPOS institutes.

I would also like to express my gratitude to the members who participated in the live streaming of the Zoom study room called 'Straight A Student'. Thank you for the company and the emotional support throughout this writing journey, especially amidst a global pandemic.

I would like to express my deepest appreciation to my family for their support throughout this research journey, especially my parents, who have given me generous financial support. I would have never survived my PhD without their constant encouragement and patience.

Finally, I would like to thank myself for remaining steadfast and resilient throughout my PhD journey in spite of the countless difficulties I encountered.

[BLANK PAGE]

Chapter 1

1. Introduction

Aerosol particles suspended in the ambient atmosphere range in size from 2 nm–10μm (Mcneill, 2017). Owing to their small size and inertial properties, fine atmospheric aerosols can remain airborne for several hours to days and be transported long distances, experiencing chemical and physical transformation, interaction with water vapour and radiation, deposition to the surface and inhalation by humans.

The organic components constitute a significant fraction of fine particulate matter, that makes non-negligible contribution (20 to 90%) to the mass of fine particulate matter in the atmosphere(Jimenez et al., 2009). These particles can be introduced to the atmosphere by emission from a variety of primary sources, such as organic matter from the sea surface microlayer, agricultural operations, industrial processes, and combustion processes (Laidlaw et al., 2012; Prospero et al., 2002) and forming of secondary organic aerosol (SOA)(Hallquist et al., 2009) via nucleation and / or condensational growth (in situ formation) (Patoulias et al., 2015). SOA, which is a major component of particulate matters in the troposphere, is associated with multiphase chemical oxidation that formed partially SOA in the atmosphere originated from oxidizing volatile organic compounds (VOCs). More specifically, VOCs are classified into two major groups: anthropogenic VOCs (e.g., emission from human activities) and biogenic VOCs (e.g., emission from nature) (Hallquist et al., 2009).

The degradation of VOCs initiated by OH, O_3, and NO_3 radicals in the ambient atmosphere sequentially forms multigeneration products through continuous oxidation leading to growing amount through continual "ageing" by functionalisation and fragmentation with differential partitioning between the gas and particle phases. The emission of VOCs and the type of oxidants differ both spatially and temporally, leading to complex chemical compositions of the SOA in the ambient atmosphere. The drivers of the SOA formation are complex and challenging to resolve due to the complexity of sources for organic aerosols, and the limitations behind isolating the chemical and microphysical processes in the atmosphere (Hallquist et al., 2009).

Chamber experiments have been widely used to provide the mechanistic understanding of SOA formation processes for systems comprising single VOCs. However, the atmosphere contains a complex mixture of biogenic and anthropogenic VOC emissions. Recent studies have reported that SOA's yield and chemical composition was influenced when there was more than one volatile organic compound in the chamber experiment (Kiendler-Scharr et al., 2009; Mcfiggans et al., 2019; Shilling et al., 2019; Berndt et al., 2018). The understanding of the dynamics and characteristic properties of SOA is necessary in understanding the effects on human health and climate but is highly uncertain and challenging given the mixture of VOC precursors.

Chamber experiments using online and offline mass spectrometric techniques can provide extensive information regarding the characterization of SOA at the elemental and molecular levels. This will thereby provide a better understanding of the fate and transformation of the primary emission to the aerosol in the realistic atmosphere. Such experiments should aim to evaluate the key processes leading to SOA formation in mixtures of complex vapors and investigate the chemical mechanisms taking place during the oxidation processes.

1.1. Thesis Overview

The work in this thesis investigated the SOA formation using the Manchester Aerosol Chamber under controlled conditions, examining the chemical characteristics of SOA from photooxidation experiments with 7 different VOCs systems, including three single VOC systems, their three binary mixtures and their ternary mixture. The work aimed to provide insights into the chemical processes involved in SOA formation in mixtures of vapors relevant to the ambient atmosphere.

Chapter 1 outlines the motivation behind investigating the SOA formation using the aerosol chamber. Chapter 2 provides a background discussion of atmospheric aerosols outlining the importance and sources of global aerosols and the tropospheric chemistry and pathways of SOA formation from anthropogenic and biogenic volatile organic species providing the foundation for the work within this thesis. Chapter 3 provides background information about the facilities, measurement techniques and instruments and analysis methods, followed by an overview of the experimental procedure in the studies. Chapter 4 describes the aims of the thesis.

Chapter 5 presents four papers, including two joint lead-authorship manuscripts, all co-authored with Aristeidis Voliotis, Yu Wang, and Mao Du, who are former PhD students at the University of Manchester, and two sole lead-authorship papers. The first joint lead paper (5.1) described the characterization of the Manchester Aerosol Chamber (MAC) that was an essential facility for the remaining investigation in this thesis. The second joint lead paper (5.2) focused on investigating the SOA particulate mass formed from the photo-oxidation of anthropogenic (*o*-cresol) and biogenic (α-pinene and isoprene) VOCs, as well as their binary and ternary mixtures in the presence of NOx and inorganic seeds conducted in the MAC. In Paper 3 (5.3), a comprehensive analysis of SOA chemical composition measurement was deployed on inorganic seeds in the chamber photo-oxidation of anthropogenic (*o*-cresol) and biogenic (α-pinene and isoprene) VOCs, including their binary and ternary mixtures in the presence of NOx by using the Orbitrap-liquid chromatography mass spectrometer. The fourth paper (5.4) expands on the third paper by employing the online high resolution time-of-flight aerodyne aerosol mass spectrometers (HR-TOF-AMS) and Iodide high-resolution time of flight chemical ionization mass spectrometer (FIGAERO-CIMS) and offline LC-Orbitrap MS techniques to characterise the SOA in all systems, focusing on investigate the potential average carbon oxidation state of SOA particle changes in complex precursor mixtures.

Finally, Chapter 6 summarizes the key findings and discusses their impacts, and Chapter 7 consists of supplementary materials from the papers in Chapter 5.

References:

Berndt, T., Scholz, W., Mentler, B., Fischer, L., Herrmann, H., Kulmala, M., and Hansel, A.: Accretion Product Formation from Self- and Cross-Reactions of RO2 Radicals in the Atmosphere, Angewandte Chemie International Edition, 57, 3820-3824, https://doi.org/10.1002/anie.201710989, 2018.

Hallquist, M., Wenger, J., Baltensperger, U., Rudich, Y., Simpson, D., Claeys, M., Dommen, J., Donahue, N., George, C., and Goldstein, A.: The formation, properties and impact of secondary organic aerosol: current and emerging issues, Atmospheric chemistry and physics, 9, 5155-5236, 2009.

Jimenez, J. L., Canagaratna, M. R., Donahue, N. M., Prevot, A. S. H., Zhang, Q., Kroll, J. H., DeCarlo, P. F., Allan, J. D., Coe, H., Ng, N. L., Aiken, A. C., Docherty, K. S., Ulbrich, I. M., Grieshop, A. P., Robinson, A. L., Duplissy, J., Smith, J. D., Wilson, K. R., Lanz, V. A., Hueglin, C., Sun, Y. L., Tian, J., Laaksonen, A., Raatikainen, T., Rautiainen, J., Vaattovaara, P., Ehn, M., Kulmala, M., Tomlinson, J. M., Collins, D. R., Cubison, M. J., Dunlea, J., Huffman, J. A., Onasch, T. B., Alfarra, M. R., Williams, P. I., Bower, K., Kondo, Y., Schneider, J., Drewnick, F., Borrmann, S., Weimer, S., Demerjian, K., Salcedo, D., Cottrell, L., Griffin, R., Takami, A., Miyoshi, T., Hatakeyama, S., Shimono, A., Sun, J. Y., Zhang, Y. M., Dzepina, K., Kimmel, J. R., Sueper, D., Jayne, J. T., Herndon, S. C., Trimborn, A. M., Williams, L. R., Wood, E. C., Middlebrook, A. M., Kolb, C. E., Baltensperger, U., and Worsnop, D. R.: Evolution of Organic Aerosols in the Atmosphere, Science, 326, 1525, 10.1126/science.1180353, 2009.

Kiendler-Scharr, A., Wildt, J., Maso, M. D., Hohaus, T., Kleist, E., Mentel, T. F., Tillmann, R., Uerlings, R., Schurr, U., and Wahner, A.: New particle formation in forests inhibited by isoprene emissions, Nature, 461, 381-384, 10.1038/nature08292, 2009.

Laidlaw, M. A. S., Zahran, S., Mielke, H. W., Taylor, M. P., and Filippelli, G. M.: Re-suspension of lead contaminated urban soil as a dominant source of atmospheric lead in Birmingham, Chicago, Detroit and Pittsburgh, USA, Atmospheric Environment, 49, 302-310, https://doi.org/10.1016/j.atmosenv.2011.11.030, 2012.

McFiggans, G., Mentel, T. F., Wildt, J., Pullinen, I., Kang, S., Kleist, E., Schmitt, S., Springer, M., Tillmann, R., and Wu, C.: Secondary organic aerosol reduced by mixture of atmospheric vapours, Nature, 565, 587, 2019.

McNeill, V. F.: Atmospheric Aerosols: Clouds, Chemistry, and Climate, Annual Review of Chemical and Biomolecular Engineering, 8, 427-444, 10.1146/annurev-chembioeng-060816-101538, 2017.

Patoulias, D., Fountoukis, C., Riipinen, I., and Pandis, S.: The role of organic condensation on ultrafine particle growth during nucleation events, Atmospheric Chemistry and Physics, 15, 6337-6350, 2015.

Prospero, J. M., Ginoux, P., Torres, O., Nicholson, S. E., and Gill, T. E.: ENVIRONMENTAL CHARACTERIZATION OF GLOBAL SOURCES OF ATMOSPHERIC SOIL DUST

IDENTIFIED WITH THE NIMBUS 7 TOTAL OZONE MAPPING SPECTROMETER (TOMS) ABSORBING AEROSOL PRODUCT, Reviews of Geophysics, 40, 2-1-2-31, https://doi.org/10.1029/2000RG000095, 2002.

Shilling, J. E., Zawadowicz, M. A., Liu, J., Zaveri, R. A., and Zelenyuk, A.: Photochemical Aging Alters Secondary Organic Aerosol Partitioning Behavior, ACS Earth and Space Chemistry, 3, 2704-2716, 10.1021/acsearthspacechem.9b00248, 2019.

[BLANK PAGE]

Chapter 2

2. Theoretical Background and Literature Review

2.1. Atmospheric Aerosol

Aerosol is an essential component of the earth's atmosphere due to its increasingly recognized vital role in various environmental processes (e.g., climate change, visibility degradation, and toxicology). Atmospheric aerosol is composed of solid and liquid particles suspended in the air, which differ in chemical complexity, size, and phase. These particles exert significant impacts on human health, visibility, air quality, and our overall climate. However, there are significant challenges in understanding how aerosols affect the climate and human health.

There are two mechanisms by which aerosols impact the climate, namely: aerosol-radiation interaction and aerosol-cloud interaction. Aerosol-radiation interaction directly impacts the climate and refers to the following: a) scattering and absorbing of solar radiation, and b) scattering, absorbing, and emission of thermal radiation, which leads to changes in radiative flux (Myhre et al., 2013; Forster et al., 2007). This direct impact strongly relates to aerosol's optical properties, which increases the attention of black and brown carbon components in the atmosphere, given their contribution to the absorption of light and broad wavelength radiation (Andreae and Gelencsér, 2006; Russo et al., 2013). Moreover, the composition of aerosols plays an important role in the radiation effect (e.g., black carbon compound strongly absorbs radiation) (Ramanathan and Carmichael, 2008). However, some inorganic and secondary aerosol components act as scattering material (Hoyle et al., 2008).

On the other hand, aerosols indirectly impact the climate through its influence on cloud formation and cloud properties. For instance, aerosols can act as cloud condensation nuclei (CCN). A higher number of smaller cloud droplets result in a longer lasting and brighter cloud, which is a consequence of an increased number of particles that act as CCN. Changing the concentration of CCN impacts the cloud's lifetime and optical properties and perturbs the planet's energy balance. Moreover, the ability of aerosols to act as CCN causes further implications on precipitation in the context of a changing climate (Stevens and Feingold, 2009; IPCC, 2013).

Although aerosols are natural components of the Earth's atmosphere, they are one of the most crucial contributors to air pollution in urban areas. Meanwhile, air pollution is reported and confirmed to cause damage to human health (e.g., There are 5.5 million premature deaths globally and 130,000 premature deaths in the United States annually associated with air pollution) (Brauer et al., 2016; Fann et al., 2012). Aerosols in the atmosphere, also commonly referred to as particulate matters, can be classified into three groups based on aerodynamic diameters, namely: PM_{10} (<10 μm), $PM_{2.5}$ (<2.5 μm), and ultra-fine particles (UFP) (<100 nm). Aerodynamic diameters play an important role in human health because small aerosol particles can penetrate deep into the lungs through inhalation, and large particles can deposit in the upper respiratory tract (Burnett et al., 2014). The deposition of aerosols can induce a series of acute and chronic diseases, from cardiovascular to respiratory issues. However, some cities continue to experience poor air quality, especially developing cities, resulting in the establishment of international guidelines and policies concerning air quality (World Health Organization and Environmental Health, 2006; Centrer For Chemical Process Safety, 2006). Identifying the sources of particulate matter, along with a study of their chemical properties, confront certain limitations. However, these efforts are essential in establishing and implementing mitigation strategies regionally.

It has been conclusively proven that organic components constitute a significant fraction of fine particulate matter (Jimenez et al., 2009). Figure 2.1 shows that these particles are introduced to the atmosphere as emissions from a variety of primary sources (e.g., biomass burning, vehicle emissions, resuspension of dust and sea salt) and as secondary aerosol formations (Hallquist et al., 2009) that are classified into coarse-mode (PM_{10} - $PM_{2.5}$) and fine-mode ($PM_{2.5}$) aerosol particles. Coarse-mode aerosol typically attributed by the primary inorganic source, including dust from deserts, sea salt from oceans, soil from vegetation debris, and bioaerosols (e.g., pollen and fungal spores) (Laidlaw et al., 2012; Prospero et al., 2002). Moreover, organic particulate matter from primary and secondary sources present as fine-mode aerosol particles that contribute to air pollution, affecting human health, as aforementioned.

Secondary organic aerosol is the major component in fine-mode aerosol particles, and understanding its formation and properties is of great importance. SOA formation involves

oxidation of volatile organic gas species that are directly emitted to the atmosphere, which leads to the production of a less volatile component (more oxidized) that either continuously nucleates or condenses into existing particles. However, details of SOA formation and properties are limited due to the complexity of natural and anthropogenic sources of SOA precursor gases and the various pathways of reactive chemistry. VOCs have different degradation rates and reactive pathways with different tropospheric oxidants, all of which affect the chemical composition of SOA. More detailed information about SOA chemical composition and formation pathways is illustrated in Section 2.4 of this thesis

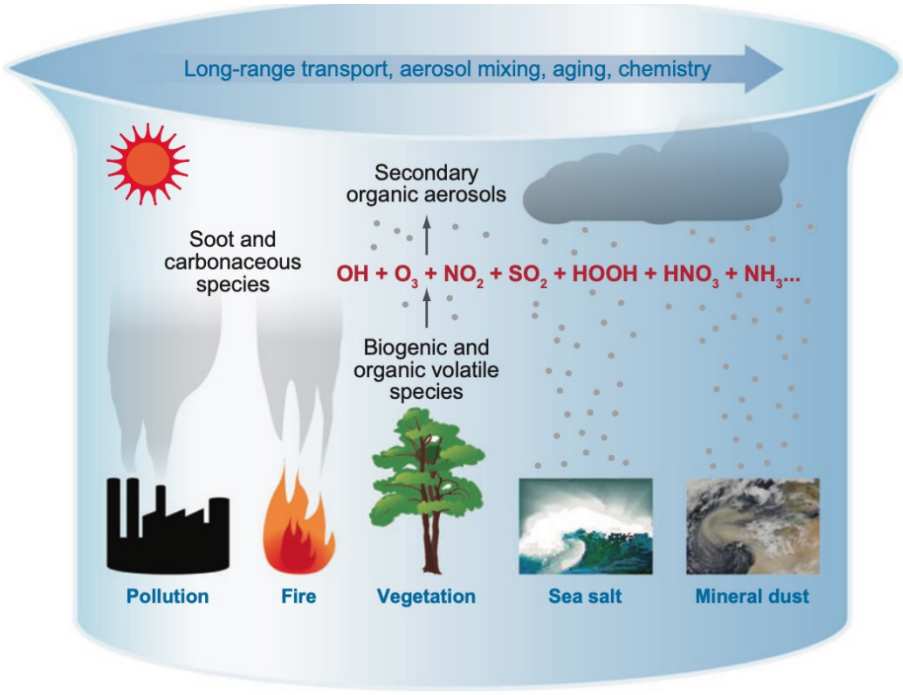

Figure 2.1 :Schematic of the natural and anthropogenic processes producing aerosols in the atmosphere(Prather et al., 2008).

2.2. Volatile Organic Compounds

Volatile organic compounds (VOCs) include a large group of organic chemical gases emitted from both human and natural sources that vaporise easily into the atmosphere under normal conditions. VOCs exhibit high volatility and mobility and have high resistance against degradation that allows them to be easily transported over long distances upon release to the environment. VOCs emitted from natural sources refer to biogenic VOCs (BVOC), which take up 75% to 90% of total VOCs in the atmosphere (Guenther et al., 1995; Lamarque et al., 2010; Carlton et al., 2009). There are

three sources of BVOCs including tree emissions, vegetation emissions, and emissions from biomass burning that is naturally caused. It has been identified that emissions from plant processes (i.e., those that involve plant growth, development, reproduction, and defense) are the dominant source of BVOCs globally (Després et al., 2012). Emissions from plants include a diverse mixture of terpenoids, such as isoprene, monoterpenes, sesquiterpenes, diterpenes, and some oxygenated BVOCs (Owen et al., 2001; Keeling and Bohlmann, 2006). According to the global model report from Guenther et al. (2012), 30% of BVOCs comprise methanol, ethanol, acetaldehyde, α-pinene, β-pinene, t- β-ocimene, limonene ethene, and propene; although isoprene (C_5H_8, 2-methyl-1,3, butadiene) is the most dominant BVOC in the Earth's systems, accounting for approximately 50% of total global BVOC emissions. Sanadze (1956) was the first to identify and describe isoprene products and emissions by plants; and Went (1960) was the first to mention the impacts of isoprene on atmospheric physics and chemistry (this initial assertion explains the blue haze observed over forested landscapes).

In recent years, anthropogenic VOCs (AVOCs) have attracted worldwide attention. AVOCs refer to volatile organic compounds generated by human activities from both domestic and industrial processes, such as hydrocarbon fuel evaporation, food extraction, traffic pharmaceutical industries, distribution and storage, and fertilizer and pesticide application (Pandey and Yadav, 2018). AVOCs contribute to photochemistry in the ambient, due to their due to their potential for ozone formation and the identification of their oxidation products in ambient aerosol (Montero-Montoya et al., 2018; Nault et al., 2021; Petit et al., 2014; Stavroulas et al., 2019). Some AVOCs are toxic and harm the ecosystem, such as benzene, toluene, ethylbenzene, and xylenes (BTEX), which account for over 60% of total VOCs in urban areas. A high BTEX concentration has been noted in fast-developing cities that have intensive industrial activities and massive vehicular traffic problems, which contribute to fuel burning (e.g., crude oil, diesel, and gasoline). In rural areas, agricultural sector-related activities such as fuel storage and consumption for agricultural implements and agricultural waste burning are sources of AVOCs, which are extensively distributed in the environment (Jürgens and Bischoff, 2017).

VOC profiles are unique across different regions of the world owing to the diversity in speciation of both BVOCs and AVOCs. The concentration and profiles of VOCs depend on land and

vegetation cover for BVOCs; fuel types, human and industrial activities for the AVOCs. Each VOC has its own fate in the ambient, which relies on its functionality and reactivity with oxidants. There is a massive volume of laboratory studies that investigate the gas phase chemistry of VOC oxidation, which leads to ozone formation and SOA formation. However, mechanistic knowledge behind SOA formation remains unclear and requires further investigation in the future.

2.3. Oxidants

VOC oxidation strongly depends on prevailing gaseous oxidants in the atmosphere. The main gaseous oxidants in the ambient mainly comprise hydroxyl (OH) radicals, ozone (O_3), and nitrate (NO_3) radicals; the first oxidant in the daytime, and the last at night. O_3 could contributes to VOC oxidation in both day and night time. Reactions between VOCs and these oxidants occur as soon as VOCs are emitted by their primary source into the atmosphere.

2.3.1. O_3 as Oxidant

It is essential to understand the pathway that leads to O_3 formation in the ambient. In the lower troposphere, ozone is almost completely formed by the photolysis of nitrogen dioxide and the subsequent reaction of oxygen atom with molecular oxygen:

$$NO_2 + hv \rightarrow O(^3P) + NO \quad (2.1)$$

$$O(^3P) + O_2 + M \rightarrow O_3 + M \quad (2.2)$$

Since O_3 reacts quickly with NO:

$$O_3 + NO \rightarrow NO_2 \quad (2.3)$$

There is a so-called photo-stationary state between NO, NO_2 and O_3 is rapidly established. The lifetime of O_3 can last several days in the ambient away from NO sources; it can persist as an oxidant (both day and night) even when all O_3 can titrate away in the presence of a strong NO source (e.g., polluted urban environments).

2.3.2. OH Radicals

The primary daytime oxidant is OH radicals, which form from the photolysis of O_3 and the subsequent reaction of approximately 10% of $O(^1D)$ that is formed with water vapor in the ambient.

$$O_3 + hv \rightarrow O(^3P) + O_2 \quad (2.4)$$

$O_3 + hv \rightarrow O(^1D) + O_2$ (2.5)

$O(^1D) + H_2O \rightarrow 2OH$ (2.6)

OH radicals are highly reactive to both saturated and unsaturated compounds, and generally last for only a few seconds under tropospheric conditions. Formation of OH radicals required to decomposed O_3 under light conditions, which is the reason have such low OH radicals concentration at night time. (Atkinson and Arey, 2003). Of note, OH radicals have different predominant source processes depending on location (i.e., urban or rural area). The regional atmosphere in urban and urban influence areas exhibit higher OH concentration compared to the rural areas. Other routes for OH radical formation in the ambient atmosphere include alkene (C_2H_{2n}) ozonolysis and photolysis of nitrous acid (HONO), hydrogen peroxide (H_2O_2), and organic peroxides. Harrison (2018) illustrated that the photolysis of nitrous acid at daytime and the decomposition of the Criegee biradical intermediate form from ozone-alkene reactions are more vital sources of OH radicals in urban polluted environments compared to rural region environments.

2.3.3. NO_3 Radicals

At nighttime, NO_3 is a major oxidant formed through the rapid reaction between NO_2 and O_3. It rapidly establishes an equilibrium with dinitrogen pentoxide as illustrated in the equations below:

$NO_2 + O_3 \rightarrow NO_3 + O_2$ (2.7)

$NO_2 + NO_3 \leftrightarrow N_2O_5$ (2.8)

The NO_3 would convert to NO_x under light condition leading to insufficient NO_3 radical concentration at daytime.

$NO_3 + hv \rightarrow NO_2 + O$ (2.9)

$NO_3 + hv \rightarrow NO + O_2$ (2.10)

According to Equation 2.8, NO_3 can persist in an equilibrium with N_2O_5, which creates an uptake by aerosols, leading to HNO_3 formation. Moreover, NO_3 will attack double bonds of the VOC precursor and form nitrate-substituted peroxy radicals, some of which may decompose into OH radicals, thereby resulting in a low OH radical concentration of the ambient atmosphere at night. Multi-functional organic nitrates are formed from the non-radical oxidation of NO_3+VOCs reaction. These compounds are likely partitioning to the atmospheric organic particles due to low vapor pressure consequence to generate secondary organic aerosols (Atkinson and Arey, 2003).

2.4. SOA Formation from VOC Oxidation

2.4.1. VOCs React with Various Oxidants

The lifetimes of VOCs in the atmosphere are different, depending on the reactivity between VOCs and various oxidants. Table 2.1 shows the calculated lifetimes of selected biogenic and anthropogenic volatile organic compounds corresponding to photolysis and reactions to OH radicals, NO_3 radicals, and O_3 (Atkinson, 2000). Terpenes (e.g., isoprene and α-pinene) that have unsaturated double bonds can be attacked by OH, O_3, and NO_3 oxidants. In contrast, aromatic compounds (e.g., 1,2,4-tmethylbenzene and o-Cresol) are typically oxidized by OH radicals compared to NO_3 and O_3 oxidants. These circumstances explain the longer atmospheric lifetimes of aromatic compounds under high O_3 concentration environments (up to a few years) compared to the presence of OH radicals and NO_3 radicals. The calculated atmospheric lifetimes of various VOCs also demonstrate that OH radicals are the main component that contributes to VOC loss in the ambient.

Table 2.1: Calculated Atmospheric lifetimes of selected volatile organic compounds in photolysis and reactions with OH radicals, NO3 and O3 radicals (Atkinson, 2000).

	Lifetime due to			
Organic	OH[b]	NO_3[c]	O_3[d]	Photolysis[e]
Propane	10 day	~ 7 yr	> 4500 yr	
n-Butane	4.7 day	2.8 yr	> 4500 yr	
n-Octane	1.3 day	240 day		
2,2,4-Trimethylpentane	3.2 day	1.4 yr		
Ethene	1.4 day	225 day	10 day	
Propene	5.3 h	4.9 day	1.6 day	
trans-2-Butene	2.2 h	1.4 h	2.1 h	
Isoprene	1.4 h	50 min	1.3 day	
α-Pinene	2.6 h	5 min	4.6 h	
Limonene	50 min	3 min	2.0 h	
Benzene	9.4 day	> 4 yr	> 4.5 yr	
Toluene	1.9 day	1.9 yr	> 4.5 yr	
m-Xylene	5.9 h	200 day	> 4.5 yr	
1,2,4-Trimethylbenzene	4.3 h	26 day	> 4.5 yr	
Styrene	2.4 h	3.7 h	1.0 day	
Phenol	5.3 h	9 min		
o-Cresol	3.3 h	2 min	65 day	
Formaldehyde	1.2 day	80 day	> 4.5 yr	4 h
Acetaldehyde	8.8 h	17 day	> 4.5 yr	6 day
Butanal	5.9 h			
Benzaldehyde	11 h	18 day		
Acetone	53 day	> 11 yr		~ 60 day
2-Butanone	10 day			~ 4 day
2-Pentanone	2.4 day			
Glyoxal	1.1 day			5 h
Methylglyoxal	9.3 h		> 4.5 yr	2 h
2,3-Butanedione	49 day			1 h
cis-Butanedial	2.6 h			~ 10 min
cis-3-Hexene-2,5-dione	2.1 h	1.5 day		~ 30 min
cis, trans-2,4-Hexadiendial	1.3 h	8.8 day		1.9 h
Pinonaldehyde	2.9 h	2.3 day	> 2.2 yr	
Methanol[f]	12 day	1 yr		
Ethanol	3.5 day	26 day		
2-Butanol	1.3 day	17 day		
Dimethyl ether	4.1 day	180 day		
Diethyl ether	11 h	17 day		
Methyl *tert*-butyl ether	3.9 day	72 day		
Ethyl *tert*-butyl ether	1.3 day	4.2 day		
tert-Butyl formate	16 day			
Methacrolein	4.1 h	11 day	15 day	~ 1 day
Methyl vinyl ketone	6.8 h	> 385 day	3.6 day	~ 2 day
Ethyl acetate	6.9 day	10 yr		
tert-Butyl acetate	21 day			
Linalool	50 min	3 min	55 min	
6-Methyl-5-hepten-2-one	50 min	4 min	1.0 h	
3-Methyl-2-buten-3-ol	2.1 h	3.8 day	1.7 day	
Methyl hydroperoxide[f]	2.1 day			~ 5 day
Ethyl nitrate	66 day			~ 7 day
2-Butyl nitrate	13 day			15–30 day

2.4.2. VOC Oxidation Pathways

The history of the scientific investigation and discussion of the atmospheric chemistry of various VOC classes can be traced to the 1980s (National Research Council, 1991; Atkinson and Carter, 1984; Atkinson, 1997; Atkinson and Aschmann, 1994). The process of VOC chemical removal in the atmosphere is complicated; and Figure 2.2 illustrates the general degradation/transformation reactions of VOCs in the ambient. In the early stage of VOC oxidation with oxidants, an alkyl radical ($R^{\cdot}$) is formed, followed by an organic peroxyl radical ($RO_2^{\cdot}$) and alkoxy radicals ($RO^{\cdot}$) intermediate. Meanwhile, termination products (e.g., organic nitrate) are formed via several termination reactions between intermediate with HO_2, NO_2, NO, or $RO_2^{\cdot}$. These termination products can alter the degree of oxidation state and stay as either gas-phase products and/or particle phase products (depending on their volatility), which is further discussed in Section 2.4.3.

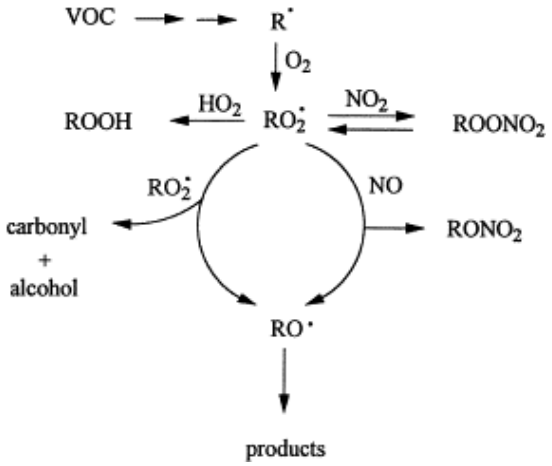

Figure 2.2: Simplified mechanisms of VOC degradation and transformation in the atmosphere (Atkinson, 2000).

As mentioned in Section 2.2, emissions from anthropogenic and biogenic sources were mainly alkene. Thus, it is crucial to understand the tropospheric chemistry of alkenes in ambient that leads to SOA formation. Oxidation pathways of specified alkene via OH radicals, NO_3 radicals, and O_3 were respectively considered in the assessment of transformation processes. This thesis exclusively addresses the oxidation pathways of VOCs at daytime. The oxidation of alkene proceeds from the initial addition of radicals to the C=C bond in alkene. For example, OH radicals exhibit major initial addition reactions to the C=C bond and subsequently form β-hydroxyalkyl radicals ($R^{\cdot}$), while a H-abstraction (minor reaction) occurs from C-H bonds of the alkyl substitute group around the C=C bonds. On the other hand, initial addition reactions of O_3 to the C=C bonds

form primary ozonides that rapidly decompose to form Criegee intermediates. Primary ozonide decomposition follows two pathways that form two sets of carbonyls and/or biradical products, depending on the molecular structure of the parent alkene (Atkinson, 1997). On the other hand, OH radicals formed from O_3 reactions with alkene lead to secondary reactions between OH radicals and alkene. These O_3 reactions with alkene involving OH radical formation and its subsequent reactions result in different product compositions and yields compared to the "actual" ozonolysis of alkene (Hakola et al., 1994). Aromatic hydrocarbon components are predominate emissions from anthropogenic activities. Aromatic hydrocarbons including benzene, toluene, and trimethyl-benzenes typically have OH radicals (daytime) and NO_3 radicals (nighttime) in the ambient. In the OH radical-initiated reaction, the H atom is abstracted from the C-H bonds of the alkyl substituted groups or the C-H bond that connect to the aromatic ring in benzene case, followed by OH radical additions to the aromatic ring, which lead to OH-aromatic adduct formation (Atkinson, 1991; Atkinson and Aschmann, 1994). Moreover, OH-aromatic adducts with O_2 were concerning in the ambient since the mechanism and products of these reactions can cause uncertainty in the tropospheric degradation of aromatic hydrocarbons. For instance, OH-benzene adducts with O_2 lead to different types of radical formations (e.g., epoxide-alkoyl radical, a bicycloalkyl radical, and peroxy radical) (Atkinson, 2000). These aforementioned species undergo subsequent reactions that form ring-opened products (e.g., unsaturated carbonyls, dicarbonyls, and epoxy-carbonyls).

2.4.3. Secondary Organic Aerosol Evolution and Phase Partitioning

Secondary organic aerosols are condense-phase compounds that proceed from volatile precursors (Donahue et al., 2012). Owing to the complexity of organic vapor reactions presented in Figure 2.2, gas-phase organic precursors are oxidized, which lead to reaction product formation with added functionality, such as oxygen containing substituents that have higher polarity and lower vapor pressure (Pandis et al., 1992). All these products can undergo further oxidation (i.e., continuously undergo the oxidation process over multiple generation steps), resulting in a highly complex mixture of organic compounds that have a wide range of chemical compositions and properties. Of note, the multiple generation steps include the following: oligomerization, fragmentation, and functionalization. A portion of these products can partition into aerosol particles that are controlled by the thermodynamics of organic mixture in the particles (Pankow et

al., 2001; Pankow and Asher, 2008). It has been reported that heavier, low-volatility organic vapors potentially form SOA much more efficiently than relatively light, high-volatility vapors. However, high-volatility vapors exhibit dominant carbon mass emissions in the ambient atmosphere (Robinson et al., 2007; Shrivastava et al., 2008). It is crucial to understand the properties and reactivities of these oxidation organic products, as they can impact the following: ozone products, the removal pathways of pollutants, and oxidant cycling and reactivity in the atmosphere.

One approach that constrains the chemical properties of the complex organic's mixture and demonstrates organic aerosol's formation and evolution is to use the Van Krevelen diagram. The diagram is a framework that illustrates how elemental composition changes during aerosol formation and evolution, which shows H:C ratios (hydrogen to carbon atomic ratios) against O:C ratios (oxygen to carbon atomic ratios) (Figure 2.3). The Van Krevelen diagram can be applied to the mass spectrometric measurement of individual species within organic aerosols (Bateman et al., 2009) and to bulk aerosol measurements (Kumar et al., 2016).

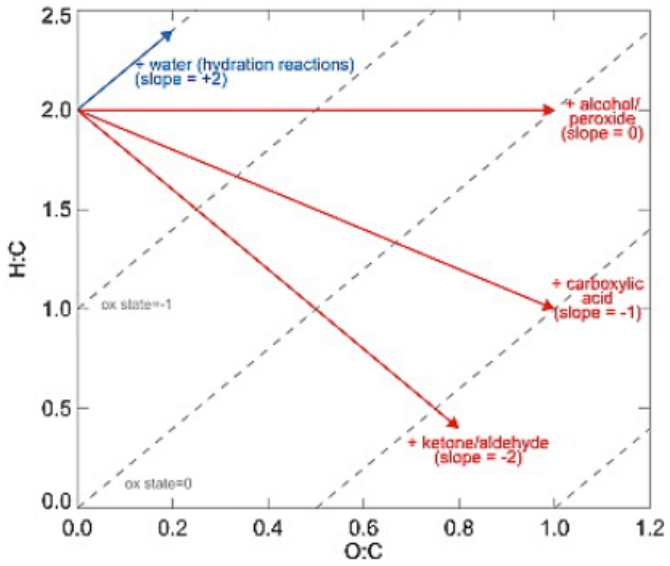

Figure 2.3: A conceptual Van Krevelen diagram for ambient organic aerosol (Heald et al., 2010).

Kroll et al. (2011) established average carbon oxidation state ($\overline{os}_C$) as a metric that describes the degree of oxidation during SOA formation and evolution. The oxidation states of individual carbon atoms within a molecule or mixture of molecules can exhibit dissimilar changes, depending on the reaction. However, the average carbon oxidation state should increase during oxidation, which may serve as a key quantity that constrains the chemical properties of complex organic mixtures

in the atmosphere. The interpretation of average carbon oxidation states associated with the identity and abundance of non-carbon atoms in organic aerosols is defined as Equation 2.11:

$$\overline{OS}_c = -\sum OS_i \frac{n_i}{n_C} \quad (2.11)$$

This equation is associated with all non-carbon elements, where OS_i is the oxidation state related to element i, and n_i/n_C refers to the molar ratios of element i to carbon. However, atmospheric organics mainly comprise carbon, hydrogen, and oxygen elements. Thus, Equation 2.11 can also be simplified to the following:

$$\overline{os}_C \approx 2\,O/C - H/C \quad (2.12)$$

The $\overline{os}_C$ coupling to nC provides a two-dimensional framework that describes the oxidation processes of atmospheric organic species relevant to the SOA evolution, in which should increase during oxidation. In theory, the end product of the oxidation of atmospheric organic species should be CO_2 (=+2) (Logan et al., 1981), which involves an addition of oxygen-containing moieties as well as breaking of C-C bonds of organic species upon oxidation. In fact, there are chemical reactions involved in the oxidative transformation of organic species, which even include non-oxidative transformation (e.g., accretion reactions). Figure 2.4 demonstrates that this two-dimensional framework ($\overline{os}_C$ vs nC) can visualize the fragmentation (breaking of C–C bonds), functionalization (addition of polar functional groups), and oligomerization (covalent association of two organic species) processes in the oxidation system. Different types of reactions result in complex movements through the $\overline{os}_C$ - nC space. Nevertheless, with adequate time, the $\overline{os}_C$ of atmospheric organic species eventually move toward the upper right corner (Kroll et al., 2011).

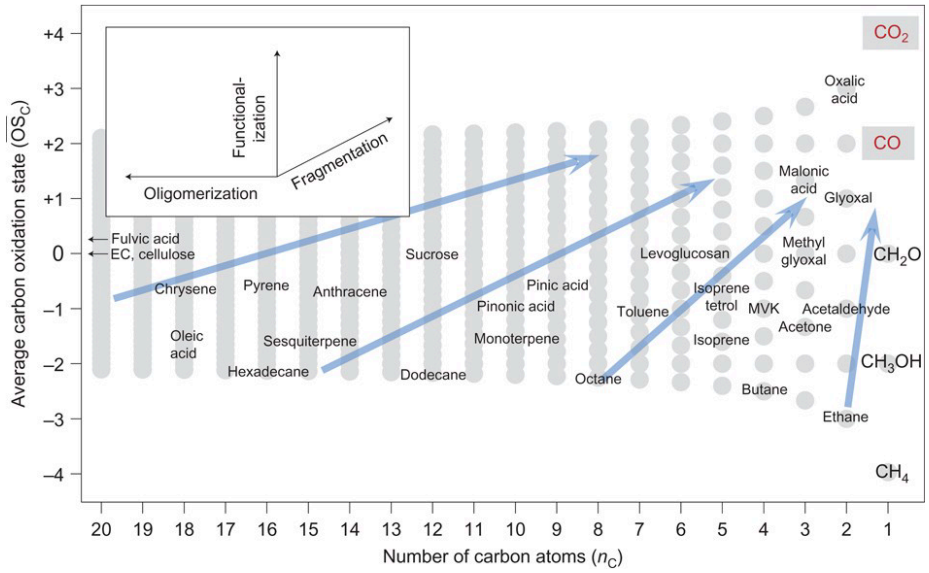

Figure 2.4: A two-dimensional framework of of $\overline{os}_C$ – nC that follows the atmospheric oxidation pathways of SOA formation (Kroll et al., 2011).

It has been studied and widely accepted that gas-phase oxidation reactions in the atmosphere (VOC oxidation) not only change the average carbon oxidation state, but also reduce volatility via addition of polar functional groups, or increase volatility via cleavage of C-C bonds (Kroll and Seinfeld, 2008). The low-volatility products can undergo subsequent phase-partitioning (gas-particle partitioning) into a condensed phase, which will either change the molecule dynamics or undergo further reaction that leads to particulate matter formations. Phase-partitioning is characterised by the saturation vapor pressure and equilibrium partitioning coefficients of molecules (Pankow, 1994). The saturation vapor pressure is directly proportional to the volatility of organic species that is strongly associated with elemental composition (Donahue et al., 2014). A two-dimensional volatility basis set developed by Donahue et al. (2012) utilized these relationships and classified atmospheric organic species according to their saturation vapor concentrations (C*), in reference to their volatility. In order of increasing volatility magnitude, organic species are classified into the following: i) extremely-low volatility organic compounds (ELVOC, $C^* < 3 \times 10^{-5} \mu g\ m^{-3}$); ii) low volatility organic compounds (LVOC, $3 \times 10^{-5} < C^* < 0.3 \mu g\ m^{-3}$); iii) semi-volatile organic compounds (SVOC, $0.3 < C* < 300 \mu g\ m^{-3}$); iv) intermediate volatility organic compounds (IVOC, $300 < C^* < 3 \times 10^6 \mu g\ m^{-3}$); and v) volatile organic compounds (VOC,$C^* > 3 \times 10^6 \mu g\ m^{-3}$).

It is vital to explore insights related to the volatility of aerosol components to investigate SOA formation and evolution comprehensively. To date, the major concept for the modern treatment of SOA predominantly involves semi-volatile organic compounds (Pankow, 1994; Lazaridis, 1999; Odum et al., 1996). Pankow (1994) proposed a theory about the absorptive portioning of pure semi-volatile organic species, which describes that partitioning coefficient K_p ($m^3\mu g^{-1}$) is inversely proportional to saturation vapor pressure (C*). Moreover, more high-volatility compounds will partition into a condense phase if a larger number of absorbing materials is present. However, it is difficult to measure all individual semi-volatile compounds in the atmosphere of SOA formation. Thus, a "two-product model" of SOA formation was proposed to represent laboratory SOA growth data (Seinfeld and Pankow, 2003; Keywood et al., 2004) and incorporate with the atmosphere chemistry model (Figure 2.5) (Chung and Seinfeld, 2002; Koo et al., 2003; Heald et al., 2005). This "two-product model" only used two surrogate semi-volatile products ($S_1$and S_2) to express volatility distribution from SOA formation, and each of the products will partition between gas phase and particle phase, which is similar to the "volatility basis set" approach (Donahue et al., 2006), as used in complex mixtures of semi-volatiles.

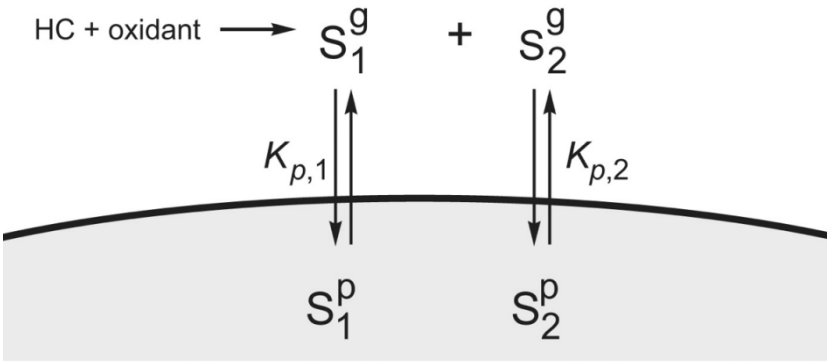

Figure 2.5: Schematic of the "two-product model" of SOA formation (Odum et al., 1996)

2.5. Aerosol Chamber Studies of SOA Formation and Its Impacts

2.5.1. SOA Formation via Photochemistry

Extensive studies have investigated SOA formation from the oxidation of volatile organic compounds by using a smog chamber, particularly those that involve VOCs in the presence of NOx for photochemical oxidation. As mentioned in Section 2.3, photolysis of NO_2 generates OH radicals and leads to ozone generation that significantly contributes to VOC degradation, resulting

in SOA formation. Interrogation of SOA yield dependence related to the type of parent precursors and NOx contents can be used to infer information about SOA formation pathways. SOA yield is defined as the ratio of the mass of organic aerosol compounds formed to the mass of parent hydrocarbon that reacted (δMo/δHC) (Ng et al., 2007).

The chemical composition of parent VOCs directly influences the SOA yield initiated by OH-radical reaction (Lim and Ziemann, 2009). SOA yield depends on the amount of organic matter (M_0) that is present, which relates to the extent of gas/particle absorptive partitioning. Adsorptive partitioning correlates to the extent of the organic condensed phase involving products that can be absorbed. Ziemann (2011) reported that SOA yield increases when the number of carbon increases in the C_8–C_{17} n-alkane reaction. It is likely that a higher number of carbon atoms in n-alkane compounds will generate lower volatility SOA precursor products through OH-radical initiation reactions, thereby enhancing partitioning to the particles phase. Moreover, the structure of VOCs may impact SOA formation. The concentration of low volatility SOA products will decrease if the alkoxy radicals become more branched; and such branching results from the atmospheric OH radical-initiated oxidation of C_7–C_{17} n-alkanes. This oxidation may result in an increase in the decomposition rate of alkoxy radicals to alkyl radicals that will enhance the yield of high volatile carbonyls and products of alkyl radicals. Thus, the average volatility of products will increase if the precursors are more branched, leading to a lower SOA yield (Ziemann, 2011; Lim and Ziemann, 2009).

Moreover, it has been reported in smog chamber experiments that the ratio between VOCs and NOx affects the pathways of SOA, resulting in changes in SOA yield. Recent studies have demonstrated that SOA yields are highest at low levels of NOx on α-pinene ozonolysis as well as the photooxidation of isoprene, benzene, toluene, and m-xylene (Kroll et al., 2006; Presto et al., 2005; Song et al., 2005; Ng et al., 2007). This observation occurred due to the competitive chemistry of peroxy radicals between NO and HO_2. This implies that the classification of SOA yield, which depends on NOx, should account for other aspects of the oxidant regime. Organic peroxy radicals (RO_2) will predominantly react with NO under high NOx conditions, and react with HO_2 under low NOx conditions, forming products from RO_2+HO_2 reactions that have lower volatility compared to RO_2+NO reactions (Presto et al., 2005; Johnson et al., 2004, 2005). On the

925 other hand, Zhang et al. (2006) suggested that the reaction between VOCs and NOx is also dependent on ozone presence. Heterogeneous ozonolysis of the exo-double bond occurring under low NOx conditions in the presence of ozone leads to the generation of condensed-phase secondary generation oxidation products. However, under high NOx conditions, gas-phase oxidation of the double bond is the dominant process.

930

Oh and Andino (2000) suggested that the presence of pre-existing submicron seed aerosols exerted catalytic effects on gas-phase reaction kinetics, leading to the promotion of SOA formation in VOC OH-initiated oxidation. Moreover, Oh and Andino (2000) and by Koehler et al. (2004) also suggested that the initial wet and dry conditions of seed particles can also impact SOA yield. 935 However, Cocker et al. (2001) disagreed with this conclusion, and indicated that SOA yield has little variation with changes in initial wet and dry conditions of ammonium sulfate seed. More laboratory experiments involving a wide variety of inorganic seeds and RH conditions are warranted.

940

2.5.2. The Impacts of Wall Effects in Aerosol Chamber on SOA Formation

The interaction between semi-volatile vapors and the Teflon chamber wall is one of the influencing factors of organic-aerosol behaviors in chamber experiments (Mcmurry and Grosjean, 1985; Loza et al., 2010; Matsunaga and Ziemann, 2010; Zhang et al., 2014; Zhang et al., 2015) In theory, the 945 SOA mass yield decreases because the loss of organic vapors on the Teflon chamber walls leads to suppression of vapor condensation to suspended particles. However, the loss of volatile organic vapors on the chamber wall is not well characterised (Matsunaga and Ziemann (2010). Matsunaga and Ziemann (2010) observed that the gas-wall partitioning of volatile organic vapors is a reversible process, and the equilibrium can be characterised by a condensation process (Figure 950 2.6). La et al. (2016) also suggested that SOA yield usually underestimates, and the inferred composition of SOA is altered in the chamber experiment due to the wall loss effect of organic vapors. This supports the idea that the gas-wall partitioning equilibrium follows Raoult's law, and the temporal concentration of semi-volatile organic compounds in the gas phase of the gas-wall process can be calculated in terms of Equation 2.13:

955

[SVOC(g)] is the concentration of SVOC in the gas phase; [SVOC(w)] are the concentrations of SVOC on the wall at a given time; and $-k_{gw}\ and\ k_{gw}$ are the rate constants.

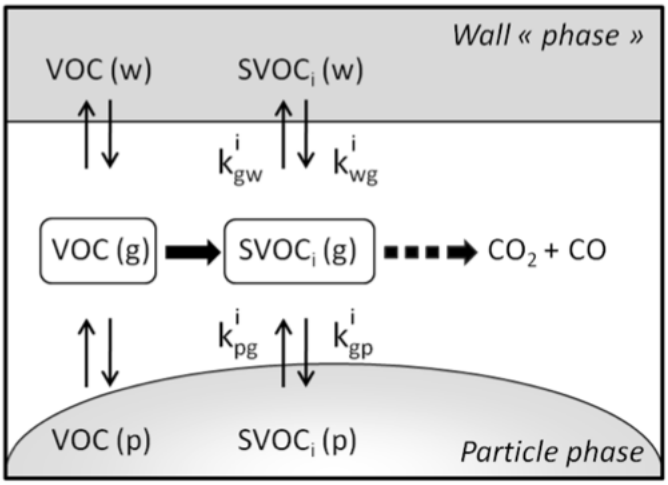

Figure 2.6: Schematic of gas-particles and gas-wall mass transfer process during gaseous oxidation of VOCs (La et al., 2016).

On the other hand, particle-wall loss process is another challenge in smog chamber experiments that affect SOA yield because aerosols can exhibit particle loss on the chamber wall via Brownian diffusion, convection, electrostatic effects, and gravitational sedimentation (Wang et al., 2018). Generally, the wall loss rate of particles in the chamber can be calculated using Equation 2.14.

$$\frac{dN(D_p,t)}{dt} = -k(D_p,t)N(D_{p,}t) \qquad (2.14)$$

N(Dp,t) refers to the number concentration of particles with diameter Dp at time t; and k refers to the function of particle size and time since a smaller particle size (less than 50nm) has a higher diffusion rate. A number of particle-wall loss correction methods have been developed and adapted in chamber studies, such as the use of size-independent and/or dependent loss rate constants and the ratio of suspended organic mass to inert seed particles (e.g., ammonium sulphate) (Pathak et al., 2007; Ng et al., 2007; Nah et al., 2017; Fry et al., 2014).

Historical investigations of wall effects on organic vapor and particles in smog chamber experiments indicate that gas-wall partitioning and particle-wall loss require routine characterisation for aerosol chamber experiments to derive SOA yield.

Reference:

Andreae, M. O. and Gelencsér, A.: Black carbon or brown carbon? The nature of light-absorbing carbonaceous aerosols, Atmos. Chem. Phys., 6, 3131-3148, 10.5194/acp-6-3131-2006, 2006.

Atkinson, R.: Kinetics and Mechanisms of the Gas-Phase Reactions of the NO3 Radical with Organic Compounds, Journal of Physical and Chemical Reference Data, 20, 459-507, 10.1063/1.555887, 1991.

Atkinson, R.: Gas-phase tropospheric chemistry of volatile organic compounds: 1. Alkanes and alkenes, Journal of Physical and Chemical Reference Data, 26, 215-290, 1997.

Atkinson, R.: Atmospheric chemistry of VOCs and NOx, Atmospheric Environment, 34, 2063-2101, https://doi.org/10.1016/S1352-2310(99)00460-4, 2000.

Atkinson, R. and Arey, J.: Gas-phase tropospheric chemistry of biogenic volatile organic compounds: a review, Atmospheric Environment, 37, 197-219, 2003.

Atkinson, R. and Aschmann, S. M.: Products of the gas-phase reactions of aromatic hydrocarbons: Effect of NO2 concentration, International Journal of Chemical Kinetics, 26, 929-944, 10.1002/kin.550260907, 1994.

Atkinson, R. and Carter, W. P. L.: Kinetics and mechanisms of the gas-phase reactions of ozone with organic compounds under atmospheric conditions, Chemical Reviews, 84, 437-470, 10.1021/cr00063a002, 1984.

Bateman, A. P., Nizkorodov, S. A., Laskin, J., and Laskin, A.: Time-resolved molecular characterization of limonene/ozone aerosol using high-resolution electrospray ionization mass spectrometry, Physical Chemistry Chemical Physics, 11, 7931-7942, 10.1039/B905288G, 2009.

Brauer, M., Freedman, G., Frostad, J., van Donkelaar, A., Martin, R. V., Dentener, F., Dingenen, R. v., Estep, K., Amini, H., Apte, J. S., Balakrishnan, K., Barregard, L., Broday, D., Feigin, V., Ghosh, S., Hopke, P. K., Knibbs, L. D., Kokubo, Y., Liu, Y., Ma, S., Morawska, L., Sangrador, J. L. T., Shaddick, G., Anderson, H. R., Vos, T., Forouzanfar, M. H., Burnett, R. T., and Cohen, A.: Ambient Air Pollution Exposure Estimation for the Global Burden of Disease 2013, Environmental Science & Technology, 50, 79-88, 10.1021/acs.est.5b03709, 2016.

Burnett, R., Pope, C., Ezzati, M., Olives, C., Lim, S., Mehta, S., Shin, H., Singh, G., Hubbell, B., Brauer, M., Anderson, H., Smith, K., Balmes, J., Bruce, N., Kan, H., Laden, F., Prüss-Ustün, A., Turner, M., Gapstur, S., and Cohen, A.: An Integrated Risk Function for Estimating the Global Burden of Disease Attributable to Ambient Fine Particulate Matter Exposure, Environmental health perspectives, 122, 10.1289/ehp.1307049, 2014.

Carlton, A. G., Wiedinmyer, C., and Kroll, J. H.: A review of Secondary Organic Aerosol (SOA) formation from isoprene, Atmos. Chem. Phys., 9, 4987-5005, 10.5194/acp-9-4987-2009, 2009.

Chung, S. and Seinfeld, J.: Global Distribution and Climate Forcing of Carbonaceous Aerosols, J. Geophys. Res, 107, 10.1029/2001JD001397, 2002.

Cocker, D. R., Clegg, S. L., Flagan, R. C., and Seinfeld, J. H.: The effect of water on gas–particle partitioning of secondary organic aerosol. Part I: α-pinene/ozone system, Atmospheric Environment, 35, 6049-6072, https://doi.org/10.1016/S1352-2310(01)00404-6, 2001.

Council, N. R.: Rethinking the Ozone Problem in Urban and Regional Air Pollution, The National Academies Press, Washington, DC, 524 pp., doi:10.17226/1889, 1991.

Després, V., Huffman, J. A., Burrows, S. M., Hoose, C., Safatov, A., Buryak, G., Fröhlich-Nowoisky, J., Elbert, W., Andreae, M., Pöschl, U., and Jaenicke, R.: Primary biological aerosol

particles in the atmosphere: a review, Tellus B: Chemical and Physical Meteorology, 64, 15598, 10.3402/tellusb.v64i0.15598, 2012.
Donahue, N. M., Kroll, J. H., Pandis, S. N., and Robinson, A. L.: A two-dimensional volatility basis set – Part 2: Diagnostics of organic-aerosol evolution, Atmos. Chem. Phys., 12, 615-634, 10.5194/acp-12-615-2012, 2012.
Donahue, N. M., Robinson, A. L., Stanier, C. O., and Pandis, S. N.: Coupled Partitioning, Dilution, and Chemical Aging of Semivolatile Organics, Environmental Science & Technology, 40, 2635-2643, 10.1021/es052297c, 2006.
Donahue, N. M., Robinson, A. L., Trump, E. R., Riipinen, I., and Kroll, J. H.: Volatility and Aging of Atmospheric Organic Aerosol, in: Atmospheric and Aerosol Chemistry, edited by: McNeill, V. F., and Ariya, P. A., Springer Berlin Heidelberg, Berlin, Heidelberg, 97-143, 10.1007/128_2012_355, 2014.
Fann, N., Lamson, A. D., Anenberg, S. C., Wesson, K., Risley, D. L., and Hubbell, B.: Estimating the national public health burden associated with exposure to ambient PM2.5 and ozone, Risk analysis : an official publication of the Society for Risk Analysis, 32 1, 81-95, 2012.
Forster, P., Ramaswamy, V., Artaxo, P., Berntsen, T., Betts, R., Fahey, D. W., Haywood, J., Lean, J., Lowe, D. C., Myhre, G., Nganga, J., Prinn, R., Raga, G., Schulz, M., and Van Dorland, R.: Changes in Atmospheric Constituents and in Radiative Forcing Chapter 2, Cambridge University Press, United Kingdom2007.
Fry, J. L., Draper, D. C., Barsanti, K. C., Smith, J. N., Ortega, J., Winkler, P. M., Lawler, M. J., Brown, S. S., Edwards, P. M., Cohen, R. C., and Lee, L.: Secondary Organic Aerosol Formation and Organic Nitrate Yield from NO3 Oxidation of Biogenic Hydrocarbons, Environmental Science & Technology, 48, 11944-11953, 10.1021/es502204x, 2014.
Guenther, A., Hewitt, C. N., Erickson, D., Fall, R., Geron, C., Graedel, T., Harley, P., Klinger, L., Lerdau, M., McKay, W. A., Pierce, T., Scholes, B., Steinbrecher, R., Tallamraju, R., Taylor, J., and Zimmerman, P.: A global model of natural volatile organic compound emissions, Journal of geophysical research, 100, 8873-8892, 10.1029/94JD02950, 1995.
Guenther, A. B., Jiang, X., Heald, C. L., Sakulyanontvittaya, T., Duhl, T., Emmons, L. K., and Wang, X.: The Model of Emissions of Gases and Aerosols from Nature version 2.1 (MEGAN2.1): an extended and updated framework for modeling biogenic emissions, Geosci. Model Dev., 5, 1471-1492, 10.5194/gmd-5-1471-2012, 2012.
Hakola, H., Arey, J., Aschmann, S. M., and Atkinson, R.: Product formation from the gas-phase reactions of OH radicals and O3 with a series of monoterpenes, Journal of Atmospheric Chemistry, 18, 75-102, 10.1007/BF00694375, 1994.
Hallquist, M., Wenger, J., Baltensperger, U., Rudich, Y., Simpson, D., Claeys, M., Dommen, J., Donahue, N., George, C., and Goldstein, A.: The formation, properties and impact of secondary organic aerosol: current and emerging issues, Atmospheric chemistry and physics, 9, 5155-5236, 2009.
Harrison, R. M.: Urban atmospheric chemistry: a very special case for study, npj Climate and Atmospheric Science, 1, 20175, 10.1038/s41612-017-0010-8, 2018.
Heald, C., Jacob, D., Park, R., Russell, L., Huebert, B., Seinfeld, J., Liao, H., and Weber, R.: A Large Organic Aerosol Source in the Free Troposphere Missing from Current Models, Geophysical Research Letters, 10.1029/2005GL023831, 2005.
Heald, C., Kroll, J. H., Jimenez, J. L., Docherty, K. S., DeCarlo, P., Aiken, A., Chen, Q., Martin, S. T., Farmer, D. K., Artaxo, P., and Weinheimer, A. J.: A simplified description of organic aerosol composition and implications for atmospheric aging, Geophys. Res. Lett, 37, 2010.

Hoyle, C., Myhre, G., Berntsen, T., and Isaksen, I.: Anthropogenic influence on SOA and the resulting radiative forcing, Atmospheric Chemistry and Physics Discussions, 8, 10.5194/acpd-8-18911-2008, 2008.

Ipcc, Stocker, T., Qin, D., Plattner, G.-K., Tignor, M., Allen, S. K., Boschung, J., Nauels, A., Xia, Y., Bex, V., and Midgley, P. M.: The physical science basis. Contribution of Working Group I to the Fifth Assessment Report of the Intergovernmental Panel on Climate Change, Climate Change 2013, 2013.

Jimenez, J. L., Canagaratna, M. R., Donahue, N. M., Prevot, A. S. H., Zhang, Q., Kroll, J. H., DeCarlo, P. F., Allan, J. D., Coe, H., Ng, N. L., Aiken, A. C., Docherty, K. S., Ulbrich, I. M., Grieshop, A. P., Robinson, A. L., Duplissy, J., Smith, J. D., Wilson, K. R., Lanz, V. A., Hueglin, C., Sun, Y. L., Tian, J., Laaksonen, A., Raatikainen, T., Rautiainen, J., Vaattovaara, P., Ehn, M., Kulmala, M., Tomlinson, J. M., Collins, D. R., Cubison, M. J., E, Dunlea, J., Huffman, J. A., Onasch, T. B., Alfarra, M. R., Williams, P. I., Bower, K., Kondo, Y., Schneider, J., Drewnick, F., Borrmann, S., Weimer, S., Demerjian, K., Salcedo, D., Cottrell, L., Griffin, R., Takami, A., Miyoshi, T., Hatakeyama, S., Shimono, A., Sun, J. Y., Zhang, Y. M., Dzepina, K., Kimmel, J. R., Sueper, D., Jayne, J. T., Herndon, S. C., Trimborn, A. M., Williams, L. R., Wood, E. C., Middlebrook, A. M., Kolb, C. E., Baltensperger, U., and Worsnop, D. R.: Evolution of Organic Aerosols in the Atmosphere, Science, 326, 1525, 10.1126/science.1180353, 2009.

Johnson, D., Jenkin, M., Wirtz, K., and Martin-Reviejo, M.: Simulating the Formation of Secondary Organic Aerosol from the Photooxidation of Toluene, Environmental Chemistry, 1, 150-165, 10.1071/en04069, 2004.

Johnson, D., Jenkin, M., Wirtz, K., and Martin-Reviejo, M.: Simulating the Formation of Secondary Organic Aerosol from the Photooxidation of Aromatic Hydrocarbons, Environmental Chemistry, 2, 35-48, 10.1071/en04079, 2005.

Jürgens, A. and Bischoff, M.: Changing odour landscapes: The effect of anthropogenic volatile pollutants on plant-pollinator olfactory communication, Functional Ecology, 31, 10.1111/1365-2435.12774, 2017.

Keeling, C. and Bohlmann, J.: Genes, enzymes and chemicals of terpenoid diversity in the constitutive and induced defence of conifers against insects and pathogens, The New phytologist, 170, 657-675, 10.1111/j.1469-8137.2006.01716.x, 2006.

Keywood, M. D., Varutbangkul, V., Bahreini, R., Flagan, R. C., and Seinfeld, J. H.: Secondary Organic Aerosol Formation from the Ozonolysis of Cycloalkenes and Related Compounds, Environmental Science & Technology, 38, 4157-4164, 10.1021/es035363o, 2004.

Koehler, C. A., Fillo, J. D., Ries, K. A., Sanchez, J. T., and De Haan, D. O.: Formation of Secondary Organic Aerosol by Reactive Condensation of Furandiones, Aldehydes, and Water Vapor onto Inorganic Aerosol Seed Particles, Environmental Science & Technology, 38, 5064-5072, 10.1021/es034672b, 2004.

Koo, B., Asif, S., and Pandis, S.: Integrated approaches to modeling the organic and inorganic atmospheric aerosol components, Atmospheric Environment, 37, 4757-4768, 10.1016/j.atmosenv.2003.08.016, 2003.

Kroll, J. H. and Seinfeld, J. H.: Chemistry of secondary organic aerosol: Formation and evolution of low-volatility organics in the atmosphere, Atmospheric Environment, 42, 3593-3624, https://doi.org/10.1016/j.atmosenv.2008.01.003, 2008.

Kroll, J. H., Ng, N. L., Murphy, S. M., Flagan, R. C., and Seinfeld, J. H.: Secondary organic aerosol formation from isoprene photooxidation, Environmental science & technology, 40, 1869-1877, 2006.

Kroll, J. H., Donahue, N. M., Jimenez, J. L., Kessler, S. H., Canagaratna, M. R., Wilson, K. R., Altieri, K. E., Mazzoleni, L. R., Wozniak, A. S., Bluhm, H., Mysak, E. R., Smith, J. D., Kolb, C. E., and Worsnop, D. R.: Carbon oxidation state as a metric for describing the chemistry of atmospheric organic aerosol, Nature Chemistry, 3, 133-139, 10.1038/nchem.948, 2011.

Kumar, B., Chakraborty, A., Tripathi, S. N., and Bhattu, D.: Highly time resolved chemical characterization of submicron organic aerosols at a polluted urban location, Environmental Science: Processes & Impacts, 18, 1285-1296, 10.1039/C6EM00392C, 2016.

La, Y. S., Camredon, M., Ziemann, P. J., Valorso, R., Matsunaga, A., Lannuque, V., Lee-Taylor, J., Hodzic, A., Madronich, S., and Aumont, B.: Impact of chamber wall loss of gaseous organic compounds on secondary organic aerosol formation: explicit modeling of SOA formation from alkane and alkene oxidation, Atmos. Chem. Phys., 16, 1417-1431, 10.5194/acp-16-1417-2016, 2016.

Laidlaw, M. A. S., Zahran, S., Mielke, H. W., Taylor, M. P., and Filippelli, G. M.: Re-suspension of lead contaminated urban soil as a dominant source of atmospheric lead in Birmingham, Chicago, Detroit and Pittsburgh, USA, Atmospheric Environment, 49, 302-310, https://doi.org/10.1016/j.atmosenv.2011.11.030, 2012.

Lamarque, J. F., Bond, T. C., Eyring, V., Granier, C., Heil, A., Klimont, Z., Lee, D., Liousse, C., Mieville, A., Owen, B., Schultz, M. G., Shindell, D., Smith, S. J., Stehfest, E., Van Aardenne, J., Cooper, O. R., Kainuma, M., Mahowald, N., McConnell, J. R., Naik, V., Riahi, K., and van Vuuren, D. P.: Historical (1850–2000) gridded anthropogenic and biomass burning emissions of reactive gases and aerosols: methodology and application, Atmos. Chem. Phys., 10, 7017-7039, 10.5194/acp-10-7017-2010, 2010.

Lazaridis, M.: Gas–particle partitioning of organic compounds in the atmosphere, Journal of Aerosol Science, 30, 1165-1170, https://doi.org/10.1016/S0021-8502(98)00788-5, 1999.

Lim, Y. B. and Ziemann, P. J.: Effects of molecular structure on aerosol yields from OH radical-initiated reactions of linear, branched, and cyclic alkanes in the presence of NO x, Environmental science & technology, 43, 2328-2334, 2009.

Logan, J., Prather, M., Wofsy, S., and McElroy, M.: Tropospheric chemistry: A global perspective, Journal of Geophysical Research, 86, 10.1029/JC086iC08p07210, 1981.

Loza, C. L., Chan, A. W. H., Galloway, M. M., Keutsch, F. N., Flagan, R. C., and Seinfeld, J. H.: Characterization of Vapor Wall Loss in Laboratory Chambers, Environmental Science & Technology, 44, 5074-5078, 10.1021/es100727v, 2010.

Matsunaga, A. and Ziemann, P. J.: Gas-Wall Partitioning of Organic Compounds in a Teflon Film Chamber and Potential Effects on Reaction Product and Aerosol Yield Measurements, Aerosol Science and Technology, 44, 881-892, 10.1080/02786826.2010.501044, 2010.

McMurry, P. H. and Grosjean, D.: Gas and aerosol wall losses in Teflon film smog chambers, Environmental Science & Technology, 19, 1176-1182, 10.1021/es00142a006, 1985.

Montero-Montoya, R., Lopez, R., and Arellano-Aguilar, O.: Volatile Organic Compounds in Air: Sources, Distribution, Exposure and Associated Illnesses in Children, Annals of Global Health, 84, 225-238, 10.29024/aogh.910, 2018.

Myhre, G., Shindell, D., Bréon, F.-M., Collins, W., Fuglestvedt, J., Huang, J., Koch, D., Lamarque, J.-F., Lee, D., Mendoza, B., Nakajima, T., Robock, A., Stephens, G., Takemura, T., and Zhang, H.: Anthropogenic and natural radiative forcing, Climate Change 2013: The Physical Science Basis. Contribution of Working Group I to the Fifth Assessment Report of the Intergovernmental Panel on Climate Change, 659-740, 10.1017/CBO9781107415324.018, 2013.

Nah, T., McVay, R. C., Pierce, J. R., Seinfeld, J. H., and Ng, N. L.: Constraining uncertainties in particle-wall deposition correction during SOA formation in chamber experiments, Atmos. Chem. Phys., 17, 2297-2310, 10.5194/acp-17-2297-2017, 2017.

Nault, B., Jo, D., McDonald, B., Campuzano-Jost, P., Day, D., Hu, W., Schroder, J., Allan, J., Blake, D., Coe, H., Coggon, M., DeCarlo, P., Diskin, G., Dunmore, R., Flocke, F., Fried, A., Gilman, J., Gkatzelis, G., and Jimenez, J.: Secondary organic aerosols from anthropogenic volatile organic compounds contribute substantially to air pollution mortality, Atmospheric Chemistry and Physics, 21, 11201-11224, 10.5194/acp-21-11201-2021, 2021.

Ng, N. L., Kroll, J. H., Chan, A. W. H., Chhabra, P. S., Flagan, R. C., and Seinfeld, J. H.: Secondary organic aerosol formation from m-xylene, toluene, and benzene, Atmos. Chem. Phys., 7, 3909-3922, 10.5194/acp-7-3909-2007, 2007.

Odum, J. R., Hoffmann, T., Bowman, F., Collins, D., Flagan, R. C., and Seinfeld, J. H.: Gas/particle partitioning and secondary organic aerosol yields, Environmental Science & Technology, 30, 2580-2585, 1996.

Oh, S. and Andino, J.: Effects of ammonium sulfate aerosols on the gas-phase reactions of the hydroxyl radical with organic compounds, Atmospheric Environment, 34, 2901-2908, 10.1016/S1352-2310(00)00071-6, 2000.

Owen, S. M., Boissard, C., and Hewitt, C. N.: Volatile organic compounds (VOCs) emitted from 40 Mediterranean plant species:: VOC speciation and extrapolation to habitat scale, Atmospheric Environment, 35, 5393-5409, https://doi.org/10.1016/S1352-2310(01)00302-8, 2001.

Pandey, P. and Yadav, R.: A Review on Volatile Organic Compounds (VOCs) as Environmental Pollutants: Fate and Distribution, International Journal of Plant and Environment, 4, 10.18811/ijpen.v4i02.2, 2018.

Pandis, S. N., Harley, R. A., Cass, G. R., and Seinfeld, J. H.: Secondary organic aerosol formation and transport, Atmospheric Environment. Part A. General Topics, 26, 2269-2282, https://doi.org/10.1016/0960-1686(92)90358-R, 1992.

Pankow, J. F.: An absorption model of the gas/aerosol partitioning involved in the formation of secondary organic aerosol, Atmospheric Environment, 28, 189-193, 1994.

Pankow, J. F. and Asher, W. E.: SIMPOL.1: a simple group contribution method for predicting vapor pressures and enthalpies of vaporization of multifunctional organic compounds, Atmos. Chem. Phys., 8, 2773-2796, 10.5194/acp-8-2773-2008, 2008.

Pankow, J. F., Seinfeld, J. H., Asher, W. E., and Erdakos, G. B.: Modeling the Formation of Secondary Organic Aerosol. 1. Application of Theoretical Principles to Measurements Obtained in the α-Pinene/, β-Pinene/, Sabinene/, Δ3-Carene/, and Cyclohexene/Ozone Systems, Environmental Science & Technology, 35, 1164-1172, 10.1021/es001321d, 2001.

Pathak, R., Stanier, C., Donahue, N., and Pandis, S.: Ozonolysis of a-pinene at atmospherically relevant concentrations: Temperature dependence of aerosol mass fractions (yields), J. Geophys. Res, 112, 10.1029/2006JD007436, 2007.

Petit, J.-E., Favez, O., Sciare, J., Canonaco, F., Croteau, P., Močnik, G., Jayne, J., Worsnop, D., and Leoz-Garziandia, E.: Submicron aerosol source apportionment of wintertime pollution in Paris, France by double positive matrix factorization (PMF²) using an aerosol chemical speciation monitor (ACSM) and a multi-wavelength Aethalometer, ATMOSPHERIC CHEMISTRY AND PHYSICS, 14, 13773-13787, 10.5194/acp-14-13773-2014, 2014.

Prather, K., Hatch, C., and Grassian, V.: Analysis of Atmospheric Aerosols, Annual review of analytical chemistry (Palo Alto, Calif.), 1, 485-514, 10.1146/annurev.anchem.1.031207.113030, 2008.

Presto, A. A., Huff Hartz, K. E., and Donahue, N. M.: Secondary Organic Aerosol Production from Terpene Ozonolysis. 2. Effect of NOx Concentration, Environmental Science & Technology, 39, 7046-7054, 10.1021/es050400s, 2005.

Prospero, J. M., Ginoux, P., Torres, O., Nicholson, S. E., and Gill, T. E.: ENVIRONMENTAL CHARACTERIZATION OF GLOBAL SOURCES OF ATMOSPHERIC SOIL DUST IDENTIFIED WITH THE NIMBUS 7 TOTAL OZONE MAPPING SPECTROMETER (TOMS) ABSORBING AEROSOL PRODUCT, Reviews of Geophysics, 40, 2-1-2-31, https://doi.org/10.1029/2000RG000095, 2002.

Ramanathan, V. and Carmichael, G.: Global and regional climate changes due to black carbon, Nature Geoscience, 1, 221-227, 10.1038/ngeo156, 2008.

Robinson, A. L., Donahue, N. M., Shrivastava, M. K., Weitkamp, E. A., Sage, A. M., Grieshop, A. P., Lane, T. E., Pierce, J. R., and Pandis, S. N.: Rethinking Organic Aerosols: Semivolatile Emissions and Photochemical Aging, Science, 315, 1259, 10.1126/science.1133061, 2007.

Russo, S., Dosio, A., Sterl, A., Barbosa, P., and Vogt, J.: Projection of occurrence of extreme dry-wet years and seasons in Europe with stationary and nonstationary Standardized Precipitation Index, Journal of Geophysical Research, 118, 7628-7639, 10.1002/jgrd.50571, 2013.

Safety, C. F. C. P.: Historical Perspective on Air Pollution Control, 10.1002/0470038071.app9, 2006.

Seinfeld, J. H. and Pankow, J. F.: Organic Atmospheric Particulate Material, Annual Review of Physical Chemistry, 54, 121-140, 10.1146/annurev.physchem.54.011002.103756, 2003.

Shrivastava, M., Lane, T. E., Donahue, N. M., Pandis, S. N., and Robinson, A. L.: Effects of gas particle partitioning and aging of primary emissions on urban and regional organic aerosol concentrations, Journal of Geophysical Research, 113, 2008.

Song, C., Na, K., and Cocker, D. R.: Impact of the Hydrocarbon to NOx Ratio on Secondary Organic Aerosol Formation, Environmental Science & Technology, 39, 3143-3149, 10.1021/es0493244, 2005.

Stavroulas, I., Bougiatioti, A., Grivas, G., Paraskevopoulou, D., Tsagkaraki, M., Zarmpas, P., Liakakou, E., Gerasopoulos, E., and Mihalopoulos, N.: Sources and processes that control the submicron organic aerosol composition in an urban Mediterranean environment (Athens): A high temporal-resolution chemical composition measurement study, Atmospheric Chemistry and Physics, 19, 901-919, 10.5194/acp-19-901-2019, 2019.

Stevens, B. and Feingold, G.: Untangling aerosol effects on clouds and precipitation in a buffered system, Nature, 461, 607-613, 10.1038/nature08281, 2009.

Wang, N., Jorga, S. D., Pierce, J. R., Donahue, N. M., and Pandis, S. N.: Particle wall-loss correction methods in smog chamber experiments, Atmos. Meas. Tech., 11, 6577-6588, 10.5194/amt-11-6577-2018, 2018.

Went, F. W.: Blue Hazes in the Atmosphere, Nature, 187, 641-643, 10.1038/187641a0, 1960.

World Health Organization, O. and Environmental Health, T.: WHO Air quality guidelines for particulate matter, ozone, nitrogen dioxide and sulfur dioxide : global update 2005 : summary of risk assessment, 2006.

Zhang, J., Huff Hartz, K. E., Pandis, S. N., and Donahue, N. M.: Secondary organic aerosol formation from limonene ozonolysis: Homogeneous and heterogeneous influences as a function of NO x, The Journal of Physical Chemistry A, 110, 11053-11063, 2006.

Zhang, X., Cappa, C. D., Jathar, S. H., McVay, R. C., Ensberg, J. J., Kleeman, M. J., and Seinfeld, J. H.: Influence of vapor wall loss in laboratory chambers on yields of secondary organic aerosol, Proceedings of the National Academy of Sciences, 111, 5802, 10.1073/pnas.1404727111, 2014.

Zhang, X., Schwantes, R., McVay, R., Hakulinen, H., Coggon, M., Flagan, R., and Seinfeld, J.: Vapor wall deposition in Teflon chambers, Atmospheric Chemistry and Physics, 15, 4197-4214, 10.5194/acp-15-4197-2015, 2015.
Ziemann, P.: Effects of molecular structure on the chemistry of aerosol formation from the OH-radical-initiated oxidation of alkanes and alkenes, International Reviews in Physical Chemistry, 30, 161-195, 2011.

[BLANK PAGE]

1300

Chapter 3

3. Methods

3.1. Manchester Aerosol Chamber

Investigating the SOA formation via laboratory experiment under controlled conditions is essential because the ambient SOA is overly complex for the sources, physicochemical properties, and aging processes to be readily understood. As a result, the atmospheric science community has extensively employed environmental simulation chambers (otherwise known as aerosol, or smog, chamber) to explore the insights related to the oxidation of VOCs since the 1960s (Carter et al., 2005; Wang et al., 2014; Babar et al., 2016). Such environmental simulation chambers were designed to isolate and elucidate the various processes that occurred in the real atmosphere (e.g., gas-phase reaction, chemical pathways of SOA formation, new particle formation, and transformation of real-world emissions) by developing a standardised system under controlled environmental conditions (Barnes and Rudzinski, 2006).

In this thesis, all experiments were conducted at the Manchester Aerosol Chamber (MAC), an indoor simulation chamber located at the University of Manchester. The MAC was established in 2005, to investigate the various sources of aerosols, such as engine, real-plant emissions, and synthetic VOCs (biogenic and anthropogenic). Briefly, the MAC operated as a batch reactor and was composed of an 18 m^3 FEP Teflon bag mounted on three rectangular aluminum frames. Moreover, the Teflon bag could freely expand and collapse since the central aluminum was fixed while the top and bottom aluminum could move vertically.

Gaseous precursors (e.g VOC precursors, and NO_x) and/or seed particles were injected into the Teflon bag to generate an oxidation reaction, while the relative humidity and temperature were controlled during the experiment. On the other hand, as the light sources for indoor photochemistry experiment, a bank of halogen lights (Solux 50W/4700K, Solux MR16, USA) were used along with the two 6 kW Xenon lamps (XBO 6000 W/HSLA OFR, Osram) mounted inside the enclosure of the chamber. In addition, a set of cooling systems, specifically an air conditioning (AC) unit and a water tank in front of each arc lamp with a circulating water system, were utilised during the photochemistry experiment to remove the unwanted heat from the light source. It should be noted

that the operation procedure of the MAC (fill/flush cycles, injection procedure, humidification, VOC bulb heating, and ozonizer operation) and the sensors (Edgetech and Sensirion sensors) for measuring temperature and relative humidity of the chamber were controlled from a PC and home-built PLC board.

Furthermore, the MAC made significant contributions in this thesis, since multiple online and offline instruments could be coupled with the MAC for measuring the gas and particulate products obtained through chamber experiments. This approach sought to explore the chemical and physical properties of aerosols, but the MAC was not fully characterised (e.g., mixing/wall effect) since previous studies did not require the quantification of aerosol amount. Moreover, a recent study by the MAC mainly evaluated the SOA formation from mixed volatile precursors (Voliotis et al., 2021; Wang et al., 2021), suggesting that the MAC must be fully characterised to ensure the reliability of the research like in Paper 1 (Chapter 5.1).

Equally important, examining the SOA formation from the mixture of VOC systems is necessary to establish a series of suitable chamber experiments (the MAC), and select typical metrics (e.g., SOA yield). This is used to quantify the SOA formation in order to understand the change of SOA formation in the mixture of VOC systems, as shown in Paper 2 (Chapter 5.2). Meanwhile, the MAC is coupled with several online and offline mass spectrometers to measure the chemical properties and seek chemical insights regarding the change in the SOA formation in the mixture of the VOC systems, as found in Papers 3 and 4 (Chapters 5.3. and 5.4). These online and offline instruments are described in Chapter 3.2.

3.2. Measurement Instrumentation

Comprehensive characterisation of the mixtures of VOC oxidation and SOA formation required techniques to measure both gas and particulate products. This section describes and details how these three methods contribute to SOA composition characterisation, including online Gas Chromatography-Mass Spectrometer (GC-MS) and High Resolution Aerosol Mass Spectrometer (HR-ToF-AMS), a Filter Inlet for Gas and Aerosols Iodine High-Resolution Time-of-Flight Chemical Ionisation Mass Spectrometer (FIGAERO-ToF-CIMS), and offline liquid chromatography ultra-high resolution mass spectrometry (UPLC-orbitrap-MS). A number of other

instruments were used to more fully describe the physical and chemical evolution in the experiments. These are not the primary focus of the thesis and are listed and described where appropriate in the first and second papers (5.1 and 5.2)

3.2.1. Gas Chromatography-Mass Spectrometer (GC-MS)

The Gas Chromatography-Mass Spectrometer was an instrument assembled by the University of York. It features the major components flow control box, thermal desorption unit, gas chromatograph (GC) (6850 Agilent), and mass spectrometer (MS) (5975C Agilent). Also, the GC-MS was designed for use in aircraft to measure the tropospheric volatile organic compound. This GC-MS instrument was coupled to MAC and used to measure gas-phase components during experiment, due to its short timescale for measurement and the ability to separate and identify a mix of species into the constituents of gas products.

The flow control box was built in-house and connected to a pump that drew gas samples from the MAC. Its function manipulated the gas samples and prepared them for subsequent GCMS analysis. The gas sample must be dried before it enters the thermal desorption unit because the water vapor within the GC column might interact with the column itself. Then, the analytes interacted with the stationary phase, causing distorted peak shapes. Moreover, the water could damage the mass spectrometer, shortening the lifetime of the ion sources. There was a built-in cold-finger device that chilled the gas stream down to -30 ℃ to remove the water vapor from the gas sample. The cold-finger device took about an hour to cool down to -30 ℃ before gas sampling since the set-up had an initial temperature that was the same as the laboratory's room temperature during the MAC research program. The air sample passed through the cold-finger devices and entered the thermal desorption unit (Markes TT24/7, UK), which used two glass traps with sorbents (Tenax TA) and had a consistently low temperature(Minaeian, 2017).

The traps preconcentrated and stored the volatile organic compounds when the gas sample passed through, followed by a flash heated. In turn, the VOCs desorbed with a flow of helium gas (chromatography grade, < 0.0001 % impurity) and then passed through the GC column through a capillary transfer line. It is worth mentioning that the thermal desorption unit contained two alternating traps to allow continuous and constant sampling (Minaeian, 2017). For instance, one

trap was collecting a sample on the absorbent, while the other was desorbing the previous sample to the GC column. The flow rate of sample collection was set at 100 ml/min, and the sampling time was set at 10 mins for each trap. Figure 3.1 illustrates a flow diagram of the thermal desorption unit.

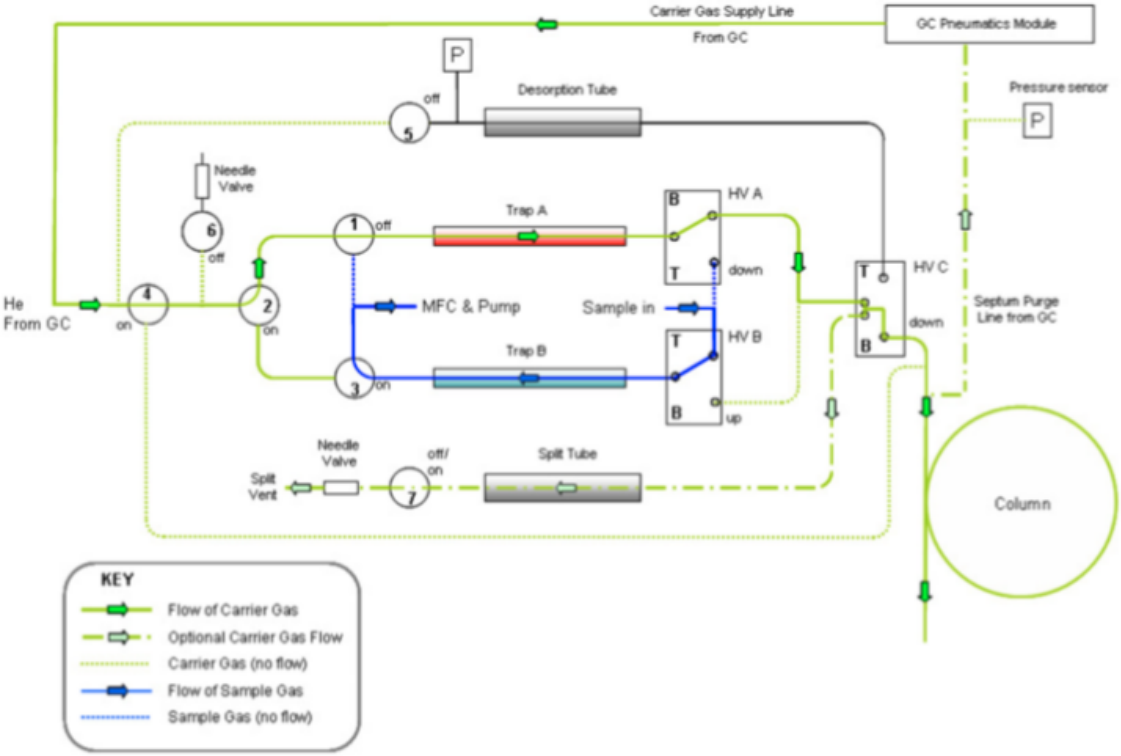

Figure 3.1. Flow diagram of the thermal desorption unit (Minaeian, 2017)

After the VOCs were desorbed from the thermal desorption unit, the gas sample was transferred to the GC column, followed by the temperature program of 40°C to 180°C with a ramp rate of 40°C/min. The GC column was internally coated with a stationary phase, and the mixed gas compounds went through the column by using the carrier gas (mobile phase). On top of that, the mixed gas compounds had different partitions with the stationary phase and mobile phase, while various compounds had distinct interactions with the stationary phase. Thus, each compound in the mixed constituents will elute at different times, also known as retention time, from the column. The differences in the retention times acted as a metric to distinguish the compounds accordingly, but some were difficult because they might have the same retention time that required the assistance of mass spectrometry.

The compounds entered the mass spectrometric detection after passing through the GC column. The ion source in the mass spectrometer used 70eV electron impact ionisation to ionize the analytes, and the ions passed through a quadrupole, which was employed to select ions based on their m/z ratios. Subsequently, the ionised ions entered the detector with a mass range set to 44 amu to 250 amu so that large organic species could be quantified as well. Also, the temperature of the transfer line between the GC and the ion source was maintained at 250℃. The mass analyser was set to 200℃ to reduce the water vapor inside the mass spectrometer, leading to better ion transmission (Minaeian, 2017).

During the MAC research program, the GCMS routinely operated a calibration procedure, comprising of running the "blank" procedure and the "standard" procedure. The GCMS was not connected to any source during the "blank" procedure, so the analysis of the air stream that flushed the trap followed the same GC method as the one mentioned above to determine the contamination on the trap and clean it. Each trap had to run the "blank" procedure twice to ensure that the traps were clean enough to proceed with further sample analysis. As soon as the traps were ensured to have insignificant contamination, we ran the "standard" procedure to connect the GCMS to the standard gas cylinder. More specifically, the standard gas cylinder was made using helium gas as the carrier gas, containing 5ppb of Isoprene, Toluene, α-pinene, limonene, and 1,3,5-trimethylbenzene, respectively, in nitrogen. Knowing the concentration and corresponding peak area of the standard gas compound could be utilised to quantify the same organic compound we used in the MAC experiment (e.g., α-pinene and isoprene).

Data processing was executed using the ChemStation software (Agilent Version 15.5) to processed the raw mass spectra, including the baseline correction, which manually integrated the peak area and identified the peak with regards to the ion's fragmentation spectra.

3.2.2. High-Resolution Aerosol Mass Spectrometer (HR-ToF-AMS)

The aerosol mass spectrometer (AMS) consists of three main components: an aerosol inlet, a particle sizing chamber, and a particle composition detection unit. Each part is separated by a small aperture and is differentially pumped. There is an inlet for particle sampling, which is connected

to the Manchester aerosol chamber for the experiments in this thesis. The particulate products from the chamber experiment continuously passed through an orifice into an aerodynamic lens and focused into a narrow beam (~1mm diameter) on entering the high vacuum region (Zhang et al., 2002).

The particles will accelerate through the particle's time of flight over a known flight path, where the velocity is inversely related to the particle's aerodynamic diameter. As shown in Figure 3.2 the particle beam then experiences flash vaporization on the heated oven, with the subsequent electron impact ionisation resulting in ion formation. In the high-resolution aerosol mass spectrometer, these ions pass into a time-of-flight mass spectrometer to determine the chemical composition. The AMS has two operating modes. First, the particle beam is blocked and unblocked alternatively to produce a comprehensive mass spectrum. Second, the particle beam is modulated via a spinning chopper wheel that produces a pulse of particles, generating size-resolved mass spectra since the particle velocity depends on their size (Sun et al., 2008).

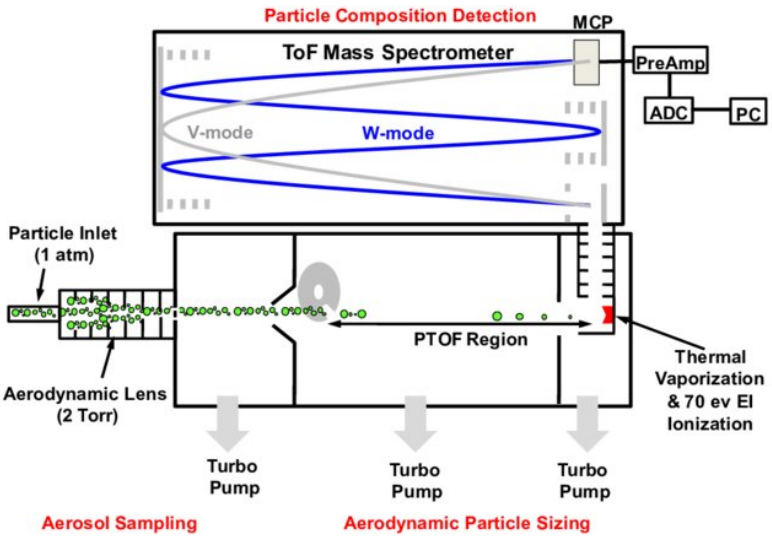

Figure 3.2. The basic components of an aerosol mass spectrometer (Sun et al., 2008)

Data processing was carried out using the ToF-AMS Analysis Software (Pika Version 1.22), written in the Igor Pro software (Wavemetrics, Lake Oswego, OR, USA). This package contains built-in procedures for the processing of raw mass spectra from .hdf files and includes two tools for data processing, specifically SQUIRREL (SeQUential Igor data RetRiEvaL) and PIKA (Peak Integration by Key Analysis), respectively (D. Sueper and collaborators, 2021). SQUIRREL is a

data management tool that eliminates the imposed limits by having to load all the data into memory so that the data can be selectively accessed, accelerating the data processing time. The PIKA tool is used for the speciation and quantification of HR-ToF-AMS mass spectra to identify the chemical components (specific ions), enhance source apportionments, and describe organic composition in terms of molecular O:C and H:C ratios within aerosols. In this thesis, both tools were applied to the HR-ToF-AMS data.

3.2.3. Liquid Chromatography Ultra-High Resolution Mass Spectrometry

Ultrahigh-performance liquid chromatography coupled with ultra-high resolution mass spectrometer (Dionex 3000-Q Exactive Orbitrap, UPLC-MS, ThermoFisher Scientific) were utilised to analyse the particulate products collected from chamber experiments. This instrument was supported by the University of York.

The principle of UPLC involves a stationary phase (e.g., solid or liquid on solid) and a mobile phase (e.g., liquid or gas). The latter phase could transport the components of the mixtures passing through the former. The components that have a stronger affinity with the stationary phase would slowly move through the column compared to the components that have weaker interaction with the stationary phase (Pitt, 2009). After separating the components of the mixtures, a heated electrospray ionisation was applied to generate the gas-phase ions. This approach can produce multiply charged ions from large molecules by applying a strong electric field into a liquid pass through a capillary tube.

The electric field was obtained between the capillary and the electrode with a potential difference of 3-6 kV that induced a charge accumulation at the liquid surface, specifically at the end of the capillary results, in forming highly charged droplets. These droplets shrank and increased the charge per unit volume since the solvent in the droplets evaporated. Moreover, the droplets deformation occurred under the strong electric field, leading to the formation of small, highly charged droplets. The solvent in these small droplets continuously evaporated until the desorption of ions from the surface took place, after flowing to the mass analyser.

The mass analyser helps separate the gas phase ions according to their mass-to-charge ratios (m/z), a physical property of ions. In this case, a new type of mass analyser (the orbitrap) was coupled with UPLC to analyse the particulate compounds. The orbitrap is comprised of electrostatic ion traps that acquire the mass spectra through the Fourier transform. Makarov (2000) first proposed and described this new concept of the mass analyser. Figure 3.3 presents the face view of the orbitrap trap in relation to Makarov's description. In this paper, the ions were tangentially injected through a hole in the external electrode and turned around the central electrode while oscillating in the traps along the z-axis when some kiloelectronvolts of direct current voltage were applied. Then, the oscillating ions induced the broadband current, which was then measured. Using the Fourier transform formula, the broadband currents were converted into individual frequencies and intensities that generated the mass spectrum.

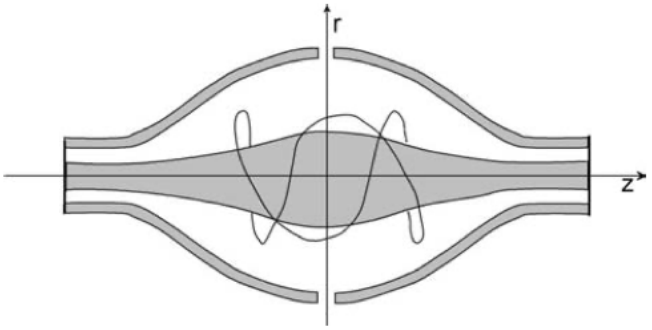

Figure 3.3. The face view of the Orbitrap component. The external part shaped like a barrel is comprised of an electrode and the internal spindle-shaped components (Makarov, 2000).

The chromatographic separation that offers the chemical specificity and Fourier transform mass spectrometers (Orbitrap) are capable of providing the molecular composition of highly complex matrices. These results produce highly significant and complex data. Scientists usually employ target approaches to reduce data complexity and increase throughput, but it provides limited compositional information (Hoffmann, 2007). Thus, this thesis applied Pereira et al. (2021) new automated methodology for non-targeted compositional analysis into the UPLC-Orbitrap-MS data. For the data processing program, the users had to decide which data files were classified as "blanks" and "samples." The "blanks" included the solvent/instrument blank data and filter blank data (the procedural blank). The artifacts detected from "blanks" were removed by the sample data if the sample compounds obeyed the following conditions: (a) same detected molecular species, (b) m/z

ratio within 2 ppm mass accuracy, (c) retention time within ±0.1 minutes, and (d) sample/artifact peak area ratio > 3.

Any compounds excluded from the data set were assigned a molecular formula, if the oxygen-to-carbon (O/C) ratio was 0.05 to 2 and the hydrogen-to-carbon (H/C) ratio was 0.5 to 3. The output for particulate matters was encoded into an Excel-readable format, including the molecular composition of detected compounds in each sample, and grouped by their elemental composition (CHO, CHON, CHONS, and CHOS) and the number of carbon atoms in each molecular formula (C_2-C_3, C_4-C_5, C_6-C_8, C_9 -C_{10}, C_{11}-C_{15}, C_{16} -C_{20} and >C_{21}). Moreover, the peak area and normalized peak area of individual compounds (normalized peak area = peak area of compound/peak area of total sample) in each sample were displayed in the output file.

3.2.4. Filter Inlet for Gas and Aerosols Iodine High-Resolution Time-of-Flight Chemical Ionisation Mass Spectrometer (FIGAERO-ToF-CIMS)

The Filter Inlet for Gas and Aerosols (FIGAERO, Aerodyne Research Inc.) (Lopez-Hilfiker et al., 2014) along with an iodine high-resolution Time-of-Flight Chemical Ionization Mass Spectrometer (Lee et al., 2014) was employed to characterize the gas and particle composition. The FIGAERO method collects particles onto a TEFLON filter that is followed by desorption with heated nitrogen into the mass spectrometer, while sampling the gas phase components. The FIGAERO can be programmed as a cyclic mode between the gas sampling, the aerosol collection, and the thermal desorption of the collected aerosol with temperatures ranging up to 200°C. The instrument has to be flushed with ultrahigh purified N_2 regularly in order to remove the potential contamination during the gas phase sampling, with an established gas-phase instrument background.

Chemical Ionization (CI) includes proton transfer, proton abstraction, and adduct formation. In this instrument, Chemical Ionization was applied to produce the ions from gas phase analytes through adducts formation, subsequent to being detected in the mass spectrometer and yielding mass spectrum. CI is a 'soft ionization' technique requiring a reagent gas to ionize the sample molecules with relatively little energy, yielding less fragmentation in mass spectrum, resulting in less structural information (Hoffmann, 2007). This instrument was run with I^- reagent ion in

negative-ion mode, which was sensitive to inorganic species, oxygenated VOCs, and Highly Oxygenated Organic Molecules (HOMs). Besides, the I^- reagent ions were generated from the gaseous CH_3I flowing through the ultra-highly purified N_2 over a ^{210}Po radioactive source. It was a challenge to quantify both gas and the particles phase components from FIGAERO-CIMS due to lack of available standards and being time consuming for calibration, despite there being several studies attempting to constrain those limitations (Lopez-Hilfiker et al., 2016, Aljawhary et al., 2013). Hence, it was presumed that the instrumental sensitivity to an entire range of detected products was uniform.

The data processing was done using the Tofware software package (versions 2.5.7 - version 3.2.0, TOFWERK AG/Aerodyne/University of Colorado), written in Igor Pro software (Wavemetrics, Lake Oswego, OR, USA) (Stark et al., 2015). A series of operation on the raw mass spectra were carried out prior to the peak identification, including time averaging, m/Q calibration, baseline determination with the determination of the peak shape, and mass resolution functions. A detailed description of the FIGAERO-CIMS used in this thesis and its explicit configuration can be found in Voliotis et al., (2021) and Du et al., (2021).

3.3. Overview of Experimental Procedure

This thesis comprises two sections that characterise a novel Manchester aerosol chamber (MAC) and understand the formation of secondary organic aerosols (SOA) from mixed biogenic and anthropogenic origins. These sections initially required a laboratory approach to provide a detailed characterization of the MAC, followed by conducting SOA formation experiments using synthetic biogenic and anthropogenic mixture components in MAC to evaluate a complex ambient mixture.

The first part of this thesis focuses on the MAC, including temperature, relative humidity, photolysis rate of NO_2 (photochemistry experiments), the wall loss rate of gaseous compounds and particles, auxiliary mechanism, and aerosol formation. This work component further investigated the potential influences of chamber contamination on the wall loss rates of gaseous compounds/particles and discussed various wall-loss correction methods of the particles, which are detailed in Chapter 5.1.

Meanwhile, the second part of this thesis concentrates on SOA from mixed BVOC and AVOC oxidation in laboratory work employing the MAC. This work component was performed after MAC characterization and involved three sections. It included designing a suitable experimental procedure for investigating and quantifying SOA formation in a VOC mixture using the reported measured and predicted SOA mass yield, as presented in Chapter 5.2. Moreover, the SOA formed from sole and mixed VOC oxidation were characterised using ultra-high resolution mass spectrometry (LC-Orbitrap MS) and employing a novel non-targeted accurate mass analysis (Pereira et al., 2021). It evaluated the chemical properties of SOA changed in mixed systems, leading to exploring the interactions in mixtures of VOC involved in ambient SOA formation, as discussed in Chapter 5.3. At last, we expand study from the previous study in chapter 5.3 by providing the real-time atomic ratios and estimated carbon oxidation state of particulate matters from all the VOCs precursor systems, detailed discussed in Chapter 5.4.

The experimental work in the second part was an extended work performed by Mcfiggans et al. (2019), which investigated the SOA formation from isoprene and α-pinene mixture precursors in the regime dominated by OH oxidation. The said study concluded that the isoprene acted as an OH scavenger, while its radical oxidation products reacted with those formed from α-pinene, thus enhancing the overall volatility of the products in the mixture. Comparably, this thesis retained the two biogenic precursors — isoprene and alpha-pinene — with a significant contribution to VOC emitted from plants globally, despite isoprene having a modest SOA formation potential and α-pinene being a more efficient SOA precursor (Hallquist et al., 2009; Mcvay et al., 2016; Dommen et al., 2006).

This thesis also added a new anthropogenic precursor (*o*-cresol) into mixture precursor systems, which had a moderate SOA yield, with a comparable reactivity towards the hydroxyl radical (OH) and a negligible reactivity towards ozone. Furthermore, it applied a concept called "initial iso-reactivity" towards the dominant oxidant (OH) to determine the precursors' initial concentration and enable a direct comparison across systems. Figure 3.4 illustrates the designed concept of VOC mixture systems. Seven experimental systems were investigated: three single precursor systems (a, b, c), three systems comprising two different VOC mixtures (a & b, b & c, a & c) and a system

mixing the three VOCs (a & b & c). These experiments were conducted in the MAC in the presence of NOx (VOC/NOx ratio: ~3–8) and seed particles (ammonium sulphate).

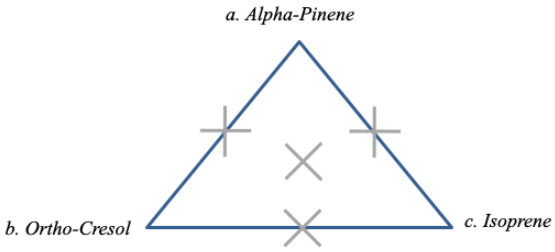

Figure 3.4. A schematic diagram of the VOC mixture systems.

This thesis was performed in collaboration with the University of York, focusing on characterising SOA composition from each particular precursor system and using these to explore the mechanism of interactions in a mixture of VOCs involved in ambient SOA formation.

References:

Aljawhary, D., Lee, A. K. Y., and Abbatt, J. P. D.: High-resolutionchemical ionization mass spectrometry (ToF-CIMS): applicationto study SOA composition and processing, Atmos. Meas. Tech.,6, 3211–3224, https://doi.org/10.5194/amt-6-3211-2013, 2013.

Barnes, I. and Rudzinski, K. J.: Environmental simulation chambers: Application to atmospheric chemical processes, Springer Science & Business Media,2006.

Babar, Z. B., Park, J.-H., Kang, J., and Lim, H.-J.: Characterization of a smog chamber for studying formation and physicochemical properties of secondary organic aerosol, Aerosol and Air Quality Research, 16, 3102-3113, 2016.

Carter, W. P., Cocker III, D. R., Fitz, D. R., Malkina, I. L., Bumiller, K., Sauer, C. G., Pisano, J. T., Bufalino, C., and Song, C.: A new environmental chamber for evaluation of gas-phase chemical mechanisms and secondary aerosol formation, Atmospheric Environment, 39, 7768-7788, 2005.

D. Sueper and collaborators, ToF-AMS Data Analysis Software Webpage, http://cires1.colorado.edu/jimenez-group/wiki/index.php/ToF-AMS_Analysis_Software"

Du, M., Voliotis, A., Shao, Y., Wang, Y., Bannan, T. J., Pereira, K. L., Hamilton, J. F., Percival, C. J., Alfarra, M. R., and McFiggans, G.: Combined application of Online FIGAERO-CIMS and Offline LC-Orbitrap MS to Characterize the Chemical Composition of SOA in Smog Chamber Studies, Atmos. Meas. Tech. Discuss., 2021, 1-42, 10.5194/amt-2021-420, 2021.

Dommen, J., Metzger, A., Duplissy, J., Kalberer, M., Alfarra, M., Gascho, A., Weingartner, E., Prevot, A., Verheggen, B., and Baltensperger, U.: Laboratory observation of oligomers in the aerosol from isoprene/NOx photooxidation, Geophysical Research Letters, 33, 2006.

Hallquist, M., Wenger, J., Baltensperger, U., Rudich, Y., Simpson, D., Claeys, M., Dommen, J., Donahue, N., George, C., and Goldstein, A.: The formation, properties and impact of secondary

organic aerosol: current and emerging issues, Atmospheric chemistry and physics, 9, 5155-5236, 2009.
Hoffmann, E. d. S. V.: Mass spectrometry : principles and applications, J. Wiley, Chichester, West Sussex, England; Hoboken, NJ2007.
Makarov, A.: Electrostatic Axially Harmonic Orbital Trapping: A High-Performance Technique of Mass Analysis, Analytical Chemistry, 72, 1156-1162, 10.1021/ac991131p, 2000.
McFiggans, G., Mentel, T. F., Wildt, J., Pullinen, I., Kang, S., Kleist, E., Schmitt, S., Springer, M., Tillmann, R., and Wu, C.: Secondary organic aerosol reduced by mixture of atmospheric vapours, Nature, 565, 587, 2019.
McVay, R. C., Zhang, X., Aumont, B., Valorso, R., Camredon, M., La, Y. S., Wennberg, P. O., and Seinfeld, J. H.: SOA formation from the photooxidation of α-pinene: systematic exploration of the simulation of chamber data, Atmos. Chem. Phys., 16, 2785-2802, 10.5194/acp-16-2785-2016, 2016.
Minaeian, J. K.: Development and Deployment of an Airborne Gas Chromatography/Mass Spectrometer to Measure Tropospheric Volatile Organic Compounds, PhD, University of York, 2017.
Pereira, K. L., Ward, M. W., Wilkinson, J. L., Sallach, J. B., Bryant, D. J., Dixon, W. J., Hamilton, J. F., and Lewis, A. C.: An Automated Methodology for Non-targeted Compositional Analysis of Small Molecules in High Complexity Environmental Matrices Using Coupled Ultra Performance Liquid Chromatography Orbitrap Mass Spectrometry, Environmental Science & Technology, 55, 7365-7375, 10.1021/acs.est.0c08208, 2021.
Pitt, J. J.: Principles and applications of liquid chromatography-mass spectrometry in clinical biochemistry, Clin Biochem Rev, 30, 19-34, 2009.
Sun, Y., Zhang, Q., MacDonald, A., K, H., Li, S., Liggio, J., Liu, P., Anlauf, K., Leaitch, W., M, C., D, W., Donkelaar, A., and Martin, R.: Size-resolved aerosol chemistry on Whistler Mountain, Canada with a High-Resolution Aerosol Mass Spectrometer during INTEX-B, Atmospheric Chemistry and Physics Discussions, 8, 10.5194/acpd-8-20749-2008, 2008.
Voliotis, A., Wang, Y., Shao, Y., Du, M., Bannan, T. J., Percival, C. J., Pandis, S. N., Alfarra, M. R., and McFiggans, G.: Exploring the composition and volatility of secondary organic aerosols in mixed anthropogenic and biogenic precursor systems, Atmos. Chem. Phys. Discuss., 2021, 1-39, 10.5194/acp-2021-215, 2021.
Wang, X., Liu, T., Bernard, F., Ding, X., Wen, S., Zhang, Y., Zhang, Z., He, Q., Lü, S., and Chen, J.: Design and characterization of a smog chamber for studying gas-phase chemical mechanisms and aerosol formation, Atmospheric Measurement Techniques, 7, 301, 2014.
Wang, Y., Voliotis, A., Shao, Y., Zong, T., Meng, X., Du, M., Hu, D., Chen, Y., Wu, Z., Alfarra, M. R., and McFiggans, G.: Phase state of secondary organic aerosol in chamber photo-oxidation of mixed precursors, Atmos. Chem. Phys., 21, 11303-11316, 10.5194/acp-21-11303-2021, 2021.
Worsnop, D., JT.Jayne, Canagaratna, M., H.Boudries, CE.Kolb, J.Jimenez, and P.Silva: Field applications of an aerosol mass spectrometer: What are we learning about aerosol chemical and microphysical properties?, ACS National Meeting Book of Abstracts 224, u350-u351, 2002.
Zhang, X., Smith, K. A., Worsnop, D. R., Jimenez, J., Jayne, J. T., and Kolb, C. E.: A Numerical Characterization of Particle Beam Collimation by an Aerodynamic Lens-Nozzle System: Part I. An Individual Lens or Nozzle, Aerosol Science and Technology, 36, 617-631, 10.1080/02786820252883856, 2002.

[BLANK PAGE]

Chapter 4

4. Aims

The aims of this thesis include the following:

1. to provide a comprehensive description and characterization of the MAC including identification of key capabilities and limitations;
2. to investigate SOA formation from mixtures of VOCs (e.g., choices of precursors, concentration, and experimental conditions) using a suitable experimental design in the MAC;
3. to understand the potential of molecular interaction of the SOA formation and composition from mixtures of biogenic and anthropogenic VOCs;
4. to explore the chemistry and detailed mechanism of interactions in a mixture of VOCs by characterising the variability of particulate products, the elemental composition, and the contribution of "unique compounds" in a mixed system resulting in potential atmospheric significance.
5. To assess the ability of the available tools to investigate the SOA particle average carbon oxidation state changes in complex precursor mixtures.

[BLANK PAGE]

Chapter 5

5. Results

1765

Paper 1: Characterisation of the Manchester Aerosol Chamber facility

This paper has been accepted in the journal of "Atmopsheric Measurement Techniques" with DOI: 10.5194/amt-2021-147

Yunqi Shao[1*], Yu Wang[1*], Mao Du[1*], Aristeidis Voliotis[1*], M. Rami Alfarra[1,2,‡] , Simon P. O'Meara[1,2], S. Fiona Turner[1,†] and Gordon McFiggans[1]

[1] Centre for Atmospheric Science, Department of Earth and Environmental Sciences, School of Natural Sciences, University of Manchester, Manchester, M13 9PL, United Kingdom
[2] National Centre for Atmospheric Science (NCAS), University of Manchester, Manchester, M13 9PL, United Kingdom

[‡] Now at Environment & Sustainability Center, Qatar Environment & Energy Research Institute, 34110, Doha, Qatar
[†] Now at AMETEK Land, Dronfield, Derbyshire, S18 1DJ, United Kingdom
*These authors all made equal contributions to this work.

Correspondence to: G. McFiggans (g.mcfiggans@manchester.ac.uk)

Abstract.

This study describes the design of the Manchester Aerosol Chamber (MAC), initially developed in 2005, and presents for the first-time its comprehensive characterisation. The MAC is designed to investigate multi-phase chemistry and the evolution of aerosol physico-chemical properties from the real-world emissions (e.g. diesel engine, plants) or of secondary organic aerosol (SOA) produced from pure volatile organic compounds (VOCs). Additionally, the generated aerosol particles in MAC can be transferred to the Manchester Ice Cloud Chamber (MICC), which enables investigation of cloud formation in warm, mixed-phase and fully glaciated conditions (with T as low as -55 °C). MAC is an 18 m^3 FEP Teflon chamber, with the potential to conduct experiments at controlled temperature (15-35 °C) and relative humidity (25-80 %) under simulated solar radiation or dark conditions. Detailed characterisations were conducted at common experimental conditions (25 °C, 50% RH) for actinometry and determination of background contamination, wall losses of gases (NO_2, O_3, and selected VOCs), aerosol particles at different sizes, chamber wall reactivity and aerosol formation. In addition, the influences of chamber contamination on the wall loss rate of gases and particles, and the photolysis of NO_2 were estimated.

1 Introduction

Atmospheric aerosols have significant effects on air quality, regional to global climate, and human health (Lohmann and Feichter, 2005; Pope et al., 2002; Katsouyanni et al., 1997). Aerosol particles range from a few nanometers to several tens of micrometers in diameter. Their composition is complex, comprising inorganic and organic compounds, dependent on their sources which may be either primary (e.g. sea salt, dust, wildfires) or secondary, from the oxidation of gaseous precursors

(Seinfeld and Pandis, 2016). Organic compounds contribute 20~90% of the mass of submicron aerosols in the Northern hemisphere (Jimenez et al., 2009; Zhang et al., 2007), and of an estimated 10000~100000 atmospheric organic compounds(Goldstein and Galbally, 2007) , only around 10% have been identified, such as alkanes, carbonyls, alcohols, easters, acids and etc (Hallquist et al., 2009; Goldstein and Galbally, 2007). Owing to this complexity, their chemical reaction pathways and properties lead to substantial outstanding challenges to the understanding of organic aerosol (OA) formation, transformation, fate and impacts (Hallquist et al., 2009). Such an inadequate understanding of aerosol particles, and particularly the organic fraction, leads to large uncertainties in understanding their role in air quality and global climate (Mcfiggans et al., 2006). Processes relating to organic-containing particles have consequently been a primary focus of studies in our chamber.

Over the last several decades, numerous field measurements have been conducted globally to characterise OA in the atmosphere (Gray et al., 1986; Hoffman and Duce, 1977; Turpin and Huntzicker, 1991; Turpin and Huntzicker, 1995; Hallquist et al., 2009; Jimenez et al., 2009; Zhang et al., 2007). However, isolation of chemical and microphysical processes from meteorology and other atmospheric processes can be challenging in ambient measurements (Becker, 2006). To better understand the sources, physicochemical properties and aging processes influencing atmospheric aerosols, simulation chamber facilities have been developed across the globe since the 1960s (Karl et al., 2004; Cocker et al., 2001b; Carter et al., 2005; Paulsen et al., 2005; Saathoff et al., 2009; Wang et al., 2011; Platt et al., 2013; Schnitzhofer et al., 2014; Wang et al., 2014; Leskinen et al., 2015; Babar et al., 2017; Gallimore et al., 2017; Leone et al., 1985). In principle, a simulation chamber is a controlled system to elucidate processes that occur in the real atmosphere (Barnes and Rudzinski, 2006), gas-phase reactions and chemical pathways (Carter and Lurmann, 1991; Seakins, 2010; Atkinson et al., 1992; Paulot et al., 2009; Surratt et al., 2010; Ehn et al., 2012; Bianchi et al., 2019 ,Thornton et al., 2020), SOA production (Hallquist et al., 2009; Carlton et al., 2009; Mcfiggans et al., 2019), new particle formation (Smith, 2016; Wang et al., 2020; Wagner et al., 2017; Dunne et al., 2016), cloud processes (Wang et al., 2011; Frey et al., 2018; Wagner et al., 2006), transformations and properties of real-world emissions (from vehicles; e.g., Liu et al. (2017), biomass burning; e.g., Hennigan et al. (2011), plants; e.g. Hohaus et al. (2016)) and health effect (Tong et al., 2018; Taylor et al., 2000).

The design of simulation chambers varies widely with respect to the light sources, chamber sizes, materials and operation conditions to address varied lines of research (Barnes and Rudzinski, 2006). The size of chamber facilities ranges from ~l to ~300 m^3 and are variously constructed from pyrex/quartz, aluminium, stainless steel and FEP Teflon. The light sources of chambers include artificial and natural solar radiation, leading to a convenient classification into indoor and outdoor chambers (Barnes and Rudzinski, 2006). Pyrex or quartz is widely used for chambers with a volume of less than 1 m^3, with a few larger, such as JPAC (1.45 m^3) (Ehn et al., 2014), Bayreuth chambers (2.4 m^3) (Behnke et al., 1988) and UAREC (>1 m^3) (Barnes et al., 1994). Owing to its reasonably inert nature and transparency towards short-wavelength lights, pyrex and quartz chambers enable ready access to radical generation studies. Also, pyrex and quartz chambers can enable temperature-dependent studies with the use of a cooling or heating bath. Metal chambers are usually built with a volume of 1~6 m^3, with exceptions such as AIDA chamber (85 m^3) (Wagner et al., 2006), MICC (10 m^3) (Connolly et al., 2012) and CERN Cloud chamber (26 m^3) (Schnitzhofer et al., 2014). The largest advantage of the rigid metal chambers is the ability of experiments under varying temperatures, enabling simulation of free tropospheric conditions (Wagner et al., 2006; Schnitzhofer et al., 2014) and warm, mixed phase and fully glaciated clouds. FEP Teflon is widely used in medium to large chambers, such as FORTH-ASC (10 m^3)(Kostenidou et al., 2013), Manchester Aerosol Chamber (MAC) (18 m^3), LEAK-LACIS (19 m^3) (Mutzel et al., 2015; Niedermeier et al., 2020), IASC (27 m^3), Caltech dual chambers (both 28 m^3)(Cocker et al., 2001a), the University of California at Riverside dual chambers (both 90 m^3)(Carter et al., 2005), PSI chamber (27 m^3) (Paulsen et al., 2005), ILMARI (29 m^3) (Leskinen et al., 2015), HELIOS (90 m^3) (Ren et al., 2017), SAPHIR (270 m^3)(Karl et al., 2004) and EUPHORE (2 × 200 m^3) (Bloss et al., 2005; Dunne et al., 2016). The transparency of Teflon enables its widespread use in both indoor and outdoor chambers, enabling transmission across the solar spectrum.

All chambers have limitations. A universal challenge is the presence of chamber walls that can act as a sink of the reacting gases and aerosol particles (Mcmurry and Grosjean, 1985) and as a surface on which they can react. Consequently, experimental results relating to gas-particle partitioning, aerosol formation rate and yield, for example, require careful interpretation (Mcmurry and Grosjean, 1985; Matsunaga and Ziemann , 2010; Zhang et al., 2014; Ye et al., 2016; Wang et al., 2018). Similarly, photochemistry experiments in indoor chambers using artificial lights requires

consideration of the wavelength dependence of the irradiance (Barnes and Rudzinski, 2006). Outdoor chambers, particularly the larger ones, are challenged by control of relative humidity and temperature due to the ambient diurnal variation, which may introduce some uncertainty (Barnes and Rudzinski, 2006). In addition, gases and particles as well as the intermediate reactants can interact with and partition into chamber walls (so-called memory effect), which can affect repeatability and reliability of the results (Carter and Lurmann, 1991; Wang et al., 2011; Wang et al., 2014; Schnitzhofer et al., 2014). This artifact due to the memory effect necessitates a clear and detailed characterisation of chamber behaviour and history.

This manuscript provides a description and characterisation of a novel indoor simulation chamber, Manchester Aerosol Chamber (MAC), located at The University of Manchester. The MAC has been well developed and predominantly used since 2005 to understand the chemical and physical properties of aerosols from different sources (e.g., engine, real-plant emissions, biogenic or anthropogenic VOC). But all these studies have not required the quantification of aerosol amount, therefore the mixing/wall effect had not been characterized at the time of many previous experiments. Recently, in order to understand the SOA formation (e.g., yield) from mixed precursors (e.g., Voliotis et al., 2021; Wang et al., 2021), a full characterization of chamber was implemented to ensure the reliability of the studies. Equipped with state-of-the-science instruments, MAC has been used to explore the aerosol formation and aging (Hamilton et al., 2011; Alfarra et al., 2012), physicochemical properties of multi-component aerosol particles (Alfarra et al., 2013; Wang et al., 2021; Voliotis et al., 2021), gas-particle partitioning (Voliotis et al., 2021), aerosol formation, properties and transformations from plant emissions (Wyche et al., 2014) and from engine emissions (Pereira et al., 2018; Liu et al., 2017). Additionally, the entire contents of the MAC can be transferred directly to the MICC (Manchester Ice Cloud Chamber) to investigate the warm, mixed phase and fully glaciated cloud formation on the aerosol particles that will act as cloud condensation nuclei (CCN) and ice nuclei (IN). A detailed description of the coupling between the facilities and its use can be found in Connolly et al. (2012) and Frey et al. (2018) and will not be discussed here.

2. Description of the MAC

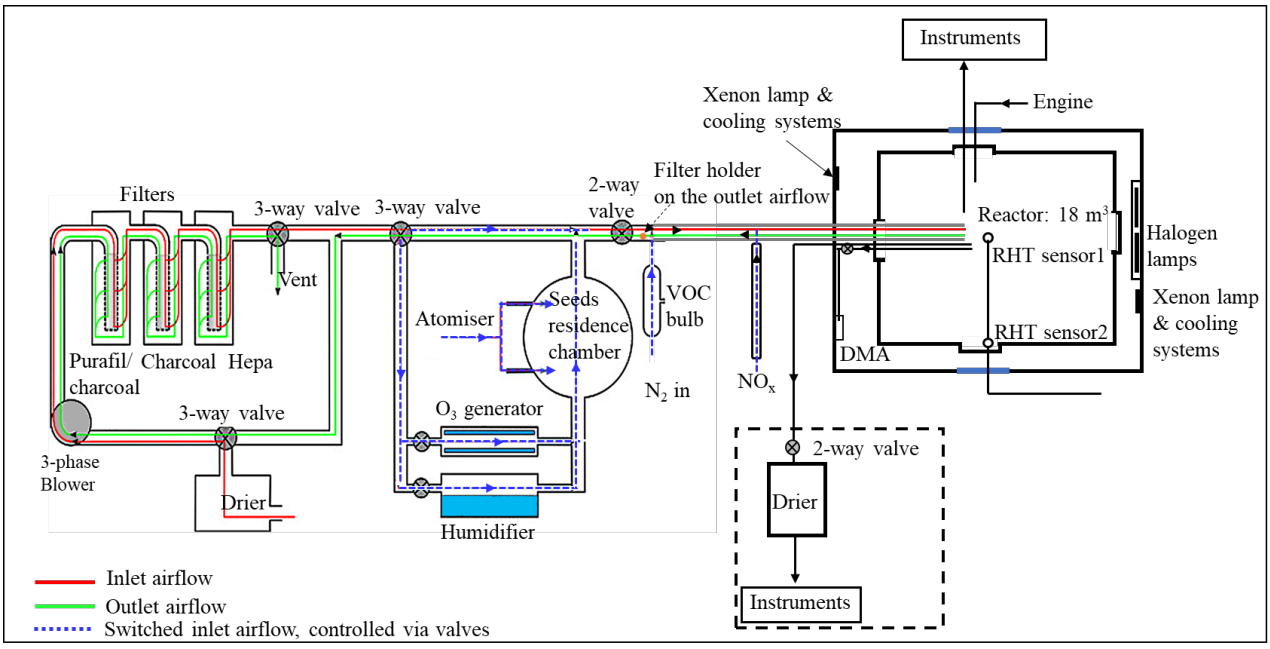

Figure 1:Schematic of the Manchester Aerosol Chamber (MAC).

The MAC is operated as a batch reactor where the composition of the gaseous precursors, pre-existing seed, oxidising environment, relative humidity and temperature are controlled throughout a typical experimental duration of several hours. It is equipped with a variable combination of gas-phase and particle-phase analytical instruments as listed in Table 1. The MAC consists of an 18 m^3 FEP Teflon bag suspended from a frame comprising a central fixed frame member and two moving members, all contained within an RH and temperature-controlled enclosure. Along with the light sources, cooling systems and air purification system, the MAC is shown in the schematic in Figure 1.

2.1 Enclosure and environmental control

The rectangular enclosure comprises an extruded aluminium framework supporting two access sides each with two bi-fold doors and two fixed sides within which the lamp enclosures and air conditioning (AC) ducts are situated. The inner walls and the ceiling of the enclosure and the floor are fully coated with a reflective space blanket to approximate an integrating sphere to maximise the chamber irradiance and provide even light intensity. The temperature and relative humidity

between the chamber and the enclosure walls is controlled by the AC allowing the temperature within the range of 15-35°C and RH between 25% and 80%. The inlet duct is positioned aloft at one end of the chamber and the outlet duct is at the bottom of the other such that conditioned air at 3 m^3s^{-1} continually passes through the 50 cm space between the bag and enclosure, agitating and mixing the air in the bag as it does so. The RH setpoints is chosen to match the dewpoint of the chamber air at the desired temperature. Temperature and dew point is measured at two points in the chamber (at the middle and on the side) using a dew point hygrometer and two thermocouples to choose the setpoint.

2.2 Teflon reactor

The reactor comprises four sections of FEP Teflon film (50μm, AdTech Polymer Engineering Ltd.). FEP Teflon film is chosen since it is chemically inert and more transparent than PVF and PTFE, having better light transmission between 290 and 800nm, and has lower rates of hydrocarbon off-gassing (Finlayson-Pitts and James N. Pitts, 2000). A weakness of the FEP film is the accumulation of electrostatic charge which can significantly increase the wall loss rates for particles with a diameter smaller than 500nm (Mcmurry and Rader, 1985; Charan et al., 2018). The chamber is suspended in the enclosure and joints between three pairs of edges of the Teflon film are made by compression-sealing between the three pairs of rectangular extruded aluminium frames. The edges of the top and bottom Teflon webs are clamped by stainless steel clips installed on the aluminium frames with expanded foam strips relieving between the frame and Teflon to ensure even compression between the Teflon sheets. This approach avoids additional contamination from glue or tapes. The central rigid frame is fixed, with the upper and lower frames free to move vertically. They are counter-weighted to enable the bag to expand and collapse when sample air is introduced and extracted in the process of fill/flush cycles and sampling. This reduces the possibility of the chamber operating under negative pressure, minimising instrumental sampling problems and contamination from laboratory air. In normal practice, around 80% of the chamber air can be extracted from the chamber within ~ 5 min at a flow rate of 3 m^3 min^{-1} in each flush cycle, after that the purified air can be filled into the chamber at the same flowrate. A low background condition is achieved in around 2-hours of continuous automated fill/flush cycles. This relatively rapid cleaning improves the duty cycle and efficiency of the chamber preparation process. The central fixed frame pair supports 3 inlet and sampling manifolds constructed of solid Teflon,

one in each of the two long sides and one in the short side of the bag, as well as mirrors and optical fibre mounting for a 2-pass broadband Differential Optical Absorption Spectroscopy (DOAS) system for retrieval of aerosol optical properties along the long axis of the chamber. One manifold is connected to the air purification system (described in 2.4) for injection of purified air, VOC precursor, NO_x, O_3, seed aerosols and transfer of sample to selected instrumentation in the upper-floor laboratory. A second manifold is used for sampling gas and particulate material from the chamber to online instrumentation next to the chamber throughout each experiment. A second port in this manifold can be used to couple the chamber to emission sources such as engines, plant chambers etc., and has been discussed elsewhere (Wyche et al., 2014; Pereira et al., 2018). The third manifold houses sensors to monitor the RH and T inside the chamber and at the chamber walls.

2.3 Chamber illumination

The irradiation source, consisting of two xenon arc lamps and a bank of halogen bulbs, is mounted inside the enclosure and is used to approximate the atmospheric actinic spectrum. Two 6 kW arc Xenon lamps (XBO 6000 W/HSLA OFR, Osram) are installed on the bottom-left and the top-right of the chamber housing, respectively. Quartz plates with optical polish (PI-KEM Ltd) of 4mm thickness in front of each arc lamp filter out unwanted UV light. The bank of 112 halogen lights, 7 rows of 16 bulbs each (Solux 50W/4700K, Solux MR16, USA), are mounted on the same enclosure wall as the bottom xenon arc lamp, facing the inlet.

The unwanted heat generated from the irradiation source is removed by the cooling system which includes the Air Conditioning (AC) unit and a water tank in front of each arc lamp with circulating water system. The chiller water circulates running through aluminium bars cooling the halogen bulb holders and through tanks in front of each arc lamp faced by the quartz filter plates, in order to dissipating heat produced by absorption of unwanted IR light by water vapour.

2.4 Chamber air purification, conditioning and injection system

Purified dry air is supplied by passing laboratory air at up to 3 m^3 min^{-1} using a 3-phase blower (Nash Elmo; model G200) through a drier (ML180, Munters) and three filters (the first canister containing Purafil/charcoal, the second containing activated charcoal, and the third with a Hepa filter to remove the NO_x, volatile organic compounds and particles). This typically results to

particle concentrations <15 particles cm^{-3}, particle mass concentration ~0μg m^{-3}, O_3 concentrations ~0ppb and NO_x concentration <10ppb (NO <8ppb and NO_2<2ppb).

The clean air can be conditioned by passing through the humidifier, ozoniser and aerosol mixing tank before entering the chamber. The ozoniser (OZV30, Waterth) generates ozone using 2 mercury lamps. The custom-built humidifier comprises a 50L tank fed with ultra-pure water (resistivity ≥18.2 MΩ-cm), producing water vapour using an immersion heater that heats the water to ~80°C. VOCs are added to the chamber by injecting the desired liquid amount into a gently heated glass bulb (to ~80 °C) and transferred using the electron capture device (ECD) grade nitrogen (N4.8; purity 99.998%; N_2) as the carrier gas. NO_x (NO and NO_2) is added to the chamber using custom-made cylinders at 10% v/v and a mass flow controller and transferred with ECD grade N_2 as the carrier gas. Seed particles are generated by an atomiser (Topaz model ATM 230) and pass through a 0.12 m^3 stainless steel aerosol residence chamber before being flushed into the chamber. All components are connected with large bore (50 mm) stainless steel pipes apart from the diversion lines for the seed, humidifier and ozoniser, which have a 25 mm bore. The flow path is controlled by several 2- and 3-way electro-pneumatic valves along the inlet system. As shown in Fig. 1, the purified lab air that is used to fill the chamber can be directed through the humidifier, the ozoniser and aerosol residence chamber and carry any of their components to the chamber while filling at high flow rate (3 m^3 min^{-1}), ensuring rapid mixing (see Section 3.2).

2.5 Control system

To regulate the chamber operational procedures and devices (fill/flush cycles, injection procedure, humidification, VOC bulb heating, ozoniser operation) conveniently, repeatably and precisely, a bespoke automated control system is used. All component switches are controlled from a home-built PLC board, with all control signals processed using ladder logic and communicating with a graphical front end in Visual Basic. All components (including the 2- and 3-way valves) shown in Fig. 1 are controlled by the PLC. Selection of the valve position controls whether clean air is injected into the chamber, or the chamber contents are flushed to exhaust. Cycles of filling and flushing are programmed to enable unsupervised operation during cleaning cycles. The humidifier and ozoniser can be bypassed by controlling the diversion line valves during the fill part of the cycle. Relative humidity and temperature of the chamber were continuously measured via the Edgetech and Sensirion sensors that are also PLC

controlled. All control data are saved automatically. Three pre-programmed operations (pre-experiment, post-experiment and fill/flush cycle) are provided in the control system to enable manual or automated operation. More details about these operational procedures are provided in section 2.7.

2.6 Modes of operation

The MAC generally operates as a batch reactor that provides a closed system without the continuous flow of reactants or dilution flow of clean air. There have been several modes of operation used. The most straightforward mode is the heated bulb injection of commercial pure VOC precursors to investigate SOA formation and transformation either in sole or mixed VOC systems (Hamilton et al., 2011; Jenkin et al., 2012). The MAC has additionally been coupled to whole combustion process and biogenic emission sources. A dynamometer, diesel engine and oxidising catalyst unit can be connected to the chamber directly, allowing controlled exhaust dilutions by controlled injection timing of exhaust fumes into the chamber under selected loads and speeds. For example, (Pereira et al., 2018) reported the effect of different engine conditions and emission control devices on unregulated diesel exhaust gas emissions. The MAC has been coupled with a custom-built plant chamber to investigate the SOA formation from the real plants under controlled conditions. (Wyche et al., 2014) deployed the chamber to investigate SOA formation from biogenic VOC precursors emitted from the silver birch and three South-east Asian tropical plant species. Also, the MAC infrastructure was recently successfully extended to continuously generate NO_3 radicals using synthesised N_2O_5, to enable studies of SOA formation and transformation under night-time conditions.

2.7 Experimental procedures

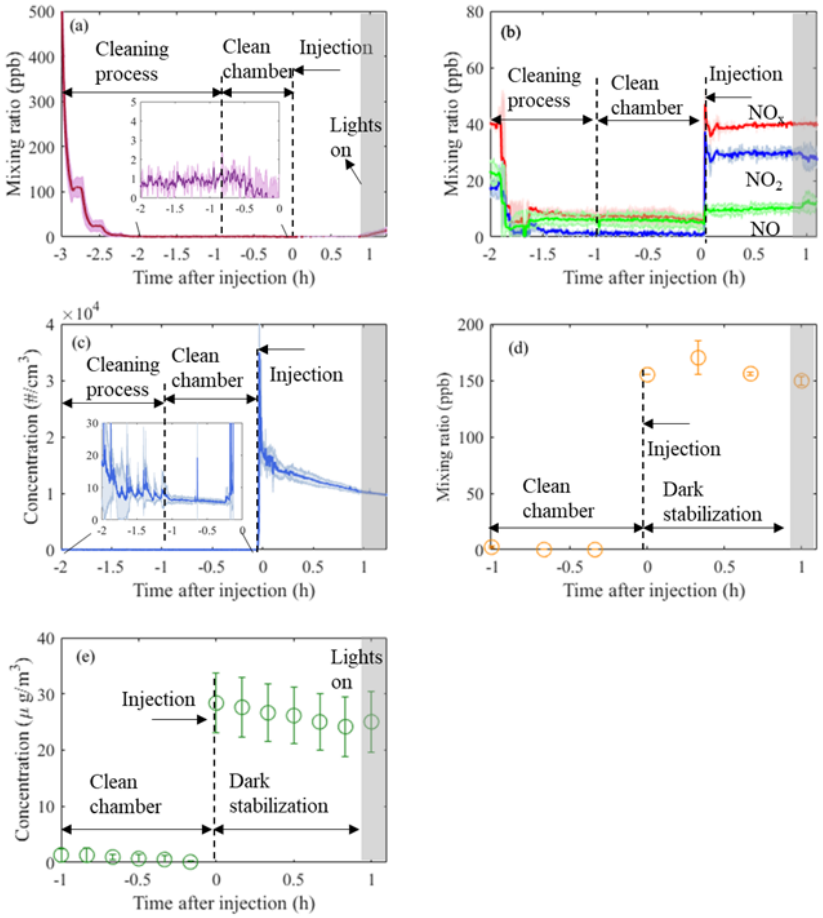

Figure 2: Time series (mean ± 1σ; n=3) of O3 (a), NOx (b), particle number (c), VOC (α-pinene; d) and particle mass (e) from three identical experiments conducted in the MAC. Annotations provide information of the related process occurring in the chamber at each time point, normalised to the injection time of the reactants. Cleaning process duration is ~2h, while subsequently the chamber is left with clean air for about 1h prior the addition of the reactants ("clean chamber"). After the addition of the reactants, the chamber is stabilised in the dark for another hour ("dark stabilization") before the lights are turned on.

To ensure reliable and reproducible control of experimental conditions, three specific experimental procedures have been programmed to be sequenced and implemented automatically or manually to ensure a lower chamber background. The first, designated the pre-experiment procedure, includes several fill/flush cycles of the chamber with clean air at a high flow rate of 3 m^3 min^{-1} for ~1.5 h. The VOC glass bulb is also cleaned in the course of the pre-experiment procedure using ECD grade N_2.

The second, conducted at the end of each experiment, is the post-experiment procedure. Again, this consists of several fill/flush cycles of the chamber with clean air at a high flow rate of 3 m^3 min^{-1} for ~1.5 h, with a subsequently fill with a high concentration of O_3 (~1ppm) to soak the chamber overnight to oxidize the residual O_3-reacting volatile species. The third, a more aggressive

"harsh cleaning" procedure is carried out weekly during experimental campaigns. In this procedure a high concentration of O_3 (~1ppm) is filled into the chamber with illumination, undergoing several hours of photooxidation at high relative humidity (~80%).

These procedures ensure a clean environment is provided in the MAC prior to SOA experiments. Gaseous and particle time series before and after injection of reactants in three α-pinene photooxidation experiments in the presence of AS seeds are shown in Figure 2. As can be observed from panels a and b, during the cleaning cycle the mixing ratios of NO_x and O_3 are sharply decreasing from ~40 and ~500 ppb, respectively, down to <10 and <1 ppb, respectively, during our automated filling cycle in less than an hour. Similarly, the particle number and mass concentration decreases down to <10 particles cm^{-3} and 0 $\mu g\ m^{-3}$, respectively, prior the injection of the reactants to chamber (Fig. 2c and e), so does the mixing ratio of a selected VOC (α-pinene) to 0 ppb (Fig. 2d). Furthermore, after ~3h of illumination in our cleaned bag (i.e., clean air + light experiments) the particle number and mass concentrations remain at the background levels, (see Fig. S1). This shows that our overall chamber gas-phase background is sufficiently low to prevent the formation of particles in the presence of light and in the absence of reactants. Overall, before the addition of the reactants to the MAC, our automated cleaning procedure ensures rapid cleaning that results in repeatably low background concentrations.

2.8 Instrumentation

A range of instruments can be used to measure the physical and chemical properties of the chamber air, as shown in Table 1. The table is separated into two parts, displaying the core instrumentation which are permanently fixed at the chamber as well as the additional instrumentation which can be coupled to the chamber and used on demand. All the instruments sampl from a number of ports in the manifolds, equipped with stainless steel or PTFE tubing extending to the middle of the chamber.

NO and NO_2 are measured using a NO_x Thermo 42i chemiluminescence analyzer. O_3 is measured by an Thermo 49C analyser. Both NO_x and O_3 analysers are regularly calibrated using certified cylinders and an ozone calibrator, respectively. Water-based condensation particle counters (wCPC; model 3785 and 3786) have been selected as core instrumentation operating in the chamber room to avoid the interference of the volatile working fluid (e.g., butanol), usually found on other CPC units, to diffuse into the chamber. A wCPC is being used to measure the total particle

number concentration in the chamber and the other is coupled to a differential mobility analyser (DMA, Brechtel Inc) as part of a custom-built differential mobility particle sizer (DMPS) system to measure particle size distributions in the 40-600 nm range. The DMA uses filtered chamber air as sheath flow to maintain the gas-particle equilibrium during the measurements.

The chamber is equipped with a removable 47mm filter holder which is located at the flushing line of the chamber (see Fig. 1) that can be loaded with the desired substrate and enable the sampling of the whole chamber contents at the end of each experiment at high flow rate ($3 m^3 min^{-1}$). In such a way, adequate amounts of particulate mass can be collected for subsequent off-line analysis.

A selection of additional instrumentation that are shared within the Centre for Atmospheric Sciences (CAS) group at the University of Manchester, are potentiallyavailable to be used on demand. Briefly, oxygenated VOCs are measured using a high-resolution time-of-flight chemical ionisation mass spectrometer (CIMS; Aerodyne/Tofware) using iodide as a reagent ion. Non-refractory PM_1 composition is measured using a high-resolution time-of-flight aerosol mass spectrometer (HR-AMS; Aerodyne) while oxygenated particulate organic composition is measured using the filter inlet for gases and aerosols (FIGAERO) when coupled to CIMS. Total organic and elemental carbon concentrations are measured using a semi-continuous carbon aerosol analyser (OC/EC; Sunset Laboratory; Model 4). Selection of particles based on their mass, or their aerodynamic size can be achieved using a centrifugal particle mass analyser (Cambustion) and an aerodynamic aerosol classifier (Cambustion), respectively. Particle hygroscopicity and volatility are measured by custom-built hygroscopicity tandem differential mobility analyser (HTDMA) and thermal denuder (TD), respectively, while cloud condensation nuclei (CCN) activity is measured by a CCN counter (Droplet measurement Technologies). Black carbon concentration and properties can be measured by a three-wavelength photoacoustic spectrometer and single particle soot photometer (Droplet measurement Tech).

Routinely, additional instruments, such as gas chromatograph coupled to a mass spectrometer (GC-MS) and proton transfer reaction ionisation scheme (PTR) were added to MAC as part of collaborative work to measure VOCs concentrations (Alfarra et al., 2013; Wyche et al., 2014; Wyche et al., 2015). Similarly, particle offline analysis using liquid chromatography-mass

spectrometry/tandem MS (LC-MS/MS) and two-dimensional GC-MS (2D-GC-MS) have been also employed occasionally to probe the chemical characteristics of the SOA particles (Hamilton et al., 2011; Wyche et al., 2015) .

2120 Table 1: List of the available instrumentation at MAC

Instrument	Model	Measured parameter	LOD/ range
Core instrumentation			
Dew point hygrometer	Edgetech; DM-C1-DS2-MH-13	Dew point	-20 – 90 ± 0.2 ºC
Sensirion capacitance sensor	Sensirion; SHT75	Temperature, relative humidity	-40 to +125, ±0.3 °C 0 – 100, ±1.8 %
NOx analyser	Thermo; 42i	NO, NO_2	0.5 to 1000 ppb
O_3 analyser	Thermo; 49C	O_3	0-0.05 to 200 ppm
CO analyser	Thermo;48i	CO	>0.04 ppm
Water-based condensation particle counter, wCPC	TSI; 3785, 3786	Particle number	$<10^7$ p/cc
Differential mobility particle sizer	Custom-built[a]	Particle size	40-600 nm
Filter collector	Custom-built[b]	Particle collection for offline analysis	
Additional instrumentation			
Condensation particle counter, CPC	TSI; 3776	Particle number	$<10^7$ p/cc
Scanning mobility particle sizer, SMPS	TSI; 3081	Particle size	10-1000 nm
Aerodynamic Aerosol Classifier, AAC	Cambustion	Selection of particles by size	25-5000 nm
Centrifugal Particle Mass Analyser	Cambustion	Selection of particles by mass	Mass accuracy: 5%
High-resolution aerosol mass spectrometer, HR-AMS	Aerodyne	PM_1 non-refractory particle composition	>0.05 μg m^{-3}
Iodide chemical ionisation mass spectrometer, I^--CIMS	Aerodyne/Tofware	Oxygenated VOC	LOD >60 ppt; Mass resolution 4000 Th/Th
Filter Inlet for Gases and AEROsols, FIGAERO	Aerodyne/Tofware	Particle composition	$>10^2$ ng
Semi-Continuous Carbon Aerosol Analyzer, OC/EC	Sunset Laboratory; Model 4	Organic/elemental carbon concentration	>0.5 μgC m^{-3}
Hygroscopicity tandem differential mobility analyser, HTDMA	Custom-built [c]	Hygroscopicity	20-350 nm

Cloud condensation nuclei counter, CCNc	Droplet measurement Tech; CCN-100)	CCN activity	>6 x 10^3 particles cm^{-3} at SS:0.2%
Thermal denuder	Custom built[d]	Volatility	Temperature range: ambient – 200°C
Three-wavelength photoacoustic spectrometer, PAS	Droplet measurement Tech	BC	0-100,000Mm^{-1}
Single Particle Soot Photometer, SP2	Droplet measurement Tech	light absorbing property of soot	>10 ng m^{-3}

[a](Alfarra et al., 2012) [b](Hamilton et al., 2011) [c](Good et al., 2010) [d](Voliotis et al., 2021)

3. MAC Characterization

This section describes the characterisation of each element of the chamber with relevance to the operation and influence on the and interpretation of the experimental results.

3.1. Temperature and relative humidity

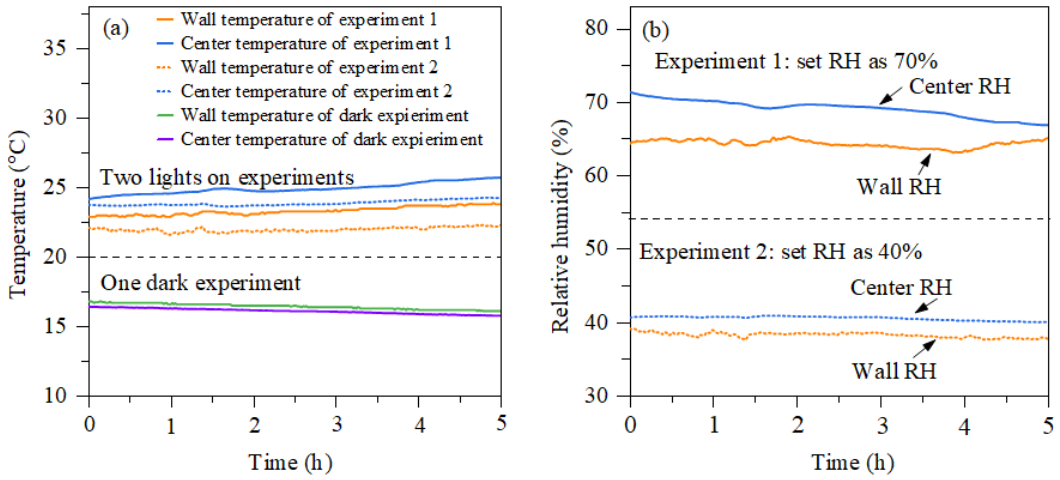

Figure 3: (a) Temperature as a function of time measured by the Edgetech (wall temperature) and Sensirion (centre temperature) in a dark experiment and a photooxidation experiment. (b) RH as a function of time in the two photooxidation experiments.

The temperature in MAC is controlled by the AC system, which compensate the releasing heat from illumination system. The calibrated dewpoint hygrometer (Edgetech sensor) is used as a reference for Sensirion capacitance sensors during dark conditions (no irradiation of the chamber) where there is no influence of temperature gradient caused by the light sources. The dark experiment at a set temperature of 16°C and two photooxidation experiments at different set points of relative humidity (40% and 70%) and a set temperature of 25 °C were conducted to examine the temperature and relative humidity homogeneity of the chamber.

Figure 3a shows the evolution of temperature at the chamber wall and at the centre of the chamber measured by the Edgetech and one Sensirion sensor, respectively, during dark and photooxidation experiments. The temperature accuracy of sensors is ± 0.3 ºC and ± 0.2 ºC for the Sensirion sensor and Edgetech sensor at 25 ºC, respectively. In photooxidation experiments, the temperature in the chamber centre (24 ± 1 ºC) is stable and slightly higher than that in the chamber wall (23 ± 1 ºC). Such a gradient might be caused by the cooler air between the chamber wall and enclosure and incomplete mixing. The temperature in dark conditions shows good agreement with the two sensors, around 16 ºC. Figure 3b shows the relative humidity results of the two photooxidation experiments measured by the Sensirion and Edgetech sensors. In the light experiment, the RH in the centre of the chamber measured by the Sensirion capacitance sensor (40 ± 1% and 70 ± 1%) was slightly higher than the RH at the wall of the chamber measured by the Edgetech hygrometer (39 ± 1% and 65 ± 1%). In the light experiments, it appears that both the temperature and humidity were higher in the centre of the MAC than that of the wall, while in the dark experiments these differences were negligible as they were within the uncertainty of our measurement. A likely explanation for this unexpected behaviour in the light experiments can be possibly to the radiative heating of the sensors in these experiments that could result in an over-estimation of the RH.

3.2. Mixing

NO, NO_2 and NO_x are selected as gas tracers to test the gas-phase mixing time inside the reactor. There are no fans or other equipment inside the chamber, however, NO_x is injected as NO_2 into the 3 m^3 min^{-1} (=50 L s^{-1}) flow through the 50 mm diameter inlet at a velocity of approximately 25 m/s, inducing near instantaneous mixing throughout the chamber. Throughout an experiment, the forceful agitation of the Teflon walls by the AC flow between the enclosure and chamber continuously maintains mixing inside the reactor. As shown in Figure 2b (for clarity see Fig. S2a), the mixing time for NO, NO_2 and NO_x gases is in the order of few minutes. Typically, the mixing time in atmospheric simulation chambers fall within the range of minutes, for example, 1 min in the CESAM chamber with 4.2 m^3 (Wang et al., 2011) and 2 mins in the GIG-CAS chamber 30 m^3 (Wang et al., 2014)

Non-acidic seed particles (ammonium sulfate, AS) were chosen to examine the mixing time of particles in the chamber. Briefly, seed particles were injected into the seed aerosol residence chamber (Fig. 1) and mixed for 1 min and subsequently introduced into the chamber at the flowrate

of 3 m^3 min^{-1}. Figure 2c (for clarity see Fig. S2b) shows the number concentration of particles measured by the wCPC as a function of time, which shows that the mixing time for seed particles in the chamber is around 2.5 mins. This time is comparable with the gases mixing time in the chamber. Furthermore, as can be seen, after the addition of NO_x and seed aerosol to the chamber and the air condition is turned on, the mixing ratios of NO_x are remaining constant within few minutes after their injection. Similarly, the number concentration of the seed aerosol shows some fluctuations over the first ~10 mins and they appear to stabilise and being subjected to the expected losses to the chamber walls. The stability in the measured concentrations of those tracers provides evidence for the effectiveness of the mixing of the components of the MAC, while the low standard deviations between the experiments (shown as shaded areas) further demonstrate the repeatability that can be achieved in our system.

3.3. Light intensity

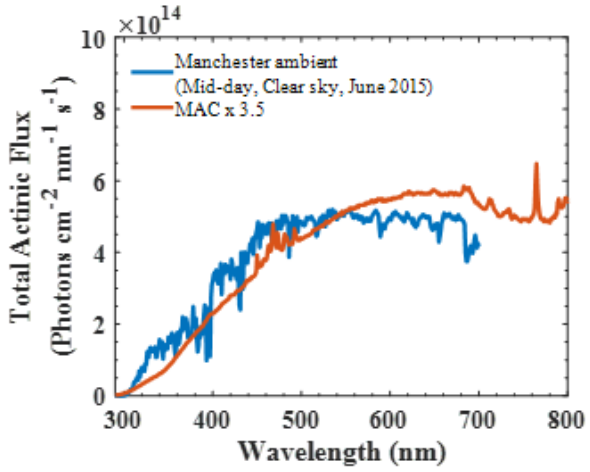

Figure 4: Total actinic flux spectrum in the MAC compared to the ambient light spectrum obtained in the city of Manchester (UK) mid-day with a clear sky in June 2015

The artificial radiation in the MAC has a broad radiation distribution owing to the chosen combination of illumination sources, producing irradiation over the wavelength range 290-800 nm to capture all wavelengths of the atmospheric actinic spectrum. Figure 4 shows the total actinic flux measured in MAC (red line) multiplied by 3.5 compared with the Manchester midday clear sky measurements on a June day. The total actinic flux in MAC was measured the centre position of chamber bag (150cm apart from the arc lamps in both vertical and horizontal axes).

The photolysis rate of NO_2 (jNO_2) estimated in steady-state actinometry can be used as a confirmation of the light intensity in the chamber (Hu et al., 2014) measured by direct spectral

radiometry. Such actinometric measurements were carried out by injecting NO_2 into the chamber and irradiating for several hours, measuring the concentration of NO, NO_2 and O_3 continuously. A series of NO_2 actinometry experiments were conducted with ~ 70ppb NO_2 injected into the chamber and irradiated for more than 3 hours, with the temperature and humidity maintained at around 25°C and 50% respectively. The photolysis frequency of NO_2 is calculated from

$$jNO_2 = \frac{k_{NO+O_3} \times [NO] \times [O_3]}{[NO_2]} \quad (1)$$

where k_{NO+O3} is the rate constant of the reaction of O_3 and NO (1.8×10^{-14} $cm^3molecule^{-1}s^{-1}$ at 298K) (Atkinson et al., 2004).

In the MAC, the photolysis rate of NO_2 (jNO_2) as derived from our steady state actinometry experiments was comparable, within our measured variability, with that directly measured from the integrated absorption across the measured wavelengths (2.25 ± 0.4 vs. 1.5×10^{-3} s^{-1}, respectively). Given that the jNO2 obtained by the actinometry experiments is an average and is estimated based on the assumption of photostationary state for trace gases in the bag, while the spectral radiometry is a point-measurement in an imperfect integrating sphere, which could not be representative for the whole chamber, these results are in a reasonable agreement. The integrated jNO_2 measured by spectral radiometry in the ambient Manchester on clear sky over the summer was 7×10^{-3} s^{-1} but had comparable light spectrum to that measured in MAC. The values obtained in MAC are more similar to those reported previously over the winter-time at Finokalia station, Greece (Gerasopoulos et al., 2012) and are generally comparable with those obtained across the broader simulation chamber community, as shown in Table 2.

3.4. Wall loss of gaseous compounds

Chamber wall adsorption had been shown to be a substantial source of gas losses inside Teflon bags (Wang et al., 2011) and will influence the gas-phase reactivity and SOA formation. In the MAC, the wall loss rates of NO_2, O_3 and several volatile organic compounds (α-pinene, toluene, 1.3.5-TMB and limonene) were investigated by injecting known concentrations into the chamber and measuring their concentration decay for an extended period under dark conditions. Approximately 50ppb concentration of NO_2 and O_3 at concentrations ranging from 120 ppb to 350ppb were injected into the chamber and monitored for 4 hours allowing sufficient time for a

measurable decay. Selecting different concentration of O_3 could assist in investigating the impact their initial concentration on the wall loss rate in the MAC. For the wall loss experiments of volatile organic species, 50ppb of each compound was injected into the chamber with the decay monitored for ~4 hours. All the wall loss experiments of gaseous species were conducted under the T and RH of ~25°C and ~50% respectively.

Measured first-order wall loss rates of selected gaseous species were calculated by considering their decay as a first-order process. The wall loss rates of NO_2 and O_3 were $9.40 \pm 7.38 \times 10^{-7} s^{-1}$ and $2.09 \pm 0.97 \times 10^{-6} s^{-1}$, respectively. Table 2 compares the wall loss rates of NO_2 and O_3 between MAC and other chambers. The NO_2 decay rate at the MAC was slightly higher than all the other chambers listed, except GIG-CAS, while the O_3 decay rate of MAC was higher than TU and KNU chamber, but lower than GIG-CAS and PSI chamber.

The first order wall loss rate of the selected anthropogenic and biogenic VOCs were $2.24 \pm 0.67 \times 10^{-5} s^{-1}$ for α-pinene, $2.08 \pm 0.54 \times 10^{-5} s^{-1}$ for limonene, $2.06 \pm 1.25 \times 10^{-5} s^{-1}$ for toluene and $12.22 \pm 0.90 \times 10^{-5}\ s^{-1}$ for 1.3.5 TMB.

Table 2: Comparison of wall loss rate of NO2 and O3, jNO2 with other chambers

Chamber	**Wall loss rate (s^{-1})**		**jNO_2 ($x10^{-3}\ s^{-1}$)**	**Reference**
	NO_2	**O_3**		
MAC	0.94×10^{-6}	2.09×10^{-6}	2.25	This study
KNU	7.45×10^{-7}	1.08×10^{-6}	2.83	Babar et al., 2016
GIG-CAS	2.32×10^{-6}	2.18×10^{-6}	8.17	Wang et al., 2014
PSI	2.17×10^{-7}	4.00×10^{-6}	-	Metzger et al., 2008
TU	6.95×10^{-7}	1.02×10^{-8}	3.83	Wu et al., 2007
UCR	-	-	3.17	Carter et al., 2005
AIOFM-CAS	-	-	3.50	Hu et al., 2014

3.5. Wall losses of particles

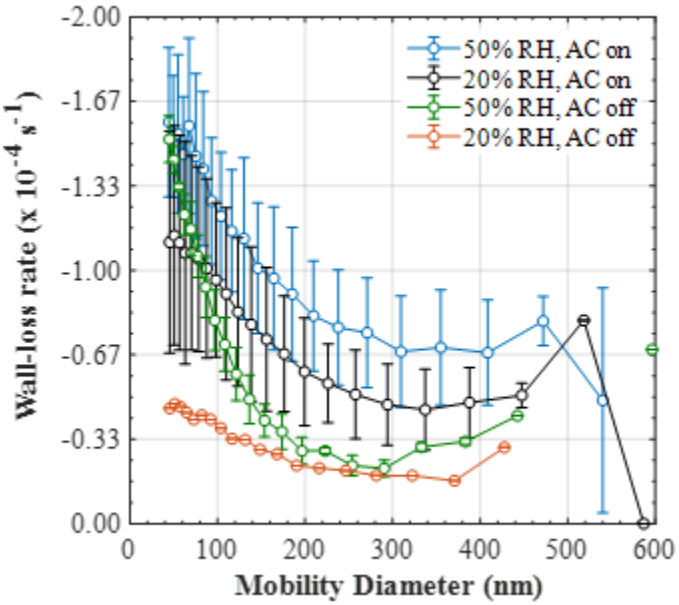

Figure 5:Mean (± 1σ) size-resolved wall loss rate (s^{-1}) of particles in the MAC at various relative humidity and mixing conditions (50% RH and mixing, n=9; 20% RH and mixing, n=5; 50% RH and no mixing, n=3; 20% RH and no mixing, n=1)

Particles are deposited to chamber walls mainly due to natural convection, diffusion, gravitational settling and electrostatic forces in addition to physical mixing (Crump et al., 1983; Pierce et al., 2008; Mcmurry and Rader, 1985). Several different approaches have been proposed to determine and account for these losses to the chamber walls that are largely size-dependent (Charan et al., 2019). Most commonly, the particle wall losses are determined by injecting particles with measurable sizes into the chambers and subsequently measuring their size-resolved loss rates by treating the decay as first-order process (Murphy et al., 2006; Zhang et al., 2007) A series of experiments were conducted to investigate the size-resolved particle lifetimes under various humidity and mixing conditions using AS seed, which was introduced to the chamber and left in the dark at the desired RH and temperature conditions for ≥4 hours. An initial seed concentration of 50-100 μg m^{-3} was used with a modal diameter of ~100 nm. The size-resolved concentration of the AS seed was monitored using a DMPS at 40-600 nm range, with a 10 min scanning time. Here, in line with the literature (Cocker et al., 2001a; Donahue et al., 2012; Gallimore et al., 2017; Smith et al., 2019), the particle wall-loss rate was retrieved by fitting an exponential function to the decay of the particle number in each size bin of the DMPS, to obtain a size-resolved decay rate coefficient.

A comparison between the application of different particle wall-loss correction methods is shown in section 3.5.1.

The mean (± 1σ) size-resolved wall loss rate (s^{-1}) of particles in the MAC at various relative humidity and mixing conditions are shown in Figure 5. The size-resolved particle wall loss rate in all experimental types showed a decreasing trend with particle size. In the size range measured here, such behaviour has been observed previously in chambers with varying volumes (Wang et al., 2018) and was attributed to the high diffusivity of the particles in the sub-100nm range, in addition to the possible contribution of coagulation when particle number concentrations of the small size particles are high. Moreover, a considerable scatter in the data obtained under our typical experimental conditions was observed (i.e., at 50% RH and with the AC on). The large deviations in the size-resolved particle wall loss rates can be possibly attributed to the changes in the chamber behaviour, considering that the experiments averaged here were conducted sporadically over a large time-period (2017-2019) and on different conditions of the bag. The latter is investigated further in Section 5. Alternatively, such deviations could be also attributed to particle and/or chamber charging effects (Charan et al., 2019). More specifically, considering that the AS particles generated in all of our experiments were not neutralised prior entering the chamber, the potential charge distribution of the particles could have been varying with consequent implications to the particle losses. Similarly, Teflon chambers are known to acquire charge when in contact with non-conductive surfaces, in turn affecting the particle losses to the walls. In spite the MAC being suspended and its operators had minimal to no contact with the bag, it is challenging to experimentally assess the potential effects of the chamber charging to the particle wall losses over such large time-period.

However, the combination of our experimental results presented in this study with those presented earlier using our newly developed PyCHAM model (O'meara et al., 2021) can provide some further insights on the latter matter. Figure 6 shows the measured size-resolved particle decay from several identical wall-loss characterisation experiments (i.e., ammonium sulfate seed in the dark), conducted over a span of 3 years and at various conditions of the MAC. Additionally, the size-resolved wall-loss rates that were required to reproduce the SOA formation in the limonene nucleation experiment presented in the O'meara et al. (2021) study are also shown. Evidently, the variation in the measured loss rates of the particles nebulised in similar manner in the MAC as a function of the chamber bag history can be substantial. Interestingly, the modelled particle losses

that required to reproduce a nucleation experiment, where no induced charge of the particles is expected, are comparable with those measured in a new bag. What is more, the model of Mcmurry and Rader (1985) suggests that the differences in the wall-loss rates of the particles having 0 and +1 charge can be as a high as 2 orders of magnitudes (or more) for particles of 100 nm in diameter (see Fig. 9 on O'Meara et al., 2021). Here, the observed differences between the potentially charged AS particles in the characterisation experiments were within the same order of magnitude to those modelled for a nucleation experiment, where no particle charge is expected. Therefore, this analysis suggests that neutralising the seed aerosols prior to injection into the MAC would have less of an effect than the usage history of the bag.

In either relative humidity conditions (e.g., 20 and 50%), the continuous agitation of the chamber walls due to the air circulation around the chamber from the AC affected the particle wall losses, showing higher wall-loss rates compared to those where the AC was disabled. The enhanced particle wall losses when the AC was enabled can be possibly attributed to the turbulence caused by AC as the chamber walls agitate, causing the particles to deposit at higher rates (Trump et al., 2016).

The amount of the water vapour also affects the particle wall-loss rate with the experiments conducted under drier conditions having lower loss rates compared to those at moderate RH conditions, however the variability was quite high to unambiguously differentiate the results from both conditions. These results suggest that the experimental conditions can have a significant impact on the particle wall-loss rates. Therefore, care should be taken when using the retrieved wall-loss rates from such experiments to correct the SOA particle mass in experiments conducted on different environmental conditions.

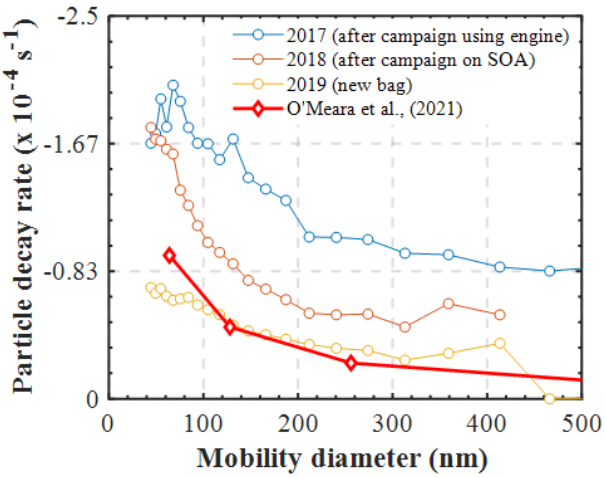

Figure 6: Measured size-dependent particle decay rates (s^{-1}) in characterisation experiments (RH=50%) conducted at different conditions of the bag. The modelled particle losses on a nucleation experiment are shown for comparison (O' Meara et al., 2021).

3.5.1. Investigation of various particle wall-loss correction methods to the SOA formation

As mentioned above, the retrieved size-resolved ammonium sulfate particle loss rates from characterisation experiments are commonly used to correct the SOA particle mass from VOC oxidation experiments (Ng et al., 2007; Fry et al., 2014; Nah et al., 2017). Several alternative numerical approaches have also been proposed (Wang et al., 2018; Pierce et al., 2008). Here, we compare two different approaches to correct the SOA particle mass from a β-caryophyllene photooxidation and a limonene ozonolysis experiment. More specifically, we use the size-resolved mass loss rates retrieved from the characterisation experiments (described in Section 3.5.) as well as the modelling approach proposed by Verheggen and Mozurkewich (2006). The results are summarised in Figure 7. It should be noted that our aim here is not to investigate the characteristics of each method, rather to demonstrate their effect when correcting for particle wall-losses in atmospheric simulation chambers.

The different approaches clearly result in substantially different wall-loss corrected SOA masses (Fig. 7). In all cases, the correction using the ammonium sulfate size-resolved wall-loss rates resulted in greater differences compared to the Verheggen and Mozurkewich (2006) model. These differences can be, at least partly, attributed to the parameters accounted in each method. The size-resolved particle correction applies the measured particle decay rates from the characterisation

experiments to the decay of the particles in the SOA experiments. Effectively, in this method it is assumed that the losses of the AS particles in the characterisation experiments (from any loss process) are the same as those formed in the SOA experiments. On the other hand, the Verheggen and Mozurkewich (2006) model employs inverse modelling to simulate the particle wall losses based on diffusion and gravitational settling, while the losses due to coagulation are indirectly inferred and the eddy diffusion and the turbulent kinetic energy are treated as empirical parameters based on the Crump et al., (1983) model. Therefore, the differences between the two approaches could be partly attributed to the particle losses due to coagulation that is indirectly accounted in the Verheggen and Mozurkewich (2006) model opposed to the size-resolved correction. Alternatively, considering that the seed aerosol generated in our experiments were not neutralised, the particle decay rates measured in the characterisation experiments account for any potential influences of the particle charge to the decay rates of the particles, opposed to the Verheggen and Mozurkewich (2006) model, thereby possibly further contributing to observed discrepancies. Clearly, treating the particle losses to atmospheric simulation chambers is not a trivial task and this could have substantial impacts for the reported SOA yields.

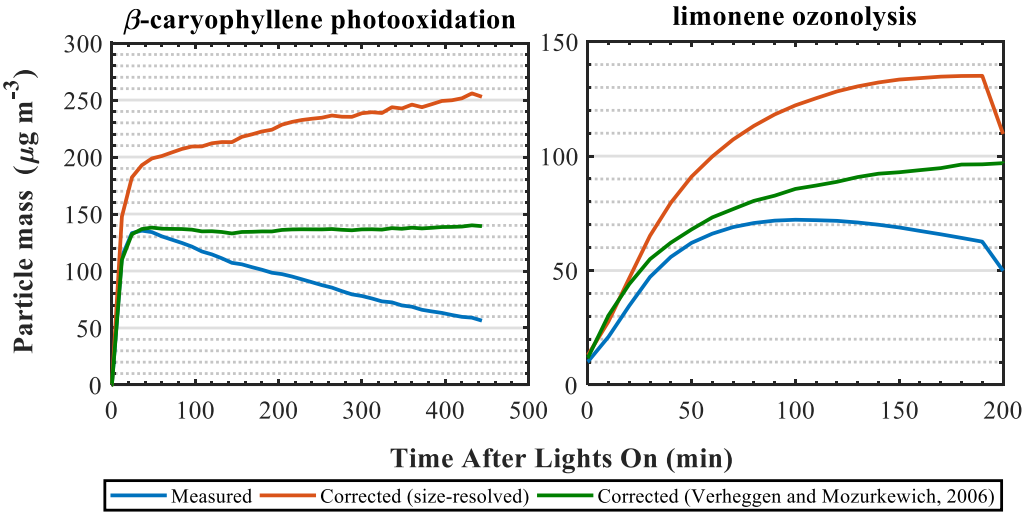

Figure 7: Measured and wall-loss corrected SOA particle mass using two different wall-loss correction approaches for a β-caryophyllene photooxidation (left panels) and a limonene ozonolysis (right panels) experiment.

3.6. Chamber wall reactivity

The chamber wall reactivity aims to describe the chamber wall activity such that it can be directly used as data set in future computer modelling to simulate the chamber experiments. A set of

experiments were conducted including simulating clean air, dark decay of NO_2 and O_3. Four non-elementary hypothetical reactions and relevant parameters used in the model are listed in Table 3. The parameters for the NO_2 and O_3 formation rate from the Teflon walls were calculated based on the off-gassing experiments under light irradiation conditions for at least 3 hours reaction. The initial concentrations of NO_2 and O_3 in the chamber were varied from 0 to 8 ppb. The light-induced formation of NO_2 and O_3 from the chamber walls were $6.95 \pm 1.26\times10^{-5}s^{-1}$ and $8.56 \pm 2.58\times10^{-5}s^{-1}$, respectively.

The decrease of NO_2 and O_3 in the gaseous phase under dark conditions for the new chamber bag had been mentioned in section 3.4. Gas phase molecules can be lost to the boundary layer of the surface chamber wall by molecular diffusion and macroscopic mixing, while their reactive uptake by the Teflon film and any deposited material is also possible. Teflon film can act as a reservoir for organic vapour deposition during chamber experiments that may contribute to O_3 loss by oxidation. Furthermore, the organic compounds deposited can act as absorptive mass, in turn influencing the mass transfer from the gas phase to the walls (Charan et al., 2019).

Table 3:Chamber wall activity and rates for chamber-dependent reactions. aProduction rate of gaseous species from wall under light condition (P w, l). bLoss rate of gaseous species to wall under dark condition (L w,d).

Parameters	**Gas Species**	**Rate (mean ±1σ) /s^{-1}**	**Experiment**
(P w,l)[a]	NO_2	$(6.95\pm1.26)\times10^{-5}$	Direct measurement of NO_2 wall production
	O_3	$(8.56\pm2.58)\times10^{-5}$	Direct measurement of NO_2 wall production
(L w,d)[b]	NO_2	$(9.40 \pm 7.39)\times10^{-7}$	Direct measurement of NO_2 wall loss
	O_3	$(2.09\pm 0.9)\times10^{-6}$	Direct measurement of O_3 wall loss

4. α -pinene photooxidation experiment

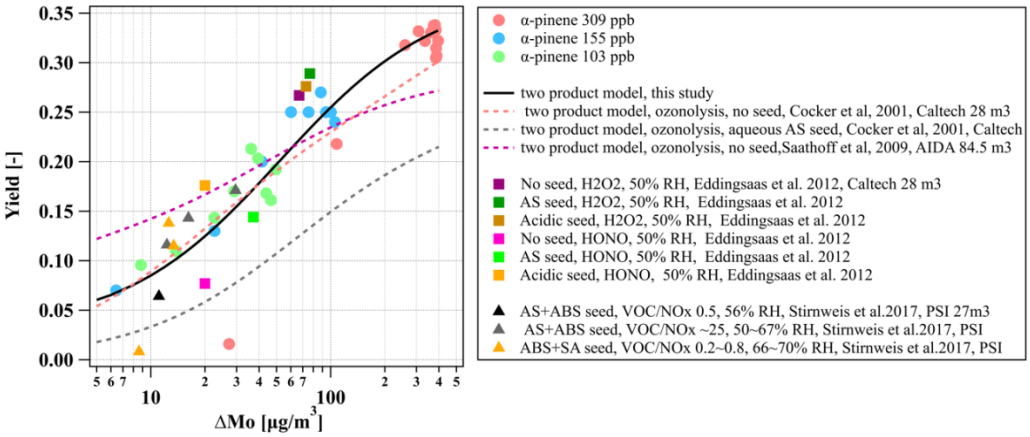

Figure 8: Yield curves derived from the photooxidation of α-pinene on aqueous AS seed conducted in this study and literature data (Cocker et al., 2001b, Saathoff et al., 2009, Eddingsaas et al., 2012, Stirnweis et al., 2017). All experiments are carried out under humid conditions. Lines represent the two-product model fit for yield curves.

To evaluate the chamber facility for the purposes of studying SOA production and transformation, α-pinene photochemistry experiments were conducted in the MAC. The initial experimental conditions are shown in Table 4. During the experiments, chemical composition (NH_4, SO_4, NO_3, OA) in the particle phase and α-pinene in the gas phase were monitored by HR-ToF-AMS and Semi-continuous GC-MS, respectively. The measured SOA mass by HR-ToF-AMS was corrected due to the non-unit collection efficiency of the instrument following standard procedures in previous studies (Jimenez, 2003; Jayne et al., 2000; Allan et al., 2003; Allan et al., 2004) and chamber wall loss effects (Wang et al., 2018).

To compare with literature data, SOA yield (Y) was used as a proxy to evaluate SOA production (Grosjean and Seinfeld, 1989), defined as the SOA mass formation (ΔM_o) from the reactive organic gas (ΔVOC) consumption as shown in Eq. (2).

$$Y = \frac{\Delta M_0}{\Delta voc} \qquad (2)$$

Here, the SOA mass is wall loss corrected using the size-resolved wall-loss rate of ammonium sulphate particles from the nearest characterisation experiment as described in Section. 3.5.1. Odum et al. (1996) incorporated gas/particle partitioning theory (Pankow, 1994b; Pankow, 1994a) into SOA formation and calculated SOA yield from individual compounds, shown in Eq. (3).

$$Y = \sum_i Y_i = C_{OA} \sum_i \left(\frac{\alpha_i K_{p,i}}{1 + K_{p,i} C_{OA}} \right) \qquad (3)$$

Here, Y_i represents the yield of compound i. α_i is a stoichiometric factor representing the ratio of the molecular weight of product i to the parent VOC. $K_{p,i}$ and C_{OA} are the partitioning coefficient of product i and the total absorbing organic mass (the same as ΔM_o herein). Furthermore, Odum et al. (1996) successfully used a two-product model parameterising SOA yield and ΔM_o as shown in Eq. (4). The α_1, α_1, $K_{p,1}$, $K_{p,2}$ can be fitted upon yield curves.

$$Y = \frac{\Delta M_0}{\Delta voc} Y = \sum_i Y_i = C_{OA} \sum_i \left(\frac{\alpha_i K_{p,i}}{1 + K_{p,i} C_{OA}} \right) Y = C_{OA} \left(\frac{\alpha_i K_{p,i}}{1 + K_{p,i} C_{OA}} + \frac{\alpha_i K_{p,i}}{1 + K_{p,i} C_{OA}} \right) \qquad (4)$$

The yield curves as a function of ΔM_o for the three α-pinene experiments in this study and the comparison with literature data (Saathoff et al., 2009; Cocker et al., 2001b; Eddingsaas et al., 2012; Stirnweis et al., 2017) are shown in Figure 8 (all yield curves are wall loss corrected). As expected from the absorptive partitioning, it can be seen that the SOA yield increased consistently with an increase of absorptive organic mass for the three *α*-pinene experiments in this study. Our results are qualitatively and quantitatively comparable with *α*-pinene photochemistry experiments under different oxidant conditions and seed initialisations in other chambers, such as with HONO & H_2O_2 as oxidant and no seed & AS seed & acidic seed in Caltech chamber (Eddingsaas et al., 2012) and with VOC/NO_x ratio in the range of 0.2 to 25 and AS/Ammonium bisulphate (ABS) seed in PSI chamber (Stirnweis et al., 2017). Additionally, we use the two-product model to fit the yield curve of three *α*-pinene experiments in this study and the fitted α_1, α_1, $K_{p,1}$, $K_{p,2}$ are 0.03, 0.34, 3.14e+006, and 0.02, respectively, as shown in Fig. 8 (black solid line). The fitted yield curve for α-pinene photochemistry with aqueous AS seed in this study is comparable to the α-pinene ozonolysis without seed (Stirnweis et al., 2017; Cocker et al., 2001b), but much higher than the ozonolysis with aqueous seed (Cocker et al., 2001b).

Table 4:Summary of initial conditions for α-pinene photochemistry experiments

Exp. Date	VOC type	$[VOC]_0$ (ppbV)	VOC/NO_x	T (°C)	RH (%)	AS Seed conc. (ug/m^3)[a]
28-Mar-2019	α-pinene	309	7.7	26.7	50.5	60.7
6-Jul-2019	α-pinene	155	6.0	25.9	53.1	61.3
13-Jul-2019	α-pinene	103	5.7	27.2	54.5	55.4

[a]measured NR-PM mass concentration by HR-ToF-AMS with corrected collection efficiency (30 mins average before lights on).

5. Effects of contamination on chamber performance

It has been shown that organic vapours can condense on the Teflon chamber walls in a similar manner to the losses of particles (Matsunaga and Ziemann, 2010; Zhang et al., 2014; Krechmer et al., 2020). The deposition of those compounds on the chamber walls can be reversible (Matsunaga and Ziemann, 2010) or quasi-irreversible (Ye et al., 2016) and proportional to each compound's volatility and chemical characteristics. Similarly, other atmospheric gases, such as HONO, have been also found to condense on chamber walls (Rohrer et al., 2005). The uptake of semi-volatile vapours from the chamber walls has been proven to substantially affect the oxidative chemistry and thereby the reported SOA formation potential (Zhang et al., 2014; Rohrer et al., 2005). It is therefore likely that both gaseous and particle deposition can lead to a build-up of contamination on chamber walls with time (Huang et al., 2018). It is not guaranteed that any cleaning procedures are completely effective, and it is important to consider the experimental history of a chamber when interpreting experimental behaviour (and particularly when comparing experiments conducted in different periods). To assess the effect of contamination from such sources on the chamber performance, we conducted the same characterisation experiments as those described in Sections 3.3-3.5, in an extensively used Teflon bag, after a series of experiments with high concentrations of particles and gases derived from diesel engines.

The photolysis rate of NO_2 (i.e., jNO_2) derived from photostationary state calculations was found to be lower in the extensively used bag compared to a newly installed bag ($1.83 \pm 0.47 \times 10^{-3}$ vs. $2.25 \pm 0.40 \times 10^{-3}$ s^{-1}, respectively). This coincided with a substantial increase in the wall loss rate of NO_2 and O_3 that was observed in the extensively used compared to the newly installed ($7.95 \pm 6.90 \times 10^{-6}$ s^{-1} vs $0.93 \pm 0.76 \times 10^{-6}$ s^{-1} for the NO_2 and $2.23 \pm 1.83 \times 10^{-5}$ s^{-1} vs. $0.20 \pm 0.08 \times 10^{-5}$ s^{-1} for the O_3, respectively). At the same time, the wall production (i.e., off-gassing) of the same gases was decreased (0.12 vs. $0.19 \pm 0.04 \times 10^{-7}$ s^{-1} for the NO_2 and 0.20 vs. $0.24 \pm 0.07 \times 10^{-7}$ s^{-1} for the O_3). Unfortunately, spectral radiometry data are not available for the extensively used bag, which could help to identify whether the reduction in the jNO_2 is attributed to the transparency of the walls over usage of the bag or the changes in the production and loss of gases from and to the chamber walls. In the absence of such information, we can only speculate that the changes in the jNO_2 over the bag history could be attributable to the differences in the wall loss rates of these gases.

.

In addition to the changes in the decay rates of gases, similar changes were observed in the wall losses of particles. Fig. 6 shows the measured size-dependent particle decay rates (s^{-1}) in characterisation experiments conducted at different conditions of the bag. More specifically, characterisation experiments conducted in an extensively used bag after a campaign using diesel engine fumes, in a used bag after a campaign on SOA formation and in a new bag are shown. Clearly, the size-dependent losses of the particles can be substantially affected by the condition and the usage of the bag. Wang et al., (2018) reported significant changes in the wall-loss rates of particles after major maintenance activities in the area where the chamber was suspended and attributed those differences to the electrostatic forces caused by friction. In our setup, the chamber is enclosed in a housing and the operators have little to no contact with its walls, so it may be unlikely this to be the main cause for the changes in the particle wall-losses over the bag usage history. Considering that the correction of the SOA mass and particle yield calculations are strongly dependent on the measured particle loss rates in characterisation experiments, at least for MAC, it is recommended to conduct more frequent particle and gas loss characterisation experiments to enable more reliable corrections.

6. Discussion and conclusions

In this work, the MAC facility was for the frist time, comprehensively described and characterised. MAC is a batch reactor and showed good temperature and relative homogeneity, parameters that can influence the SOA formation and partitioning(Cocker et al., 2001b; Saathoff et al., 2009; Stirnweis et al., 2017). Although our reported experiments in this study were performed only under certain conditions, the results shown demonstrate that MAC can provide controlled temperature and relative humidity conditions, which are important for any systematic chamber study. MAC however is limited to a RH range of 25-80% and temperature of 15-35 ºC, owing to the heat generated by the lamps and the capacity of the AC unit.

Due to its explicit setup, the generated light spectrum mimics well the ambient solar radiation spectrum, comparable to that in Manchester, yet having lower total actinic flux by a factor of ~3.5. Furthermore, fast mixing times are effected by the injection of the reactants at high flow rates, while the air circulation around the chamber housing continuously agitates the chamber walls resulting in sufficient mixing of its components during the experiments but enhances wall losses.

The bespoke control system of the MAC allows the generation of automated procedures that can improve the duty cycle and enhance the comparability across experiments. Moreover, due to its design, gases and particles generated via a number of sources can be introduced to the chamber and studied in detail. In addition, its unique capability of transferring the whole contents of MAC to MICC provides the grounds for aerosol-cloud interaction studies (e.g., Frey et al., 2018).

Different wall loss rates of NO_2 were observed between MAC and other chambers, as shown in Section 3.4. Possibly, the wall loss rates of gaseous compounds are affected by experimental conditions (such as temperature and RH), mixing, and chamber sizes (Metzger et al., 2008; Wang et al., 2011). Importantly, we showed that the usage history can influence the wall loss of gases with a higher wall loss rate of NO_2 and O_3, which may result in the lower jNO_2 in an extensively used bag, as showing in Section 5. Higher particle decay rates were also observed in an extensively

used bag after "dirty" experiments compared to newly installed bag. It is more likely that the contaminated chamber walls may provide additional sinks to absorb more particles and gases irreversibly. Additionally, the various methods for the particle wall-loss correction led to different wall-loss corrected SOA masses, which in turn can have substantial implications for the derived SOA yields (Odum et al., 1996; Wang et al., 2018; Hoffmann et al., 1997), as shown in Section 3.5.1. This illustrates that using different approaches or experimental dataset to conduct such corrections may result in bias in the SOA yields (Cocker et al., 2001b; Saathoff et al., 2009; Stirnweis et al., 2017).

Our measured SOA yield curve from the photo-oxidation of α-pinene in the presence of seed particles, appeared to be comparable with other studies that conducted ozonolysis experiments in the absence of seed particles(Cocker et al., 2001a; Stirnweis et al., 2017), but much higher than the ozonolysis with aqueous seed (Cocker et al., 2001b), as showing in Fig. 8. However, it should be considered that the comparison of yield curves between different laboratories and facilities is quite complicated as there are many factors (seed/no seed, oxidants, relative humidity, VOC/NOx ratios, wall loss correction methods and etc,) that will affect the yields curves. Also, the characterization parameters of a chamber (e.g., gases and particles wall-loss rates) may also play an important role in the SOA formation as shown in Section 3.5.1. and discussed further above. Furthermore, the loss of condensable vapours to the chamber walls can result in a lower SOA formation even for high seed concentration conditions (Zhang et al., 2014).

Based on our results, regular characterisation experiments are recommended in order to track chamber's performance while accounting for any potential changes to the interpretation of the results. Considering that the atmospheric simulation chambers are composed by various materials and they come in different designs, sizes and shapes, in turn affecting their performance and behaviour, the comparability of their results should be a crucial priority of the scientific community. The results presented here highlight the need in developing a set of simple, standardised experiments and/or procedures that can be used from chambers across the globe in an effort to elucidate the characteristics of each facility and the interpretation of their results.

Competing interests

The authors declare that they have no conflict of interest.

Data Availability

The data that support the findings of this study are openly available in EUROCHAMP-2020 programme (https://data.eurochamp.org/data-access/chamber-experiments/).

Author contributions

GM, MRA, AV, YW, MD and YS conceived the study. GM, MRA and SFT designed the MAC. SPO provided the modelling results. AV, YW, YS and MD conducted the experiments, the data analysis and wrote the manuscript with inputs from all authors.

Acknowledgements

The Manchester Aerosol Chamber was supported by the EUROCHAMP2020 research programme funded by the European Union's Horizon 2020 research and innovation programme under grant agreement no. 730997. AV and MD acknowledge the financial support from Presidents Doctoral Scholarship from the University of Manchester. AV acknowledges the support by the Natural Environment Research Council (NERC) EAO Doctoral Training Partnership. YW acknowledges CSC scholarship support. MRA acknowledges funding support from the Natural Environment Research Council (NERC) through the UK National Centre for Atmospheric Science (NCAS). Instrumentational support was funded through the NERC Atmospheric Measurement and Observational Facility (AMOF).

References

Alfarra, M. R., Good, N., Wyche, K. P., Hamilton, J. F., Monks, P. S., Lewis, A. C., and McFiggans, G.: Water uptake is independent of the inferred composition of secondary aerosols derived from multiple biogenic VOCs, Atmospheric Chemistry and Physics, 13, 11769-11789, 10.5194/acp-13-11769-2013, 2013.

Alfarra, M. R., Hamilton, J. F., Wyche, K. P., Good, N., Ward, M. W., Carr, T., Barley, M. H., Monks, P. S., Jenkin, M. E., Lewis, A. C., and McFiggans, G. B.: The effect of photochemical ageing and initial precursor concentration on the composition and hygroscopic properties of β-caryophyllene secondary organic aerosol, Atmospheric Chemistry and Physics, 12, 6417-6436, 10.5194/acp-12-6417-2012, 2012.

Allan, J. D., Jimenez, J. L., Williams, P. I., Alfarra, M. R., Bower, K. N., Jayne, J. T., Coe, H., and Worsnop, D. R.: Quantitative sampling using an Aerodyne aerosol mass spectrometer 1. Techniques of data interpretation and error analysis, Journal of Geophysical Research: Atmospheres, 108, n/a-n/a, 10.1029/2002jd002358, 2003.

Allan, J. D., Delia, A. E., Coe, H., Bower, K. N., Alfarra, M. R., Jimenez, J. L., Middlebrook, A. M., Drewnick, F., Onasch, T. B., Canagaratna, M. R., Jayne, J. T., and Worsnop, D. R.: A generalised method for the extraction of chemically resolved mass spectra from Aerodyne aerosol mass spectrometer data, Journal of Aerosol Science, 35, 909-922, 10.1016/j.jaerosci.2004.02.007, 2004.

Atkinson, R., Aschmann, S. M., and Arey, J.: Reactions of hydroxyl and nitrogen trioxide radicals with phenol, cresols, and 2-nitrophenol at 296 .+-. 2 K, Environmental Science & Technology, 26, 1397-1403, 10.1021/es00031a018, 1992.

Atkinson, R., Baulch, D. L., Cox, R. A., Crowley, J. N., Hampson, R. F., Hynes, R. G., Jenkin, M. E., Rossi, M. J., and Troe, J.: Evaluated kinetic and photochemical data for atmospheric chemistry: Volume I - gas phase reactions of O_x, HO_x, NO_x and SO_x species, Atmos. Chem. Phys., 4, 1461-1738, 10.5194/acp-4-1461-2004, 2004.

Babar, Z. B., Park, J.-H., Kang, J., and Lim, H.-J.: Characterization of a Smog Chamber for Studying Formation and Physicochemical Properties of Secondary Organic Aerosol, Aerosol and Air Quality Research, 16, 3102-3113, 10.4209/aaqr.2015.10.0580, 2017.

Barnes, I. and Rudzinski, K. J.: Environmental simulation chambers: Application to atmospheric chemical processes, Springer Science & Business Media2006.

Barnes, I., Becker, K. H., and Mihalopoulos, N.: An FTIR product study of the photooxidation of dimethyl disulfide, Journal of Atmospheric Chemistry, 18, 267-289, 10.1007/BF00696783, 1994.

Becker, K. H.: Overview on the Development of Chambers for the Study of Atmospheric Chemical Processes, Environmental Simulation Chambers: Application to Atmospheric Chemical Processes, Dordrecht, 2006//, 1-26,

Behnke, W., Holländer, W., Koch, W., Nolting, F., and Zetzsch, C.: A smog chamber for studies of the photochemical degradation of chemicals in the presence of aerosols, Atmospheric Environment (1967), 22, 1113-1120, https://doi.org/10.1016/0004-6981(88)90341-1, 1988.

Bianchi, F., Kurtén, T., Riva, M., Mohr, C., Rissanen, M. P., Roldin, P., Berndt, T., Crounse, J. D., Wennberg, P. O., Mentel, T. F., Wildt, J., Junninen, H., Jokinen, T., Kulmala, M., Worsnop, D. R., Thornton, J. A., Donahue, N., Kjaergaard, H. G., and Ehn, M.: Highly Oxygenated Organic Molecules (HOM) from Gas-Phase Autoxidation Involving Peroxy Radicals: A Key Contributor to Atmospheric Aerosol, Chemical Reviews, 119, 3472-3509, 10.1021/acs.chemrev.8b00395, 2019.

Bloss, C., Wagner, V., Bonzanini, A., Jenkin, M. E., Wirtz, K., Martin-Reviejo, M., and Pilling, M. J.: Evaluation of detailed aromatic mechanisms (MCMv3 and MCMv3.1) against environmental chamber data, Atmos. Chem. Phys., 5, 623-639, 10.5194/acp-5-623-2005, 2005.

Carlton, A. G., Wiedinmyer, C., and Kroll, J. H.: A review of Secondary Organic Aerosol (SOA) formation from isoprene, Atmospheric Chemistry and Physics, 9, 4987-5005, 10.5194/acp-9-4987-2009, 2009.

Carter, W., Cockeriii, D., Fitz, D., Malkina, I., Bumiller, K., Sauer, C., Pisano, J., Bufalino, C., and Song, C.: A new environmental chamber for evaluation of gas-phase chemical mechanisms and secondary aerosol formation, Atmospheric Environment, 39, 7768-7788, 10.1016/j.atmosenv.2005.08.040, 2005.

Carter, W. P. L. and Lurmann, F. W.: Evaluation of a detailed gas-phase atmospheric reaction mechanism using environmental chamber data, Atmospheric Environment. Part A. General Topics, 25, 2771-2806, 10.1016/0960-1686(91)90206-m, 1991.

Charan, S. M., Huang, Y., and Seinfeld, J. H.: Computational Simulation of Secondary Organic Aerosol Formation in Laboratory Chambers, Chemical Reviews, 119, 11912-11944, 10.1021/acs.chemrev.9b00358, 2019.

Charan, S. M., Kong, W., Flagan, R. C., and Seinfeld, J. H.: Effect of particle charge on aerosol dynamics in Teflon environmental chambers, Aerosol Science and Technology, 52, 854-871, 10.1080/02786826.2018.1474167, 2018.

Cocker, D. R., Flagan, R. C., and Seinfeld, J. H.: State-of-the-Art Chamber Facility for Studying Atmospheric Aerosol Chemistry, Environmental Science & Technology, 35, 2594-2601, 10.1021/es0019169, 2001a.

Cocker, D. R., Clegg, S. L., Flagan, R. C., and Seinfeld, J. H.: The effect of water on gas–particle partitioning of secondary organic aerosol. Part I: α-pinene/ozone system, Atmospheric Environment, 35, 6049-6072, https://doi.org/10.1016/S1352-2310(01)00404-6, 2001b.

Connolly, P. J., Emersic, C., and Field, P. R.: A laboratory investigation into the aggregation efficiency of small ice crystals, Atmospheric Chemistry and Physics, 12, 2055-2076, 10.5194/acp-12-2055-2012, 2012.

Crump, J. G., Flagan, R. C., and Seinfeld, J. H.: Particle Wall Loss Rates in Vessels, Aerosol Science and Technology, 2, 303-309, 10.1080/02786828308958636, 1983.

Donahue, N. M., Kroll, J. H., Pandis, S. N., and Robinson, A. L.: A two-dimensional volatility basis set – Part 2: Diagnostics of organic-aerosol evolution, Atmos. Chem. Phys., 12, 615-634, 10.5194/acp-12-615-2012, 2012.

Dunne, E. M., Gordon, H., Kurten, A., Almeida, J., Duplissy, J., Williamson, C., Ortega, I. K., Pringle, K. J., Adamov, A., Baltensperger, U., Barmet, P., Benduhn, F., Bianchi, F., Breitenlechner, M., Clarke, A., Curtius, J., Dommen, J., Donahue, N. M., Ehrhart, S., Flagan, R. C., Franchin, A., Guida, R., Hakala, J., Hansel, A., Heinritzi, M., Jokinen, T., Kangasluoma, J., Kirkby, J., Kulmala, M., Kupc, A., Lawler, M. J., Lehtipalo, K., Makhmutov, V., Mann, G., Mathot, S., Merikanto, J., Miettinen, P., Nenes, A., Onnela, A., Rap, A., Reddington, C. L., Riccobono, F., Richards, N. A., Rissanen, M. P., Rondo, L., Sarnela, N., Schobesberger, S., Sengupta, K., Simon, M., Sipila, M., Smith, J. N., Stozkhov, Y., Tome, A., Trostl, J., Wagner, P. E., Wimmer, D., Winkler, P. M., Worsnop, D. R., and Carslaw, K. S.: Global atmospheric particle formation from CERN CLOUD measurements, Science, 354, 1119-1124, 10.1126/science.aaf2649, 2016.

Eddingsaas, N. C., Loza, C. L., Yee, L. D., Chan, M., Schilling, K. A., Chhabra, P. S., Seinfeld, J. H., and Wennberg, P. O.: α-pinene photooxidation under controlled chemical conditions – Part 2:

SOA yield and composition in low- and high-NO_x environments, Atmospheric Chemistry and Physics, 12, 7413-7427, 10.5194/acp-12-7413-2012, 2012.

Ehn, M., Kleist, E., Junninen, H., Petäjä, T., Lönn, G., Schobesberger, S., Dal Maso, M., Trimborn, A., Kulmala, M., Worsnop, D. R., Wahner, A., Wildt, J., and Mentel, T. F.: Gas phase formation of extremely oxidized pinene reaction products in chamber and ambient air, Atmos. Chem. Phys., 12, 5113-5127, 10.5194/acp-12-5113-2012, 2012.

Ehn, M., Thornton, J. A., Kleist, E., Sipilä, M., Junninen, H., Pullinen, I., Springer, M., Rubach, F., Tillmann, R., Lee, B., Lopez-Hilfiker, F., Andres, S., Acir, I.-H., Rissanen, M., Jokinen, T., Schobesberger, S., Kangasluoma, J., Kontkanen, J., Nieminen, T., Kurtén, T., Nielsen, L. B., Jørgensen, S., Kjaergaard, H. G., Canagaratna, M., Maso, M. D., Berndt, T., Petäjä, T., Wahner, A., Kerminen, V.-M., Kulmala, M., Worsnop, D. R., Wildt, J., and Mentel, T. F.: A large source of low-volatility secondary organic aerosol, Nature, 506, 476-479, 10.1038/nature13032, 2014.

Finlayson-Pitts, B. J. and James N. Pitts, J.: Chemistry of the Upper and Lower Atmosphere, 10.1016/b978-0-12-257060-5.X5000-x, 2000.

Frey, W., Hu, D., Dorsey, J., Alfarra, M. R., Pajunoja, A., Virtanen, A., Connolly, P., and McFiggans, G.: The efficiency of secondary organic aerosol particles acting as ice-nucleating particles under mixed-phase cloud conditions, Atmospheric Chemistry and Physics, 18, 9393-9409, 10.5194/acp-18-9393-2018, 2018.

Fry, J. L., Draper, D. C., Barsanti, K. C., Smith, J. N., Ortega, J., Winkler, P. M., Lawler, M. J., Brown, S. S., Edwards, P. M., Cohen, R. C., and Lee, L.: Secondary organic aerosol formation and organic nitrate yield from NO3 oxidation of biogenic hydrocarbons, Environ Sci Technol, 48, 11944-11953, 10.1021/es502204x, 2014.

Gallimore, P. J., Mahon, B. M., Wragg, F. P. H., Fuller, S. J., Giorio, C., Kourtchev, I., and Kalberer, M.: Multiphase composition changes and reactive oxygen species formation during limonene oxidation in the new Cambridge Atmospheric Simulation Chamber (CASC), Atmospheric Chemistry and Physics, 17, 9853-9868, 10.5194/acp-17-9853-2017, 2017.

Gerasopoulos, E., Kazadzis, S., Vrekoussis, M., Kouvarakis, G., Liakakou, E., Kouremeti, N., Giannadaki, D., Kanakidou, M., Bohn, B., and Mihalopoulos, N.: Factors affecting O3 and NO2photolysis frequencies measured in the eastern Mediterranean during the five-year period 2002–2006, Journal of Geophysical Research: Atmospheres, 117, https://doi.org/10.1029/2012JD017622, 2012.

Goldstein, A. H. and Galbally, I. E.: Known and Unexplored Organic Constituents in the Earth's Atmosphere, Environmental Science & Technology, 41, 1514-1521, 2007.

Good, N., Coe, H., and McFiggans, G.: Instrumentational operation and analytical methodology for the reconciliation of aerosol water uptake under sub- and supersaturated conditions, Atmos. Meas. Tech., 3, 1241-1254, 10.5194/amt-3-1241-2010, 2010.

Gray, H. A., Cass, G. R., Huntzicker, J. J., Heyerdahl, E. K., and Rau, J. A.: Characteristics of atmospheric organic and elemental carbon particle concentrations in Los Angeles, Environ Sci Technol, 20, 580-589, 10.1021/es00148a006, 1986.

Grosjean, D. and Seinfeld, J. H.: Parameterization of the formation potential of secondary organic aerosols, Atmospheric Environment (1967), 23, 1733-1747, 10.1016/0004-6981(89)90058-9, 1989.

Hallquist, M., Wenger, J. C., Baltensperger, U., Rudich, Y., Simpson, D., Claeys, M., Dommen, J., Donahue, N. M., George, C., Goldstein, A. H., Hamilton, J. F., Herrmann, H., Hoffmann, T., Iinuma, Y., Jang, M., Jenkin, M. E., Jimenez, J. L., Kiendler-Scharr, A., Maenhaut, W., McFiggans, G., Mentel, T. F., Monod, A., Prévôt, A. S. H., Seinfeld, J. H., Surratt, J. D., Szmigielski, R., and

Wildt, J.: The formation, properties and impact of secondary organic aerosol: current and emerging issues, Atmospheric Chemistry and Physics, 9, 5155-5236, 10.5194/acp-9-5155-2009, 2009.
Hamilton, J. F., Rami Alfarra, M., Wyche, K. P., Ward, M. W., Lewis, A. C., McFiggans, G. B., Good, N., Monks, P. S., Carr, T., White, I. R., and Purvis, R. M.: Investigating the use of secondary organic aerosol as seed particles in simulation chamber experiments, Atmospheric Chemistry and Physics, 11, 5917-5929, 10.5194/acp-11-5917-2011, 2011.
Hennigan, C. J., Miracolo, M. A., Engelhart, G. J., May, A. A., Presto, A. A., Lee, T., Sullivan, A. P., McMeeking, G. R., Coe, H., Wold, C. E., Hao, W. M., Gilman, J. B., Kuster, W. C., de Gouw, J., Schichtel, B. A., Collett, J. L., Kreidenweis, S. M., and Robinson, A. L.: Chemical and physical transformations of organic aerosol from the photo-oxidation of open biomass burning emissions in an environmental chamber, Atmospheric Chemistry and Physics, 11, 7669-7686, 10.5194/acp-11-7669-2011, 2011.
Hoffman, E. J. and Duce, R. A.: Organic carbon in marine atmospheric particulate matter: Concentration and particle size distribution, Geophysical Research Letters, 4, 449-452, 10.1029/GL004i010p00449, 1977.
Hoffmann, T., Odum, J. R., Bowman, F., Collins, D., Klockow, D., Flagan, R. C., and Seinfeld, J. H.: <HOFFMANN1997_Article_FormationOfOrganicAerosolsFrom.pdf>, Journal of Atmospheric Chemistry, 26, 189-222, 10.1023/a:1005734301837, 1997.
Hohaus, T., Kuhn, U., Andres, S., Kaminski, M., Rohrer, F., Tillmann, R., Wahner, A., Wegener, R., Yu, Z., and Kiendler-Scharr, A.: A new plant chamber facility, PLUS, coupled to the atmosphere simulation chamber SAPHIR, Atmospheric Measurement Techniques, 9, 1247-1259, 10.5194/amt-9-1247-2016, 2016.
Hu, C.-j., Cheng, Y., Pan, G., Gai, Y.-b., Gu, X.-j., Zhao, W.-x., Wang, Z.-y., Zhang, W.-j., Chen, J., Liu, F.-y., Shan, X.-b., and Sheng, L.-s.: A Smog Chamber Facility for Qualitative and Quantitative Study on Atmospheric Chemistry and Secondary Organic Aerosol, Chinese Journal of Chemical Physics, 27, 631-639, 10.1063/1674-0068/27/06/631-639, 2014.
Huang, Y., Zhao, R., Charan, S. M., Kenseth, C. M., Zhang, X., and Seinfeld, J. H.: Unified Theory of Vapor–Wall Mass Transport in Teflon-Walled Environmental Chambers, Environmental Science & Technology, 52, 2134-2142, 10.1021/acs.est.7b05575, 2018.
Jayne, J. T., Leard, D. C., Zhang, X., Davidovits, P., Smith, K. A., Kolb, C. E., and Worsnop, D. R.: Development of an Aerosol Mass Spectrometer for Size and Composition Analysis of Submicron Particles, Aerosol Science and Technology, 33, 49-70, 10.1080/027868200410840, 2000.
Jenkin, M. E., Wyche, K. P., Evans, C. J., Carr, T., Monks, P. S., Alfarra, M. R., Barley, M. H., McFiggans, G. B., Young, J. C., and Rickard, A. R.: Development and chamber evaluation of the MCM v3.2 degradation scheme for β-caryophyllene, Atmospheric Chemistry and Physics Discussions, 12, 2891-2974, 10.5194/acpd-12-2891-2012, 2012.
Jimenez, J. L.: Ambient aerosol sampling using the Aerodyne Aerosol Mass Spectrometer, Journal of Geophysical Research, 108, 10.1029/2001jd001213, 2003.
Jimenez, J. L., Canagaratna, M. R., Donahue, N. M., Prevot, A. S., Zhang, Q., Kroll, J. H., DeCarlo, P. F., Allan, J. D., Coe, H., Ng, N. L., Aiken, A. C., Docherty, K. S., Ulbrich, I. M., Grieshop, A. P., Robinson, A. L., Duplissy, J., Smith, J. D., Wilson, K. R., Lanz, V. A., Hueglin, C., Sun, Y. L., Tian, J., Laaksonen, A., Raatikainen, T., Rautiainen, J., Vaattovaara, P., Ehn, M., Kulmala, M., Tomlinson, J. M., Collins, D. R., Cubison, M. J., Dunlea, E. J., Huffman, J. A., Onasch, T. B., Alfarra, M. R., Williams, P. I., Bower, K., Kondo, Y., Schneider, J., Drewnick, F., Borrmann, S., Weimer, S., Demerjian, K., Salcedo, D., Cottrell, L., Griffin, R., Takami, A., Miyoshi, T.,

Hatakeyama, S., Shimono, A., Sun, J. Y., Zhang, Y. M., Dzepina, K., Kimmel, J. R., Sueper, D., Jayne, J. T., Herndon, S. C., Trimborn, A. M., Williams, L. R., Wood, E. C., Middlebrook, A. M., Kolb, C. E., Baltensperger, U., and Worsnop, D. R.: Evolution of organic aerosols in the atmosphere, Science, 326, 1525-1529, 10.1126/science.1180353, 2009.

Karl, M., Brauers, T., Dorn, H. P., Holland, F., Komenda, M., Poppe, D., Rohrer, F., Rupp, L., Schaub, A., and Wahner, A.: Kinetic Study of the OH-isoprene and O3-isoprene reaction in the atmosphere simulation chamber, SAPHIR, Geophysical Research Letters, 31, n/a-n/a, 10.1029/2003gl019189, 2004.

Katsouyanni, K., Touloumi, G., Spix, C., Schwartz, J., Balducci, F., Medina, S., Rossi, G., Wojtyniak, B., Sunyer, J., Bacharova, L., Schouten, J. P., Ponka, A., and Anderson, H. R.: Short-term effects of ambient sulphur dioxide and particulate matter on mortality in 12 European cities: results from time series data from the APHEA project. Air Pollution and Health: a European Approach, BMJ, 314, 1658-1663, 10.1136/bmj.314.7095.1658, 1997.

Kostenidou, E., Kaltsonoudis, C., Tsiflikiotou, M., Louvaris, E., Russell, L. M., and Pandis, S. N.: Burning of olive tree branches: a major organic aerosol source in the Mediterranean, Atmos. Chem. Phys., 13, 8797-8811, 10.5194/acp-13-8797-2013, 2013.

Krechmer, J. E., Day, D. A., and Jimenez, J. L.: Always Lost but Never Forgotten: Gas-Phase Wall Losses Are Important in All Teflon Environmental Chambers, Environ Sci Technol, 54, 12890-12897, 10.1021/acs.est.0c03381, 2020.

Leone, J. A., Flagan, R. C., Grosjean, D., and Seinfeld, J. H.: An outdoor smog chamber and modeling study of toluene–NOx photooxidation, International Journal of Chemical Kinetics, 17, 177-216, https://doi.org/10.1002/kin.550170206, 1985.

Leskinen, A., Yli-Pirilä, P., Kuuspalo, K., Sippula, O., Jalava, P., Hirvonen, M. R., Jokiniemi, J., Virtanen, A., Komppula, M., and Lehtinen, K. E. J.: Characterization and testing of a new environmental chamber, Atmospheric Measurement Techniques, 8, 2267-2278, 10.5194/amt-8-2267-2015, 2015.

Liu, D., Whitehead, J., Alfarra, M. R., Reyes-Villegas, E., Spracklen, Dominick V., Reddington, Carly L., Kong, S., Williams, Paul I., Ting, Y.-C., Haslett, S., Taylor, Jonathan W., Flynn, Michael J., Morgan, William T., McFiggans, G., Coe, H., and Allan, James D.: Black-carbon absorption enhancement in the atmosphere determined by particle mixing state, Nature Geoscience, 10, 184-188, 10.1038/ngeo2901, 2017.

Lohmann, U. and Feichter, J.: Global indirect aerosol effects: a review, Atmospheric Chemistry and Physics, 5, 715-737, 10.5194/acp-5-715-2005, 2005.

Matsunaga, A. and Ziemann, P. J.: Gas-Wall Partitioning of Organic Compounds in a Teflon Film Chamber and Potential Effects on Reaction Product and Aerosol Yield Measurements, Aerosol Science and Technology, 44, 881-892, 10.1080/02786826.2010.501044, 2010.

McFiggans, G., Artaxo, P., Baltensperger, U., Coe, H., Facchini, M. C., Feingold, G., Fuzzi, S., Gysel, M., Laaksonen, A., Lohmann, U., Mentel, T. F., Murphy, D. M., O'Dowd, C. D., Snider, J. R., and Weingartner, E.: The effect of physical and chemical aerosol properties on warm cloud droplet activation, Atmos. Chem. Phys., 6, 2593-2649, 10.5194/acp-6-2593-2006, 2006.

McFiggans, G., Mentel, T. F., Wildt, J., Pullinen, I., Kang, S., Kleist, E., Schmitt, S., Springer, M., Tillmann, R., Wu, C., Zhao, D., Hallquist, M., Faxon, C., Le Breton, M., Hallquist, A. M., Simpson, D., Bergstrom, R., Jenkin, M. E., Ehn, M., Thornton, J. A., Alfarra, M. R., Bannan, T. J., Percival, C. J., Priestley, M., Topping, D., and Kiendler-Scharr, A.: Secondary organic aerosol reduced by mixture of atmospheric vapours, Nature, 565, 587-593, 10.1038/s41586-018-0871-y, 2019.

McMurry, P. H. and Grosjean, D.: Gas and aerosol wall losses in Teflon film smog chambers, Environ Sci Technol, 19, 1176-1182, 10.1021/es00142a006, 1985.
McMurry, P. H. and Rader, D. J.: Aerosol Wall Losses in Electrically Charged Chambers, Aerosol Science and Technology, 4, 249-268, 10.1080/02786828508959054, 1985.
Metzger, A., Dommen, J., Gaeggeler, K., Duplissy, J., Prevot, A. S. H., Kleffmann, J., Elshorbany, Y., Wisthaler, A., and Baltensperger, U.: Evaluation of 1,3,5 trimethylbenzene degradation in the detailed tropospheric chemistry mechanism, MCMv3.1, using environmental chamber data, Atmospheric Chemistry and Physics, 8, 6453-6468, 10.5194/acp-8-6453-2008, 2008.
Murphy, D. M., Cziczo, D. J., Froyd, K. D., Hudson, P. K., Matthew, B. M., Middlebrook, A. M., Peltier, R. E., Sullivan, A., Thomson, D. S., and Weber, R. J.: Single-particle mass spectrometry of tropospheric aerosol particles, Journal of Geophysical Research: Atmospheres, 111, https://doi.org/10.1029/2006JD007340, 2006.
Mutzel, A., Poulain, L., Berndt, T., Iinuma, Y., Rodigast, M., Böge, O., Richters, S., Spindler, G., Sipilä, M., Jokinen, T., Kulmala, M., and Herrmann, H.: Highly Oxidized Multifunctional Organic Compounds Observed in Tropospheric Particles: A Field and Laboratory Study, Environmental Science & Technology, 49, 7754-7761, 10.1021/acs.est.5b00885, 2015.
Nah, T., McVay, R. C., Pierce, J. R., Seinfeld, J. H., and Ng, N. L.: Constraining uncertainties in particle-wall deposition correction during SOA formation in chamber experiments, Atmospheric Chemistry and Physics, 17, 2297-2310, 10.5194/acp-17-2297-2017, 2017.
Ng, N. L., Kroll, J. H., Chan, A. W. H., Chhabra, P. S., Flagan, R. C., and Seinfeld, J. H.: Secondary organic aerosol formation from <i>m</i>-xylene, toluene, and benzene, Atmospheric Chemistry and Physics, 7, 3909-3922, 10.5194/acp-7-3909-2007, 2007.
Niedermeier, D., Voigtländer, J., Schmalfuß, S., Busch, D., Schumacher, J., Shaw, R. A., and Stratmann, F.: Characterization and first results from LACIS-T: a moist-air wind tunnel to study aerosol–cloud–turbulence interactions, Atmos. Meas. Tech., 13, 2015-2033, 10.5194/amt-13-2015-2020, 2020.
O'Meara, S. P., Xu, S., Topping, D., Alfarra, M. R., Capes, G., Lowe, D., Shao, Y., and McFiggans, G.: PyCHAM (v2.1.1): a Python box model for simulating aerosol chambers, Geosci. Model Dev., 14, 675-702, 10.5194/gmd-14-675-2021, 2021.
Odum, J. R., Hoffmann, T., Bowman, F., Collins, D., Flagan, R. C., and Seinfeld, J. H.: Gas/Particle Partitioning and Secondary Organic Aerosol Yields, Environ Sci Technol, 30, 2580–2585, https://doi-org.manchester.idm.oclc.org/10.1021/es950943+, 1996.
Pankow, J. F.: An absorption model of gas/particle partitioning of organic compounds in the atmosphere, Atmospheric Environment, 28, 185-188, 10.1016/1352-2310(94)90093-0, 1994a.
Pankow, J. F.: An absorption model of the gas/aerosol partitioning involved in the formation of secondary organic aerosol, Atmospheric Environment, 28, 189-193, 1994b.
Paulot, F., Crounse John, D., Kjaergaard Henrik, G., Kürten, A., St. Clair Jason, M., Seinfeld John, H., and Wennberg Paul, O.: Unexpected Epoxide Formation in the Gas-Phase Photooxidation of Isoprene, Science, 325, 730-733, 10.1126/science.1172910, 2009.
Paulsen, D., Dommen, J., Kalberer, M., Prevot, A. S., Richter, R., Sax, M., Steinbacher, M., Weingartner, E., and Baltensperger, U.: Secondary organic aerosol formation by irradiation of 1,3,5-trimethylbenzene-NOx-H2O in a new reaction chamber for atmospheric chemistry and physics, Environ Sci Technol, 39, 2668-2678, 10.1021/es0489137, 2005.
Pereira, K. L., Dunmore, R., Whitehead, J., Alfarra, M. R., Allan, J. D., Alam, M. S., Harrison, R. M., McFiggans, G., and Hamilton, J. F.: Technical note: Use of an atmospheric simulation chamber to investigate the effect of different engine conditions on unregulated VOC-IVOC diesel

exhaust emissions, Atmospheric Chemistry and Physics, 18, 11073-11096, 10.5194/acp-18-11073-2018, 2018.
Pierce, J. R., Engelhart, G. J., Hildebrandt, L., Weitkamp, E. A., Pathak, R. K., Donahue, N. M., Robinson, A. L., Adams, P. J., and Pandis, S. N.: Constraining Particle Evolution from Wall Losses, Coagulation, and Condensation-Evaporation in Smog-Chamber Experiments: Optimal Estimation Based on Size Distribution Measurements, Aerosol Science and Technology, 42, 1001-1015, 10.1080/02786820802389251, 2008.
Platt, S. M., El Haddad, I., Zardini, A. A., Clairotte, M., Astorga, C., Wolf, R., Slowik, J. G., Temime-Roussel, B., Marchand, N., Ježek, I., Drinovec, L., Močnik, G., Möhler, O., Richter, R., Barmet, P., Bianchi, F., Baltensperger, U., and Prévôt, A. S. H.: Secondary organic aerosol formation from gasoline vehicle emissions in a new mobile environmental reaction chamber, Atmospheric Chemistry and Physics, 13, 9141-9158, 10.5194/acp-13-9141-2013, 2013.
Pope, C. A., 3rd, Burnett, R. T., Thun, M. J., Calle, E. E., Krewski, D., Ito, K., and Thurston, G. D.: Lung cancer, cardiopulmonary mortality, and long-term exposure to fine particulate air pollution, JAMA, 287, 1132-1141, 10.1001/jama.287.9.1132, 2002.
Ren, Y., Grosselin, B., Daële, V., and Mellouki, A.: Investigation of the reaction of ozone with isoprene, methacrolein and methyl vinyl ketone using the HELIOS chamber, Faraday Discussions, 200, 289-311, 10.1039/C7FD00014F, 2017.
Rohrer, F., Bohn, B., Brauers, T., Brüning, D., Johnen, F. J., Wahner, A., and Kleffmann, J.: Characterisation of the photolytic HONO-source in the atmosphere simulation chamber SAPHIR, Atmospheric Chemistry and Physics, 5, 2189-2201, 10.5194/acp-5-2189-2005, 2005.
Saathoff, H., Naumann, K. H., Möhler, O., Jonsson, Å. M., Hallquist, M., Kiendler-Scharr, A., Mentel, T. F., Tillmann, R., and Schurath, U.: Temperature dependence of yields of secondary organic aerosols from the ozonolysis of <i>α</i>-pinene and limonene, Atmospheric Chemistry and Physics, 9, 1551-1577, 10.5194/acp-9-1551-2009, 2009.
Schnitzhofer, R., Metzger, A., Breitenlechner, M., Jud, W., Heinritzi, M., De Menezes, L. P., Duplissy, J., Guida, R., Haider, S., Kirkby, J., Mathot, S., Minginette, P., Onnela, A., Walther, H., Wasem, A., and Hansel, A.: Characterisation of organic contaminants in the CLOUD chamber at CERN, Atmospheric Measurement Techniques, 7, 2159-2168, 10.5194/amt-7-2159-2014, 2014.
Seakins, P. W.: A brief review of the use of environmental chambers for gas phase studies of kinetics, chemical mechanisms and characterisation of field instruments, EPJ Web of Conferences, 9, 143-163, 10.1051/epjconf/201009012, 2010.
Seinfeld, J. H. and Pandis, S. N.: Atmospheric Chemistry and Physics: From Air Pollution to Climate Change, John Wiley & Sons, Inc2016.
Smith, D. M., Fiddler, M. N., Sexton, K. G., and Bililign, S.: Construction and Characterization of an Indoor Smog Chamber for Measuring the Optical and Physicochemical Properties of Aging Biomass Burning Aerosols, Aerosol and Air Quality Research, 19, 467-483, 10.4209/aaqr.2018.06.0243, 2019.
Smith, H. J.: Nanoparticle growth in the CLOUD chamber, Science, 352, 1422-1422, 10.1126/science.352.6292.1422-a, 2016.
Stirnweis, L., Marcolli, C., Dommen, J., Barmet, P., Frege, C., Platt, S. M., Bruns, E. A., Krapf, M., Slowik, J. G., Wolf, R., Prévôt, A. S. H., Baltensperger, U., and El-Haddad, I.: Assessing the influence of NO_{<i>x</i>} concentrations and relative humidity on secondary organic aerosol yields from <i>α</i>-pinene photo-oxidation through smog chamber experiments and modelling calculations, Atmospheric Chemistry and Physics, 17, 5035-5061, 10.5194/acp-17-5035-2017, 2017.

Surratt, J. D., Chan, A. W. H., Eddingsaas, N. C., Chan, M., Loza, C. L., Kwan, A. J., Hersey, S. P., Flagan, R. C., Wennberg, P. O., and Seinfeld, J. H.: Reactive intermediates revealed in secondary organic aerosol formation from isoprene, Proceedings of the National Academy of Sciences, 107, 6640, 10.1073/pnas.0911114107, 2010.

Taylor, L., Reist, P. C., Boehlecke, B. A., and Jacobs, R. R.: Characterization of an aerosol chamber for human exposures to endotoxin, Appl Occup Environ Hyg, 15, 303-312, 10.1080/104732200301629, 2000.

Thornton, J. A., Shilling, J. E., Shrivastava, M., D'Ambro, E. L., Zawadowicz, M. A., and Liu, J.: A Near-Explicit Mechanistic Evaluation of Isoprene Photochemical Secondary Organic Aerosol Formation and Evolution: Simulations of Multiple Chamber Experiments with and without Added NOx, ACS Earth and Space Chemistry, 4, 1161-1181, 10.1021/acsearthspacechem.0c00118, 2020.

Tong, H., Lakey, P. S. J., Arangio, A. M., Socorro, J., Shen, F., Lucas, K., Brune, W. H., Poschl, U., and Shiraiwa, M.: Reactive Oxygen Species Formed by Secondary Organic Aerosols in Water and Surrogate Lung Fluid, Environ Sci Technol, 52, 11642-11651, 10.1021/acs.est.8b03695, 2018.

Trump, E. R., Epstein, S. A., Riipinen, I., and Donahue, N. M.: Wall effects in smog chamber experiments: A model study, Aerosol Science and Technology, 50, 1180-1200, 10.1080/02786826.2016.1232858, 2016.

Turpin, B. J. and Huntzicker, J. J.: Secondary formation of organic aerosol in the Los Angeles basin: A descriptive analysis of organic and elemental carbon concentrations, Atmospheric Environment. Part A. General Topics, 25, 207-215, 10.1016/0960-1686(91)90291-e, 1991.

Turpin, B. J. and Huntzicker, J. J.: Identification of secondary organic aerosol episodes and quantitation of primary and secondary organic aerosol concentrations during SCAQS, Atmospheric Environment, 29, 3527-3544, 10.1016/1352-2310(94)00276-q, 1995.

Verheggen, B. and Mozurkewich, M.: An inverse modeling procedure to determine particle growth and nucleation rates from measured aerosol size distributions, Atmos. Chem. Phys., 6, 2927-2942, 10.5194/acp-6-2927-2006, 2006.

Voliotis, A., Wang, Y., Shao, Y., Du, M., Bannan, T. J., Percival, C. J., Pandis, S. N., Alfarra, M. R., and McFiggans, G.: Exploring the composition and volatility of secondary organic aerosols in mixed anthropogenic and biogenic precursor systems, Atmos. Chem. Phys., 21, 14251-14273, 10.5194/acp-21-14251-2021, 2021.

Wagner, R., Bunz, H., Linke, C., Möhler, O., Naumann, K.-H., Saathoff, H., Schnaiter, M., and Schurath, U.: Chamber Simulations of Cloud Chemistry: The AIDA Chamber, Dordrecht, 67-82,

Wagner, R., Yan, C., Lehtipalo, K., Duplissy, J., Nieminen, T., Kangasluoma, J., Ahonen, L. R., Dada, L., Kontkanen, J., Manninen, H. E., Dias, A., Amorim, A., Bauer, P. S., Bergen, A., Bernhammer, A.-K., Bianchi, F., Brilke, S., Mazon, S. B., Chen, X., Draper, D. C., Fischer, L., Frege, C., Fuchs, C., Garmash, O., Gordon, H., Hakala, J., Heikkinen, L., Heinritzi, M., Hofbauer, V., Hoyle, C. R., Kirkby, J., Kürten, A., Kvashnin, A. N., Laurila, T., Lawler, M. J., Mai, H., Makhmutov, V., Mauldin Iii, R. L., Molteni, U., Nichman, L., Nie, W., Ojdanic, A., Onnela, A., Piel, F., Quéléver, L. L. J., Rissanen, M. P., Sarnela, N., Schallhart, S., Sengupta, K., Simon, M., Stolzenburg, D., Stozhkov, Y., Tröstl, J., Viisanen, Y., Vogel, A. L., Wagner, A. C., Xiao, M., Ye, P., Baltensperger, U., Curtius, J., Donahue, N. M., Flagan, R. C., Gallagher, M., Hansel, A., Smith, J. N., Tomé, A., Winkler, P. M., Worsnop, D., Ehn, M., Sipilä, M., Kerminen, V.-M., Petäjä, T., and Kulmala, M.: The role of ions in new particle formation in the CLOUD chamber, Atmospheric Chemistry and Physics, 17, 15181-15197, 10.5194/acp-17-15181-2017, 2017.

Wang, J., Doussin, J. F., Perrier, S., Perraudin, E., Katrib, Y., Pangui, E., and Picquet-Varrault, B.: Design of a new multi-phase experimental simulation chamber for atmospheric photosmog,

aerosol and cloud chemistry research, Atmospheric Measurement Techniques, 4, 2465-2494, 10.5194/amt-4-2465-2011, 2011.
Wang, M., Kong, W., Marten, R., He, X. C., Chen, D., Pfeifer, J., Heitto, A., Kontkanen, J., Dada, L., Kurten, A., Yli-Juuti, T., Manninen, H. E., Amanatidis, S., Amorim, A., Baalbaki, R., Baccarini, A., Bell, D. M., Bertozzi, B., Brakling, S., Brilke, S., Murillo, L. C., Chiu, R., Chu, B., De Menezes, L. P., Duplissy, J., Finkenzeller, H., Carracedo, L. G., Granzin, M., Guida, R., Hansel, A., Hofbauer, V., Krechmer, J., Lehtipalo, K., Lamkaddam, H., Lampimaki, M., Lee, C. P., Makhmutov, V., Marie, G., Mathot, S., Mauldin, R. L., Mentler, B., Muller, T., Onnela, A., Partoll, E., Petaja, T., Philippov, M., Pospisilova, V., Ranjithkumar, A., Rissanen, M., Rorup, B., Scholz, W., Shen, J., Simon, M., Sipila, M., Steiner, G., Stolzenburg, D., Tham, Y. J., Tome, A., Wagner, A. C., Wang, D. S., Wang, Y., Weber, S. K., Winkler, P. M., Wlasits, P. J., Wu, Y., Xiao, M., Ye, Q., Zauner-Wieczorek, M., Zhou, X., Volkamer, R., Riipinen, I., Dommen, J., Curtius, J., Baltensperger, U., Kulmala, M., Worsnop, D. R., Kirkby, J., Seinfeld, J. H., El-Haddad, I., Flagan, R. C., and Donahue, N. M.: Rapid growth of new atmospheric particles by nitric acid and ammonia condensation, Nature, 581, 184-189, 10.1038/s41586-020-2270-4, 2020.
Wang, N., Jorga, S. D., Pierce, J. R., Donahue, N. M., and Pandis, S. N.: Particle wall-loss correction methods in smog chamber experiments, Atmospheric Measurement Techniques, 11, 6577-6588, 10.5194/amt-11-6577-2018, 2018.
Wang, X., Liu, T., Bernard, F., Ding, X., Wen, S., Zhang, Y., Zhang, Z., He, Q., Lü, S., Chen, J., Saunders, S., and Yu, J.: Design and characterization of a smog chamber for studying gas-phase chemical mechanisms and aerosol formation, Atmospheric Measurement Techniques, 7, 301-313, 10.5194/amt-7-301-2014, 2014.
Wang, Y., Voliotis, A., Shao, Y., Zong, T., Meng, X., Du, M., Hu, D., Chen, Y., Wu, Z., Alfarra, M. R., and McFiggans, G.: Secondary organic aerosol phase behaviour in chamber photo-oxidation of mixed precursors, Atmos. Chem. Phys. Discuss., 2021, 1-25, 10.5194/acp-2021-105, 2021.
Wyche, K. P., Monks, P. S., Smallbone, K. L., Hamilton, J. F., Alfarra, M. R., Rickard, A. R., McFiggans, G. B., Jenkin, M. E., Bloss, W. J., Ryan, A. C., Hewitt, C. N., and MacKenzie, A. R.: Mapping gas-phase organic reactivity and concomitant secondary organic aerosol formation: chemometric dimension reduction techniques for the deconvolution of complex atmospheric data sets, Atmos. Chem. Phys., 15, 8077-8100, 10.5194/acp-15-8077-2015, 2015.
Wyche, K. P., Ryan, A. C., Hewitt, C. N., Alfarra, M. R., McFiggans, G., Carr, T., Monks, P. S., Smallbone, K. L., Capes, G., Hamilton, J. F., Pugh, T. A. M., and MacKenzie, A. R.: Emissions of biogenic volatile organic compounds and subsequent photochemical production of secondary organic aerosol in mesocosm studies of temperate and tropical plant species, Atmospheric Chemistry and Physics, 14, 12781-12801, 10.5194/acp-14-12781-2014, 2014.
Ye, P., Ding, X., Hakala, J., Hofbauer, V., Robinson, E. S., and Donahue, N. M.: Vapor wall loss of semi-volatile organic compounds in a Teflon chamber, Aerosol Science and Technology, 50, 822-834, 10.1080/02786826.2016.1195905, 2016.
Zhang, Q., Jimenez, J. L., Canagaratna, M. R., Allan, J. D., Coe, H., Ulbrich, I., Alfarra, M. R., Takami, A., Middlebrook, A. M., Sun, Y. L., Dzepina, K., Dunlea, E., Docherty, K., DeCarlo, P. F., Salcedo, D., Onasch, T., Jayne, J. T., Miyoshi, T., Shimono, A., Hatakeyama, S., Takegawa, N., Kondo, Y., Schneider, J., Drewnick, F., Borrmann, S., Weimer, S., Demerjian, K., Williams, P., Bower, K., Bahreini, R., Cottrell, L., Griffin, R. J., Rautiainen, J., Sun, J. Y., Zhang, Y. M., and Worsnop, D. R.: Ubiquity and dominance of oxygenated species in organic aerosols in anthropogenically-influenced Northern Hemisphere midlatitudes, Geophysical Research Letters, 34, https://doi.org/10.1029/2007GL029979, 2007.

Zhang, X., Cappa, C. D., Jathar, S. H., McVay, R. C., Ensberg, J. J., Kleeman, M. J., and Seinfeld, J. H.: Influence of vapor wall loss in laboratory chambers on yields of secondary organic aerosol, Proc Natl Acad Sci U S A, 111, 5802-5807, 10.1073/pnas.1404727111, 2014.

[BLANK PAGE]

Paper2: Chamber investigation of the formation and transformation of secondary organic aerosol in mixtures of biogenic and anthropogenic volatile organic compounds

This paper is currently under review in the journal of "Atmospheric Chemistry and Physics" and can be found on: https://acp.copernicus.org/preprints/acp-2021-1080/

Aristeidis Voliotis[1,*], Mao Du[1,*], Yu Wang[1,*], Yunqi Shao[1,*], M. Rami Alfarra[1,2,‡], Thomas J. Bannan[1], Dawei Hu[1], Kelly L. Pereira[3], Jaqueline F. Hamilton[3], Mattias Hallquist[4], Thomas F. Mentel[5], Gordon McFiggans[1]

[1]Centre for Atmospheric Science, Department of Earth and Environmental Sciences, School of Natural Sciences, University of Manchester, Manchester, M13 9PL, UK

[2]National Centre for Atmospheric Science (NCAS), University of Manchester, Manchester, M13 9PL, UK

[3]Wolfson Atmospheric Chemistry Laboratories, Department of Chemistry, University of York, York, YO10 5DD, UK

[4]Department of Chemistry and Molecular Biology, Atmospheric Science, University of Gothenburg, Gothenburg SE-412 96, Sweden

[5]Institut für Energie und Klimaforschung, IEK-8, Forschungszentrum Jülich, Jülich, Germany

‡ now at Environment & Sustainability Center, Qatar Environment & Energy Research Institute, Doha, Qatar

* these authors all made equal contribution to the work and manuscript

Correspondence to: *g.mcfiggans@manchester.ac.uk*

Abstract. A comprehensive investigation of the photochemical secondary organic aerosol (SOA) formation and transformation in mixtures of anthropogenic (o-cresol) and biogenic (α-pinene and isoprene) volatile organic compound (VOC) precursors in the presence of NOx and inorganic seed particles was conducted. Initial iso-reactivity was used to enable direct comparison across systems, adjusting the initial reactivity of the systems towards the assumed dominant oxidant (OH). Comparing experiments conducted in single precursor systems at various initial reactivity levels

(referenced to a nominal base case VOC reactivity) and their binary and ternary mixtures, we show that the molecular interactions from the mixing of the precursors can be investigated and discuss limitations in their interpretation. The observed average SOA yields in descending order were found for the α-pinene (32±7%), α-pinene/o-cresol (28±9%), α-pinene at ½ initial reactivity (21±5%), α-pinene/isoprene (16±1%), α-pinene at ⅓ initial reactivity (15±4%), o-cresol (13±3%), α-pinene/o-cresol/isoprene (11±4%), o-cresol at ½ initial reactivity (11±3%), o-cresol/isoprene (6±2%) and isoprene systems (0±0%). We find a clear suppression of the SOA yield from α-pinene when it is mixed with isoprene, whilst the addition of isoprene to o-cresol may enhance the mixture's SOA formation potential, however, the difference was too small to be unequivocal. The α-pinene/o-cresol system yield appeared to be increased compared to that calculated based on the additivity, whilst in the α-pinene/o-cresol/isoprene system the measured and predicted yield were comparable. However, in mixtures where more than one precursor contributes to the SOA mass it is unclear whether changes in the SOA formation potential are attributable to physical or chemical interactions, since the reference basis for the comparison is complex. Online and offline chemical composition and SOA particle volatility, water uptake and "phase" behaviour measurements that were used to interpret the SOA formation and behaviour are introduced and detailed elsewhere.

1. Introduction

The fine fraction of particulate matter (PM) plays the dominant role in the impact of air pollution on human health and of aerosol on climate through direct radiative effects and cloud adjustments. Ambient $PM_{2.5}$ was the fifth-ranking global mortality risk factor in 2015, with exposure to it causing 4.2 million deaths and 103.1 million disability-adjusted life-years (DALYs), 7.6% of total global deaths and 4.2% of global DALYs (Cohen et al., 2017). Moreover, fine PM is responsible for the aerosol effects that make the single greatest contributory uncertainty to radiative forcing (IPCC, 2013).

Organic material makes a major contribution to the mass of fine PM in the atmosphere (Jimenez et al., 2009) and secondary organic aerosol (SOA) is the major contributor (Hallquist et al., 2009). Nonetheless, our ability to predict the atmospheric burden and hence impacts of fine secondary aerosol particles (Kanakidou et al., 2005; Tsigaridis and Kanakidou, 2018) has been limited by basic understanding of the formation of this organic component (Hallquist et al., 2009).

Photochemistry dictates the levels of NO_2, O_3 and the SOA fraction of PM. Whilst it is relatively straightforward to understand and control primary pollutants, these secondary pollutants make a substantial contribution to air quality degradation that are set to become increasingly important as primary pollutants are cleaned up. However, understanding the rate and extent of SOA formation in the real atmosphere presents a number of challenges. There are tens of thousands of isolated organic compounds in the atmosphere, ranging across more than 12 orders of magnitude in volatility (Goldstein and Galbally, 2007) with possible oxidation products running to many millions (Aumont et al., 2005). They have extensive biogenic and anthropogenic sources and are spatially heterogeneous. Their reactivity ranges over many orders of magnitude and their lifetimes at ambient oxidant levels consequently range from less than a second to several years. An unknown but substantial proportion of the organic compounds have the potential to act as SOA precursors and the degree to which this is influenced by the complex atmospheric mixture is unclear.

It has long been established that prediction of the formation of secondary gaseous pollutants in the troposphere requires knowledge of the nature of the mixture of volatile organic compounds (VOC), their abundance and the chemical regime (e.g. VOC : NO_x ratio) and airmass history. In contrast, the formation of SOA in the real atmosphere is conventionally considered less mechanistically. Against the backdrop of the near unimaginable complexity of the atmospheric mixture of SOA precursors, the basis for our understanding of SOA formation has been primarily derived from experimental investigations of single component systems (Thornton et al., 2020; Donahue et al., 2012; Jenkin et al., 2012). A wealth of literature derived from chamber experiments on biogenic (Thornton et al., 2020; Carlton et al., 2009) and anthropogenic (Schwantes et al., 2017; Nakao et al., 2012) precursors under a range of chemical environments combined with fundamental kinetic studies (Ziemann and Atkinson, 2012; Cash et al., 2016) has enabled numerous representations of atmospheric SOA at varying levels of detail (Shrivastava et al., 2017; Charan et al., 2019). There have additionally been studies of SOA formation in source-oriented mixtures from diesel (Weitkamp et al., 2007; Nakao et al., 2011) and gasoline (Nordin et al., 2013; Platt et al., 2013) exhaust, woodburning (Tiitta et al., 2016), cooking (Reyes-Villegas et al., 2018; Kaltsonoudis et al., 2017) and from macroalgal (McFiggans et al., 2004) and plant (Joutsensaari et al., 2005; VanReken et al., 2006; Pinto et al., 2007; Mentel et al., 2009; Hao et al., 2009; Wyche et al., 2014) emissions. Building on a well-established framework first suggested by Pankow (1994) to account for absorptive partitioning of mixtures of organic components in the atmosphere, attempts have

been made to provide empirically constrained and mechanistically augmented conceptual frameworks of organic aerosol (Donahue et al., 2006; Donahue et al., 2011; Schervish and Donahue, 2020), but there is currently no universally accepted mechanistic basis for SOA understanding in the complex atmosphere.

Evidence suggests that it is necessary to take a more mechanistic approach in order to capture observed behaviour of SOA formation in mixtures. It was established that the scavenging of the OH radical by addition of isoprene significantly inhibits new particle formation in plant chamber studies (Kiendler-Scharr et al., 2009), though the atmospheric implication was questioned by Berndt et al. (2018) since OH will likely not be controlled by isoprene. More recent studies have indicated that the mass and yield of SOA formed from individual precursors may similarly be influenced by the presence of other VOC (McFiggans et al., 2019). In addition to the observed suppression of particle mass and yield from α-pinene being attributed to the established scavenging of oxidant by the lower SOA yield isoprene, it was found that the C_5 peroxy radical isoprene oxidation products scavenged highly oxygenated C_{10} peroxy radicals that would otherwise form extremely low volatility condensable compounds. This had also been reported by Berndt et al. (2018) who demonstrated a similar scavenging of C_{10} radical products in the presence of ethylene. McFiggans et al. (2019) further reported such product scavenging and consequent reduction in α-pinene SOA yield by CO and CH_4. Such interactions should be no surprise, given our understanding of peroxy radical cross reactions and termination fates in controlling production of secondary gaseous pollutants. Moreover, the existence of such interactions in mixtures is somewhat obvious in the light of the understanding that has emerged over recent years (e.g., Bianchi et al., 2019) of the roles of atmospheric autoxidation of VOC producing highly oxygenated organic molecules (HOM). Following the early postulations of the role of autoxidation in atmospheric VOC degradation (Crounse et al., 2013), the importance of HOM in SOA formation has been widely established and quantified in monoterpene oxidation (Ehn et al., 2012; Ehn et al., 2014; Jokinen et al., 2015; Berndt et al., 2016; Berndt et al., 2018; Bianchi et al., 2019). The termination of the RO_2 formed via autoxidation ("HOM-RO_2") will depend on the chemical conditions (the abundance of NO_x, HO_2 and the numerous other RO_2 species present in the mixture) as well as the formation rate of the HOM-RO_2. Schervish and Donahue (2020) provide a discussion of the determinants of the fate of HOM-RO_2 and potential consequences on the distribution of low, extremely low and ultra-low volatility organic compound (LVOC, ELVOC and ULVOC

respectively) products and hence on SOA formation in α-pinene oxidation. Autoxidation is widespread and common and, in atmospheric systems, is unlikely to be restricted to monoterpenes (though unsaturated compounds may be expected to be more susceptible). Indeed, the application of recently developed mass spectrometric techniques has revealed the presence of HOM in the oxidation of aromatic compounds (Wang et al., 2017; Wang et al., 2020; Molteni et al., 2018; Tsiligiannis et al., 2019; Garmash et al., 2020; Mehra et al., 2020; Priestley et al., 2021). The degree to which the HOM distribution results from direct autoxidation or from multigenerational pathways is unclear, though the prevalence of HOM-RO_2 during aromatic oxidation is clear. The attention on aromatic compounds has been driven by their relevance as anthropogenic VOC emissions, making significant manmade contributions to the VOC burden in the polluted troposphere. Given the prevalence and diversity of autoxidation mechanisms, it is probable that HOM would be detected on the application of modern mass spectrometry to the investigation of many classes of atmospheric VOC. The recent focus on interactions via autoxidation in mixtures has added to more well-established mechanistic linkages in the oxidation of VOCs for understanding gas phase photochemistry. The implications on production of aerosol particle precursors are less well studied. Since the fractional contribution of HOM to particle mass is unclear, the role of autoxidation and influences of interactions on the HOM contributions to SOA mass formation in mixtures is unquantified. It is therefore important to additionally maintain a focus on influences of the non-HOM components on SOA formation in oxidation of VOC mixtures.

Given the potential diversity in VOC sources contributing to the pollutant mixture in the ambient atmosphere, it is important to establish the experimental basis for an understanding of SOA formation beyond the recently studied "simple" biogenic mixed systems (Berndt et al., 2018; McFiggans et al., 2019; Shilling et al., 2019). The importance of establishing a framework to understand interactions in systems of mixed anthropogenic and biogenic VOC stretches well beyond speculative curiosity. Such a framework may be a key to explaining observed non-linearities when natural and manmade pollution mixes (Spracklen et al., 2011; Emanuelsson et al., 2013). Using such considerations as motivation, a series of experiments was conceived to explore SOA formation from typical biogenic and anthropogenic VOC precursors and their binary and ternary mixtures. The binary α-pinene/isoprene system reported elsewhere was used as a biogenic mixture with established mechanistic interactions in its photo-oxidation. *o*-cresol was chosen as a representative anthropogenic VOC, being both emitted as a primary pollutant and formed through

oxidation of other aromatic compounds. The construction of the study is detailed in the methodology section below. The experiments were conducted in the 18m^3 Manchester Aerosol Chamber (MAC), a photochemical chamber operating in batch mode. The design of experiments on mixed VOCs is complex and requires consideration of aspects not encountered in single VOC experiments. This paper explores many of these elements and associated challenges with a view to inform best practice in their planning and executions. The objectives were broad and diverse and aimed to:

i) establish the suitability of the experimental design for investigating SOA formation in VOC mixtures;

ii) establish the suitability of conventionally reported metrics such as SOA mass yield for quantifying SOA formation in VOC mixtures;

iii) using these metrics, quantify any interactions in VOC mixtures leading to changes in the SOA formation from that may be expected based on single precursor experiments;

iv) using a suite of online and offline measurements of chemical and physical properties, to probe the chemistry and physics leading to these interactions and the properties of particles resulting from them, of potential atmospheric significance.

This paper will address the first three of these and provide an introduction to the findings related to the fourth, which will be detailed in a number of companion manuscripts. It is envisaged that the programme will act as a springboard to investigate the detailed mechanisms of interactions in mixtures of VOC involved in ambient SOA formation.

Importantly, this paper aims to explore whether SOA experiments using multiple VOC precursors can reveal aspects of the multiphase atmospheric systems inaccessible to experiments using a single precursor species.

2. Experimental design

The mixture of atmospheric VOCs and variability in prevailing oxidising environment is so complex that the choice of precursors, concentrations and experimental conditions makes a comprehensive programme intractable. Besides challenges associated with representativeness of

atmospheric complexity and concentrations in the multiphase system, numerous infrastructural considerations and measurement challenges must be considered. There are additional conflicts in the requirements needed to fully address specific objectives of the study. In this section, these criteria and the bounds placed on the study are addressed and the approaches to experimental design in response to these restrictions and requirements are discussed along with the choices made. Finally, the capabilities and likely consequences and compromises inherent in these choices are listed, before outlining the methodology employed.

2.1. VOC mixture and oxidant "representativeness"

Of the tens of thousands (or perhaps millions) of atmospheric organic compounds present in the vapour phase, only a handful have been studied in previous chamber SOA experiments and fewer in mixtures. The selection of compounds for the study of mixed SOA precursors is simultaneously simple and complex; simple, insofar as study of a random mixture will yield novel results, but complex, in that care is required to maximise their importance. Disregarding chlorine atoms and the Criegee radicals as "exotic", the dominant oxidants at night are the nitrate radical (NO_3) and ozone and during the day, the hydroxyl radical (OH) and ozone. Whilst arguments (such as likely / possible dominance of daytime oxidising capacity and pathways to SOA over night-time) can be used to select the oxidant combination of interest, this is fairly arbitrary and open, and we have selected daytime oxidation conditions for the present study.

Similarly arbitrary is the selection of NO_x regime. Whilst VOC:NO_x ratio dependence of SOA formation from some precursors has been well studied (e.g. Pullinen et al. 2020), this is not the case for mixtures of VOC. It is established for certain systems that SOA formation pathways in low and high NO_x regimes change dramatically and consequently influence SOA particle mass yield (e.g. Sarrafzadeh et al. 2016). Challenges associated with the comparability of experimental configurations and conditions lead to apparently conflicting findings and controversies remain surrounding the influence of NOx on SOA formation, requiring unambiguous mechanistic resolution. Truly low NO_x regimes probably do not occur widely in the ambient atmosphere, at least not in the perturbed northern hemisphere. Moreover, in light of selection (see below) of an anthropogenic SOA precursor in the mixture, it would be unreasonable to expect there to be a complete absence of NO_x. For reasons outlined below (sections 2.4 and 2.5) related to the chosen

concentrations and contributions to reactivity, this study uses moderate VOC:NO_x ratios (between roughly 3 and 8) broadly corresponding to a perturbed background chemical regime.

The reactivity of gaseous VOCs towards ambient oxidants spans several orders of magnitude and the ratio of reactivity towards each oxidant varies substantially. In particular, reactivity towards ozone will be negligible for saturated VOCs but can lead to lifetimes of a few minutes for reactive sesquiterpenes. In order for each VOC in a mixture to contribute significantly to the distribution of oxidation products in a chamber experiment and thereby influence the pathways to, and potential for, SOA formation, it is desirable for them to have comparable reactivity towards the available oxidants. In such a mixture, similar concentrations of each VOC might be reasonably expected to provide a comparable rate of change of oxidation products into the mix and hence contribute to SOA production pathways. Our approach to this is outlined in section 2.4.

As with reactivity, the SOA particle formation potential of VOCs can vary widely, from unmeasurably low to having particle mass yields of several tens of percent. Intuitively, the presence of a higher yield VOC might be expected to contribute more mass than a lower yield VOC and consequently increase the yield of the mixture. What is less clear is the degree to which a lower yield component might reduce the yields of a higher yield VOC and vice versa – i.e. how strongly is the chemistry coupled and how do such interactions influence SOA particle formation? More fundamentally, the reference for and calculation of yields in VOC mixtures is a challenge depending on the often arbitrary selected definition (see results and discussion sections 4 and 5).

A final consideration is the sort of atmosphere that the experiment aims to represent. McFiggans et al (2019), in their choice of α-pinene and isoprene, have looked at binary mixtures of abundant biogenically-emitted VOCs (as did Jaoui and Kamens, 2003, previously, in looking at mixtures of α- and β-pinene). Much of the global atmosphere is perturbed by anthropogenic pollutants and contributions from natural and manmade sources at any location or time will depend upon the mixture and strength of, and distance from, upwind sources (amongst a multitude of other factors). This study builds on previous insight from the binary mixture of low and high yield biogenic SOA precursors to add a moderate yield anthropogenic VOC. Studies could equally be focused on a range of high, low or moderate SOA yield manmade VOCs or numerous other combinations. Indeed, such extension and broadening of the current approach will be of substantial interest.

2.2. Infrastructural and instrumentational considerations

This study employs a mixture of VOCs as SOA precursors – i.e. compounds almost entirely in the vapour phase under normal temperate surface atmospheric conditions. This straightforwardly takes advantage of the heated glass bulb arrangement in the MAC for the injection of small amounts of liquid organic components and enables comparability with other studies using conventional SOA precursors. Future work could readily use materials from solid stock for studies of "unconventional" SOA precursors that have had much recent attention, such as those falling into the intermediate volatility (IVOC) and semi-volatile (SVOC) classes.

All experiments employed ammonium sulphate seed particles. This was primarily to enable greater reproducibility by providing sufficient particulate mass to act as a condensation sink for partitioning compounds, suppressing nucleation and its attendant stochastic elements. In chamber experiments, there is a competition for condensable vapours between the walls and any existing particles such that seeded experiments enable earlier formation of SOA particle mass. Moreover, detection of this particle mass, and determination of their composition and properties is more straightforward with instruments that require particles to be greater than a certain size. Whilst we previously pioneered the technique of generation of SOA particle seeds for use in chamber experiments (Hamilton et al., 2011), use of ammonium sulphate avoids the additional complication of the chemistry by residual VOC oxidation products. Ammonium sulphate is nebulised into a stainless-steel retaining drum prior to entrainment into the final fill cycle for the experiment (see methods section 3, below). It is recognised that inorganic seeds may not present the most effective absorptive medium for condensational uptake of organic vapours, but the seed generation process is highly reproducible and an implicit assumption of the likelihood of comparable efficiency as an absorptive medium across the systems of choice is made. Acidic seeds are not accessible in the MAC, because uptake of background ambient NH_3 leads to neutralisation of H^+ at any reasonable seed mass loading.

Instrumental detection limits and sampling requirements dictate the accessible range of concentrations for the experiments (see table 2). State-of-the-science sampling and measurement techniques are employed throughout. Many are capable of very high precision and time resolution measurement at low concentrations. Some are capable of single particle detection or particle ensemble measurement by number concentration. Most of the approaches employ online, or semi-

continuous, operation and low concentrations could be readily accommodated by increasing instrument integration times. Filters are collected for molecular determination of SOA particle composition by the evacuation of the entire chamber through pre-fired quartz filters (section 3). Collection of sufficient mass provides a lower limit to the mass concentration loadings and dictates moderately high injected VOC concentration (dependent on the particle mass yield of the mixture). The consequences of higher-than-ambient VOC and PM mass loadings are discussed in section 5.

Very low NO_x studies are not accessible in the MAC, owing to variable and sometimes elevated NO_x concentrations in our chamber laboratory in the centre of Manchester. Such conditions limit the ability of our Purafil scrubber to completely remove NO_x at our high inlet flow and may potentially lead to the increase in NO_x by diffusion through the Teflon film. Such effects would be non-negligible when attempting sub-ppbv NO_x experiments but present modest challenges at higher NO_x conditions, unnoticeable under the chosen VOC concentrations and moderate VOC:NO_x ratios of the current programme.

The chemical conditions in all experiments were controlled by photo-oxidation under a simulated solar spectrum at moderate VOC:NO_x ratio, with NO_x injected as NO_2. In all experiments, neutral ammonium sulphate was injected to provide a condensation sink sufficiently large to compete effectively with the wall for condensable vapours. Table 1 shows the initial conditions of all experiments.

2.3. Ideal, desirable and realistic objectives

It is not the intention to quantitatively establish the extent and nature of interactions between VOC precursors in the photochemical processes leading to SOA particle formation in ambient mixtures and the consequent impacts on SOA composition and properties in the real atmosphere. The VOC mixtures and set of experimental conditions is a small sample across a large chemical and physical space. The current programme aims to reveal examples of the behaviours in mixed systems and provide indicative quantifications of potential interactions and consequences. A focus is placed on the physical properties and chemical composition of the evolving particle distribution throughout the photochemistry driving its formation and transformation. Less emphasis is placed on the

quantification of the radical chemistry and oxidative environment although some characterisation of the transformations of the oxidation products in the gas phase and their influence on the particle formation is attempted. The experimental design and instrumentational payload are used so far as possible to contribute to addressing the objectives outlined in section 1.

Table 1: List of initial experimental conditions for all the experiments in the campaign.

Exp. No	Exp. Type	VOC	NOx (ppb)	VOC (ppb)[a]	VOC/NOx (ppb/ppb)	Seed (µg m^{-3})	SOA mass (µg m^{-3})
	Single						
1		α-pinene	40	309	7.7	72.6	273.2
2		α-pinene	43	309	7.2	67.6	283.1
3		α-pinene	50	309	6.2	39.4	-
4		α-pinene	26	155	6.0	45.7	68.6
5		α-pinene	35	155	4.4	47.8	109.5
6		α-pinene	18	103	5.7	51.0	31.5
7		o-cresol	98	400	4.1	50.8	28.2
8		o-cresol	44	400	9.1	47.8	56.0
9		o-cresol	71	400	5.6	36.0	-
10		o-cresol	40	200	5.0	51.3	22.8
11		isoprene	24	164	6.8	64.1	0.0
12		isoprene	23	164	7.1	101.9	0.0
13		isoprene	14	55	3.9	42.2	0.0
	Binary						
14		o-cresol/isoprene	34	282 (200/82)	8.3	49.6	11.2
15		o-cresol/isoprene	-	282 (200/82)	-	57.0	9.4
16		α-pinene/o-cresol	52	355 (155/200)	6.8	48.3	122.3
17		α-pinene/o-cresol	65	355 (155/200)	5.5	72.9	-
18		α-pinene/o-cresol	-	355 (155/200)	-	42.5	130.1
19		α-pinene/isoprene	33	237 (155/82)	7.2	63.7	96.6
20		α-pinene/isoprene	39	237 (155/82)	6.1	62.0	100.9
21		α-pinene/isoprene	24	237 (155/82)	9.9	50.5	75.2
	Ternary						
22		α-pinene/o-cresol/isoprene	80	291 (103/133/55)	3.6	45.6	55.5
23		α-pinene/o-cresol/isoprene	60	291 (103/133/55)	4.9	49.0	51.4
24		α-pinene/o-cresol/isoprene	78	291 (103/133/55)	3.7	45.8	58.0

[a]All nominal reported initial VOC concentrations have a ± 15% measurement uncertainty. The individual VOC concentration in the binary and ternary mixtures shown in brackets correspond to the precursor VOC listing. A dash indicates missing data owing to instrument problems.

2.4. Concept behind the experimental design

Taking into account the constraints and challenges outlined above, the programme was constructed to investigate a single ternary system comprising one anthropogenic and two biogenic VOCs. The biogenic VOCs were chosen as *α*-pinene and isoprene to enable comparison of batch reactor experiments with previous flowtube (Berndt et al., 2018), well-mixed continuously stirred tank reactor (McFiggans et al., 2019) or flow-through chamber studies (Shilling et al., 2019). The anthropogenic aromatic OVOC *o*-cresol was chosen for its fairly rapid rate constant with OH (4.1 x 10^{-11} $cm^3molec^{-1}s^{-1}$), such that it would exhibit comparable reactivity towards OH as a similar concentration of *α*-pinene or isoprene. A concept of "initial isoreactivity" towards OH was employed to select ratios of the initial concentrations of the VOCs. This meant that the initial mixing ratios were injected at an *α*-pinene : isoprene : *o*-cresol ratio of 309 : 164 : 400 based on the ratios of the inverse of their IUPAC-recommended rate constants at 298K (Atkinson et al., 2006; Mellouki et al., 2021). In order to construct a systematic investigation of the single precursor, binary and ternary mixtures, individual VOC experiments were conducted at full-, half- and third-reactivity for comparison of SOA particle mass, composition and properties. Using previously reported values for the SOA particle mass yields, it was expected that an initial full-reactivity mixing ratio in the 100s ppbv range would provide the 10 to a few 100 μgm^{-3} required to provide enough particle mass on the filter at the end of an experiment (at a final chamber volume of around 10 m^3) for molecular characterisation.

2.5. Compromises in the experimental plan and consequences

OH is only one of the likely oxidants under the chosen photo-oxidation conditions, and the unsaturated biogenic compounds will each react with ozone with appreciable reactivity. *o*-cresol exhibits negligible reactivity towards ozone. Ozone is the first oxidant to be formed through photolysis of NO_2, and there will be appreciable formation of biogenic oxidation products prior to formation of those from *o*-cresol (see section 4).

In addition to the differential reactivity towards the two dominant oxidants, there will be differences in the product formation rates in the single VOC experiments with varying concentrations owing to the use of a single VOC:NOx ratio. This will result from the reduced NO_x at reduced VOC, which will lead to reduced OH concentration owing to reduction in the NO +

HO_2 flux. Though there will also be a reduced rate of production of ozone in these experiments, non-linearity will lead to changes in the O_3: OH ratio and hence changes in the contributions of the oxidation pathways for the biogenic VOCs. There may be less expected influence on the pathways for *o*-cresol oxidation, though the rate of oxidation will nevertheless be slowed.

Ambient atmospheric OH reactivity can be estimated from the quantification of VOC abundance or from direct measurements of OH lifetime. Using the latter, Whalley et al. (2016) reported central London diurnal average morning peaks of around 27 s^{-1} and a campaign maximum of around 116 s^{-1}. Our full reactivity experiments have an OH reactivity around 465 s^{-1}, some 4 times higher with only one, two or three VOCs for single precursor, binary or ternary experiments respectively. It would be desirable to work with lower concentrations. In addition to challenges associated with maintaining oxidant levels at such high VOC concentrations, there is likelihood that the chemical regime, particularly with respect to radical concentrations may introduce biases in observed system behaviour. In our systems, OH reactivity is provided by C_5, C_7 and C_{10} VOC compounds (in addition to that provided by NO_2 and VOC oxidation products formed by the oxidation). This will lead to a high abundance of relatively large peroxy-radical, RO_2, species. OH reactivity in the ambient atmosphere is likely to be distributed amongst a high diversity of small (including CO and CH_4) and larger components (including carbonyls and other oxygenates). The distribution of RO_2 and the ratio of RO_2 : HO_2 may be substantially different. Nonetheless, it is not the intention or objective of the current study to mimic the atmospheric chemical regime, more to explore the potential for mixed VOC systems to reveal interactions in SOA formation processes.

A further consideration is the selection of neutral seed experiments. The systems studied will more reflect direct partitioning of gaseous oxidation products rather than accounting for products of condensed phase, particularly acid catalysed, reactions. Again, the intention is not to comprehensively mimic the atmosphere and this is recognised in the interpretation and discussed in further detail in section 5.

3. Methodology

All experiments were performed in the MAC; a 18m^3 FEP Teflon bag mounted on three pairs of rectangular extruded aluminium frames and housed in an air-conditioned enclosure. In the MAC,

ground-level solar illumination is simulated using two 6 kW Xenon arc lamps and a bank of halogen lamps, mounted on the inner aluminium wall of the enclosure which is lined with reflective "space blanket" material to maximise and homogenise the light intensity across the chamber. Removal of unwanted heat from the lamps is provided by the temperature and RH conditioned air introduced between the bag and the enclosure at 3 m^3 s^{-1} and active water cooling of the mounting bars of the halogen lamps and of the filter in front of the arc lamps. In addition to removing the heat from the arc lamp, the water in the filters removes unwanted IR radiation and the 4mm quartz plates forming the filter windows remove all UV radiation below 290 nm and increasingly transmit light up to a 100% transmission above 305 nm. The inlet comprises a high flowrate blower, feeding dried laboratory air through 50 mm diameter stainless steel pipework to a series of high-capacity filters and variously via a series of two- and three-way electropneumatic valves to a humidifier, ozoniser and aerosol generation drum before delivering it to the chamber through a Teflon manifold. This is mounted on the top frame of the central rigidly fixed pair of frames. The upper and lower pairs of frames are counter-weighted and free to track vertically, allowing the bag to expand and collapse as it is filled and flushed, by switching the valve positioning.

All controls are automated, and a series of pre- and post-experimental procedures have been programmed, comprising repeatable, characterised sequences of filling and flushing. The pre-experiment sequence is conducted prior to each experiment to ensure an adequately low background of indicative particulate and gaseous contaminants, monitored by CPC, NO_x and O_3 analysers. A one-hour long chamber background characterisation procedure, following the pre-experiment sequence, is conducted to ensure that a baseline contamination level has been established. This is followed by injection of the VOCs, NO_x and seed particles and a one-hour collection of data from the experimental background in the dark, during which the chamber conditions and all instrumentation are stabilised. A post-experiment sequence is conducted after each experiment to flush the chamber of all residual contaminants and leave a clean bag for the next experiment. The final fill of the post-experiment sequence contains ppm levels of ozone which is used to soak the chamber overnight between subsequent experiments. A weekly vigorous clean is conducted with full illumination with no UV filter on the arc lamps and ppm levels of ozone at high RH for maximum OH production.

Ammonium sulphate seed particles are atomised into a 50L stainless steel drum for pre-concentration prior to injection into the chamber. The seed concentration in the chamber is controlled by altering the injection time into the drum and the concentration of the stock solution (0.01 g/ml). After the final pre-experiment flush cycle, the fill flow is diverted through the drum. Liquid α-pinene, isoprene and *o*-cresol are injected as required through the septum of a heated glass bulb and evaporated into an N_2 carrier flow into this final fill along with NO_x as NO_2 from a cylinder, also carried by N_2. Photochemistry is initiated by irradiating the VOC at moderate VOC / NO_x ratio using the lamps as described above. Online instrumentation is used to continuously monitor the concentration of NO_x, O_3, particle number and mass throughout each experiment. It should be noted that *o*-cresol was found to interfere with O_3 measurement as a result of its UV absorption. The decay of CIMS-measured *o*-cresol was used to correct the O_3 data in all *o*-cresol containing experiments. The dark *o*-cresol measured before introduction of O_3 into the MAC was used to calibrate the O_3 analyser signal for absorption by *o*-cresol. The decay rate of the CIMS *o*-cresol signal was used to correct the O_3 measurements during the experiment. It should be noted that any UV absorption from the oxidation products of *o*-cresol cannot be captured and O_3 is thus reported as an upper limit in *o*-cresol containing systems.

Table 2: List of instrumentation employed over the course of the study

Instrument	Model	Measured parameter	LOD/ range
Dew point hygrometer	Edgetech (DM-C1-DS2-MH-13)	Dew point	-20 – 90 ± 0.2 °C
NOx analyser	Thermo 42i	NO, NO_2	0.5 to 1000 ppb
O_3 analyser	Thermo 49C	O_3	0-0.05 to 200 ppm
Water-based condensation particle counter	TSI 3786	Particle number	$<10^7$ p/cc
Differential mobility particle sizer	Custom-built[a]	Particle size	40-600 nm
Filter collector	Custom-built[b]	Particle collection for offline analysis	
Condensation particle counter	TSI 3776	Particle number	$<10^7$ p/cc
Scanning mobility particle sizer	TSI 3081	Particle size	10-1000 nm
High-resolution aerosol mass spectrometer	Aerodyne	PM_1 non-refractory particle composition	>0.05 μg m^{-3}

Iodide chemical ionisation mass spectrometer	Aerodyne/Tofware	Oxygenated VOC	LOD >60 ppt; Mass resolution 4000 Th/Th
Filter Inlet for Gases and AEROsols	Aerodyne/Tofware	Particle composition	$>10^2$ ng
Semi-continuous gas-chromatograph mass spectrometer	6850 and 5975C Agilent	VOC concentration	>0.4 ppb
Liquid chromatograph – orbitrap mass spectrometery	Dionex 3000, Orbitrap QExactive, ThermoFisher Scientific	Particle composition	
Hygroscopicity tandem differential mobility analyser	Custom.built[c]	Hygroscopicity	20-350 nm
Cloud condensation nuclei counter	Droplet measurement Tech (model CCN-100)	CCN activity	>6 x 10^3 particles cm^{-3} at SS:0.2%
Thermal denuder	Custom.built[d]	Volatility	Temperature range: ambient – 200°C
Three arm bounce impactor	Custom.built[e]	Particle bounce	20-500 nm, < 10^4 particles cm^3

[a]Alfarra et al. (2012)
[b]Hamilton et al. (2011)
[c]Good et al. (2010)
[d]Voliotis et al. (2021a)
[e]Liu et al. (2017)

A high-resolution time-of-flight Aerosol Mass Spectrometer (HR-ToF-AMS; Aerodyne Inc.) is used to measure particle composition by mass, a Filter Inlet for Gases and Aerosols coupled to an iodide chemical ionisation mass spectrometer (FIGAERO-I^--CIMS; Aerodyne Inc.) for gas and particle phase oxygenated component measurement, a scanning mobility particle sizer (SMPS; TSI Inc.) for particle size distribution retrieval, a home-built hygroscopicity tandem differential mobility analyser (HTDMA) for hygroscopic growth factor determination, a cloud condensation nucleus counter (CCNc; DMT Inc.) for cloud droplet potential evaluation and a home-built three arm bounce impactor for particle rebound determination. Some of the online instrumentation was switched after several hours to cycle between sampling after a home-built thermodenuder (TD)

and directly from the chamber. Finally, a semi-continuous 2-trap Gas Chromatograph with Mass Spectrometric detection (GC-MS; Agilent) was used to monitor VOC concentrations. Table 2 provides a list of all instrumentation employed throughout the programme. At the end of each 6-hour experiment, the entire remaining contents of the bag are flushed through a Whatman Quartz microfibre filter (pre-fired at 550°C for 5.5 hours) to collect the particles. The filters were then wrapped in foil and stored at -18°C prior to analysis by LC-electrospray Orbitrap MS.

Actinometry and off-gassing experiments were conducted regularly through the programme in order to establish the consistency of the chamber's performance, evaluate the effectiveness of the cleaning procedure and confirm cleanliness of the chamber. Background filters were collected from the actinometry and off-gassing experiments.

4. Results

Photolysis of NO_2 under the simulated solar irradiation in the MAC forms O_3 and they rapidly move towards photostationary state with NO. The O_3 is photolysed at wavelengths below 310 nm to yield $O(^3P)$ and $O(^1D)$, the latter reacting with available water vapour to form the hydroxyl radical, OH. The O_3 will attack the double bond in unsaturated compounds such as α-pinene and isoprene, initiating oxidation and yielding secondary OH. The OH will attack all VOCs in the system, either by hydrogen abstraction or OH-addition. Owing to the isoreactivity concept employed in the experiments, the initial VOC destruction rate, and first-generation oxidation product production rate, at a *given* OH concentration will be the same, enabling the opportunity to explore interactions in the mixed systems. However, owing to the indirect method used to produce OH (and hence its production and loss rate and steady-state concentration) the loss rate of each VOC will be different, dependent on the differential reactivity of the VOC towards O_3, and turnover of products from each will depend on this loss rate and the reactivity of their oxidation products to the prevailing oxidants. A currently unquantified contribution to the OH concentration will likely be contributed by the release from the walls of HONO, as has been seen in previous studies in Teflon reactors (Rohrer et al., 2005). This is under investigation and will influence the photochemical environment in the MAC, but does not directly change the results reported here.

To provide the photochemical context for example systems, Figure 1 shows time series of NO_2, NO and O_3 from experiments in the following 4 systems: α-pinene, isoprene, α-pinene/isoprene and *o*-cresol. Note that, in the presence of *o*-cresol, O_3 measurement by UV absorption was influenced by UV absorption by *o*-cresol and Figure 1(d) is corrected as explained in the methods section. Figure S1 shows the NO_2, NO and O_3 for all systems, similarly corrected for *o*-cresol containing systems.

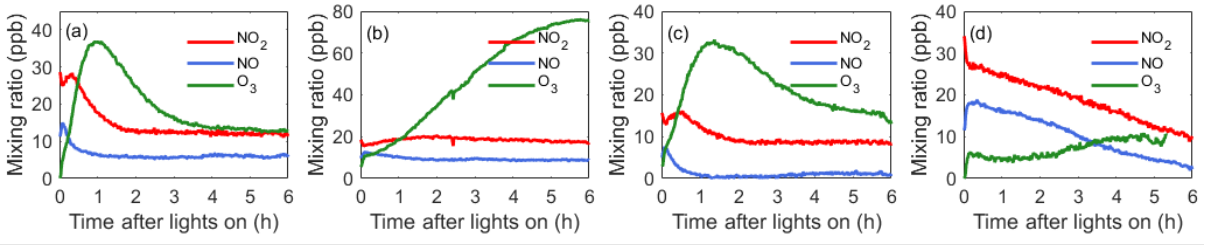

Figure 1: NO_2, NO and O_3 time series in example single and mixed VOC experiments (a) α-pinene, (b) isoprene, (c) α-pinene/isoprene, (d) *o*-cresol.

O_3 will move towards photo-stationary state (PSS) with NO and NO_2 according to reactions R1, R2 and R3:

$$NO_2 + h\nu \rightarrow NO + O(^3P) \qquad (@\ \lambda < 424\ nm) \qquad (R1)$$

$$O(^3P) + O_2\ (+ M) \rightarrow O_3\ (+ M) \qquad (R2)$$

$$NO + O_3 \rightarrow NO_2 + O_2 \qquad (R3)$$

Some insight into the trajectory towards PSS across the systems can be gained by inspection of Supplementary Figure S2, which provides a comparative summary of the Leighton Ratio (Leighton 1961) for all systems and the O_3 calculated assuming PSS, i.e. Leighton Ratio of 1, shown for the o-cresol containing systems. The Leighton Ratio is given by

$$\varphi = j_{NO2}\,[NO_2]/k_{O3+NO}[O_3][NO] \qquad (1)$$

In the polluted high-NOx atmosphere, PSS universally applies and φ is unity. In moderately polluted conditions, radical reactions are increasingly important in conversion of NO to NO_2 and typically φ >1. This is because HO_2 and RO_2 will compete with the O_3 reaction for NO (R3) according to reactions (R4 and R5):

$$HO_2 + NO \rightarrow NO_2 + OH \qquad (R4)$$

$RO_2 + NO \rightarrow NO_2 + RO$ (R5)

where RO_2 arise from biogenic VOC or *o*-cresol. Note that, in the ambient atmosphere, RO_2 can stem from a very wide pool of VOCs. Further deviation from PSS and consequent increase in φ will occur when O_3 loss processes other than R3 become important. These can include reactions of O_3 with NO_2, alkenes and radicals. In our chamber systems, the O_3 reactions with α-pinene and isoprene and radical reactions with NO, are competitive and provide substantial deviation from PSS. The NO_x and O_3 trajectories in the various systems can be seen to vary substantially. Nevertheless, in all systems, illumination of the chamber leads to the expected onset of significant photochemistry to initiate the VOC photo-oxidation.

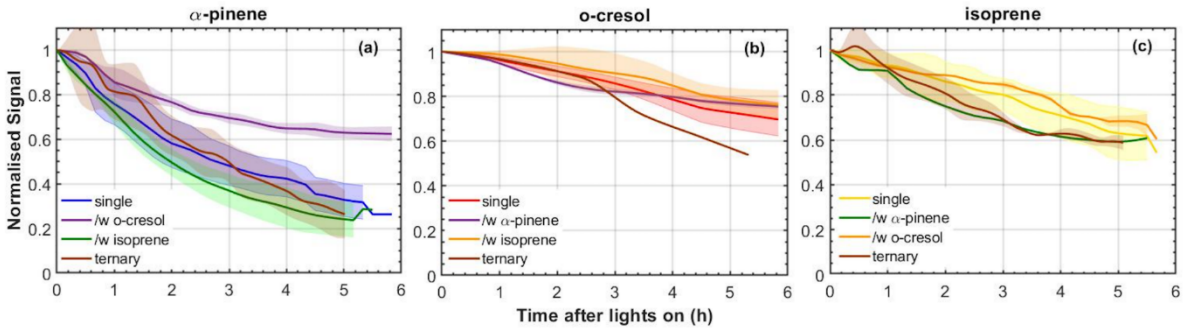

Figure 2: Decay rates of each VOC across all mixtures; a) α-pinene, b) isoprene and c) *o*-cresol. All lines (and shaded areas) containing blue correspond to experiments including α-pinene, containing red to those including *o*-cresol and yellow to isoprene. For example, purple lines correspond to an α-pinene /*o*-cresol binary mixture and brown to the ternary mixture. The shaded areas represent 1 standard deviation around the solid line mean value of all experiments.

From Figure 2, it can be seen that the rate of decay is not the same in each experiment, despite the attempt at initial isoreactivity, as explained in section 2.5. Oxidation products from each VOC will nevertheless be present in appreciable quantities in each experiment, satisfying the objectives of the design to enable exploration of interactions of oxidation products in SOA particle formation.

Figure 3 shows the time series of SOA particle mass in all experiments (with shading representing ± 1σ of the measurement across all experiments) in all precursor systems studied. It can be seen that the greatest SOA mass was generated in α-pinene containing systems, which is unsurprising, given the known efficiency with which it forms particle mass. It was found that *o*-cresol and *o*-cresol containing mixtures were the next most efficient at producing particle mass. This might be

expected with its reported moderate SOA particle producing potential. Negligible SOA particles were formed in all single VOC isoprene experiments. Only when isoprene was in a mixture was any mass formed and, in all cases, this was lower than the mass formed from the other VOC alone. Again, this is not too surprising, given the low or negligible particle mass yield reported for isoprene on neutral particle seeds. As seen in Figure 2, not all VOC was consumed in all experiments and it can be seen that the particle mass may not have fully peaked in all *o*-cresol and *o*-cresol / isoprene experiments. Nevertheless, the mass peak was observed in most experiments before they were completed, and the chamber contents flushed through the filter for compositional analysis. Panel b) in Figure 3 shows the SOA particle mass corrected for the losses of particles to the chamber walls. This was conducted by calculating the exponential decay of particles of each size from a targeted ammonium sulphate wall loss correction experiment performed close to the experiment of interest. Details of the wall loss correction can be found in Shao et al. (2021a).

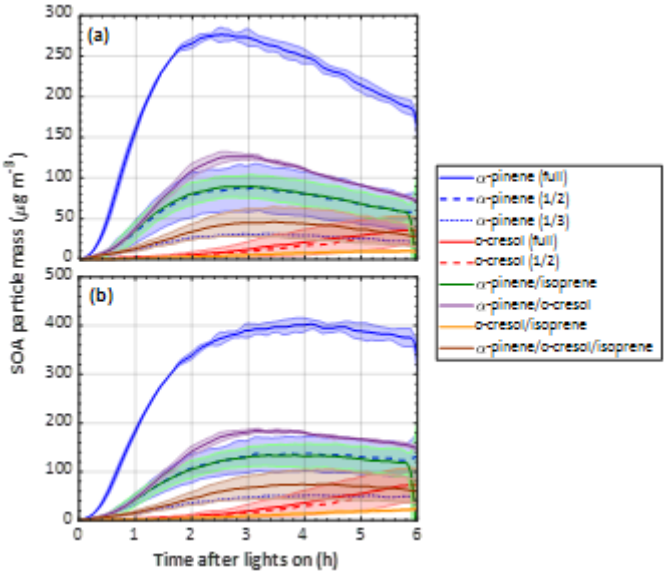

Figure 3: SOA particle mass (mean ± 1δ as shaded areas) in each system, a) raw measurements and b) particle wall-loss corrected mass. Note that this is organic mass determined from AMS measurements and so does not include the ammonium sulphate seed particles. The same colour scheme is used as in Figure 2.

Figure S3 shows the total particle wall loss corrected particle component mass ratios in each system indicating the inorganic and organic component evolution as measured by AMS. As shown in panel a), the mass ratio of organic to inorganic seed follows the production of SOA particle

mass and the loss of total particle mass to the walls. In the wall loss correction, the size-resolved loss of multi-component organic-inorganic aerosol particles is assumed to be the same as that for size-resolved ammonium sulphate seeds loss rate measured in dedicated experiments (see methodology). The decrease in SO_4^{2-}/ NO_3^- shown in panel b) follows the wall loss of total particle mass (and hence SO_4^{2-}) and simultaneous oxidation of NO_2 by OH to form HNO_3 (and hence particulate NO_3^-). NH_4^+ was found to be in ion balance with the sum of NO_3^-/SO_4^{2-} in all experiments.

Particle mass yield is a widely used metric that aims to represent the effectiveness of a VOC in forming SOA particle mass. In single precursor systems it is relatively straightforward the particle mass formed per unit of VOC consumed:

$$Y = \frac{\Delta[SOA]}{\Delta[VOC]} \quad (2)$$

Frequently the yield is reported as a single number and this may be taken from measurements at maximum SOA particle mass formed in the experiment, at the maximum VOC consumed, or perhaps more arbitrarily, at the end of an experiment. Such approaches may be reasonably applied for comparisons between precursors in identical oxidation conditions in the same chamber. Owing to significant particle losses to chamber walls, it can be seen from Figure 3 that it is important to correct the particle mass formed in the yield calculations for such losses. It is noted that the yields need to be corrected for VOC or OVOC product losses to the walls, too as discussed in section 5. Table 3 shows the calculated yields for all individual VOC and mixture experiments. The first 9 rows show the yields for single VOC experiments. Following the particle mass plots shown in Figure 3, it is clear that the efficiency in forming particle mass is in the order α-pinene > *o*-cresol > isoprene, with no mass yield observed in isoprene oxidation though appreciable isoprene consumption was observed as shown in Figure 2. For α-pinene and *o*-cresol it can be seen that the yield increased with increasing initial concentration. The *o*-cresol and *o*-cresol / isoprene experiments were not continued to the point of maximum mass formation (as shown in Figure 3) and so the maximum VOC consumption and mass formation both correspond to the end of the experiments in these systems. Figure 4 shows the yield plotted against SOA particle mass for α-pinene and *o*-cresol for all individual VOC experiments, indicating that the yield increases monotonically with particle mass within propagated experimental uncertainties. Such behaviour is

expected and is consistent with absorptive partitioning considerations. Note that organic mass formation in the "full reactivity" (i.e. 309 ppb α-pinene) experiment is so rapid that VOC data are only available for yield calculation beyond 100 µg m^{-3}. Supplementary Figure S4 alternatively shows the SOA particle mass yield plotted against the total particle mass in the chamber, including the ammonium sulphate seed particles that provide a condensation sink for the condensable vapours produced by VOC oxidation.

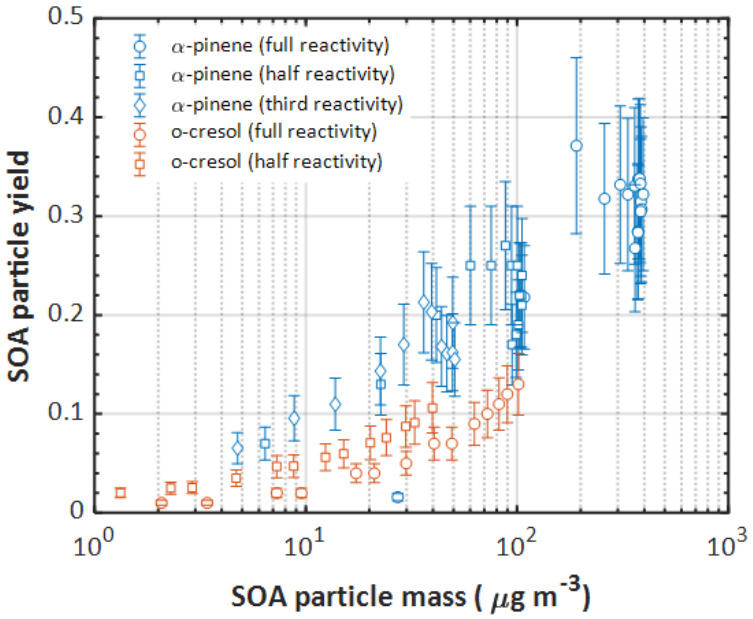

Figure 4: SOA particle mass yield as a function of mass formed in the single precursor α-pinene and *o*-cresol experiments at all initial concentrations. Error bars represent the propagated uncertainties in all measurements and in the particle wall loss corrections applied.

Since there is no SOA particle mass formed from isoprene, Table 3 additionally presents yield data omitting the consumption of isoprene in the denominator of equation 2, accordingly increasing the yield. Figure 5 shows the yield curves for typical experiments in all systems. The yield curves allow comparison between the systems, both including and excluding isoprene in the denominator of equation 2. The two-product model (Odum et al., 1996) was used to fit the yield curves for α-pinene and *o*-cresol. These are included to guide the eye. Here, the two-product model parameterised the relation of overall SOA yield and the adsorptive mass assuming only two products to exist in the system. The equation of the two-product model is shown in eq.3. α, K_p and C_{OA} represent the stoichiometric factor, the partitioning coefficient of product and the total absorbing organic mass, respectively. The α_1, α_2, $K_{p,1}$, $K_{p,2}$ can be fitted from the yield curves.

Table 3: Measured and particle wall-loss corrected SOA particle mass yields for all systems calculated at maximum particle mass and maximum VOC consumed. For mixtures containing isoprene, which had zero yield on the neutral seeds injected, the yields were calculated excluding the consumption of isoprene in the system allowing them to be referenced to the mixtures without isoprene. Yield was calculated with the density of organic matter of 1.4μg m^{-3}. The maximum mass used in the yield at maximum mass calculation is given in Table 1. The uncertainties in SOA particle mass yield was calculated by propagating the ± 1□ uncertainties of measured ΔSOA and ΔVOC.

	Reactivity	Yield at max. mass	Yield at max. VOC consumed	Yield at max. mass (Isoprene excluded)	Yield at max. VOC consumed (Isoprene excluded)
α-pinene	Full	0.32 ± 0.08	0.27 ± 0.06		
	1/2	0.21 ± 0.05	0.17 ± 0.04		
	1/3	0.16 ± 0.04	0.13 ± 0.03		
isoprene	Full	0	0		
	1/2	-	-		
	1/3	0	0		
o-cresol	Full	0.13 ± 0.03	0.13 ± 0.03		
	1/2	0.11 ± 0.03	0.11 ± 0.03		
	1/3	-	-		
α-pinene/isoprene	Full	0.16 ± 0.05	0.13 ± 0.04	0.19 ± 0.05	0.16 ± 0.04
α-pinene/*o*-cresol	Full	0.29 ± 0.09	0.22 ± 0.07		
o-cresol/isoprene	Full	0.06 ± 0.02	0.06 ± 0.02	0.08 ± 0.02	0.07 ± 0.02
α-pinene/*o*-cresol/isoprene	Full	0.11 ± 0.04	0.08 ± 0.03	0.12 ± 0.04	0.08 ± 0.03

In addition to the measured points, Figure 5 shows "predicted" yields for the mixtures, based on the organic mass at the same VOC consumption measured in the single VOC experiments and additively combining them according to:

$$Yield = C_{OA}\left(\frac{\alpha_1 K_{p,1}}{1+K_{p,1}C_{OA}} + \frac{\alpha_2 K_{p,2}}{1+K_{p,2}C_{OA}}\right) \quad (3)$$

and

$$Yield_{pred.} = \frac{\Delta m_{\Delta VOC1} + \Delta m_{\Delta VOC2} + \Delta m_{\Delta VOC3}}{\Delta_{VOC1} + \Delta_{VOC2} + \Delta_{VOC3}} \quad (4)$$

The parameters for the two-product fit from the single VOC half- and third-reactivity experiments were used to generate a yield-mass-ΔVOC look-up-table. This was then used to calculate the particle mass formed from each precursor at the consumption of the VOC at each point in the binary and ternary systems.

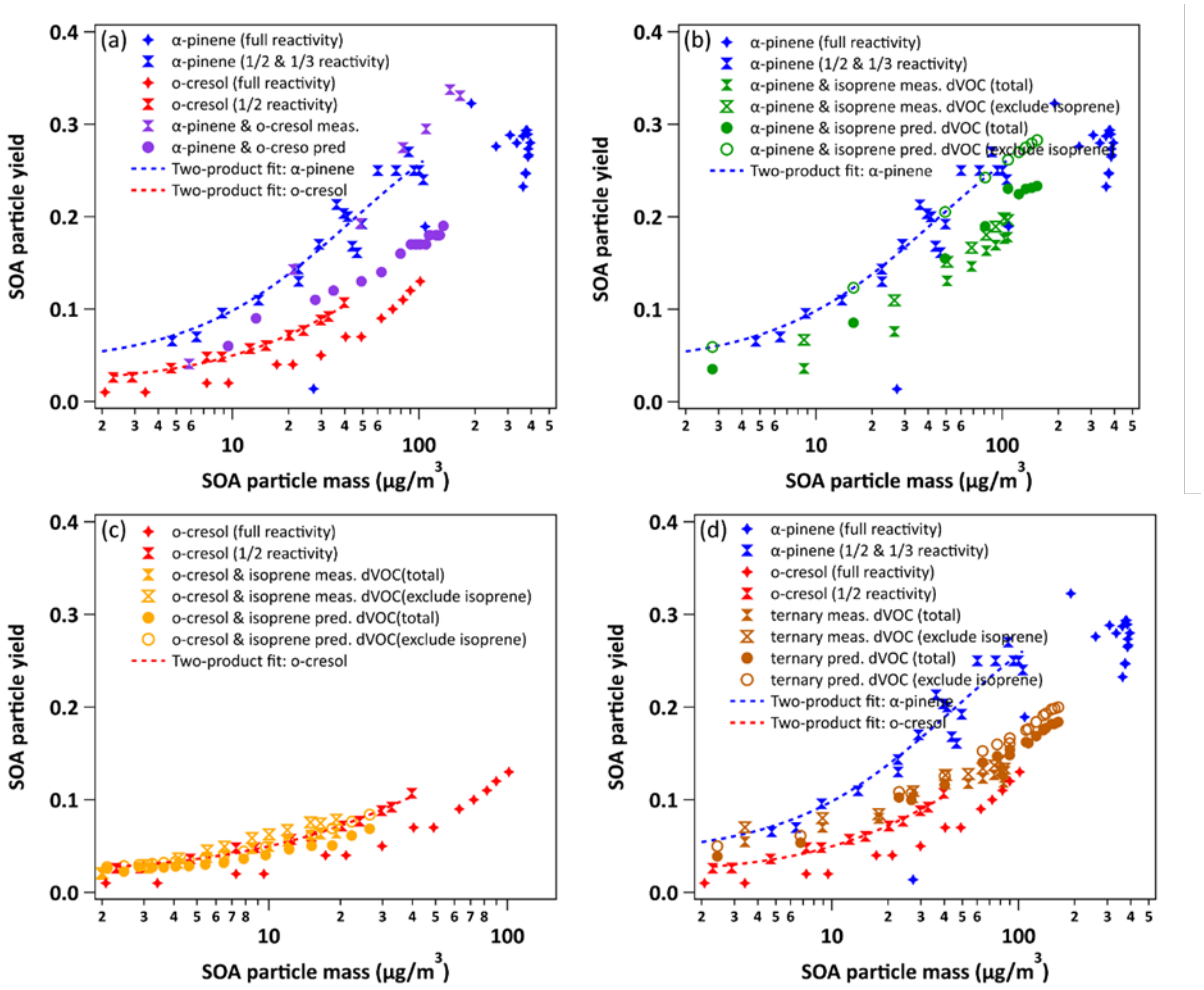

Figure 5: Yield data for selected representative experiments in all systems (with 2-product yield curves for α-pinene and *o*-cresol single VOC experiments). Panel a) shows the binary α-pinene / *o*-cresol mixture and its constituents, b) the binary α-pinene / isoprene mixture, c) the *o*-cresol / isoprene mixture (expanded y-axis plot shown in Figure S5) and d) the ternary α-pinene / *o*-cresol / isoprene mixture. Yields "predicted" from the linear combination of yields from the individual VOC experiments using equation 4 are shown for each mixture.

Using this look-up table, the predicted yield from the binary α-pinene / *o*-cresol mixture photo-oxidation is below that measured in the *α*-pinene / *o*-cresol mixture experiment and slightly higher than that in the individual *o*-cresol experiment at 50% reactivity. Indeed, the yield measured in the mixture is comparable to that of *α*-pinene at one half and one third reference reactivity. For the isoprene-containing binary mixtures, clearly the predicted yield excluding isoprene in the denominator is identical to that of the 2-product curve fitted to the single VOC experiment derived yield of other components in the mixtures. In the *α*-pinene / isoprene system, the predicted yield accounting for the consumption of both *α*-pinene and isoprene is higher than that measured but, as

shown in Tables 3 and 4, comparable to the measured yield referenced only to the consumption of *α*-pinene. In the *o*-cresol / isoprene system, the predicted yield accounting for the consumption of both *o*-cresol and isoprene is lower than that measured (at higher mass loadings), there is little difference within uncertainty at a lower mass. The predicted yield accounting for the consumption of *o*-cresol alone is lower than that measured when referenced to the same total VOC consumption, but comparable to the measured yield referenced to the consumption of both *o*-cresol and isoprene. Finally, in the ternary system, the predicted yield excluding isoprene consumption is similarly (and obviously) higher than that including its consumption, but both predictions are between the yields of single *α*-pinene and *o*-cresol experiment measurements. The measured yields accounting for only *α*-pinene and *o*-cresol consumption in the ternary mixture are also similarly (and obviously) higher than that including isoprene consumption. There is insufficient difference between the measurements or the predictions to state whether inclusion or exclusion of isoprene consumption gives a much better agreement, though there is an indication that the predicted yields show a steeper gradient with SOA particle mass than the measured slope, which more closely follows that of the *o*-cresol than that of *α*-pinene. Table 4 distils the predictions based on the yield from single VOC experimental data at the same consumption as in the mixtures into single values predicted at maximum SOA particle mass, maximum VOC consumption, both with and without isoprene decay in the calculation.

To explore the likely fate of the parent VOCs in the MAC, we used the measured O_3 concentrations and VOC decay rates and exploited the differential reactivities of the VOCs to investigate the decay attributable to each oxidant and also overcome measurement difficulties encountered in the experiments. For example, knowing that *o*-cresol has a negligible rate of reaction with O_3, we are able to calculate the OH concentration from the *o*-cresol decay curve. This can then be used to attribute the fraction of the decay of isoprene and *α*-pinene to OH and O_3 in their binary mixtures with *o*-cresol. This is important, since the measurement of O_3 by UV absorption in the presence of *o*-cresol is challenging and requires correction for the additional absorption by *o*-cresol. In systems without *o*-cresol, the decremental decay attributable to O_3 can be constructed for *α*-pinene and isoprene using the O_3 measurements and (reaction rates of 9.6 and 1.28 x 10^{-17} $cm^3 molecules^{-1}$ s^{-1}, respectively; Cox et al., 2020), by comparing with the actual *α*-pinene and isoprene, the residual decay can be attributed to OH. An example of this oxidant reconciliation is shown in Figure 6 for the binary *α*-pinene / isoprene system.

Table 4 SOA predicted yield for the 4 mixtures at maximum SOA particle mass produced and maximum VOC consumed. The uncertainties in SOA particle mass yield was calculated by propagating the ± 1δ uncertainties of predicted ΔSOA and measured ΔVOC.

Predicted Yield at:				
	Max. SOA particle mass	**Max. VOC consumption**	**Max. SOA particle mass excl. isoprene**	**Max. VOC consumption excl. isoprene**
α-pinene/isoprene	0.19± 0.08	0.15±0.06	0.21±0.08	0.17±0.06
α-pinene/*o*-cresol	0.17±0.07	0.14±0.05	0.17±0.07	0.14±0.05
isoprene/*o*-cresol	0.10±0.04	0.09±0.04	0.11±0.04	0.11±0.04
α-pinene/isoprene/*o*-cresol	0.13±0.06	0.11±0.05	0.14±0.05	0.12±0.05

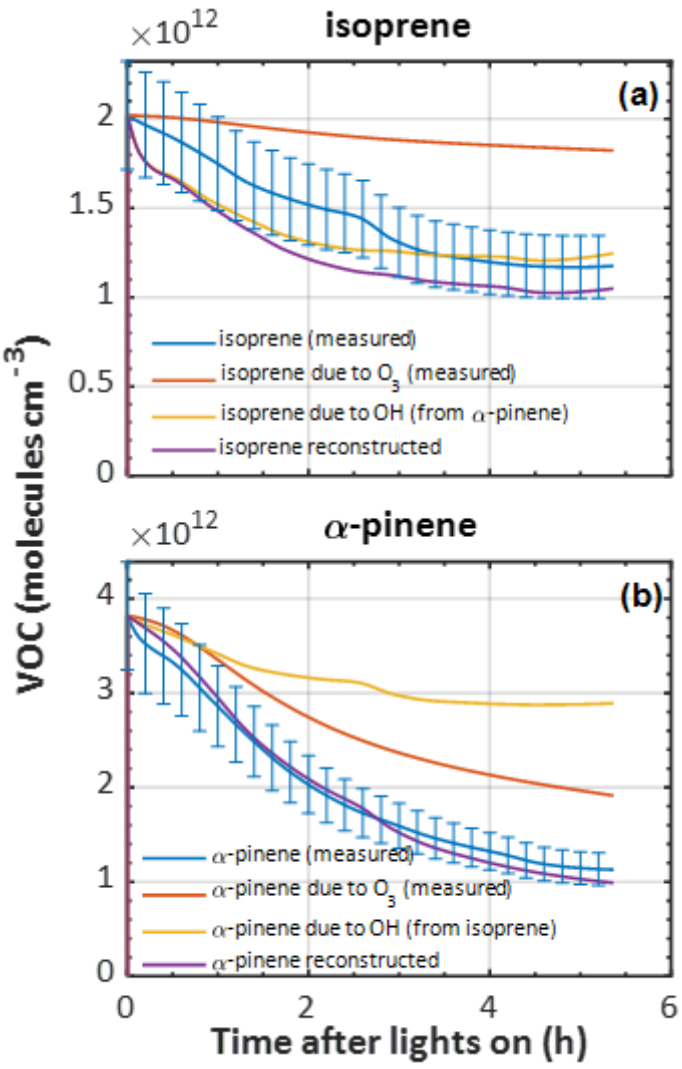

Figure 6: Measured (±15% error) and reconstructed (a) isoprene and (b) α-pinene decay in a α-pinene & isoprene binary experiment. Initially, in each case the decay of the VOC due to ozone was predicted based on the O_3 concentration, the reaction rate of each VOC toward O_3 and the initial VOC concentration. Subsequently, the OH concentration from each VOC was estimated from the difference in the VOC decay attributed to O_3, and the measured VOC decay. Finally, the OH concentration from each precursor was used to reconstruct the decay of the other (i.e. OH from isoprene was used to reconstruct the decay of α-pinene and vice versa.

In the example shown in Figure 6, it can be seen that roughly twice as much loss of α-pinene can be attributed to O_3 as to OH and roughly 4 times as much isoprene loss attributed to OH as to O_3. The inability to control isoreactivity towards all oxidants through controlling the initial VOC concentrations will influence prediction of SOA particle mass yields owing to the differences in tendency to condense of oxidation products from different oxidants. These aspects are discussed in section 5.

Differences in the SOA particle oxgenation trajectory between the systems are illustrated in Figure 7 by the percentages of the AMS total signal at m/z=44 (f_{44}) and 43 (f_{43}) respectively to represent more and less oxygenated contribution to the SOA particle mass.

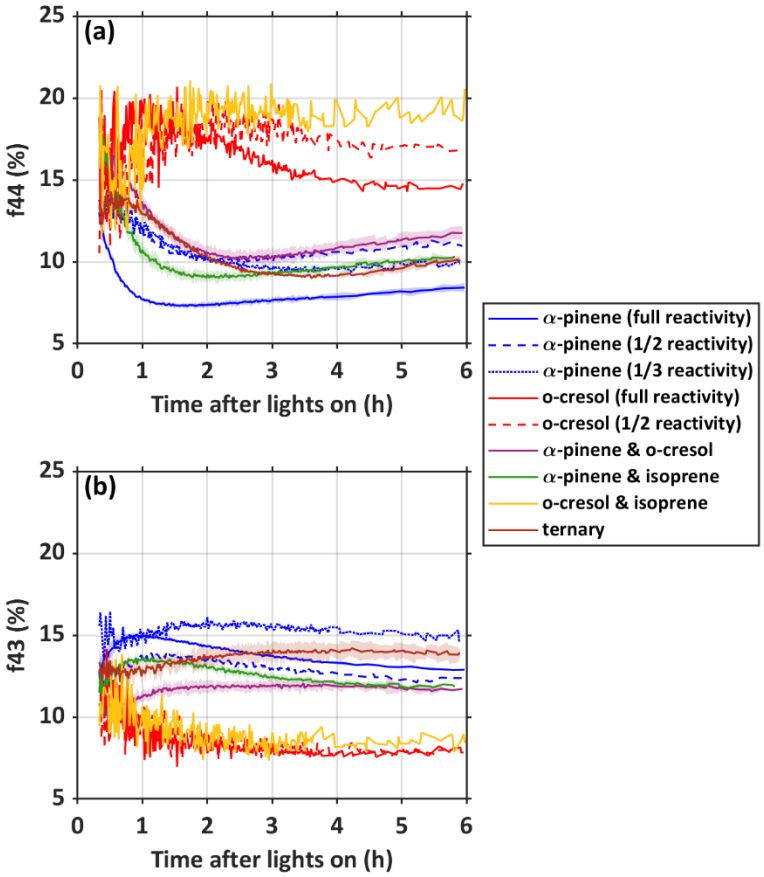

Figure 7: Aerosol Mass Spectrometer time series of f_{44} and f_{43} in all systems.

With some simplification *m/z*=44 is the CO_2^+ fragment thought to be formed by decarboxylation on the AMS vapouriser and *m/z*=43 corresponds to the presence of less oxidised components like carbonyls (though with a small contribution from unoxidised alkyl fragment ions that was not substracted). The full reactivity single VOC α-pinene experiment has the lowest f_{44} and highest f_{43} of all systems. Systems that do not contain α-pinene can be seen to comprise a persistently higher f_{44} and lower f_{43} than all α-pinene containing systems. This is attributable to a higher contribution of the mass from products of α-pinene with a lower degree of oxygenation, when it is present in the mixture. However, there is a substantial difference in the fractional contributions of the

fragments with concentration in the single VOC α-pinene experiments, with higher f_{44} in the lower concentration experiments forming lower mass. This may be partly explained in terms of absorptive partitioning, with lower absorptive mass enabling condensation of only the lower volatility (and more oxidised and higher f_{44} products). However, such effects would likely be small since the mass reduction is not large. Moreover, the difference between f_{44} at full and half reactivity might be expected to be smaller than that between half and third reactivity since the mass difference is smaller between the former pair of experiments. However, the reverse is true. The high f_{44} generated in the *o*-cresol systems and persisting through to high masses later in the experiments is notable and suggests that a high degree of oxygenation is required to enable partitioning of these compounds to the particles (Emanuelsson et al., 2013) . Compared with the lower degree of oxygenation required in the α-pinene systems, it may indicate the requirement for molecules derived from the smaller C_7 precursor to be more oxygenated than those from its C_{10} counterpart. The attribution of the m/z=44 fragment to di- and polycarboxylic acids is interesting in this context, given the high fractional signal contribution of $C_7H_7NO_4$ isomers from CIMS and UPLC-Orbitrap MS, see text below and Figure 10. This chemical behaviour has been re-expressed in Figure S6 following the approach first described in Ng et al. (2010). It can be seen that the systems all fall to the right of the delineated triangular area bracketing ambient atmospheric behaviour – a finding frequently observed in many chamber systems (see e.g. Figure 4 in Alfarra et al., 2013). A more thorough analysis of the composition from analysis of the high resolution AMS data is the subject of a separate manuscript (Shao et al., 2021a, in prep.).

A further illustration of the differences in the chemical trajectories can be provided by the time series of gaseous and particulate components derived from the FIGAERO-I^--CIMS instrument. Figure 8 illustrates the changes in particulate mass spectra of single α-pinene and *o*-cresol experiments and their mixture. These mass spectra have been normalised to the same reagent ion concentration. There is a clear increasing signal in the m/z range from 200 to 600 (I- adducts) after 5.5-hour reactions in single and mixture systems corresponding to the increase in detected particulate products with the increase in SOA particle mass with time. Additionally, some unique peaks (e.g., m/z 358, 403, 419, 439, etc) are only detected in the mixture mass spectra. Peak assignment of these mass spectra has been used to attribute signal to the molecular formulae and hence to broad chemical groupings in all single VOC and mixed systems. A full analysis and discussion can be found in Du et al., 2021 (in prep).

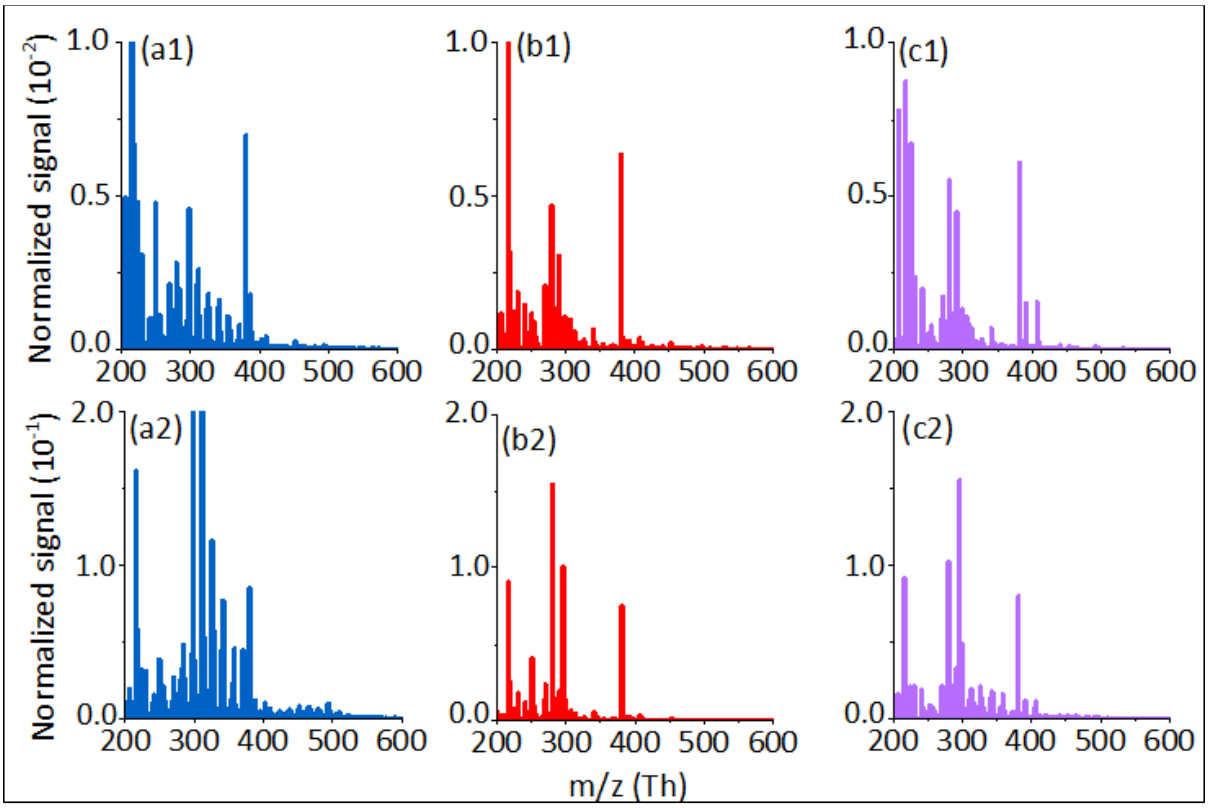

Figure 8: FIGAERO-CIMS Mass spectra taken in the single precursor α-pinene (a1 and a2), o-cresol (b1 and b2) and mixed α-pinene / o-cresol system (c1 and c2) at 0.5 hour (a1, b1 and c1) and 5.5 hours (a2,b2 and c2) after the onset of photochemistry in the MAC.

Owing to its separation and accurate mass resolution, the LC-Orbitrap MS analysis of extracts of particles from the filters collected at the end of the experiments provide molecular information to gain insight into interactions in the mixed systems. Figure 9 illustrates the ability to attribute signal in the filter extracts of particles in the ternary *o*-cresol / α-pinene / isoprene mixture to the individual parent VOC (by matching the attributed formulae to those identified in the individual precursor experiments) and thereby identify molecules found only in the mixture with their associated fractional signal contribution. This is shown for molecules detected in negative, panel a), and positive ionisation mode, c). These "unique-to-mixture" components have been split by contribution to the signal by carbon number in panels b) and d) for negative ion and positive ion mode respectively. These analyses are presented and expanded upon for all mixtures in Shao et al., 2021b (in prep.). Clearly a substantial fraction of the unique-to-mixture signal is found at carbon number greater than any precursor VOC (in -ve ionisation mode 57% of the signal in 48 individual peaks with nC > 10 and in +ve mode 60% in 115). Whether such components result from gaseous

or condensed phase reactions is not accessible from these measurements, but they clearly result from interactions in the mixture.

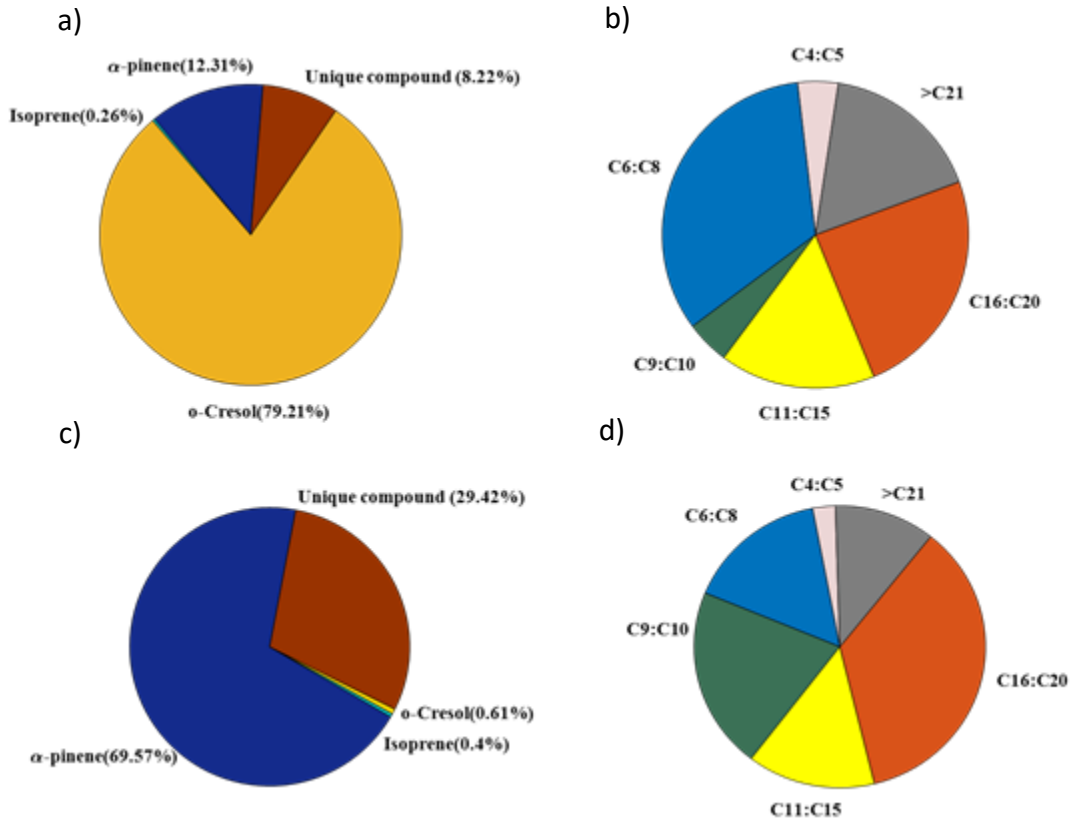

Figure 9: Molecular resolved compounds in the particle phase for the ternary *o*-cresol / *α*-pinene / isoprene mixture obtained using UPLC-Obitrap MS of filter extracts: a) fraction of signal in negative mode, b) fraction of signal by carbon number in the unique-to-mixture compounds, c) fraction of signal in positive mode, d) fraction of signal by carbon number in the unique-to-mixture compounds

Panel a) in Figure 10 expands on the molecular attribution by LC-Orbitrap MS to demonstrate the ability to separate isomeric contributions to the signal normalised to the total detected signal in single precursor and mixed systems. The example shown is for $C_7H_7NO_4$ (methyl-nitrocatechol and its isomers) in *o*-cresol containing systems. It can be seen that the isomer at an LC retention time of 9 minutes dominates the signal in all systems, whilst the isomer at retention time of 6.1minutes displays negligible signal fractions in all systems. In contrast, the I^--CIMS is incapable of separating structural isomers. Panel b) shows the time series of the total signal at m/z=296 (normalised to the total attributed signal) corresponding to the combined signal from all $C_7H_7NO_4$ isomers in the same systems.

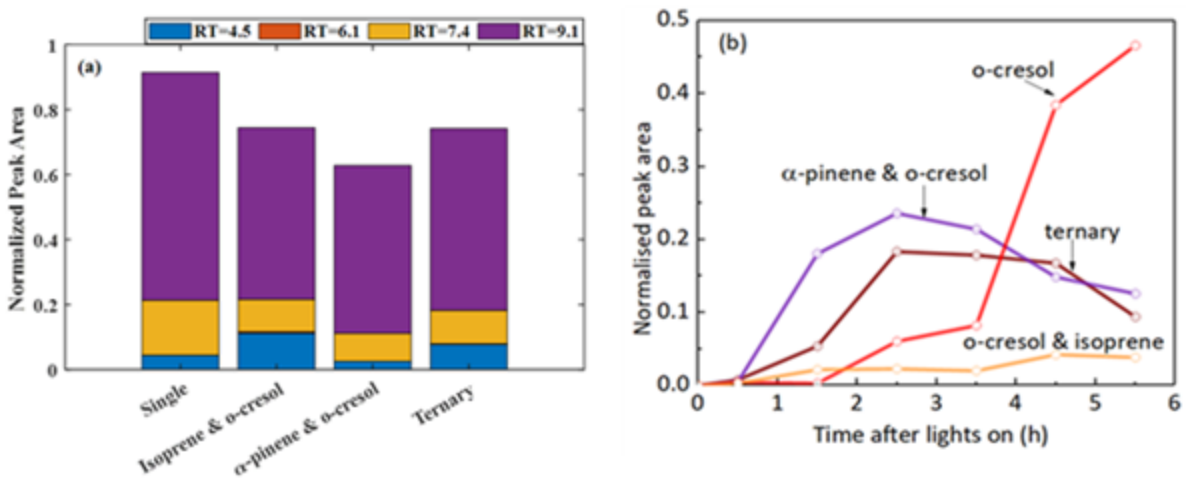

Figure 10: a) changes in the isomeric fractions of $C_7H_7NO_4$ across *o*-cresol containing systems from LC-Orbitrap MS analysis of the filter extracts collected at the end of each experiment; b) time series of particulate $C_7H_7NO_4$ from FIGAERO-CIMS

The attribution of elemental composition in the high resolution FIGAERO-CIMS analysis enables a comprehensive mapping of the particulate oxygen to carbon ratio (O:C) as a function of carbon number, as shown in Figure 11 for each system. It can be seen that the majority of signal in the *o*-cresol single system comprises compounds at the same carbon number, C_7, as the parent and, on average, with slightly higher O:C ratios than C_{10}, products dominating the *α*-pinene single VOC system. A significant fraction of the signal in all *α*-pinene containing systems is found at carbon numbers corresponding to the "dimer" range and these are all found predominantly in the particle phase (showing a low volatility). Interestingly, these low volatility products are absent in the mixtures containing *α*-pinene and *o*-cresol, suggesting a potential increase of the overall volatility. At the same time, a range of new products appear in mixtures (e.g. *α*-pinene / *o*-cresol, *o*-cresol / isoprene) with higher carbon numbers (nC=11-16), lower O:C (O:C<0.5) and varying volatility ($\log_{10}C^*$=1-3), indicating that the molecular interactions influences the overall SOA particle volatility. A more complete discussion of the chemical composition variation across the mixtures in the gas and particle phases can be found in Du et al. (2021, in prep.) and Voliotis et al. (2021b, in prep.).

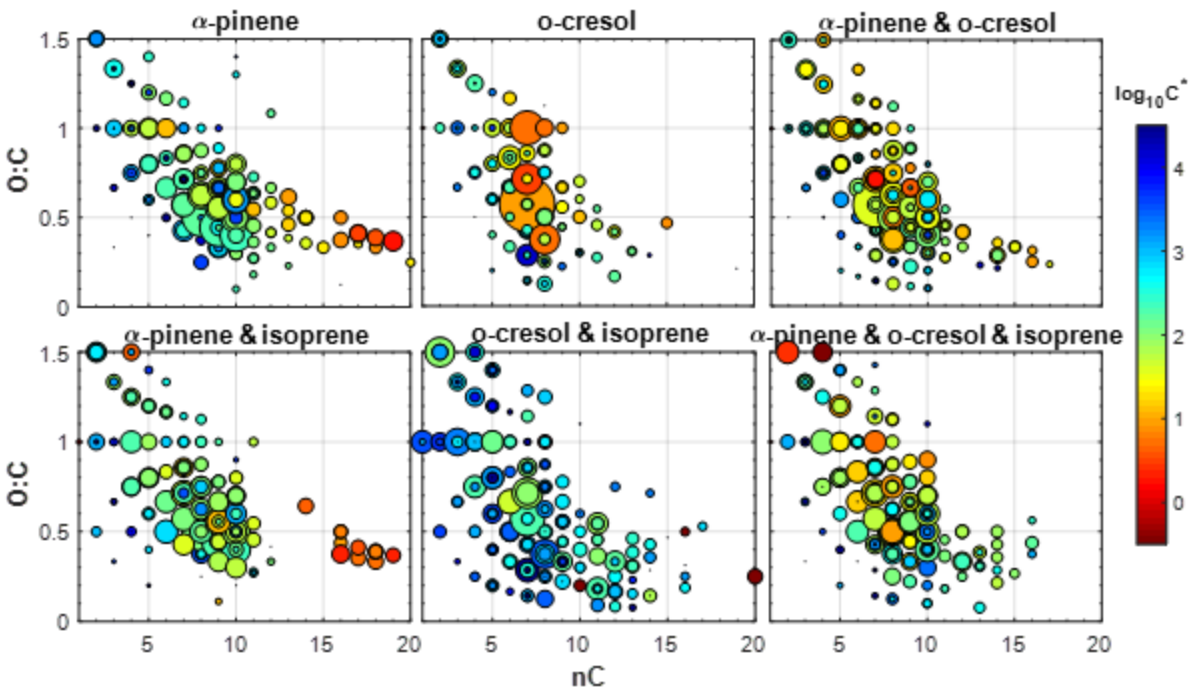

Figure 11: Oxygen to carbon ratio (O:C) vs carbon number (nC) of all the products identified by the FIGAERO-I⁻-CIMS in the particle phase at the end of each experiment in characteristic experiments in each system. Dots are sized based on the square root of the contribution of each product to the total signal and coloured according to their effective saturation concentration (C*). The C* was calculated using the gas to particle ratio of each ion and absorptive partitioning calculations.

The calculation of the C^* of all identified formulae by performing partitioning calculations using the gas to particle ratio of the ions (Voliotis et al., 2021a) can be used to assemble the volatility distribution of the products, as shown for the single VOCs, their binary and ternary mixtures in Figure 12. It can be seen that the volatility distributions of particles in the mixture experiments can be similar (*α*-pinene / isoprene) or quite different (*o*-cresol/isoprene) to those in the experiments using the single precursor. These observations suggest that the effect of mixing precursors can have a varying effect on the resultant particle volatility. A full discussion of the chemical composition and its influence on volatility in all systems can be found in Voliotis et al. (2021b, in prep.)

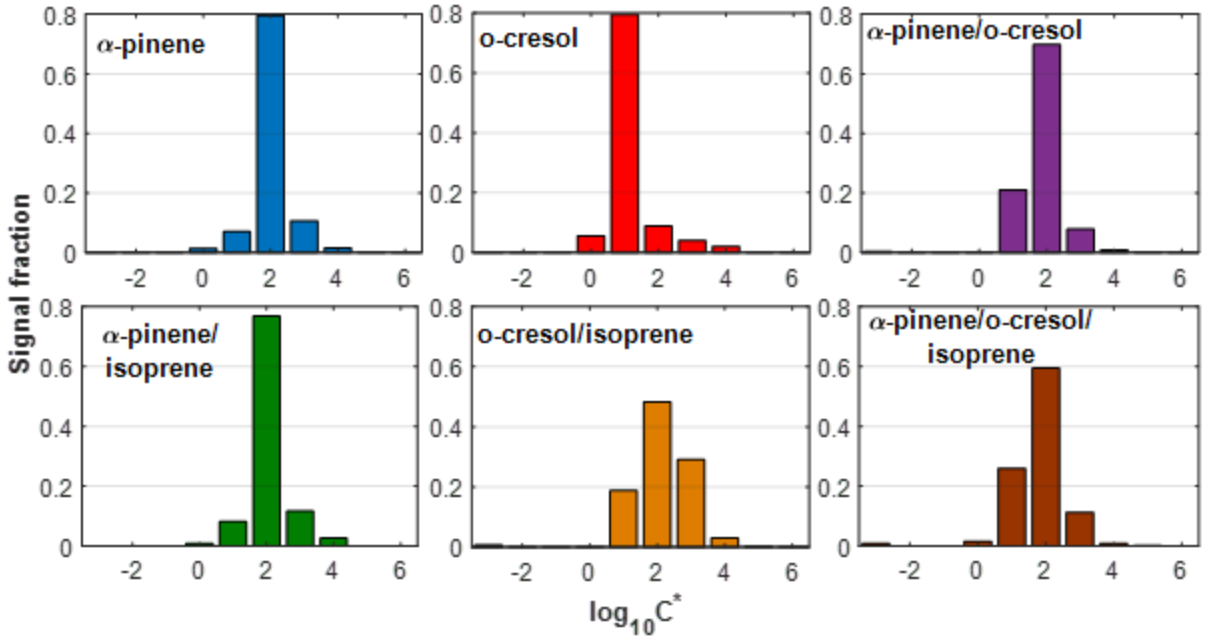

Figure 12: Volatility distributions expressed as effective saturation concentration (C*) in the volatility basis set framework of all the products identified by the FIGAERO-CIMS as a function of the total particle phase signal in example experiments in all systems. The C* was calculated using the gas to particle ratio of each ion and absorptive partitioning calculations.

The differences in evolution of the SOA particle components and the total mass formed directly influences the particle properties as expected. Since the particles are grown on inorganic seeds, the physical properties in all systems are initially dominated by the inorganic components as shown in Figure 13. This shows the relationship between the multicomponent particle composition, the hygroscopic growth factor and the rebound fraction of particles (indicative of their phase state) as the SOA to inorganic mass fraction of the particles develops in 3 example systems (*o*-cresol / isoprene, *o*-cresol and *α*-pinene). The hygroscopicity much more rapidly decreases in systems where organic material is more rapidly formed and the transition to a higher fraction of particles rebounding on a filter at high RH is similarly more rapid. It is clear that the rate of change of organic to inorganic ratio plays a controlling role in physical behaviour of the particles. The evolution of both these properties across all systems is discussed in detail in Wang et al. (2021a, b).

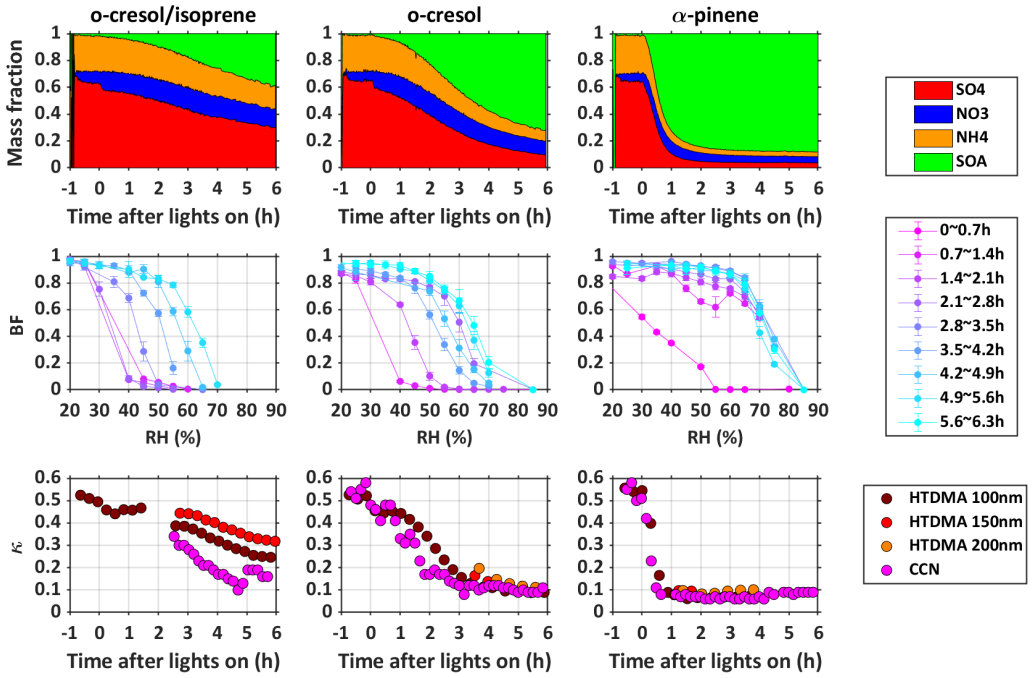

Figure 13: top row: AMS chemical composition showing rate of production of SOA and hence rate of increase in organic to inorganic ratio moving from left to right (from *o*-cresol / isoprene to *o*-cresol to *α*-pinene); middle row: the corresponding increasingly rapid transition to increased Bounce Fraction (BF) at higher RH; bottom row: the corresponding increasingly rapid reduction in the hygroscopicity parameter, k.

5. Discussion

5.1. Experimental conditions and photochemistry

The control of photochemical conditions in VOC mixtures is challenging. The chemical space is multidimensional and non-linear, and it is unclear how best to define the regime for direct comparison across systems. The approach taken in the current study, to start with concentrations of each VOC isoreactive towards a single oxidant cannot account for the differential reactivity towards the two oxidants, O_3 and OH, present in the system. This is particularly true when the production of oxidants is tightly coupled to the VOC oxidation itself and secondary oxidant production can be at a comparable level to primary production. The combination of oxidants can lead to significantly different VOC decay and hence turnover of oxidants and products. This is an unavoidable feature of VOC mixtures that will occur in the real atmosphere and such differences need to be carefully considered in the interpretation of the results.

It can be seen from Figures 1 and S1 that the time profiles of NOx and O_3 vary substantially across the single precursor experiments and the mixtures. This is a characteristic of the method of initiating photochemistry in our experiments, through photolysis of a VOC / NOx mixture in the initial absence of O_3. Within the same single VOC systems, the O_3 concentration temporal profile can vary with VOC concentration at the similar VOC/NOx values. It is particularly notable in the α-pinene experiments owing to its reactivity towards O_3. As expected, there is a more ozone production in some systems (notably those containing isoprene). The Leighton ratios shown in Figure S2 indicate wide variation in the deviation from PSS across the systems, with the high concentration single VOC *o*-cresol experiments and the α-pinene / *o*-cresol and α-pinene / isoprene binary mixtures showing the greatest +ve deviation (i.e. greatest ability for RO_2 and HO_2 to compete with O_3 for NO), whereas the single VOC isoprene and α-pinene, binary isoprene / *o*-cresol and ternary systems all move towards low φ -values.

It was shown in Figure 2 that the turnover of each VOC was different, likely resulting from the differential reactivity of each VOC towards the different oxidants present in the systems at any one time. However, it can be seen that the turnover of each individual VOC was comparable across each system (with the notable exceptions of decreased α-pinene turnover in its binary mixture with *o*-cresol and slightly increased *o*-cresol turnover in the ternary mixture). This may be i) coincidental, ii) indicative that the oxidant regimes remain comparable between experiments or iii) indicative that the turnover is relatively insensitive to the change in oxidant regimes between the mixtures in our experiments. Figure 1 and S1 show the differences in O_3 across systems, so the differences in oxidants are likely to be non-negligible (option ii)). In relation to the turnover with respect to each oxidant in a mixed oxidant system, it should be borne in mind when comparing the results from different studies that results may diverge if the dominant oxidant changes. For example, Figure 6 shows that in the MAC α-pinene / isoprene experiments, roughly twice as much α-pinene consumption was due to O_3 reaction as to OH consumption. By contrast, in the experiments in the Julich Plant Aerosol Chamber reported in McFiggans et al. (2019) around 90% of the consumption was estimated to result from OH reaction.

Control of the oxidant regime in chamber experiments is strongly dictated by the goals of the study. It is perhaps most straightforward in a dark system in the absence of NOx, where only O_3 is being introduced with a single unsaturated VOC. Even then, the chemical regime can change as the

oxidant is consumed and moves from excess to limited. Moreover, the yield of OH from ozonolysis can be non-negligible, such that the VOC consumption from the OH oxidation must be considered. A dark OH source (such as ozonolysis of TME) can be used for oxidation of a saturated VOC to access the OH decay relatively "cleanly", though the possibility for interaction between the source VOC and SOA precursor derived RO_2 must be remembered. Dark oxidation by continuously injected NO_3 in the absence of O_3 can also provide a "clean" system with relatively few interfering pathways. NO_3 generated from O_3 reaction with NO_2 starts to become quite complex. The competition between oxidants in establishing the dark consumption of unsaturated VOC will be challenging, though the NO_3 reaction can dominate in systems containing phenolic compounds such as *o*-cresol. In illuminated systems, the oxidant regime becomes complex quite quickly. Photo-oxidation in the absence of NOx can access OH consumption of saturated compounds more straightforwardly than for unsaturated VOCs, where ozonolysis (and its associated secondary OH source) must be considered. Photo-oxidation in the presence of NOx introduces about as much complexity as can be envisaged. Photo-oxidation of multiple VOCs in the presence of NOx multiplies this complexity. The study of McFiggans et al. (2019) avoided many of the challenges faced in the current study by considering the mixture of biogenic VOCs in the absence of NOx and in a regime dominated by OH oxidation. This can be considered reasonable, since mixtures of these VOCs might exist in the clean troposphere, remote from anthropogenic sources. In studying mixtures of anthropogenic and biogenic VOCs, it might be considered less reasonable since anthropogenic VOCs would seldom exist in the absence of appreciable NOx. Related to this, it should also be noted that, whilst maintaining the VOC : NO_x ratio relatively constant across the systems is desirable, with reduced VOC concentrations this will lead to reduced NO concentrations. This will inevitably lead to reduced OH concentrations and hence VOC turnover. This is of importance when comparing the single VOC experiments at different concentrations, but less important when considering the initially isoreactive mixtures, since the VOCs have been chosen for their reactivity such that their concentrations are at least of comparable magnitude at comparable mixture reactivity.

One feature of chamber experiments using mixtures of VOCs is the ability to exploit their differential reactivity towards the oxidants present in the system to attribute their decay to each of them. This reconciliation of the VOC decay, as shown in Figure 6, is potentially a powerful interpretive tool for diagnosis of the concentration of oxidants in the system and understanding of

the turnover of VOCs in the system practice. In our systems when *o*-cresol is present, there are limitations owing to the interference of the direct O_3 measurements owing to absorption of UV by *o*-cresol. However, the reconciliation in these cases can be used to aid validation of the correction based on CIMS measurement of *o*-cresol (see methods section 3). It should be noted any absorption by *o*-cresol oxidation products can still lead to bias in the reconciliation since O_3 will be underestimated. Clearly, direct measurement of OH could provide additional confidence in the oxidant field but adequate constraint can be provided by the indirect method described here.

A final consideration relates to the exploratory nature of the current study which aims to establish the suitability of the approach to reveal aspects of SOA formation in mixed VOC atmospheric systems inaccessible to experiments using a single precursor species. The broad suite of analytical techniques employed to investigate these aspects have varying requirements and some compromises have been necessary. Most importantly, the offline filter analyses require a minimum particle mass loading with the corresponding consumption of VOCs with varying yield. This has necessitated the use of initial VOC concentrations above ambient levels. Whilst such concentrations have been commonplace in chamber experiments, they do introduce limitations. Figure S2 indicates that the deviation from PSS is likely to be significantly affected by the reactions of RO_2 (and / or HO_2) with NO in some of the binary mixtures. One further important limitation arises from the non-scalability involved with processes that are higher than first order. Peroxy radical terminations often involves their cross-reaction which will be in competition with other bimolecular pathways; so, reactions that are second order in peroxy radical concentration will be in competition with those that are first order. This will be important in the termination of peroxy radicals formed during autoxidation leading to HOM formation. In particular, the reactions of large HOM-RO_2 with other large peroxy radicals leading to gas phase formation of accretion products in the "dimer" range may be over-represented at higher concentrations. Under clean ambient conditions, their reaction partners would likely be dominated by HO_2 from CO oxidation, or smaller organic peroxy radicals such as CH_3O_2 from CH_4 oxidation. Under more polluted conditions, the alkoxy pathways from NO reaction will be competitive or even dominant. Each of these aspects should also be considered when interpreting the interactions in mixed VOC systems.

5.2. Yield calculation and reporting

The representation of effectiveness of a VOC to produce SOA particle mass in a given system by its incremental yield is conceptually simple when there is only one VOC being oxidised. Equation (2) can be applied quite straightforwardly, but with consideration of the oxidant regime. There are, however, a number of considerations in the calculation and presentation of yield that should be discussed for single VOC experiments and several more that are of relevance for mixtures.

In Figure 3 we present a summary of the SOA particle mass in the various single VOC systems and their mixtures. It can be seen that the corrections made to account for the losses of particles to the chamber walls are substantial, with peak mass concentrations typically 30 to 40% higher than those measured, and no substantial decay after the peak mass has been formed (as expected). Whilst not without uncertainty, the loss of particles to the walls can be relatively straightforwardly estimated. This is not the case for the interactions of the walls with vapours, which has been the subject of extensive debate (Zhang et al., 2014;Loza et al., 2010;Ye et al., 2016;Krechmer et al., 2020). A full discussion of this subject and characterisation of vapour interaction with the Teflon chamber walls is not provided here (fluxes to and from the chamber walls). We acknowledge that these effects will likely be substantial and that these are unquantified in our reported SOA particle mass corrections and yields. In the comparisons between different systems in our chamber, it must therefore be noted that we are implicitly assuming the vapour-wall interactions are comparable. This will introduce unquantifiable errors, since there will likely be significant vapour pressure differences between products and vapour pressure dependencies of wall interactions. Most importantly, it means that, whilst the comparisons may (or may not) be valid across systems in our chamber, our reported yields are very likely not comparable with those in other chambers without further considerations. More broadly, any comparison of yields between chambers should be approached with extreme caution without full confidence that the vapour interactions with the walls of the specific chamber for the specific system have been well quantified.

Single value yields presented in Table 3 calculated at maximum SOA particle mass and maximum VOC consumed can provide useful classifications for comparisons of systems where temporal and mass dependence of yields are comparable. The mass dependent curves shown in Figures 4 and 5 capture further details of the behaviour throughout the experiments and fitting the “Odum” curves to the single VOC experiments enables the “predictions” of the yields presented in the figures and

as single values in Table 4 (as described in results section 4). There are a number of considerations when assessing whether it should be expected that such predictions will be valid. The first of these is the inclusion of the decay of all VOCs in the yield calculation. Whether the consumption of all VOCs in a mixture should be considered in calculating the mixed yield will depend on the question being addressed. It may be inappropriate to consider the consumption of a VOC that would not contribute to formation of SOA particles when investigating the change in yield of a VOC mixture. In the present study, and consistent with previous work, isoprene was consistently found to generate no measurable SOA particles above the background chamber concentration (<1 μg m^{-3}) at any initial isoprene concentration and hence exhibited negligible yield. Therefore, under the conditions of our experiments, when replacing half the reactivity of a higher yield VOC with isoprene in a binary mixture, it may be considered obvious that the SOA particle mass will be reduced. This is the case in the *α*-pinene / isoprene and *o*-cresol / isoprene mixtures. Instead, it may be more insightful to consider whether the yield of the *α*-pinene and *o*-cresol in the binary mixtures is reduced in the presence of isoprene, using their single VOC system yields as reference. This follows the approach for neutral seeded experiments in McFiggans et al. (2019). As reported in Table 4 and shown in Figure 5b), the measured binary yield is indeed below that of *α*-pinene alone (either including or excluding isoprene in the calculation). For the *o*-cresol / isoprene mixture, the effect is more ambiguous, mainly because the SOA mass had not finished increasing at the conclusion of the experiments, but also because the yields are lower and deviations between the yields more difficult to measure. It should be mentioned that the particle mass yield of isoprene has been measured to be substantial in the presence of acidic seeds (which were not used in our experiments) and cannot be ignored. This raises an interesting question: should there be a threshold below which the reference for mixture yield should exclude a component? Clearly a zero SOA yield component such as CO or CH_4 would not be expected to contribute any particle mass in a mixture and would be expected to reduce the overall mixture yield when replacing reactivity of a non-negligible yield SOA precursor. In such cases, and in the case of isoprene with a neutral seed, it appears to make sense to inspect the yield at the consumption of a known SOA precursor with reference to that of the precursor for any enhancement or suppression. In mixtures of multiple VOCs with non-negligible individual particle mass yields, it makes sense to compare the particle mass yield of the mixture to the linear combination of the individual precursor's yields at the same VOC consumption. The "prediction" based on the individual precursor experimental yields is

lower than the measurement in the α-pinene / o-cresol binary mixture, possibly indicating enhancement of the mass in the mixed experiment above that which would result from the yields of the individual VOCs. The "predictions" with and without isoprene consumption are comparable to the measurements in the ternary mixture. Without additional composition measurements, this could be interpreted as no interactions taking place, or possibly as the suppression of yield by the presence of isoprene offsetting the enhancement of the mass resulting from the combined oxidation of *α*-pinene and *o*-cresol. However, such predictions may be oversimplistic. Clearly the oxidation conditions vary significantly across the mixtures (as seen from Figure 1 and S1) and the differences in the chemical trajectories and the time series of the ratios of oxidants between the systems give reason to question the validity of the yield predictions. This is likely to be important in *α*-pinene containing systems. Here the particle mass yield from ozonolysis and OH consumption have been reported to differ substantially and Figure 6 shows that about twice as much *α*-pinene results from consumption by O_3 as that by OH in the *α*-pinene / isoprene system. In the single VOC *α*-pinene system, the consumption by each oxidant was found to comprise roughly 50% of the total, based on the assumption that the consumption not attributable to the measured O_3 was attributable to OH (not shown). A final consideration when reporting yields relates to the use of seeds as absorptive mass. Conventionally, SOA particle yield curves are plotted against absorptive mass which, in nucleation experiments, is equivalent to the SOA particle mass. In the seeded experiments in the current study, the seeds are used to provide a condensation sink to suppress nucleation, to compete effectively with the walls for condensable vapour and to facilitate measurement by ensuring particles are of a detectable size for composition measurement from early in the experiments. The seeds are nebulised from solution and introduced (and presumably maintained) as metastable aqueous electrolyte solution aerosol at the RH of the experiment. It is clear that they act as absorptive mass, since organic mass is observed early in the experiments by AMS (Figure 7 and S5) and they are internally mixed throughout the experiments, as evidenced by HTDMA measurements (shown in Figure 13). Whether the total inorganic mass should be included when interpreting yield data is not clear. Figure S4 depicts the yield behaviour with the inclusion of inorganic seed in the total particle mass, assuming it acts as an effective mass for absorptive partitioning. The added insight provided by such a plot is unclear, though there is a strong argument for dependence on total absorptive mass in the representation of absorptive partitioning even if this is reduced by a factor (analogous to a mass-based activity coefficient to account for non-ideal

mixing effects). Note here that inorganic nitrate formation from OH oxidation of NO_2 and subsequent neutralisation of the HNO_3 by available NH_3 leads to the changes in inorganic components throughout the experiments as shown in the top panels of Figure 13. Effects of changing inorganic seed composition could usefully provide the subject of future studies.

5.3. Chemical composition

The addition of measurements of particle chemical composition will provide important insights into the development of the photo-oxidation in mixtures and the resulting particle yields. Online measurements by AMS in Figures 7 and S5 indicate that single VOC *o*-cresol and its binary mixture with isoprene rapidly exhibit, and then maintain through to significant particle mass production, a higher degree of oxygenation than the other systems as represented by the f_{44}. This contrasts sharply with the lower f_{44} of all α-pinene-containing systems. Since α-pinene frequently dominates the mass owing to its high yield, this may offset any *o*-cresol-derived high f_{44} in systems containing both α-pinene and *o*-cresol. Clearly a less coarse diagnostic of composition is required to interrogate the reasons for the observed differences, though Shao et al. (2021a) provides more insight from the high-resolution AMS analyses. The FIGAERO-CIMS data shown in Figure 8 provide an indication of the sorts of analytical products that can aid this interpretation. Whilst the additional analyses presented in Du et al. (2021) can more fully explore the impacts of the mixing of SOA precursors, several features can be directly observed from the mass spectra. First, there is an evident increase in the contribution of higher mass ions with time in the α-pinene single VOC system that is not observed in either the *o*-cresol single VOC system or their binary mixture. Second, there is clear evidence for signal contributions from components in the mixture that are not present in the individual systems from the beginning of the experiment. This is expanded upon in Figure 9, which shows that much of the signal in analyses of the filters taken at the end of the in the ternary mixture is not found at masses corresponding to those found in individual component VOC oxidation. Such high-resolution analyses are required to unambiguously identify the specific products resulting from interactions in the system and to postulate mechanisms leading to their formation. It is not yet possible to state whether the "unique-to-mixture" molecules are formed by gas phase cross-reaction, condensed phase accretion in the particles or on the filter. Neither is it currently possible to unambiguously state that this signal corresponds to the same fraction of the

mass, owing to potential differential sensitivity. These aspects are discussed in detail in Shao et al. (2021b). Nonetheless, it can be stated that these compounds are only found in the mixed system. An important challenge with such identification and attributions is the requirement for substantial sampled mass. This may provide a lower limit to the yield and / or initial concentration of precursors that can be studied in this way. Nevertheless, the power of such analyses is further exploited in separating the isomeric contributions to particle components as shown in Figure 10a). Combining the power of offline and online analyses, this separation of $C_7H_7NO_4$ isomers in all *o*-cresol-containing systems may be used to interpret the significant differences in the time trends of $C_7H_7NO_4$ shown in the FIGAERO-CIMS data in Figure 10b). Whilst this may be indicative of mechanistic differences, there will be confounding differences in the rate of SOA particle mass formation between the systems (and hence abundance of absorptive mass) in addition to potential differences in the sensitivity in the different systems and total signal used for the normalisation because of the different FIGAERO filter loadings. These considerations are discussed in detail in Du et al. (2021) for all systems. Nonetheless, the differences in the fractional isomeric contributions and in the timeseries reveal substantial changes in the $C_7H_7NO_4$ contributions between the systems.

5.4. Properties: volatility, water uptake and phase

Figure 11 exploits the high-resolution analysis of the FIGAERO-CIMS data to present the changes in the O:C ratio of detected particle compounds as a function of their carbon number in all systems at the end of the experiments. Combining this with the ratio of signal in the particle and gas samples is used to indicate likely influences of the mixing of precursors on particle volatility. Whilst there are uncertainties associated with the partitioning, and hence volatility derivations it is evident that changes in the components present in mixtures can lead to change in the volatility and potentially yield, reported in detail in Voliotis et al. (2021a, b). This is extended in Figure 12, which re-expresses the FIGAERO-CIMS data as volatility distributions, further highlighting the differences between the particle volatility in the mixture and that in the single VOC systems. This is clearly complex but is broadly consistent with the observed yield behaviour for most systems. For example, the SOA particle volatility in the single α-pinene experiment at half reactivity is fairly similar to that measured in the binary system with isoprene, consistent with their comparable yields. Similarly, the measured volatility in the α-pinene and *o*-cresol binary and in the ternary systems

appear to be roughly between those obtained in the single precursor experiments, in line with the measured yields that were found to be higher than those in single *o*-cresol but equal or lower that those obtained in the single α-pinene experiments. Substantial apparent inconsistencies were found in the *o*-cresol and isoprene binary system, where the measured volatility appeared to be substantially higher than that in the single *o*-cresol system, whilst the SOA yields were somewhat comparable. The reason is unclear and additional investigation might focus on reconciliation of the discrepancies between the volatility and yield behaviour in this system. Figure 13 shows the behaviour of particle water uptake and the rebound fraction of particles in an impactor in three example systems. These have been chosen for their differences in rate of formation of SOA particle mass and, in our seeded experiments, the associated organic: inorganic particle mass ratio. Clearly the rate of decrease of particle hygroscopicity and of increase of rebound fraction at higher RH follows the rate of SOA particle mass increase in the system. This is a clear indication of the influence of the mixing of precursors on the change in particle properties through the change in rate of formation of condensable material (as explored in Wang et al., 2021a, b).

6. Further work

Whilst it is important to explore mixtures including multiple SOA particle precursors under controlled conditions to understand behaviour in the real atmosphere, and measurements in such mixtures can reveal features inaccessible to single VOC experiment, the experimental design will determine their usefulness. Alternative and supplementary methodologies may allow more direct resolution of outstanding questions related to precursor mixing. The effects of mixed and variable oxidant concentrations throughout chamber experiments is both problematic and insightful. Clearly secondary production of oxidants (both OH and ozone) may differentially influence the decay of VOCs in the mixture and it may not be possible to scavenge secondary oxidants, certainly without influencing the oxidation product distribution. In any case, secondary oxidant formation will occur in the real atmosphere and cannot be overlooked. More control over the primary oxidants may be achieved through use of "cleaner" sources, such as photolysis of H_2O_2. Care is required in the interpretation of condensed phase composition under the high peroxide concentrations required in such experiments, but the avoidance of O_3 from injection or NO_2 photolysis may be advantageous. Nevertheless, secondary O_3 will react with any unsaturated

compounds present. Selection of VOCs with low OH yields from ozonolysis may allow isolation of its pathways, but will limit the choice of mixtures. Augmentation of broadband illumination with discrete intense light sources such as in the JPAC chamber in the McFiggans et al. (2019) study may push up the $OH:O_3$ ratio such that the OH channels dominate, though care is necessary to avoid excessively high OH concentrations. Unless conducted at very low NOx concentrations, significant VOC consumption in batch mode chamber experiments will lead to variable VOC:NOx ratios. This will lead to variable production rate of ozone as well as changes in the relative importance of the NO-mediated alkoxy radical pathways. Mechanistic interpretation of such experiments must account for these changes. In any case, isolation of individual mechanistic pathways and probing details of kinetics and product yields may be more suited to more targeted laboratory studies than to chamber experiments. If it is not possible to control the oxidising environment across complex mixtures, then systematic exploration of mixtures with direct and more comprehensive oxidant and peroxy radical measurements would be of benefit. Such well-instrumented studies will be able to take full advantage of the trajectories through chemical space afforded by relatively long batch mode chamber experiments. Movement towards more atmospherically representative chemical regimes would benefit from lower VOC concentration experiments. However, moving towards a more realistic radical termination regime but would present detection limit challenges to composition measurements. A more comprehensive coverage of speciated VOC and OVOC measurements using modern online mass spectrometry methods and improved resolution of such temporally resolved instruments may avoid the need to combine online and offline techniques. Whilst they reveal important impacts of the temporal changes in VOC mixtures, the batch reactor experiments in the present study are complex. Use of well-mixed flow reactor experiments to look at multiple steady states can enable focus of batch reactor experiments on sensitive areas of the chemical regime. The range of potential mixtures is not finite and so there is a need to focus on targeted areas of importance. It is not immediately obvious how this should be done, though it should be remembered that oxidation and SOA formation will occur during both day and night and mixed night-time oxidation by NO_3 should not be forgotten.

7. Conclusions

A comprehensive suite of instrumentation was deployed to investigate the formation of SOA particulate mass on inorganic seeds in chamber photo-oxidation of anthropogenic (*o*-cresol) and

biogenic (α-pinene and isoprene) VOCs and their binary and ternary mixtures in the presence of NOx. Whilst compromises were necessary in the experimental design and the complexity of the systems introduced substantial challenges to their interpretation, a number of important observations were possible.

First, the photochemical trajectory is understandably system dependent and the rates of consumption of each VOC by each oxidant consequently variable.

Second, the yield concept typically used for an individual VOC requires careful consideration when adapting it for use with complex mixtures. In order to account for the dependence of condensed mass on available adsorptive mass, it will be necessary to use the individual component yield at the same mass as in the mixtures. However, in order to compare the mass formed at the same VOC consumption, it is necessary to reference this to the corresponding single precursor experiment at that same VOC consumption and therefore not that calculated at the same adsorptive mass.

In mixtures where the majority of the mass is contributed by only one component precursor, it is possible to identify the existence of, and quantify, any interactions in terms of SOA mass or yield. Thus, as shown in Figure 5 there is clear indication of suppression of the yield of α-pinene in its mixture with isoprene, but as with the *o*-cresol / isoprene mixture there is a possible indication of enhancement, though this is too small to be unambiguous.

It is straightforward to make a comparison between the predicted and measured yield in mixtures of precursors both with appreciable yield. It is straightforward to make a comparison between the measured yield of single components with its yield in a mixture with a precursor of zero yield. Where two components with appreciable yield are mixed with another VOC with no yield the reference point for the comparison is complex.

The mixed α-pinene / *o*-cresol system is measured to have enhanced yield above that expected from additivity of the individual VOC yield at the same consumption. In such mixtures, where there is a significant contribution to the SOA mass from more than one component precursor, we are unable to unambiguously attribute any discrepancies in predicted and measured mass to physical or chemical interactions. This is because yield and partitioned mass will depend both on

available adsorptive mass and upon the rate of consumption of individual VOC and production of condensable oxidation products. In the ternary system, the measured yield is comparable to that calculated from additivity of the component yields. It is unclear whether this is attributable to cancelling of suppression and enhancement effects, but chemical interactions are evident from the unique-to mixture components.

The trajectories of physical properties such as water uptake and phase behaviour of the particles will depend on the rates of formation of SOA particle mass, so changes in these rates in mixtures will control changes in particle physical properties.

Mixing experiments are crucial and highly beneficial for our understanding on atmospheric chemical interactions. However, the interpretation quickly becomes complex and both the experimental design and evaluation needs to be scrutinised carefully. Here, advanced online and offline compositional measurements can reveal substantial additional information to aid in the interpretation of yield data, including components uniquely found in mixtures and physicochemical property changes in the SOA formed from mixtures of VOCs.

Acknowledgments

The Manchester Aerosol Chamber received funding from the European Union's Horizon 2020 research and innovation programme under grant agreement no. 730997, which supports the EUROCHAMP2020 research programme. AV and MD acknowledge the Presidents Doctoral Scholarship from the University of Manchester and AV, the support from the Natural Environment Research Council (NERC) EAO Doctoral Training Partnership (grant no. NE/L002469/1). YW acknowledges CSC scholarship support. MRA acknowledges funding support from the Natural Environment Research Council (NERC) through the UK National Centre for Atmospheric Science (NCAS). Instrumentational support was funded through the NERC Atmospheric Measurement and Observational Facility (AMOF). We acknowledge Dr. Zhijun Wu from Peking University, China, for providing Bounce behaviour instrument through Trans-National Access (TNA) of EUROCHAMP-2020. MH and TFM acknowledge the strategic research area MERGE, the Swedish Research Council (grant number 2018-04430), the Formas (grant number 2019-586). TFM acknowledges the support from the EU Project FORCeS (grant agreement no. 821205).

Competing interests

The authors declare that they have no conflict of interest

Author contributions

GM, MRA, MH, TFM AV, YW, YS and MD conceived the study. AV, YW, YS and MD conducted the experiments and data analysis. TJB, DH and KP provided on-site support with the instrument deployment and data analysis procedures. JFH provided scientific advice. GM, AV, YW, YS and MD wrote the manuscript with inputs from all co-authors.

Data Availability

All the data used in this study are available upon request from the corresponding author(s)

References

Alfarra, M. R., Hamilton, J. F., Wyche, K. P., Good, N., Ward, M. W., Carr, T., Barley, M. H., Monks, P. S., Jenkin, M. E., Lewis, A. C., and McFiggans, G. B.: The effect of photochemical ageing and initial precursor concentration on the composition and hygroscopic properties of β-caryophyllene secondary organic aerosol, Atmos. Chem. Phys., 12, 6417-6436, 10.5194/acp-12-6417-2012, 2012.

Alfarra, M. R., Good, N., Wyche, K. P., Hamilton, J. F., Monks, P. S., Lewis, A. C., and McFiggans, G.: Water uptake is independent of the inferred composition of secondary aerosols derived from multiple biogenic VOCs, Atmos. Chem. Phys., 13, 11769-11789, 10.5194/acp-13-11769-2013, 2013.

Atkinson, R., Baulch, D. L., Cox, R. A., Crowley, J. N., Hampson, R. F., Hynes, R. G., Jenkin, M. E., Rossi, M. J., Troe, J., and Subcommittee, I.: Evaluated kinetic and photochemical data for atmospheric chemistry: Volume II – gas phase reactions of organic species, Atmos. Chem. Phys., 6, 3625-4055, 10.5194/acp-6-3625-2006, 2006.

Aumont, B., Szopa, S., and Madronich, S.: Modelling the evolution of organic carbon during its gas-phase tropospheric oxidation: development of an explicit model based on a self generating approach, Atmos. Chem. Phys., 5, 2497-2517, 10.5194/acp-5-2497-2005, 2005.

Bannan, T. J., Le Breton, M., Priestley, M., Worrall, S. D., Bacak, A., Marsden, N. A., Mehra, A., Hammes, J., Hallquist, M., Alfarra, M. R., Krieger, U. K., Reid, J. P., Jayne, J., Robinson, W., McFiggans, G., Coe, H., Percival, C. J., and Topping, D.: A method for extracting calibrated volatility information from the FIGAERO-HR-ToF-CIMS and its experimental application, Atmos Meas Tech, 12, 1429-1439, 10.5194/amt-12-1429-2019, 2019.

Berndt, T., Richters, S., Jokinen, T., Hyttinen, N., Kurtén, T., Otkjær, R. V., Kjaergaard, H. G., Stratmann, F., Herrmann, H., Sipilä, M., Kulmala, M., and Ehn, M.: Hydroxyl radical-induced formation of highly oxidized organic compounds, Nature Communications, 7, 13677, 10.1038/ncomms13677, 2016.

Berndt, T., Mentler, B., Scholz, W., Fischer, L., Herrmann, H., Kulmala, M., and Hansel, A.: Accretion Product Formation from Ozonolysis and OH Radical Reaction of α-Pinene: Mechanistic Insight and the Influence of Isoprene and Ethylene, Environmental Science & Technology, 52, 11069-11077, 10.1021/acs.est.8b02210, 2018.

Bianchi, F., Kurten, T., Riva, M., Mohr, C., Rissanen, M. P., Roldin, P., Berndt, T., Crounse, J. D., Wennberg, P. O., Mentel, T. F., Wildt, J., Junninen, H., Jokinen, T., Kulmala, M., Worsnop, D. R., Thornton, J. A., Donahue, N., Kjaergaard, H. G., and Ehn, M.: Highly Oxygenated Organic

Molecules (HOM) from Gas-Phase Autoxidation Involving Peroxy Radicals: A Key Contributor to Atmospheric Aerosol, Chem Rev, 119, 3472-3509, 10.1021/acs.chemrev.8b00395, 2019.

Carlton, A. G., Wiedinmyer, C., and Kroll, J. H.: A review of Secondary Organic Aerosol (SOA) formation from isoprene, Atmos. Chem. Phys., 9, 4987-5005, 10.5194/acp-9-4987-2009, 2009.

Cash, J. M., Heal, M. R., Langford, B., and Drewer, J.: A review of stereochemical implications in the generation of secondary organic aerosol from isoprene oxidation, Environmental Science: Processes & Impacts, 18, 1369-1380, 10.1039/C6EM00354K, 2016.

Charan, S. M., Huang, Y., and Seinfeld, J. H.: Computational Simulation of Secondary Organic Aerosol Formation in Laboratory Chambers, Chem Rev, 119, 11912-11944, 10.1021/acs.chemrev.9b00358, 2019.

Cohen, A. J., Brauer, M., Burnett, R., Anderson, H. R., Frostad, J., Estep, K., Balakrishnan, K., Brunekreef, B., Dandona, L., Dandona, R., Feigin, V., Freedman, G., Hubbell, B., Jobling, A., Kan, H., Knibbs, L., Liu, Y., Martin, R., Morawska, L., Pope, C. A., III, Shin, H., Straif, K., Shaddick, G., Thomas, M., van Dingenen, R., van Donkelaar, A., Vos, T., Murray, C. J. L., and Forouzanfar, M. H.: Estimates and 25-year trends of the global burden of disease attributable to ambient air pollution: an analysis of data from the Global Burden of Diseases Study 2015, The Lancet, 389, 1907-1918, 10.1016/S0140-6736(17)30505-6, 2017.

Cox, R. A., Ammann, M., Crowley, J. N., Herrmann, H., Jenkin, M. E., McNeill, V. F., Mellouki, A., Troe, J., and Wallington, T. J.: Evaluated kinetic and photochemical data for atmospheric chemistry: Volume VII – Criegee intermediates, Atmos. Chem. Phys., 20, 13497–13519, https://doi.org/10.5194/acp-20-13497-2020, 2020

Crounse, J. D., Nielsen, L. B., Jørgensen, S., Kjaergaard, H. G., and Wennberg, P. O.: Autoxidation of Organic Compounds in the Atmosphere, The Journal of Physical Chemistry Letters, 4, 3513-3520, 10.1021/jz4019207, 2013.

Donahue, N. M., Robinson, A. L., Stanier, C. O., and Pandis, S. N.: Coupled partitioning, dilution, and chemical aging of semivolatile organics, Environmental Science & Technology, 40, 2635-2643, 2006.

Donahue, N. M., Epstein, S. A., Pandis, S. N., and Robinson, A. L.: A two-dimensional volatility basis set: 1. organic-aerosol mixing thermodynamics, Atmos. Chem. Phys., 11, 3303-3318, 10.5194/acp-11-3303-2011, 2011.

Donahue, N. M., Henry, K. M., Mentel, T. F., Kiendler-Scharr, A., Spindler, C., Bohn, B., Brauers, T., Dorn, H. P., Fuchs, H., Tillmann, R., Wahner, A., Saathoff, H., Naumann, K.-H., Möhler, O., Leisner, T., Müller, L., Reinnig, M.-C., Hoffmann, T., Salo, K., Hallquist, M., Frosch, M., Bilde, M., Tritscher, T., Barmet, P., Praplan, A. P., DeCarlo, P. F., Dommen, J., Prévôt, A. S. H., and Baltensperger, U.: Aging of biogenic secondary organic aerosol via gas-phase OH radical reactions, 109, 13503-13508, 10.1073/pnas.1115186109 %J Proceedings of the National Academy of Sciences, 2012.

Du, M., Voliotis, A., Shao, Y., Wang, Y., Bannan, T. J., Pereira, K., Hamilton J. F., Percival C. J., Alfarra, M. R., McFiggans, G.: Combined application of on-line FIGAERO-CIMS and off-line

Orbitrap LC-MS to characterize the chemical composition of SOA in smog chamber studies. In preparation for Atmos. Chem. Phys. Discuss., 2021a

Ehn, M., Kleist, E., Junninen, H., Petäjä, T., Lönn, G., Schobesberger, S., Dal Maso, M., Trimborn, A., Kulmala, M., Worsnop, D. R., Wahner, A., Wildt, J., and Mentel, T. F.: Gas phase formation of extremely oxidized pinene reaction products in chamber and ambient air, Atmos. Chem. Phys., 12, 5113-5127, 10.5194/acp-12-5113-2012, 2012.

Ehn, M., Thornton, J. A., Kleist, E., Sipilä, M., Junninen, H., Pullinen, I., Springer, M., Rubach, F., Tillmann, R., Lee, B., Lopez-Hilfiker, F., Andres, S., Acir, I.-H., Rissanen, M., Jokinen, T., Schobesberger, S., Kangasluoma, J., Kontkanen, J., Nieminen, T., Kurtén, T., Nielsen, L. B., Jørgensen, S., Kjaergaard, H. G., Canagaratna, M., Maso, M. D., Berndt, T., Petäjä, T., Wahner, A., Kerminen, V.-M., Kulmala, M., Worsnop, D. R., Wildt, J., and Mentel, T. F.: A large source of low-volatility secondary organic aerosol, Nature, 506, 476-479, 10.1038/nature13032, 2014.

Emanuelsson, E. U., Hallquist, M., Kristensen, K., Glasius, M., Bohn, B., Fuchs, H., Kammer, B., Kiendler-Scharr, A., Nehr, S., Rubach, F., Tillmann, R., Wahner, A., Wu, H. C., and Mentel, T. F.: Formation of anthropogenic secondary organic aerosol (SOA) and its influence on biogenic SOA properties, Atmos. Chem. Phys., 13, 2837-2855, 10.5194/acp-13-2837-2013, 2013.

Garmash, O., Rissanen, M. P., Pullinen, I., Schmitt, S., Kausiala, O., Tillmann, R., Zhao, D., Percival, C., Bannan, T. J., Priestley, M., Hallquist, Å. M., Kleist, E., Kiendler-Scharr, A., Hallquist, M., Berndt, T., McFiggans, G., Wildt, J., Mentel, T. F., and Ehn, M.: Multi-generation OH oxidation as a source for highly oxygenated organic molecules from aromatics, Atmos. Chem. Phys., 20, 515-537, 10.5194/acp-20-515-2020, 2020.

Goldstein, A. H., and Galbally, I. E.: Known and unexplored organic constituents in the earth's atmosphere, Environmental Science & Technology, 41, 1514-1521, 2007.

Good, N., Coe, H., and McFiggans, G.: Instrumentational operation and analytical methodology for the reconciliation of aerosol water uptake under sub- and supersaturated conditions, Atmos. Meas. Tech., 3, 1241-1254, 10.5194/amt-3-1241-2010, 2010.

Hallquist, M., Wenger, J. C., Baltensperger, U., Rudich, Y., Simpson, D., Claeys, M., Dommen, J., Donahue, N. M., George, C., Goldstein, A. H., Hamilton, J. F., Herrmann, H., Hoffmann, T., Iinuma, Y., Jang, M., Jenkin, M. E., Jimenez, J. L., Kiendler-Scharr, A., Maenhaut, W., McFiggans, G., Mentel, T. F., Monod, A., Prévôt, A. S. H., Seinfeld, J. H., Surratt, J. D., Szmigielski, R., and Wildt, J.: The formation, properties and impact of secondary organic aerosol: current and emerging issues, Atmos. Chem. Phys., 9, 5155-5236, 10.5194/acp-9-5155-2009, 2009.

Hamilton, J. F., Alfarra, M. R., Wyche, K. P., Ward, M. W., Lewis, A. C., McFiggans, G. B., Good, N., Monks, P. S., Carr, T., White, I. R., and Purvis, R. M.: Investigating the use of secondary organic aerosol as seed particles in simulation chamber experiments, Atmospheric Chemistry and Physics, 11, 5917-5929, 10.5194/acp-11-5917-2011, 2011.

Hao, L. Q., Yli-Pirilä, P., Tiitta, P., Romakkaniemi, S., Vaattovaara, P., Kajos, M. K., Rinne, J., Heijari, J., Kortelainen, A., Miettinen, P., Kroll, J. H., Holopainen, J. K., Smith, J. N., Joutsensaari, J., Kulmala, M., Worsnop, D. R., and Laaksonen, A.: New particle formation from the oxidation

of direct emissions of pine seedlings, Atmos. Chem. Phys., 9, 8121-8137, 10.5194/acp-9-8121-2009, 2009.

IPCC: Climate Change 2013: The Physical Science Basis. Contribution of Working Group I to the Fifth Assessment Report of the Intergovernmental Panel on Climate Change, Cambridge University Press, Cambridge, United Kingdom and New York, NY, USA, 1535 pp., 2013.

IPCC: Global Warming of 1.5oC

IPCC, 2018: Summary for Policymakers. In: Global warming of 1.5°C. An IPCC Special Report on the impacts of global warming of 1.5°C above pre-industrial levels and related global greenhouse gas emission pathways,in the context of strengthening the global response to the threat of climate change, sustainable development, and efforts to eradicate poverty, World Meteorological Organization, 2018.

Jaoui, M., and Kamens, R. M.: Gaseous and Particulate Oxidation Products Analysis of a Mixture of α-pinene + β-pinene/O3/Air in the Absence of Light and α-pinene + β-pinene/NOx/Air in the Presence of Natural Sunlight, Journal of Atmospheric Chemistry, 44, 259-297, 10.1023/A:1022977427523, 2003.

Jenkin, M. E., Wyche, K. P., Evans, C. J., Carr, T., Monks, P. S., Alfarra, M. R., Barley, M. H., McFiggans, G. B., Young, J. C., and Rickard, A. R.: Development and chamber evaluation of the MCM v3.2 degradation scheme for β-caryophyllene, Atmos. Chem. Phys., 12, 5275-5308, 10.5194/acp-12-5275-2012, 2012.

Jokinen, T., Berndt, T., Makkonen, R., Kerminen, V.-M., Junninen, H., Paasonen, P., Stratmann, F., Herrmann, H., Guenther, A. B., Worsnop, D. R., Kulmala, M., Ehn, M., and Sipilä, M.: Production of extremely low volatile organic compounds from biogenic emissions: Measured yields and atmospheric implications, 112, 7123-7128, 10.1073/pnas.1423977112 %J Proceedings of the National Academy of Sciences, 2015.

Joutsensaari, J., Loivamäki, M., Vuorinen, T., Miettinen, P., Nerg, A. M., Holopainen, J. K., and Laaksonen, A.: Nanoparticle formation by ozonolysis of inducible plant volatiles, Atmos. Chem. Phys., 5, 1489-1495, 10.5194/acp-5-1489-2005, 2005.

Kaltsonoudis, C., Kostenidou, E., Louvaris, E., Psichoudaki, M., Tsiligiannis, E., Florou, K., Liangou, A., and Pandis, S. N.: Characterization of fresh and aged organic aerosol emissions from meat charbroiling, Atmos. Chem. Phys., 17, 7143-7155, 10.5194/acp-17-7143-2017, 2017.

Kanakidou, M., Seinfeld, J. H., Pandis, S. N., Barnes, I., Dentener, F. J., Facchini, M. C., Van Dingenen, R., Ervens, B., Nenes, A., Nielsen, C. J., Swietlicki, E., Putaud, J. P., Balkanski, Y., Fuzzi, S., Horth, J., Moortgat, G. K., Winterhalter, R., Myhre, C. E. L., Tsigaridis, K., Vignati, E., Stephanou, E. G., and Wilson, J.: Organic aerosol and global climate modelling: a review, Atmos. Chem. Phys., 5, 1053-1123, 10.5194/acp-5-1053-2005, 2005.

Kiendler-Scharr, A., Wildt, J., Maso, M. D., Hohaus, T., Kleist, E., Mentel, T. F., Tillmann, R., Uerlings, R., Schurr, U., and Wahner, A.: New particle formation in forests inhibited by isoprene emissions, Nature, 461, 381-384, 10.1038/nature08292, 2009.

Krechmer, J. E., Day, D. A., and Jimenez, J. L.: Always Lost but Never Forgotten: Gas-Phase Wall Losses Are Important in All Teflon Environmental Chambers, Environmental Science & Technology, 54, 12890-12897, 10.1021/acs.est.0c03381, 2020.

Leighton, P. A.: Photochemistry of air pollution, 9, Phys. Chem., 300 pp., 1961.

Liu, Y., Wu, Z., Wang, Y., Xiao, Y., Gu, F., Zheng, J., Tan, T., Shang, D., Wu, Y., Zeng, L., Hu, M., Bateman, A. P., and Martin, S. T.: Submicrometer Particles Are in the Liquid State during Heavy Haze Episodes in the Urban Atmosphere of Beijing, China, Environ Sci Tech Let, 4, 427-432, 10.1021/acs.estlett.7b00352, 2017.

Loza, C. L., Chan, A. W. H., Galloway, M. M., Keutsch, F. N., Flagan, R. C., and Seinfeld, J. H.: Characterization of Vapor Wall Loss in Laboratory Chambers, Environmental Science & Technology, 44, 5074-5078, 10.1021/es100727v, 2010.

McFiggans, G., Coe, H., Burgess, R., Allan, J., Cubison, M., Alfarra, M. R., Saunders, R., Saiz-Lopez, A., Plane, J. M. C., Wevill, D., Carpenter, L., Rickard, A. R., and Monks, P. S.: Direct evidence for coastal iodine particles from Laminaria macroalgae – linkage to emissions of molecular iodine, Atmos. Chem. Phys., 4, 701-713, 10.5194/acp-4-701-2004, 2004.

McFiggans, G., Mentel, T. F., Wildt, J., Pullinen, I., Kang, S., Kleist, E., Schmitt, S., Springer, M., Tillmann, R., Wu, C., Zhao, D., Hallquist, M., Faxon, C., Le Breton, M., Hallquist, A. M., Simpson, D., Bergstrom, R., Jenkin, M. E., Ehn, M., Thornton, J. A., Alfarra, M. R., Bannan, T. J., Percival, C. J., Priestley, M., Topping, D., and Kiendler-Scharr, A.: Secondary organic aerosol reduced by mixture of atmospheric vapours, Nature, 565, 587-593, 10.1038/s41586-018-0871-y, 2019.

Mehra, A., Wang, Y., Krechmer, J. E., Lambe, A., Majluf, F., Morris, M. A., Priestley, M., Bannan, T. J., Bryant, D. J., Pereira, K. L., Hamilton, J. F., Rickard, A. R., Newland, M. J., Stark, H., Croteau, P., Jayne, J. T., Worsnop, D. R., Canagaratna, M. R., Wang, L., and Coe, H.: Evaluation of the chemical composition of gas- and particle-phase products of aromatic oxidation, Atmos. Chem. Phys., 20, 9783-9803, 10.5194/acp-20-9783-2020, 2020.

Mellouki, A., Ammann, M., Cox, R. A., Crowley, J. N., Herrmann, H., Jenkin, M. E., McNeill, V. F., Troe, J., and Wallington, T. J.: Evaluated kinetic and photochemical data for atmospheric chemistry: volume VIII – gas-phase reactions of organic species with four, or more, carbon atoms (≥ C4), Atmos. Chem. Phys., 21, 4797-4808, 10.5194/acp-21-4797-2021, 2021.

Mentel, T. F., Wildt, J., Kiendler-Scharr, A., Kleist, E., Tillmann, R., Dal Maso, M., Fisseha, R., Hohaus, T., Spahn, H., Uerlings, R., Wegener, R., Griffiths, P. T., Dinar, E., Rudich, Y., and Wahner, A.: Photochemical production of aerosols from real plant emissions, Atmos. Chem. Phys., 9, 4387-4406, 10.5194/acp-9-4387-2009, 2009.

Molteni, U., Bianchi, F., Klein, F., El Haddad, I., Frege, C., Rossi, M. J., Dommen, J., and Baltensperger, U.: Formation of highly oxygenated organic molecules from aromatic compounds, Atmos. Chem. Phys., 18, 1909-1921, 10.5194/acp-18-1909-2018, 2018.

Nakao, S., Shrivastava, M., Nguyen, A., Jung, H., and Cocker, D.: Interpretation of Secondary Organic Aerosol Formation from Diesel Exhaust Photooxidation in an Environmental Chamber, Aerosol Sci Tech, 45, 964-972, 10.1080/02786826.2011.573510, 2011.

Nakao, S., Liu, Y., Tang, P., Chen, C. L., Zhang, J., and Cocker Iii, D. R.: Chamber studies of SOA formation from aromatic hydrocarbons: observation of limited glyoxal uptake, Atmos. Chem. Phys., 12, 3927-3937, 10.5194/acp-12-3927-2012, 2012.

Ng, N. L., Canagaratna, M. R., Zhang, Q., Jimenez, J. L., Tian, J., Ulbrich, I. M., Kroll, J. H., Docherty, K. S., Chhabra, P. S., Bahreini, R., Murphy, S. M., Seinfeld, J. H., Hildebrandt, L., Donahue, N. M., DeCarlo, P. F., Lanz, V. A., Prévôt, A. S. H., Dinar, E., Rudich, Y., and Worsnop, D. R.: Organic aerosol components observed in Northern Hemispheric datasets from Aerosol Mass Spectrometry, Atmos. Chem. Phys., 10, 4625-4641, 10.5194/acp-10-4625-2010, 2010.

Nordin, E. Z., Eriksson, A. C., Roldin, P., Nilsson, P. T., Carlsson, J. E., Kajos, M. K., Hellén, H., Wittbom, C., Rissler, J., Löndahl, J., Swietlicki, E., Svenningsson, B., Bohgard, M., Kulmala, M., Hallquist, M., and Pagels, J. H.: Secondary organic aerosol formation from idling gasoline passenger vehicle emissions investigated in a smog chamber, Atmos. Chem. Phys., 13, 6101-6116, 10.5194/acp-13-6101-2013, 2013.

Odum, J. R., Hoffmann, T., Bowman, F., Collins, D., Flagan, R. C., and Seinfeld, J. H.: Gas/Particle Partitioning and Secondary Organic Aerosol Yields, Environmental Science & Technology, 30, 2580-2585, 10.1021/es950943+, 1996.

Pankow, J. F.: An absorption-model of gas-particle partitioning of organic-compounds in the atmosphere, Atmos. Environ., 28, 185–188, 10.1016/1352-2310(94)90093-0, 1994.

Pinto, D. M., Tiiva, P., Miettinen, P., Joutsensaari, J., Kokkola, H., Nerg, A.-M., Laaksonen, A., and Holopainen, J. K.: The effects of increasing atmospheric ozone on biogenic monoterpene profiles and the formation of secondary aerosols, Atmos Environ, 41, 4877-4887, 10.1016/j.atmosenv.2007.02.006, 2007.

Platt, S. M., El Haddad, I., Zardini, A. A., Clairotte, M., Astorga, C., Wolf, R., Slowik, J. G., Temime-Roussel, B., Marchand, N., Ježek, I., Drinovec, L., Močnik, G., Möhler, O., Richter, R., Barmet, P., Bianchi, F., Baltensperger, U., and Prévôt, A. S. H.: Secondary organic aerosol formation from gasoline vehicle emissions in a new mobile environmental reaction chamber, Atmos. Chem. Phys., 13, 9141-9158, 10.5194/acp-13-9141-2013, 2013.

Priestley, M., Bannan, T. J., Le Breton, M., Worrall, S. D., Kang, S., Pullinen, I., Schmitt, S., Tillmann, R., Kleist, E., Zhao, D., Wildt, J., Garmash, O., Mehra, A., Bacak, A., Shallcross, D. E., Kiendler-Scharr, A., Hallquist, Å. M., Ehn, M., Coe, H., Percival, C. J., Hallquist, M., Mentel, T. F., and McFiggans, G.: Chemical characterisation of benzene oxidation products under high- and low-NOx conditions using chemical ionisation mass spectrometry, Atmos. Chem. Phys., 21, 3473-3490, 10.5194/acp-21-3473-2021, 2021.

Pullinen, I., Schmitt, S., Kang, S., Sarrafzadeh, M., Schlag, P., Andres, S., Kleist, E., Mentel, T. F., Rohrer, F., Springer, M., Tillmann, R., Wildt, J., Wu, C., Zhao, D., Wahner, A., and Kiendler-Scharr, A.: Impact of NOx on secondary organic aerosol (SOA) formation from α-pinene and β-pinene photooxidation: the role of highly oxygenated organic nitrates, Atmos. Chem. Phys., 20, 10125–10147, https://doi.org/10.5194/acp-20-10125-2020, 2020.

Reyes-Villegas, E., Bannan, T., Le Breton, M., Mehra, A., Priestley, M., Percival, C., Coe, H., and Allan, J. D.: Online Chemical Characterization of Food-Cooking Organic Aerosols: Implications

for Source Apportionment, Environmental Science & Technology, 52, 5308-5318, 10.1021/acs.est.7b06278, 2018.

Rohrer, F., Bohn, B., Brauers, T., Brüning, D., Johnen, F. J., Wahner, A., and Kleffmann, J.: Characterisation of the photolytic HONO-source in the atmosphere simulation chamber SAPHIR, Atmos. Chem. Phys., 5, 2189-2201, 10.5194/acp-5-2189-2005, 2005.

Sarrafzadeh, M., Wildt, J., Pullinen, I., Springer, M., Kleist, E., Tillmann, R., Schmitt, S. H., Wu, C., Mentel, T. F., Zhao, D., Hastie, D. R., and Kiendler-Scharr, A.: Impact of NOx and OH on secondary organic aerosol formation from β-pinene photooxidation, Atmos. Chem. Phys., 16, 11237–11248, 10.5194/acp-16-11237-2016, 2016.

Schervish, M., and Donahue, N. M.: Peroxy radical chemistry and the volatility basis set, Atmos. Chem. Phys., 20, 1183-1199, 10.5194/acp-20-1183-2020, 2020.

Schwantes, R. H., Schilling, K. A., McVay, R. C., Lignell, H., Coggon, M. M., Zhang, X., Wennberg, P. O., and Seinfeld, J. H.: Formation of highly oxygenated low-volatility products from cresol oxidation, Atmospheric Chemistry and Physics, 17, 3453-3474, 10.5194/acp-17-3453-2017, 2017.

Shao, Y., Wang, Y., Du, M., Voliotis, A., Alfarra, M. R., Turner, S. F., and McFiggans, G.: Characterisation of the Manchester Aerosol Chamber facility, Atmos. Meas. Tech. Discuss., 2021, 1-50, 10.5194/amt-2021-147, 2021a.

Shao, Y., Voliotis, A., Du, M., Wang, Y., Pereira, K., Hamilton, J., Alfarra, M. R., McFiggans, G.: Chemical composition of secondary organic aerosol particles formed from mixtures of anthropogenic and biogenic precursors. In preparation for Atmos. Chem. Phys. Discuss., 2021b.

Shao, Y., Voliotis, A., Du, M., Wang, Y., Pereira, K., Hamilton, J., Alfarra, M. R., McFiggans, G.: Characterisation of the oxidation state of secondary organic aerosols in mixed precursor systems. In preparation for Atmos. Chem. Phys. Discuss., 2021c.

Shilling, J. E., Zawadowicz, M. A., Liu, J. M., Zaveri, R. A., and Zelenyuk, A.: Photochemical Aging Alters Secondary Organic Aerosol Partitioning Behavior, Acs Earth Space Chem, 3, 2704-2716, 10.1021/acsearthspacechem.9b00248, 2019.

Shrivastava, M., Cappa, C. D., Fan, J., Goldstein, A. H., Guenther, A. B., Jimenez, J. L., Kuang, C., Laskin, A., Martin, S. T., Ng, N. L., Petaja, T., Pierce, J. R., Rasch, P. J., Roldin, P., Seinfeld, J. H., Shilling, J., Smith, J. N., Thornton, J. A., Volkamer, R., Wang, J., Worsnop, D. R., Zaveri, R. A., Zelenyuk, A., and Zhang, Q.: Recent advances in understanding secondary organic aerosol: Implications for global climate forcing, 55, 509-559, 10.1002/2016rg000540, 2017.

Spracklen, D. V., Jimenez, J. L., Carslaw, K. S., Worsnop, D. R., Evans, M. J., Mann, G. W., Zhang, Q., Canagaratna, M. R., Allan, J., Coe, H., McFiggans, G., Rap, A., and Forster, P.: Aerosol mass spectrometer constraint on the global secondary organic aerosol budget, Atmos. Chem. Phys., 11, 12109-12136, 10.5194/acp-11-12109-2011, 2011.

Thornton, J. A., Shilling, J. E., Shrivastava, M., D'Ambro, E. L., Zawadowicz, M. A., and Liu, J.: A Near-Explicit Mechanistic Evaluation of Isoprene Photochemical Secondary Organic Aerosol

Formation and Evolution: Simulations of Multiple Chamber Experiments with and without Added NOx, Acs Earth Space Chem, 4, 1161-1181, 10.1021/acsearthspacechem.0c00118, 2020.

Tiitta, P., Leskinen, A., Hao, L., Yli-Pirilä, P., Kortelainen, M., Grigonyte, J., Tissari, J., Lamberg, H., Hartikainen, A., Kuuspalo, K., Kortelainen, A. M., Virtanen, A., Lehtinen, K. E. J., Komppula, M., Pieber, S., Prévôt, A. S. H., Onasch, T. B., Worsnop, D. R., Czech, H., Zimmermann, R., Jokiniemi, J., and Sippula, O.: Transformation of logwood combustion emissions in a smog chamber: formation of secondary organic aerosol and changes in the primary organic aerosol upon daytime and nighttime aging, Atmos. Chem. Phys., 16, 13251-13269, 10.5194/acp-16-13251-2016, 2016.

Tsigaridis, K., and Kanakidou, M.: The Present and Future of Secondary Organic Aerosol Direct Forcing on Climate, Current Climate Change Reports, 4, 84-98, 10.1007/s40641-018-0092-3, 2018.

Tsiligiannis, E., Hammes, J., Salvador, C. M., Mentel, T. F., and Hallquist, M.: Effect of NOx on 1,3,5-trimethylbenzene (TMB) oxidation product distribution and particle formation, Atmos. Chem. Phys., 19, 15073-15086, 10.5194/acp-19-15073-2019, 2019.

VanReken, T. M., Greenberg, J. P., Harley, P. C., Guenther, A. B., and Smith, J. N.: Direct measurement of particle formation and growth from the oxidation of biogenic emissions, Atmos. Chem. Phys., 6, 4403-4413, 10.5194/acp-6-4403-2006, 2006.

Voliotis, A., Wang, Y., Shao, Y., Du, M., Bannan, T. J., Percival, C. J., Pandis, S. N., Alfarra, M. R., and McFiggans, G.: Exploring the composition and volatility of secondary organic aerosols in mixed anthropogenic and biogenic precursor systems, Atmos. Chem. Phys., 21, 14251-14273, 2021a

Voliotis, A., Wang, Y., Shao, Y., Du, M., Bannan, T. J., Percival, C. J., Pandis, S. N., Alfarra, M. R., and McFiggans, G.: The influence of the addition of a reactive low SOA yield VOC on the volatility of particles formed from photo-oxidation of anthropogenic – biogenic mixtures, in prep for Atmos. Chem. Phys. Discuss., 2021b

Wang, S., Wu, R., Berndt, T., Ehn, M., and Wang, L.: Formation of Highly Oxidized Radicals and Multifunctional Products from the Atmospheric Oxidation of Alkylbenzenes, Environmental Science & Technology, 51, 8442-8449, 10.1021/acs.est.7b02374, 2017.

Wang, Y., Mehra, A., Krechmer, J. E., Yang, G., Hu, X., Lu, Y., Lambe, A., Canagaratna, M., Chen, J., Worsnop, D., Coe, H., and Wang, L.: Oxygenated products formed from OH-initiated reactions of trimethylbenzene: autoxidation and accretion, Atmos. Chem. Phys., 20, 9563-9579, 10.5194/acp-20-9563-2020, 2020.

Weitkamp, E. A., Sage, A. M., Pierce, J. R., Donahue, N. M., and Robinson, A. L.: Organic Aerosol Formation from Photochemical Oxidation of Diesel Exhaust in a Smog Chamber, Environmental Science & Technology, 41, 6969-6975, 10.1021/es070193r, 2007.

Whalley, L. K., Stone, D., Bandy, B., Dunmore, R., Hamilton, J. F., Hopkins, J., Lee, J. D., Lewis, A. C., and Heard, D. E.: Atmospheric OH reactivity in central London: observations, model

predictions and estimates of in situ ozone production, Atmos. Chem. Phys., 16, 2109-2122, 10.5194/acp-16-2109-2016, 2016.

Wyche, K. P., Ryan, A. C., Hewitt, C. N., Alfarra, M. R., McFiggans, G., Carr, T., Monks, P. S., Smallbone, K. L., Capes, G., Hamilton, J. F., Pugh, T. A. M., and MacKenzie, A. R.: Emissions of biogenic volatile organic compounds and subsequent photochemical production of secondary organic aerosol in mesocosm studies of temperate and tropical plant species, Atmos. Chem. Phys., 14, 12781-12801, 10.5194/acp-14-12781-2014, 2014.

Ye, P., Ding, X., Hakala, J., Hofbauer, V., Robinson, E. S., and Donahue, N. M.: Vapor wall loss of semi-volatile organic compounds in a Teflon chamber, Aerosol Sci Tech, 50, 822-834, 10.1080/02786826.2016.1195905, 2016.

Zhang, X., Cappa, C. D., Jathar, S. H., Mcvay, R. C., Ensberg, J. J., Kleeman, M. J., and Seinfeld, J. H.: Influence of vapor wall loss in laboratory chambers on yields of secondary organic aerosol, P Natl Acad Sci USA, 111, 5802-5807, 10.1073/pnas.1404727111, 2014.

Ziemann, P. J., and Atkinson, R.: Kinetics, products, and mechanisms of secondary organic aerosol formation, Chemical Society Reviews, 41, 6582-6605, 10.1039/C2CS35122F, 2012.

[BLANK PAGE]

Paper 3: Chemical composition of secondary organic aerosol particles formed from mixtures of anthropogenic and biogenic precursors

This paper is going to be submitted in the journal of "Atmopsheric Chemistry and Physics" within 2021

Yunqi Shao[1], Aristeidis Voliotis[1], Mao Du[1], Yu Wang[1], Kelly Pereira[3], Jacqueline Hamilton[3], M. Rami Alfarra[1,2 ‡], Gordon McFiggans[1]

[1]School of Earth and Environmental Science, University of Manchester, Manchester, M13, 9PL, UK
[2]National Centre for Atmospheric Science
[3] Wolfson Atmospheric Chemistry Laboratories, Department of Chemistry, University of York, York, YO105DD, UK
‡ now at Environment & Sustainability Center, Qatar Environment & Energy Research Institute, Doha, Qatar

Correspondence to: Yunqi.Shao (Yunqi.Shao@Mancheste.ac.uk)

Abstract.

A series of experiments were designed and conducted in the Manchester Aerosol Chamber (MAC) to study the photooxidation of single and mixed biogenic (isoprene and α-pinene) and anthropogenic (*o*-cresol) precursors in the presence of NOx and ammonium sulphate seed particles. Several online techniques (HR-TOF-AMS, Semi-Continuous GC-MS, NOx and O_3 analyser) were coupled to the MAC to monitor the gas and particle mass concentrations. Secondary Organic Aerosol (SOA) particles were collected onto a quartz fibre filter at the end of each experiment and analysed using liquid chromatography ultra-high resolution mass spectrometry (LC-Orbitrap MS). The SOA particle chemical composition in single and mixed precursor systems was investigated using non-targeted accurate mass analysis of measurements in both negative and positive ionization modes to significantly reduce data complexity and analysis time, resulting in rapid extraction of useful chemical information. This non-targeted analysis is not widely used in environmental science and never previously in atmospheric simulation chamber studies. Products from α-pinene were found to dominate the binary mixed α-pinene / isoprene system in terms of signal contributed and the number of particle components detected. Isoprene photooxidation was found to generate negligible SOA particle mass under the investigated experimental conditions and isoprene-derived products made a negligible contribution to particle composition in the α-pinene / isoprene system. No compounds uniquely found in this system contributed sufficiently to be reliably considered as a tracer compound for the mixture. Methyl-nitrocatechol isomers ($C_7H_7NO_4$) and methyl-nitrophenol ($C_7H_7NO_3$) from *o*-cresol oxidation made dominant

contributions to the SOA particle composition in both the *o*-cresol / isoprene and *o*-cresol / α-pinene binary systems in negative ionization mode. In contrast, interactions in the oxidation mechanisms led to the formation of compounds uniquely found in the mixed *o*-cresol containing binary systems in positive ionization mode. $C_9H_{11}NO$ and $C_8H_8O_{10}$ made large signal contributions in the *o*-cresol / isoprene binary system. The SOA molecular composition in the *o*-cresol / α-pinene system in positive ionization mode is mainly driven by the large molecular weight compounds (e.g. $C_{20}H_{31}NO_4$, and $C_{20}H_{30}O_3$) uniquely found in the mixture. The SOA particle chemical composition formed in the ternary system is more complex. The molecular composition and signal abundance are both markedly similar to those in the single α-pinene system in positive ionization mode, with major contributions from *o*-cresol products in negative ionization mode.

1. Introduction

1.1. Organic Aerosols and its impacts

Atmospheric aerosols affect climate directly through scattering or absorbing solar-radiation (Novakov and Penner, 1993; Andreae and Crutzen, 1997) and indirectly by acting as cloud condensation nuclei (CCN) (Mcfiggans et al., 2006). Exposure to particulate matter has also been directly linked to adverse impacts on human health (WHO, 2016). Organic aerosol significantly contributes to fine particulate matter (PM) in the atmosphere (Fiore et al., 2012; Jimenez et al., 2009),and can affect human health through the deep penetration of small aerosol particles into the lungs through inhalation, and the deposition of larger particles in the upper respiratory tract (Burnett et al., 2014). Fine PM has a wide variety of primary (e.g. agricultural operations, industrial processes, and combustion processes) and secondary sources. In addition to secondary inorganic contributions from nitrate and sulphate, secondary organic aerosol (SOA) formed from the oxidation of atmospheric volatile organic vapours (VOCs) can make a major contribution (Hallquist et al., 2009).

1.2. SOA and its formation pathways

The chemical diversity of volatile organic compounds (VOCs) and their oxidation pathways substantially influence SOA chemical composition (Lim and Ziemann, 2009). VOCs can be both anthropogenic and biogenic in origin (Li et al., 2018). Common and abundant anthropogenic

VOCs include aromatic hydrocarbons such as benzene, toluene and cresol, emitted from a wide variety of human activities, e.g. cooking and biomass-burning (Atkinson and Arey, 2003), with the latter being an oxidation product of the former two compounds (Schwantes et al., 2017). Biogenic VOCs, including isoprene and monoterpenes (e.g. α-pinene) are emitted in large quantities by vegetation, oceanic macroalgae and microalgae (Bravo-Linares et al., 2010; Atkinson and Arey, 2003). Once emitted into the atmosphere, VOCs undergo oxidation by the prevailing atmospheric oxidants; the hydroxyl radical (OH) during daytime, the nitrate radical (NO_3) at night-time, and the unsaturated fraction by ozone during both day and night (Atkinson, 1997). The oxidation of VOCs can result in the formation of both more and less volatile organic products (Jimenez et al., 2009). Low volatility organic products can condense onto existing particles or form new particles through nucleation if sufficiently low in volatility, as described by the gas-particle partitioning framework (Schervish and Donahue, 2020; Donahue et al., 2011). VOC oxidation can result in a range of multi-functional products. Multiple generations of gas phase oxidation results in continually evolving chemical speciation either in the gas or particulate phase (Mcneill, 2015; Shrivastava et al., 2017) and owing to the complexity of gaseous and particulate phase oxidation pathways, SOA formation mechanisms remain unclear and require further investigation .

1.3. Prior studies of using offline techniques

Whilst techniques for online or semi-continuous SOA compositional measurements have recently become more widely adopted (Zhang et al., 2011; Ahlberg et al., 2017; Schwantes et al., 2017; Hamilton et al., 2021; Lopez-Hilfiker et al., 2014; Decarlo et al., 2006)), offline techniques can can generally still provide more detailed insight into molecular compositon . Offline techniques such as gas chromatography mass spectrometry (GC-MS) (Ono-Ogasawara et al., 2008; Saldarriaga-Noreña et al., 2018; Cropper et al., 2018), liquid chromatography mass spectrometry (LC-MS) (Coscollà et al., 2008; Buiarelli et al., 2017; Pereira et al., 2015) and inductively coupled plasma mass spectrometry (ICP-MS) (Kulkarni et al., 2007; Danadurai et al., 2011) can identify the chemical composition for thousands of organic compounds, with some of the techniques revealing information about compound's structure, alluding to potential sources and formation mechanisms (Liu et al., 2007; Singh et al., 2011; Ono-Ogasawara et al., 2008; Carlton et al., 2009; Kroll et al., 2005a; Ng et al., 2008; Nestorowicz et al., 2018; Eddingsaas et al., 2012). LC-MS has been widely employed for the chemical characterisation of laboratory generated SOA and ambient

SOA. For example, targeted analysis of SOA products using high-performance liquid chromatography time-of-flight mass spectrometry (HPLC-ToF-MS) illustrated a new pathway for the formation of 3-methyl-1,2,3-butane-tricarboxylic acid (MBTCA) through the further oxidation of nopinone, a known product in the oxidation of β-pinene by OH (Mutzel et al. (2016). Hamilton et al. (2021) used targeted LC-Orbitrap MS analysis of ambient Beijing filter samples to identify tracers of isoprene nitrate formation pathways in both gas and particle phases indicating a strong dependence on nitrate radicals from early afternoon onwards. These targeted approaches are somewhat limited in their inability to comprehensively account for the entire mass of SOA components, though it is impractical to extract the non-targeted chemical information by manual data processing in complex ambient systems. Non-targeted screening tools have been widely employed in metabolite and protein analysis to reduce data analysis time but are uncommon in environmental science applications. Chromatographic technique coupled with fourier transform mass spctrometers (e.g., Orbitrap) have sufficient resolution to characterise the chemical composition of complex particulate matter with the ability to distinguish structural isomers. Exploiting this capability, a methodology for automated non-targeted screening was presented by Pereira et al (2021) using ultrahigh-performance liquid chromatography–Orbitrap MS data. This non-targeted screening tool has been rigorously tested by authentic standards, and aims to providing molecular formula assignments and plausible structure information (among other information) for all detected compounds within a sample dataset. Moreover, the accurate mass spectrometry employed has a mass resolution of >6 decimal places, leading to substantial increase in the signal/noise ratio and enhanced quantification of low concentration species. Mehra et al. (2021) is one of the few studies applying automated non-targeted method in environmental matrices. This study aims to study the anthropogenic and biogenic contributions to organic aerosol by applying the automated non-targeted method for LC-Oribitrap MS data to characterize the SOA from the low-NOx oxidation of 1-methylnaphthalene, propylbenzene and 1,3,5-trimethylbenzene in laboratory measurement, alongside a characterization of the SOA from filters that were collected in an urban area. This study also compared the result with online technique a time-of-fight chemical ionisation mass spectrometer using an iodide ionisation system (I-CIMS), which show good agreement between observation of online I-CIMS results and results of offline LC-Orbitrap MS in negative ionization mode. In our present study, we will apply this automated non-targeted screening tool in SOA that generated in aerosol chamber, which will be a brand-new attempt.

1.4. Summary of studies on similar SOA systems

There are numerous studies investigating SOA formation from the oxidation of biogenic VOCs, particularly for terpenoid compounds (Stroud et al., 2001; Surratt et al., 2006; Dommen et al., 2006; Carlton et al., 2009; Camredon et al., 2010; Surratt et al., 2010; Henry et al., 2012; Ahlberg et al., 2017; Hoffmann et al., 1997; Odum et al., 1996). Isoprene (C_5H_8) is the most abundant biogenic VOC emission and α-pinene ($C_{10}H_{16}$) is one of the most abundant and widely studied biogenic monoterpene (Hallquist et al., 2009). Whilst oxidation products from these two biogenic precursors are both considered to contribute substantially to the global SOA budget, there are marked differences in their SOA particle mass yield; α-pinene has a yield in the range of 17 to 45% (Mcvay et al., 2016; Ng et al., 2007; Eddingsaas et al., 2012), while isoprene has a much lower yield in the range of 0 to5% (Dommen et al., 2006; Kroll et al., 2005a; Kroll et al., 2006; Pandis et al., 1991; Carlton et al., 2009). The reason for the low isoprene SOA yield is in part a result of the high volatility oxidation products. However, the yield of isoprene SOA strongly acid-dependent and closely related to the particle-phase acidity, which might be the reason found higher isoprene SOA yield in ambient (Surratt et al., 2007a) . Xu et al. (2021) demonstrated that over 98% of isoprene oxidized organic molecules by mole were classified as semi-VOC (SVOC) and intermediate-VOC (IVOC) with volatility ($\log_{10}C^*$, ug m^{-3}) range of -0.5 to 5, while about 1.3% of isoprene oxidation products were considered as low-VOC (LVOC). Conversely, the larger C_{10} monoterpene skeleton of α-pinene typically results in the formation of less volatile oxidation products. Lee et al. (2011) reported that the SOA from α-pinene ozonolysis required 80 ºC for complete volatilisation, and the volatility of α-pinene SOA strongly depended on the VOC/NOx ratios, forming volatile nitrate containing species under high NOx conditions.

There are many studies reporting the chemical characterisation of SOA formed in smog chambers from α-pinene and isoprene using liquid chromatography mass spectrometry (LC-MS). (Yasmeen et al., 2012; Surratt et al., 2006; Kahnt et al., 2014; Pereira et al., 2014; Winterhalter et al., 2003). Winterhalter et al. (2003) used LC-MS to demonstrated thet major particulate phase compounds from the O_3 and OH oxidation of α-pinene, such as cis-pinic acid, cis-pinonic acid, hydroxy-pinonic acid isomers, and possibly hydroxy-carboxylic acid. It is worth to noting that this study suggested the ozonolysis reaction is the main driven pathway of aerosol formation regard to its

performance of various experiments. Similarly, Surratt et al. (2006) studied isoprene photooxidation under various NOx conditions. The chemical composition of isoprene SOA products was analysed by a series of online and offline techniques (including LC-MS) and indicated that oligomerisation plays an important role in SOA formation pathways, especially under high NOx conditions, forming acidic products.

SOA can also be produced from anthropogenic VOCs (e.g. o-Cresol), although global biogenic SOA production (~88 TgC per year) is thought to dominate over the anthropogenic SOA production (~10 TgC per year) (Hallquist et al., 2009). Schwantes et al. (2017) studied the formation of low-volatility products from *o*-cresol photooxidation under various NOx conditions using chamber experiments with chemical ionization mass spectrometry (CIMS) and direct analysis in real time mass spectrometry (DART-MS). This study identified several *o*-cresol oxidation products, including the first generation product (methyl-catechol), second generation products (trihydroxy toluene and hydroxy methyl benzoquinone) and third generation products (tetrahydroxy toluene and dihydroxy methyl benzoquinone), indicating successive addition of OH radicals onto the aromatic ring during the oxidation, following expected mechanistic pathways (Atkinson and Aschmann, 1994; Olariu et al., 2002)

Despite the wealth of knowledge of gaseous and particulate phase product formation from the oxidation of single VOC precursors using chamber experiments, there is a comparative lack of understanding in the real atmosphere Online measurements of the OA composition by Aerodyne High Resolution Aerosol Mass Spectrometer (HR-TOF-AMS) and VOC by Ionicon Proton Transfer Reaction Mass Spectrometer (PTR-MS) during the CARES campaign in the vicinity of Sacramento, California indicated that the mixing of anthropogenic emissions from Sacramento with isoprene-rich air from the foothills enhance the production of OA (Shilling et al., 2013). This study suggested anthropogenic/biogenic interactions enhances OA production from biogenic species, suggesting the amount of isoprene SOA strongly depends on VOC/NOx ratio. However, the physical and chemical reasons for such interactions remain unclear and warrant further investigation. There have been several laboratory studies investigating the SOA formation in mixed VOC systems. Ahlberg et al. (2017) investigated SOA from VOC mixtures including biogenic (a-pinene, myrcene and isoprene) and anthropogenic VOCs (m-xylene) in an oxidation

flow reactor (OFR) equipped with high-resolution time-of-flight aerosol mass spectrometry (HR-ToF-AMS). Their results showed that the SOA mass yield formed from a VOC mixture containing myrcene was higher than expected, possibly a result of myrcene nucleating particles leading to an increased condensation sink under the conditions of the OFR. This study also found that the SOA particle size was larger in VOC mixtures with isoprene and unlimited oxidant supply. However, other studies indicate that isoprene could inhibit new particle formation by scavenging oxidant and forming relatively high volatility organic products than nucleating precursors (Kiendler-Scharr et al., 2009; Kiendler-Scharr et al., 2012). Mcfiggans et al. (2019) reported a reduction in SOA mass and yield from the VOC mixture of α-pinene and isoprene with an increasing fraction of isoprene in the mixture. This was attributed to isoprene acting as an OH scavenger and its radical oxidation products reacting with those formed from α-pinene, enhancing the overall volatility of the products in the mixture. This study indicates that interactions between VOC products should be considered to enable a mechanistic understanding of SOA formation in the ambient atmosphere. Shilling et al. (2019) reported that freshly formed isoprene-SOA did not fully mix with pre-existing SOA in isoprene/ α-pinene mixture system (e.g. aged isoprene-SOA and aged α-pinene SOA) over the 4 hours experimental time scale in the sequential condensation experiment, without observing notable suppression of SOA formation in α-pinene/isoprene mixture system.

1.5. This present study

In this study, we designed a series of chamber experiments using single binary and tertiary VOC systems, expanding on the work performed by McFiggans et al., (2019), with the aim of better understanding the chemical composition and interactions during SOA formation in mixed VOC systems. We move beyond the consideration of SOA formation from anthropogenic VOC precursors to consider the effect of their mixture with biogenic VOC. Ortho-cresol (*o*-cresol) was chosen as an anthropogenic precursor with a moderate SOA yield, with a comparable reactivity towards the hydroxyl radical (OH) and a negligible reactivity towards ozone. We retained the two biogenic precursors studied in McFiggans et al. (2019); isoprene being the dominant VOC emitted from plants globally, but with modest SOA formation potential and alpha-pinene (α -pinene), similarly widely emitted in lower amounts, but a more efficient SOA precursor.

The objectives of the present study are to investigate, using offline analysis of SOA chemical composition, whether (i) high yield precursors dominate the contribution to SOA formation of mixture systems and (ii) cross-products from mechanistic interactions in the oxidation of precursors feature strongly in the mixed precursor systems. A series of photochemical oxidation experiments were designed and conducted to produce SOA from the selected VOCs (α-pinene, isoprene and *o*-cresol) and their mixtures in the presence of neutral seed particles (ammonium sulphate) and NOx. The experimental programme included three single precursor systems, three binary precursor mixtures and one ternary mixture of precursors. The aerosol samples were collected onto a filter from each experiment and analysed offline using liquid chromatography ultra high resolution mass spectrometry with an automated non-targeted data processing methodology recently described in Pereira et. al (2021).

2. Method

2.1. Chamber description

All experiments were performed in the 18m^3 Manchester Aerosol Chamber (MAC). Briefly, the MAC operates as a batch reactor to study the atmospheric processing of multicomponent aerosols under controlled conditions. The chamber comprises an FEP Teflon bag mounted on three rectangular extruded aluminium frames, housed in an air-conditioned enclosure. Two 6 kW Xenon arc lamps (XBO 6000 W/HSLA OFR, Osram) and a bank of halogen lamps (Solux 50 W/4700 K, Solux MR16, USA) are mounted in the inner aluminium wall of the enclosure which is lined with reflective "space blanket" material to provide maximum and homogenous light intensity to simulate the realistic day-time atmospheric environment. To remove unwanted radiation flux below 300 nm, a quartz filter was mounted in front of each arc lamp. Removal of unwanted heat from the lamps and temperature and RH control of the chamber was assisted by conditioned air introduced between the bag and the enclosure at 3 m^3 s^{-1} and active water cooling of the mounting bars of the halogen lamps and of the filter in front of the arc lamps. Regular steady state actinometry experiments were conducted through the entire campaign and indicated that the photolysis rate of NO_2 (JNO_2) in a range of 1.83-3 x10^{-3}s^{-1} during experimental period. Photolysis of NO_2 leads to O_3 formation, which further photolyses to produce OH radicals in our moist experiments. Humidity and temperature are controlled by the humidifier and by controlling the air conditioning set-point during the experiment and continuously monitored using a dewpoint

hygrometer and a series of thermocouples and resistance probes throughout the chamber. Additional online instruments included a semi-continuous gas chromatography mass spectrometer (GCMS) for VOC measurement (Minaeian, 2017), a water-based condensation particles counter, a differential mobility particle sizer (DMPS) and an aerosol mass spectrometer (AMS) for particulate-phase compound measurement (Canagaratna et al., 2007). The filter collection, extraction, measurement and analysis techniques are described below. Full details of the MAC characterisation, the experimental procedure and instrumentation payload is provided in Shao et al. (2021).

2.2. Experimental Strategy

The experimental programme was conceived using a concept of "initial iso-reactivity" towards OH, with the intention of allowing a reasonably comparable contribution of oxidation products from each VOC at the chosen concentration and experimental conditions. Clearly this does not take into account consumption by oxidants other than OH formed during the experiment (notably ozone) and also neglects the reactivity of the subsequent oxidation products. The injected precursor mass was therefore chosen according to its reactivity towards OH (Atkinson, 2004). SOA composition was determined using analysis of chamber filter samples by liquid chromatography ultra-high mass spectrometry (LC-Orbitrap MS) and automated non-targeted data processing for all single precursor and mixed VOC systems.

2.3. Experimental Procedure

Programmed "pre-experiment" and "post- experiment" procedures were routinely conducted before and after each SOA experiment to minimize the possible contamination in the chamber. The "pre-experiment" and "post-experiment" are comprised of multiple automated fill/flush cycles with an approximate air flow rate of $3m^3$ min^{-1}, for cleaning the chamber. The upper and lower frames were free to move vertically to expand and collapse the bag during the fill/flush cycle. Filtered air was sequentially injected into and extracted from the bag, reducing contaminants in the bag with each cycle. Several instruments (e.g. WCPC, Model 49C O_3 analyser, Thermo Electron Corporation) and Model 42i NO-NO_2-NOx analyser, Thermo Scientific) were continuously connected to the chamber during the pre-experiment to monitor the concentration of particles, concentration of ozone and NOx, and to ensure the bag was sufficiently clean (with all aforementioned factors close to zero) to conduct the chamber background procedure. When

conducting this procedure, there were no reactants in the bag and the bag was stabilised for at least an hour for the instruments to establish the baseline of the clean chamber. In the following stage, VOC precursor(s), NOx and seed particles were injected into the chamber sequentially in dark conditions and the chamber remained steady for an hour for the instruments to obtain a baseline of the initial chamber conditions (e.g., experimental background) before the SOA experiment. The baselines of chamber background and experimental background were subsequently subtracted from the experimental measurements.

Ammonium sulphate seed particles were generated via atomization from ammonium sulphate solution (Puratonic, 99.999% purity) using a Topaz model ATM 230 aerosol generator. The concentration of seed particles in the chamber was controlled by altering the injection time and concentration of the prepared solution (0.01g/ml). The accumulating seed particles injected into the stainless-steel residence chamber for 1 min then diverting the main chamber injection flow for 30s during the final fill cycle of pre-experiment procedure. The liquid α-pinene, isoprene and *o*-cresol (Sigma Aldrich, GC grade ≥99.99% purity) were injected as required through the septum of a heated glass bulb and evaporated into an N_2 carrier flow into the chamber during this final fill along with NO_x as NO_2 from a cylinder, also carried by N_2. The injected VOC mass was calculated using the "initial OH isoreactivity" approach described above. Photochemistry was initiated by irradiating the VOC at a moderate VOC / NO_x ratio using the lamps as described above. The concentration of NO_x and O_3, particles number concentration and mass concentration were monitored during the experiment using the online instruments. SOA particles were collected on a blank filter (Whatman Quartz microfiber, 47 mm) mounted in a bespoke holder built into the flush pipework by flushing the remaining chamber contents after a 6-hour experiment. The filters were then wrapped in foil and stored at -18°C prior to analysis. Quartz fibre filters were pre-conditioned by heating in a furnace at 550℃ for 5.5 hours. Actinometry and off-gassing experiments were conducted regularly after several of SOA experiments to establish the consistency of the chamber's performance, evaluate the effectiveness of the cleaning procedure and confirm cleanliness of the chamber. "Background" filters were collected from the actinometry and off-gassing experiments. A summary of experimental conditions is given in Table 1.

Table 1: Experimental descriptions, VOC mixing ratios, VOC:NOx ratio and mass concentration of seed particles in chamber.

Experiment type	Experiment	Experimental conditions		
		Nominal VOC (ppbv)	Nominal VOC:NOx	Mass conc. $(NH_4)_2SO_4$ (ug/m^3)
Single Precursor	(a)	α-pinene: 309	7.7	72.6
	(b)	Isoprene: 164	7.1	101.9
	(c)	*o*-cresol: 400	9.1	47.8
Mixed Precursors (Binary)	(d)	α-pinene: 155 Isoprene: 82	9.9	50.5
	(e)	α-pinene: 155 *o*-cresol: 200	-	42.5
	(f)	Isoprene: 82 *o*-cresol: 200	8.3	49.6
Mixed Precursors (Ternary)	(g)	α-pinene: 103 Isoprene: 55 *o*-cresol: 133	3.7	45.8

2.4. Offline Analysis of the Filter Samples

2.4.1. Sample preparation

Filter samples of SOA particles were extracted using the following procedure. Each filter was cut into small pieces into pre-cleaned 20 mL scintillation vial. 4 mL of (Fisher Scientific FB15051of methanol (Optima LC-MS grade, ThermoFisher Scientific) was added to the vial. The sample was then wrapped in foil and left for 2 hours at ambient temperature, sonicated for 30 minutes and the extractant filtered through a 0.22 μm pore size PDVF filter using a BD PlasticPak syringe. An additional1 ml of methanol was added to the vial and filtered through the same syringe membrane to minimise sample loss. . The filtered extractant was then evaporated to dryness using solvent evaporator (Biotage, model V10) at 36°C and 8 mbar pressure and redissolved in 1 ml of a 90:10 water: methanol (Optima LC-MS grade) for LC-Orbitrap MS analysis.

2.4.2. Liquid Chromatography Mass Spectrometry Analysis

Samples were analysed using ultra-performance liquid chromatography ultra-high resolution mass spectrometry (Dionex 3000, Orbitrap QExactive, ThermoFisher Scientific). A reverse-phase C18 column (aQ Accucore, ThermoFisher Scientific) 100 mm (long) × 2.1 mm (wide), with a 2.6 μm particle size was used for compound separation. The flow rate was set to 0.3 ml/min, with 2μL

sample injection volume. The autosampler temperature was set to 4ºC and the column at 40ºC. The mobile phase solvent included (A) water and (B) methanol that both contain 0.1% (v/v) formic acid (Sigma Aldrich, 99% purity). Gradient elution was performed starting at 90 % (A) with a 1-minute post-injection hold, decreasing to 10% (A) over 26 minutes, before returning to the initial mobile phase conditions at 28 minutes, followed by a 2 minute column re-equilibration. Electrospray ionisation (ESI) was used with a mass-to-charge (*m/z)* scan range of 85 to 750. The ESI parameters were set as follows: 320ºC for capillary and auxiliary gas temperature ,70 (arbitrary units) and 3 (arbitrary units) flow rate for sheath gas and auxiliary gas respectively. (Pereira et al., 2021). Compound fragmentation was achieved using higher-energy collision induced dissociation (MS^2). A fragmentation spectrum is generated for each selected precursor, which allows structural identification through the elucidation of fragmentation patterns (Mcluckey and Wells, 2001). This fragmentation spectra can aid in the structural identification of isomeric species (i.e. compounds with the same molecular formula, but different structural arrangement). Accurate mass calibration was performed prior to sample analysis in positive and negative ESI mode using the manufacturer recommended calibrants (Thermo Scientific). A procedural control (i.e. pre-conditioned blank filter subject to the same sample extraction procedure) was analysed, along with solvent blanks (consisting of 90:10 water: methanol) which were frequently run throughout the sample analysis sequence, allowing any instrument or extraction artefacts to be detected.

Automated non-targeted data analysis was performed using Compound Discoverer version 2.1 (Thermo Fisher Scientific). Full details of the data processing methodology can be found in Pereira et al. (2021). Briefly, the chemical information of all detected compounds in each sample data file are extracted. The method provides molecular formulae assignment of detected compounds using the following elemental restrictions: unlimited carbon, hydrogen and oxygen atoms, up to 5 nitrogen and sulphur atoms, and in positive ionisation mode, 2 sodium and 1 potassium atom are also allowed. Molecular formulae were attributed if the mass error < 3 ppm, signal-to-noise ratio > 3, and the isotopic intensity tolerance was within ± 30 % of the measured and theoretical isotopic abundance. Instrument artefacts were removed from sample data if the same detected molecular species had a retention time within 0.1 minutes and sample/artefact peak area ratio < 3. The automated Python program generates a list of detected compounds, assigned molecular formulae and tentatively assigned mass spectral library identifications (see Pereira et. al (2021) for further

information). The mass spectra for both ESI modes from each VOCs system, are shown in supporting information (Figure S1 and S2).

For the LC-Orbitrap MS sample data, the compounds detected in "Background" filter were removed from sample data if the same detected molecular species had a retention time within 0.1 minutes and sample/background peak area ratio < 3. Meanhwhile, the compounds have sample/background peak area ratio >3 were conserved in sample data with a new peak area (New peak area= Sample peak area – Background peak area).

To provide confidence in the components in each system detected by the non-targeted data, only those compounds found in all replicate experiments and not found in any background "clean" experiments were attributed to a particular single precursor or mixed system. The approach taken thus ensures the most conservative assignment of compounds to a particular precursor system. Where quantities are analysed and presented from "representative" experiments, only those relating to compounds found in all replicate experiments are confidently attributed to this particular system. Compounds that were found above detection limit in only a subset of the experiments in a single system were not attributed to the system and were considered "inconclusive". Moreover, the common compounds were only considered to be the same detected molecular species if they had a retention time within 0.1 minutes and sample/artefact peak area ratio > 3 in all replicate experiments. Section 3.2.1 and section 3.2.3 only considers the compounds which can be confidently attributed to a particular system. For the elemental characterization in section 3.2.2, both the confident and inconclusive components are presented, with only the compounds confidently attributed analysed according to carbon number.

3. Results and Discussion

3.1. SOA particle mass formation in the experiments

The formation of SOA particle mass in the seven experimental systems is shown alongside the VOC concentration, NOx and O_3 mixing ratio time series in Figure 1. As shown in figure 1(a), the particle wall-loss corrected SOA mass in all α-pinene containing systems reaches a maximum value within the 6-hour experimental timeframe. α-pinene produced the highest SOA particle mass (~400ug/m^3) of all systems at nominal "full" VOC reactivity with the most rapid onset and rate of

mass formation. The SOA particle mass continued to increase at the end of the experiment in the single VOC *o*-cresol and binary isoprene/*o*-cresol systems. No measurable SOA particle mass above background (~0 ug/m^3) was produced within the 6-hour duration in any single VOC precursor isoprene experiment.

As shown in Fig.1 (b), NOx was observed to decay in all systems where significant SOA mass was formed, but little NOx consumption was observed in the single isoprene system or in the binary isoprene / o-cresol mixture. The reduction of NOx will result from i) reaction between OH radicals and NO_2 leading to HNO_3 formation with subsequent loss to the chember walls or particles as inorganic nitrates. ii) termination reactions between NO and RO_2 radicals or NO_2 and RO_2 radicals leading to formation of nitrogen-containing organic ($NOROO_2$ and NO_2ROO_2) compounds(Atkinson, 2000).

Noting that there was no O_3 initially in any experiment, Fig. 1(c) illustrates ozone concentration time series in each system. Ozone can be seen to increase during the initial stage of experiment in most experiments, with most modest rises in the single *o*-cresol and binary isoprene/*o*-cresol systems. An initial rise is expected owing to the fairly rapid photolysis of NO_2 tending towards photo-stationary state (PSS) between NO_2, NO and O_3. The onset of VOC oxidation will result in a consumption of O_3 when the unsaturated α-pinene and isoprene are present. At the same time NO will react with RO_2 and HO_2 radicals formed in the VOC degradation, resulting in NO_2 and OH radical formation. The reduction in the proportion of NO reacting with O_3 and photolysis of the NO_2 produced results in net O_3 production and deviation from PSS.

The time profile of the VOC concentration from experiments in all single and mixed precursor systems are shown in Fig.1 (e-f). A rapid and pronounced onset of VOC consumption in each system is observed after illumination, attributable to reaction with OH radicals, and O_3 in α-pinene and isoprene-containing systems. Panels (d) to (f), plotted logarithmically for clarity, show the VOC decay profile in each experiment reflecting their differences in reactivity and the variable oxidant regime in each experiment. Individual VOCs have comparable decay rates in each mixture except for i) α-pinene in the binary α-pinene / *o*-cresol system, which had a significantly lower decay rate than it had in other α-pinene-containing systems systems and ii) isoprene, which had a

faster decay rate in the binary α-pinene / isoprene system than in other isoprene-containing systems. No VOC was entirely consumed in any system by the end of the 6 hours experiments, with consumption continuing until the end.

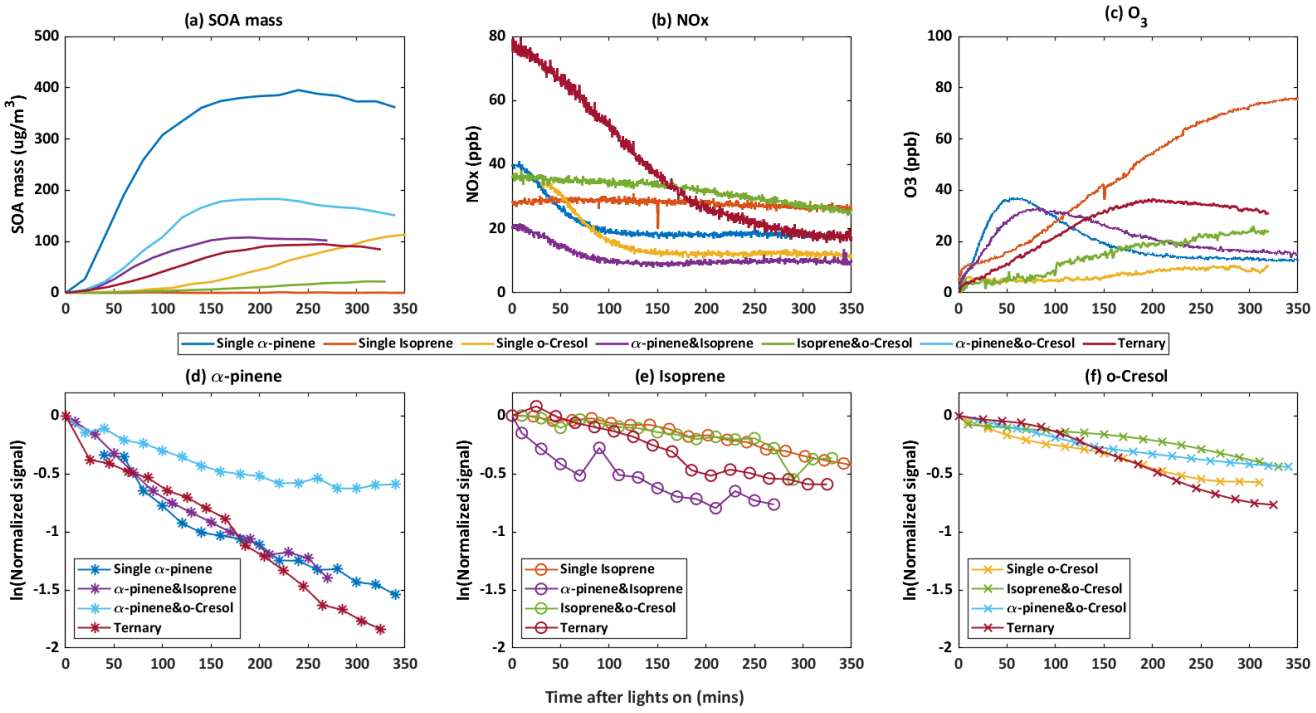

Figure 1 : Evolution of gas and total SOA particle mass measurements during the photo-oxidation of VOCs after chamber illumination. (a) The SOA mass was measured using a high-resolution time-of-flight aerosol mass spectrometer (HR-ToF-AMS) during single, binary and ternary experiment. (b)–(c): Concentration of NOx and O3 against time in all of single, binary and ternary experiments (data was unavailable for the binary α-pinene/o-cresol experiment). (d)-(f): decay rata of VOC across all systems in. α-pinene (b), isoprene(c) and o-cresol(d) in single, binary and ternary experiments respectively.

3.2. Characterisation of Components by LC-Orbitrap MS

3.2.1. Characterisation by number of discrete compounds in each system

The number of discrete peaks extracted using the Compound Discoverer software from the LC-Orbitrap MS data for all experiments in each SOA system is listed in Table 2 and illustrated using Venn diagrams showing the compounds found in more than one system (henceforth referred to as "common" compounds) and those found solely in a single system (referred to as "unique") in Figures 2 and 3 (in negative and positive ionisation modes respectively).

As seen in Table 2, all α-pinene-containing systems were found to contain a greater number of compounds than any system not containing α-pinene. The binary α-pinene / isoprene system contained the highest number of all systems, with 377 in negative ionization mode and 439 in positive ionization mode. A total of 644 total compounds were seen in the single VOC α-pinene system across both negative and positive ionization modes, fewer than in the binary α-pinene/isoprene system with 816 compounds, but higher than the α-pinene/ *o*-cresol system with 483 compounds. The total number of discrete products in the ternary system is lower than in the single α-pinene and binary α-pinene system. The single VOC isoprene system generated the lowest total number of products of all systems above detection limit. This is unsurpriseing, since undetectable mass concentration was found by the online instrumentation in these experiments. Multifunctional compounds can be detected in both negative and positive ionization mode. Negative ionization mode typically exhibits high sensitivity towards compounds containing alcohol and carboxylic acid functionalities, whereas positive ionization mode typically has a greater affinity for compounds with functional groups that are readily protonated (e.g. -NH, -O- or -S-, -CH2-,-C=O,-SO_2- group) (Glasius et al., 1999; Steckel and Schlosser, 2019).

Table 2: Number of compounds detected in SOA sample in negative and positive ionization mode from single, binary and ternary precursor's system.

	Number of Detected Compounds	
Experiment	**Negative Mode**	**Positive Mode**
α-pinene	282	362
Isoprene	28	68
o-cresol	84	53
a-pinene/Isoprene	377	441
a-pinene/o-cresol	339	144
o-cresol/Isoprene	72	87
a-pinene/Isoprene/o-cresol	112	188

a) Negative Ionization Mode

Fig. 2 shows a Venn diagram of the number of discrete compounds identified in negative ionisation mode in each of the individual and binary precursor experiments. Figure. 2(a) and Figure 2(b) show that the number of discrete compounds from α-pinene dominated those found in the binary

mixture system compared to those from the other precursors. 182 compounds found in all α-pinene single precursor experiments were also found in the binary α-pinene / isoprene mixed system; approximately 45 times greater than the 4 compounds also found in all single isoprene experiments. Similarly, 99 common compounds were found between the single precursor α-pinene experiments and those found in the binary α-pinene/ *o*-cresol system; roughly three times higher than the number of *o*-cresol-derived products that were also found in binary mixed system. More than half of the total number of compounds in the α-pinene / isoprene and α-pinene / *o*-cresol binary systems were unique to the mixtures and not observed in any of single precursor experiments. In the isoprene / *o*-cresol system a lower total number of compounds were detected in every repeat experiment, with more compounds in the mixture also found in the *o*-cresol system than the isoprene system (Fig.2(c)).

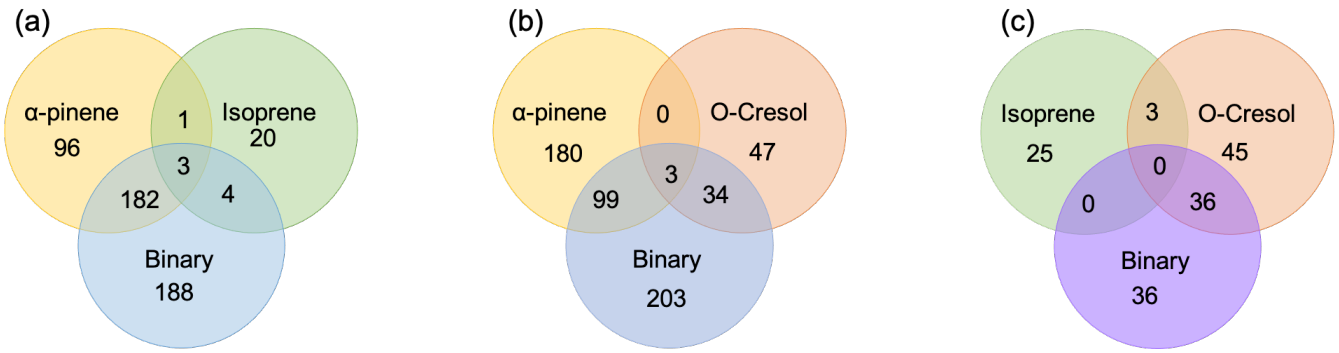

Figure 2：Number of common compounds and unique compounds in single and binary precursors mixed experiments detected by negative ionization mode LC-Orbitrap MS. Product are considered identical in the mixed and single precursor systems if the compound has the same empirical formula and a retention time difference <0.1min.

b) Positive Ionization Mode

Fig.3 shows the number of discrete SOA compounds identified in positive ionisation mode in the single and binary systems. There are 226 compounds found in all α-pinene single precursor experiments that were also found in the binary α-pinene / isoprene system; about 32 times more than also found in the isoprene-only experiments (Fig.3(a)). 48 α-pinene derived compounds were also found in binary α-pinene/ *o*-cresol system; 16 times greater than those also found in all *o*-cresol only experiments (Fig.3(b)). In both α-pinene containing binary mixtures, around or more than half of all detected compounds were unique to the mixture. In the binary isoprene / *o*-cresol

system shown in Fig.3(c)), *o*-cresol derived compounds were more numerous than those in the isoprene experiments, with 23 compounds observed.

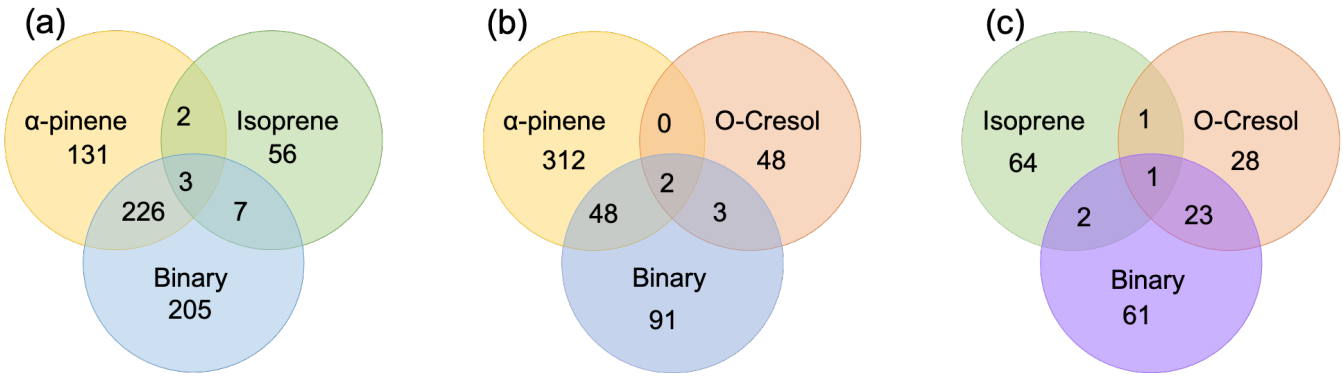

Figure 3 : Number of common compounds and unique compounds in single and binary precursors mixed experiments detected by positive ionization mode LC-Orbitrap MS. Products are considered identical in mixed and single precursor systems if a compound has the same empirical formula and the retention time difference <0.1min.

The Venn diagrams for both ionization modes indicate the importance of α-pinene oxidation products in both binary systems, with large number of binary SOA compounds found to be present in the single precursor α-pinene system. In contrast, there are few common compounds observed between single isoprene and binary systems, possibly a result of the majority of isoprene derived products remaining in the gas-phase, or the isoprene products participating in cross-product formation in mixed precursor systems.

3.2.2. Characterization of Organic Particulates by Elemental Groups

3.2.2.1. Negative Ionization Mode

Elemental groupings are used here to provide insights into the SOA chemical composition in each system. All detected molecular formulae in each system were classified into the following four categories based on their elemental compositions: CHO, CHON, CHOS, and CHONS (C, H, O, N and S corresponding to the atoms in the molecule) and separated into seven carbon number categories. The measured peak area of each compound was normalised to the total sample peak area as shown in Fig.4 and described in Pereira et. al (2021). Fig.4 presents the signal fraction of compounds in representative experiments that can be confidently attributed as found in each of the systems (i.e. that are found in every repeat experiment in this system) in the coloured stacked bars

according to their carbon number and classified according to their elemental groupings. The fractional contributions of compounds that confidently stated are similar for each experiment in a particular system. Also shown in the grey bar is the signal fraction of compounds that are inconclusively found in the experiment in each system classified by elemental grouping, but not found in all repeat experiments and chamber background experiment.

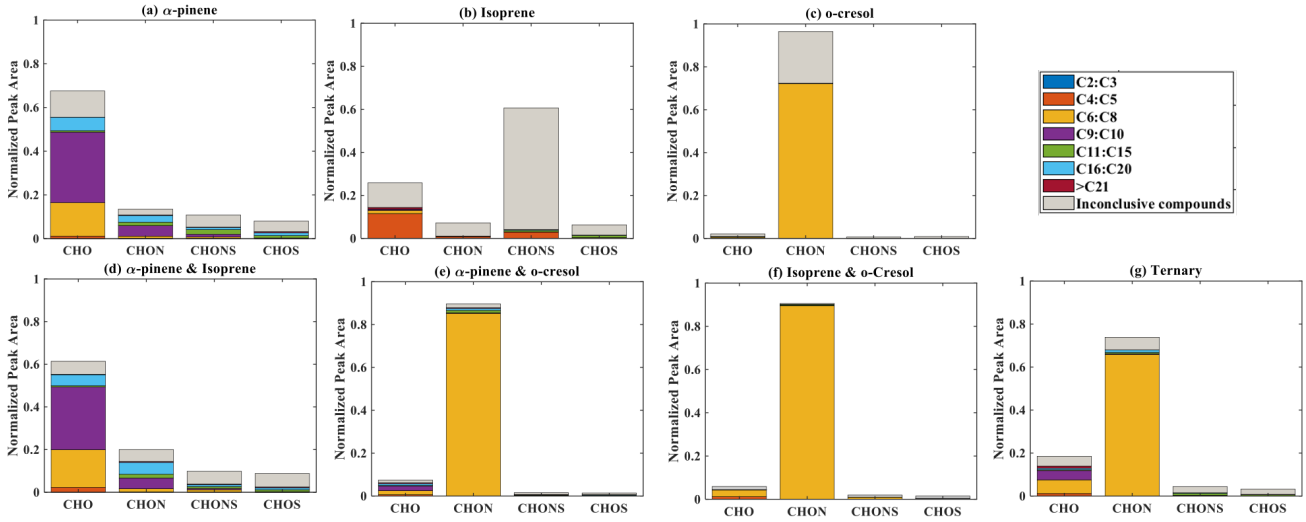

Figure 4：The normalized signal intensity distribution of different compound categories (CHO, CHON, CHOS, and CHONS) for various single and mixed precursor systems in Negative Ionisation mode ESI (-) by LC-Orbitrap MS. The grey bar (inconclusive compounds) signal attributed to compounds that were not universally found in all repeat experiments.

a) α-pinene

As shown in in Fig 1(a), the SOA particle mass produced in the single precursor α-pinene system was greater than in any other system, at ~362 μg/m^3. In the α-pinene single precursor representative experiment, ~ 55.6% of signal was found in molecules identified in each repeat experiment and containing only C, H and O atoms with the majority consisting of 6 to 10 carbon atoms (47.5 %). Larger compounds were also observed with carbon numbers ranging from C_{16} and C_{20} (representing 6.1 % of the total signal fraction) (Fig.4a)). Compounds confidently found in this system in the CHON , CHONS and CHOS groupings represented 10.8%, 5.2% and 3.2% of the signal abundance, respectively, again concentrated at C_9-C_{10} and C_{16}-C_{20}. C_{11}-C_{15} molecules represent 2.2% and 1.1% of the signal in the CHONS and CHOS categories respectively.

Inconclusively attributed compounds contributed 25% of the total signal abundance; 11.9% of them containing only C, H, and O atoms.

C_6 to C_{10} compounds will include those produced through both functionalization (addition oxygenated function group) and fragmentation (cleavage of C-C bond) pathways during α-pinene oxidation (Eddingsaas et al., 2012). It has been further suggested that particle-phase dimerization and oligomerization reactions (e.g alcohol + carbonyl to form hemiacetals and acetals, hydroperoxide + carbonyl to form peroxyhemiacetals and peroxyacetals, carboxylic acid + alcohol to form esters, and aldehyde self-reactions to form aldols) can play an important role in α-pinene oxidation(Ziemann and Atkinson, 2012; Gao et al., 2004a; Gao et al., 2004b), resulting in formation of large molecules (nC>10), potentially accounting for the C_{16} to C_{20} abundance. Recent studies have additionally identified gas-phase autoxidation as playing a pivotal role in formation of highly oxygenated molecules (HOMs)(Tomaz et al., 2021; Crounse et al., 2013; Bianchi et al., 2019; Zhao et al., 2018). HOM may condense on existing seed particles or lead to new particle formation, depending on their vapour pressure (Tröstl et al., 2016). Autoxidation of RO_2 radicals in gas-phase occurs rapidly via inter/intramolecular hydrogen abstraction leading to forming R radicals with subsequent O_2 addition (Mentel et al., 2015; Jokinen et al., 2014). The new RO_2 radicals can undergo further autoxidation reaction, or react with RO_2 to generate dimer accretion products (Zhao et al., 2018; Berndt et al., 2018). Autoxidation may therefore contribute to CHO products with carbon numbers 16 – 20 in α-pinene oxidation. It has also been found that the uptake of α-pinene oxidation products on ammonium sulphate particles can lead to formation of organosulphate and nitrooxy organosulphate (Eddingsaas et al., 2012; Iinuma et al., 2009), contributing to the CHOS and CHONS groupings.

b) isoprene

As also seen in Fig.1(a), negligible SOA particle mass was generated in the single precursor isoprene system (~0 $\mu g/m^3$, close to our chamber background) and the total signal in Fig 4(b) therefore corresponds to extremely low SOA particle mass. Nevertheless, the presence of compounds in all repeat experiments but not on any filters taken in background experiments, allows identification and attribution to isoprene products. Similar to the α-pinene system, compounds found in all repeat experiments containing CHO were the most abundant in the single

precursor isoprene experiment shown in Figure 4(b), with normalized sample abundance of 14.3 %, mainly comprising compounds with 4 or 5 carbon atoms. Similarly, compounds in the CHONS classification can be confidently stated to make a non-negligible contribution to the total signal fraction, with a normalised abundance of 4.1%, also mainly comprising C_4-C_5 compounds. CHON (1%) and CHOS (1.5%) each contributed significantly less than the other molecular groupings. Fig.4(b) shows that the majority of the signal in this single isoprene representative experiment was composed of compounds (78.9% nomalized of total signal fraction) that were not found in all isoprene experiments (and / or were also found in background filters) and are therefore inconclusively assigned.

The presence of C_4-C_5 CHO compounds in single isoprene photo-oxidation system can be readily explained by established oxidation pathways. For example, it is well-known that the double bond in isoprene is oxidized to form C_4 and C_5 compounds, such as methacrolein (C_4) and C_5-hydroxycarbonyls as first-generation products, and 2-methylglyceric acid (C_4) and isoprene tetrol (C_5) as second-generation products (Wennberg et al., 2018; Stroud et al., 2001; Carlton et al., 2009). However, it is less clear how such small compounds readily partition to the particle phase, owing to their relatively high vapour pressures, though it has been suggested that small compounds such as glyoxal (CHOCHO) have extremely high activity coefficients when partitioning to aqueous particles, leading to low effective vapour pressures (Volkamer et al., 2009).

The negligible SOA particle mass formed in the isoprene single precursor system is consistent with the literature observations (Kroll et al., 2005a; Kroll et al., 2005b; Kroll et al., 2006; Carlton et al., 2009). However, condensed phase reactions on acidic seeds would be expected to appreciably increase this yield (Surratt et al., 2010; Surratt et al., 2007a; Carlton et al., 2009). The large normalised signal contribution corresponds to the high number of inconclusively assignable compounds detected in this system. Most of these inconclusive compounds contained a large number of carbon atoms (nC>15). These compounds are likely to have been formed via particle-phase accretion reactions, such as oligomerisation and organosulfate formation, even in the absence of acidity in our experiments, leading to low volatility higher molecular weight accretion products (Berndt et al., 2019; Carlton et al., 2009). Whether these products are formed on the filter medium or are present in the suspended particle mass requires investigation. While these

components are the most abundant, this still corresponds to a very small mass compared to all other systems and were not found in all repeat experiments.

c) *o*-cresol

The particle wall-loss corrected SOA mass concentration at the end of the presented *o*-cresol experiment was approximately 101 μg/m^3 (Fig 1. (a)). Fig.4(c) shows ~26.6% of the normalized signal abundance in inconclusively assigned compounds, mainly in the CHON classification. However, the key characteristic in the single precursor *o*-cresol system is that the most abundant compounds that are confidently found in all repeat experiments were found in the CHON category with between 6 and 8 carbon atoms (Fig 4(c)) with around 72.1% of the normalised signal. CHO, CHONS and CHOS groupings comprised around 1% of the total sample abundance. These three groups of compounds should not be completely neglected since the SOA particle mass concentration of this system was appreciable compared to other systems. It might be expected to find a significant contribution of CHO compounds arising from formation of organic acids (e.g. acetyl acrylic acid and glyoxylic acid) under high NOx *o*-cresol photo-oxidation (Schwantes et al., 2017).

Nitro-compounds retaining the carbon number of the parent VOC dominated the CHON grouping. The C_6-C_8 components were identified as methyl-nirocatechol, $C_7H_7NO_4$, isomers (See Table(S1)). OH reaction with o-cresol forms various dihydroxy toluene isomers via addition of OH group to different positions on the ring (Olariu et al. (2002). Subsequent hydrogen abstraction followed by NO_2 addition on the ring at the moderate NOx concentrations of our experiments was a likely dominant fate of dihydroxy toluene in the current study to form the observed dihydroxy nitrotoluene. Further discussion of these isomers is presented in section 3.2.3.1(e). Schwantes et al. (2017) reported that H abstraction was not the dominant pathway in dihydroxy toluene oxidation, with dihydroxy nitrotoluene only detected at low concentrations by CIMS, with a significant number of highly oxygenated multi-generational products (mainly CHO compounds) detected by offline direct analysis in real-time mass spectrometry (DART-MS). It should be noted that the high signal contribution of CHON compounds, dominated by nitro-aromatics in *o*-cresol photo-oxidation (Kitanovski et al., 2012), in Fig. 4(c) may be influenced by their high negative mode sensitivity using electrospray ionisation (Kiontke et al., 2016).

d) binary α-pinene / isoprene mixture

The binary α-pinene/ isoprene mixture generated considerable particle wall-loss corrected SOA particle mass in all experiments (~101 μg/m^3 in the representative one shown here); lower than in the single precursor α-pinene system, but much higher than in the isoprene system. The distribution of elemental categories of the particle phase products in this system was very similar to that in the single precursor α-pinene experiments, with CHO compounds dominating the total signal, mainly with between 6 and 10 carbon atoms or between 16 and 20 (Fig.4(d)). The normalised signal contribution of compounds confidently found in each repeat in the CHON group was slightly increased in the binary α-pinene/isoprene system (14.4%) compared to single α-pinene system (10.8%) with a modest enhancement of compounds with greater than 15 carbon atoms (from 3.3% to 6.0%). In addition, the contribution of large compounds (nC >15) was enhanced in the CHON and CHONS categories in the binary system compared to single VOC α-pinene system.

This profile is consistent with the domination of the chemical composition in the mixture by α-pinene products, which is unsurprising since α-pinene is established as a much high yield SOA yield compound than isoprene, especially under neutral seed conditions (Ahlberg et al., 2017; Eddingsaas et al., 2012; Henry et al., 2012).

e) binary systems containing o-cresol

As shown in fig.1(a), the isoprene/*o*-cresol system produces a low particle mass concentration (~22μg/m^3) whilst the α-pinene/*o*-cresol mixture generated the second highest particle wall-loss corrected SOA mass concentration (~150μg/m^3). Compounds found across repeat experiments in these mixtures containing *o*-cresol show the same dominance of CHON signal as the single precursor *o*-cresol experiment (α-pinene/*o*-Cresol, Isoprene/*o*-Cresol) (Fig 4(e) and 4(f)). The contribution of CHON compounds to the total SOA increased to approximately 87.8% and 96.0% when α-pinene and isoprene were introduced into the mixed precursor systems, respectively. Moreover, the contribution of CHO signal intensity increased in both binary *o*-cresol mixed systems compared to the single precursor *o*-cresol system. Also, the *o*-cresol / isoprene binary mixture (Fig.4(f)) showed an slightly increased proportion of signal in CHONS compounds at 1.0%. (compared with 0.6% in the single precursor *o*-cresol system (Fig.4(c)), though noting that the total mass concentration in the mixed system at the end of the experiment was a factor of 5 lower than in single VOC *o*-cresol system.

The presence of biogenic precursors leads to additional formation of CHO compounds, while the relative signal contribution of CHON compounds is reduced in each binary system compared to single VOC *o*-cresol system. A plausible explanation for this observation could be the increase in O_3 generated in the binary mixture, increasing the ozonolysis of 1st generation *o*-cresol products with double bonds and hence a CHO contribution than in the sole *o*-cresol system.Overall, the negative ionisation mode signal from the SOA components in a binary mixture containing both biogenic and anthropogenic precursors in our systems were dominated by categories of components found in the single anthropogenic precursor system, specifically the CHON group dominated by nitro-aromatics. This may be considered somewhat surprising in the case of the mixture with α-pinene, since α-pinene (as widely reported and shown in Fig.1) produces higher SOA mass concentration than *o*-cresol under the same initial conditions as the mixture experiment.

f) ternary α-pinene / isoprene / o-cresol mixture

Figure 4 (g) shows the group contribution of the signals in the ternary mixed VOC system corresponding to its moderately high SOA particles mass concentration (~85μg/m^3) shown in fig.1(a). Across the compounds found in all repeat experiments, whilst not as completely dominant as in the *o*-cresol containing binary systems, the substantial (65.7%) C_6-C_8 CHON contribution again shows that the *o*-cresol-derived nitrocatechols play a significant role. CHO compounds make a significant contribution in particulate products with normalized abundance ~14%. Whilst the CHON compounds mainly consist of C_6-C_8 compounds, the CHO compounds comprise both C_6-C_8 and C_9-C_{10} compounds. SOA production in the ternary system appears not to be entirely driven by any single precursor and additionally, the overwhelming negative mode CHON dominance which may be controlled by sensitivity of the electrospray method, does not appear to the same degree in the ternary system as it does in the *o*-cresol-containing binaries.

There was a small contribution to the CHO group from compounds with more than 15 C atoms. Whilst relatively low in normalised signal contribution, they were found in all ternary repeat experiments and can be presumed to be accretion products. As an indication of the relative contribution of accretion products to the SOA particle mass in each system, table S2 shows the signal-attributed mass concentration of molecules with nC>21 that were observed confidently in all repeat experiments, by scaling the fractional signal contribution to the measured PM mass at

the end of the experiment. The signal-attributed mass concentration of these large molecules is around 6, 575 and 80 times lower in the single VOC isoprene system (0.002μg/m^3) than in the isoprene / *o*-cresol (0.013 μg/m^3), α-pinene / isoprene (1.15 μg/m^3) and ternary (0.16 μg/m^3) mixtures respectively.

3.2.2.2. Negative Ionisation Aggregate Particle Component Properties

This section describes average properties of the SOA PM mass using a variety of metrics including molar carbon number (nC), molar hydrogen to carbon ratio (H/C), oxygen to carbon ratio (O/C), average oxidation state ($\overline{OSc}$), double bond equivalent (DBE) and double bond equivalent to carbon ratio (DBE/C). The molar carbon number reflects to the average size of SOA particle components and often the major condensed-phase products retain the same carbon number as the precursor (Romonosky et al., 2015). The H/C and O/C provides summary information about chemical composition of bulk organics, and OSc corresponds to the average degree of oxidation of carbon in the organic species (value of $\overline{OSc}$ increasing upon oxidation)(Daumit et al., 2013; Safieddine and Heald, 2017). The OSc values were calculated by using 2*O/C-H/C for CHO, CHONS, and CHOS compounds due to the low measured abundances fractions of two species in the oxidation products we observed in section 3.2.2.1 and 3.2.2.3. For CHON compound, equation $\overline{OSc}$ =2*O/C-H/C-(OS_N*N/C) was used to determined the $\overline{OSc}$. The OS_N=+5 if nO>=3 and OS_N=+3 if nO <3 for CHON compounds (Kroll et al., 2011). It is common to used DBE and DBE/C to quantify the unsaturated bonds (and aromaticity) in a molecule. The DBE corresponds to the sum of unsaturated bonds (including aromatic and cycloalkene ring) and increasing DBE/C ratios indicates increasing contribution of the signal from molecules containing aromatic rings (Koch and Dittmar, 2006).

Table 3 shows the signal-weighted chemical metrics from compounds detected in all repeat experiments in each system. All properties were normalised to the total detected compound abundance. All parameters in the single VOC α-pinene and binary α-pinene/isoprene systems are similar, consistent with the dominance of α-pinene-derived particle mass in the binary system. In contrast, the H/C value decrease from 1.46 to 1.03 and the O/C value remain constant (~0.5) in binary α-pinene /*o*-cresol compared to the single VOC α-pinene system. Indeed, the signal-intensity weighted average values of all chemical parameters shows that the *o*-cresol single VOC

system aggregate properties are very similar to those in both *o*-cresol containing binary system, with an understandably high level of aromaticity (DBE/C >=0.67) (Koch and Dittmar, 2006), indicating that oxidation and partitioning to the particles in the unary and binary *o*-cresol systems is largely ring preserving. The OSc value decreased from -0.55 to -0.63 in α-pinene / *o*-cresol compared to the single VOC *o*-cresol system suggests a less oxidation degree of products were formed when introducing α-pinene precursors into single o-cresol system. The abundance-weighted average values of all chemical parameters in the particles in the ternary mixture do not show common features with any single precursors system, with the coincidental exception of the nC and O/C value that are similar to that in the *o*-cresol system.

Table 3: Intensity Weighted Average Values from negative ionization mode LC-Orbitrap MS for O/C, H/C, Osc, DBE/C, DBE and the number of carbons present (nC) for SOA filters extracts from single and mixed precursor experiments

Chemical parameters	**α-pinene**	**Isoprene**	***o*-cresol**	**α-pinene/ Isoprene**	**Isoprene/ *o*-cresol**	**α-pinene/ *o*-cresol**	**α-pinene/ Isoprene/ *o*-cresol**
nC	11.57	7.08	7.01	10.63	7.03	7.56	7.75
H/C	1.46	1.27	0.99	1.46	1.00	1.03	1.08
O/C	0.51	0.81	0.57	0.52	0.48	0.52	0.55
$\overline{OSc}$	-0.58	0.26	-0.55	-0.57	-0.7	-0.63	-0.55
DBE/C	0.39	0.57	0.71	0.40	0.70	0.68	0.65
DBE	4.28	3.90	5.01	4.37	4.98	5.02	4.89

The weighted average number of carbons in α-pinene experiment (~11) indicated that a modest accretion reaction (including oligomerization and functionalization) occurred in oxidation, and that the α-pinene particle phase oxidation products had significant impact on α-pinene / Isoprene binary system. The average carbon number of isoprene SOA particles was larger than the isoprene precursor (C_5), implying particle-phase accretion reactions such as organosulfate formation though forming very little particle mass in the current study. The similarity of properties between the single VOC *o*-cresol system and its binary mixtures suggest that common compounds dominate the signals, and from Fig.4(c) , (e) and (f) it can be seen that these are compounds in the CHON elemental category. In addition, the DBE/C values indicate dominance of the major oxidation products in these *o*-cresol containing systems by condensed aromatic structure, consistent with the finding in Ahlberg et al. (2017).

3.2.2.3. Positive Ionization mode

Figure 5 presents the positive ionisation mode signal fraction of compounds in representative experiments that can be confidently stated as found in each of the systems (i.e. found in every repeat experiment in this system) in the coloured stacked bars according to their carbon number and classified according to their elemental CHO, CHON, CHOS, and CHONS categories. Also shown in the grey bar is the signal fraction of compounds that are inconclusively found in the experiment in each system classified by elemental grouping, but not found in all repeat experiments and chamber background. The fractional contributions of condifently stated as products are similar for each experiment in a particular system.

It is evident that there is a generally a greater fraction of the positive ionisation mode signal that is inconclusive than in negative ionisation mode as shown in Figure 4. This indicates a larger variability in composition between repeat experiments with some compounds not found in some repeats experiments, or a larger fraction of the signal from compounds also found on chamber background filters.

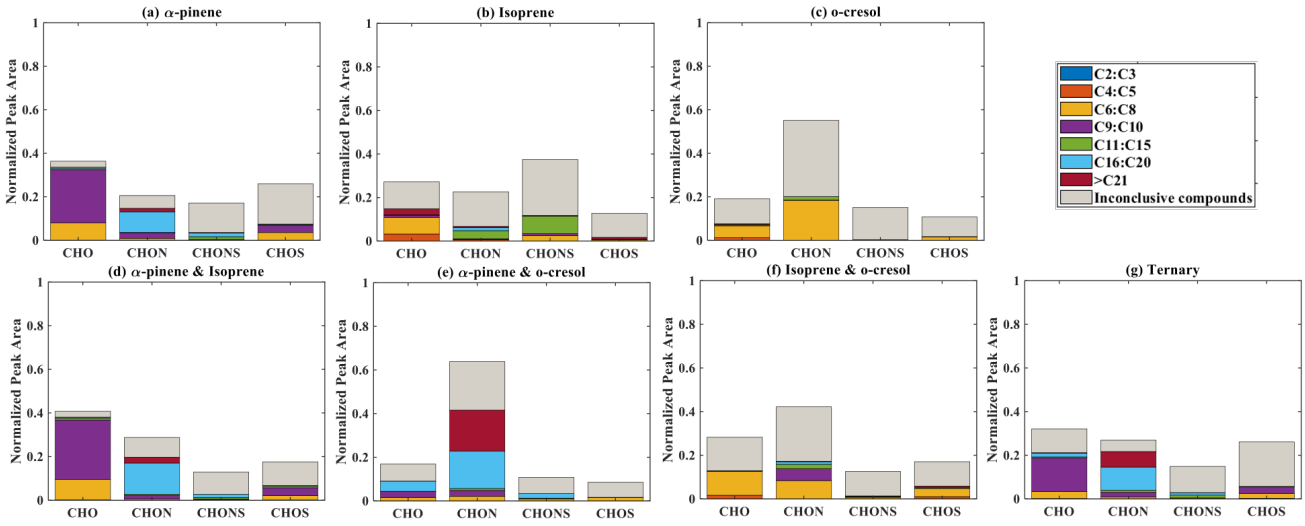

Figure 5 : The normalized signal intensity distribution of different compound categories (CHO, CHON, CHOS, and CHONS) for various single and mixed precursor systems in Positive ionization mode by LC-Orbitrap MS. The grey bar (inconclusive compounds) signal attributed to compounds that were not universally found in all repeat experiments.

a) α-pinene

In the single precursor α-pinene system (Fig 5. (a)), 33.5% of the total signal abundance was from CHO compounds found in each repeat experiment with the majority of molecules containing

between 6 and 10 carbon atoms. The compounds confidently found in the CHOS category provided 7.4% of the signal fraction, also mainly comprising compounds with 6 to 10 carbon atoms. The remainder of signal was observed in CHON (14.6%) and CHONS (3.5%) categories, which were found in all repeat experiments in this system mainly comprised large compounds, with some nC<11 molecules in these CHON category.

The contribution of C_9 to C_{10} molecules in the CHO and CHONS categories are consistent with previous studies of α-pinene ozonolysis and OH oxidation in the presence of NOx and seed particles (Winterhalter et al., 2003, Yasmeen et al., 2012). The signal contribution of CHO compounds and CHOS with carbon number 6 to 8 suggested that fragmentation plays an important role. It is likely that these compounds formed from fragmentation of alkoxy radicals (RO_2+ NO→RO+NO_2)(Pullinen et al., 2020).

The CHOS and CHONS compounds may be attributed to esterification of α-pinene SOA. Experimental results from Surratt et al. (2007b) reported that the sulphate ester and/or its derivatives has significant contribution in SOA formation of α-pinene photo-oxidation in the presence of ammonium sulphate seed. The large molecules in CHON and CHONS groups suggest the occurrence of accretion reactions between peroxy-peroxy radicals containing nitrogen and sulfur (RO_2+ R'O_2→ROOR'+O_2) (Pullinen et al., 2020).

b) Isoprene

Considering only the compounds found in all repeat experiments and not on the background filter, the dominant contribution in the isoprene signal in its single VOC photo-oxidation system were observed in the CHO category with a normalized signal of 14.8%, with molecules mostly comprising 5-8 carbon atoms or larger molecules with carbon number greater than 9 (Fig 5(b)). CHONS compounds are the next largest constituent, with 11.7% of the total signal. More than half of the CHONS signal is from large molecules (nC>11), the rest of the CHONS compounds mainly comprising molecules with carbon number 6 to 10. The remainder of the signal was found in the CHON and CHOS categories with carbon number greater than 11. Compounds which could not be confidently attributed to the isoprene system owing to their sole presence in every repeat experiment made a significant contribution (~65%) to the total signal, though an even greater fraction of inconclusive signal (78.9%) was observed in negative ionization mode (likely resulting from the extremely low total mass yield).

Clearly accretion reactions dominated the isoprene system in the positive (as well as negative) ionisation modes. Contribution of CHONS compounds in total SOA are consistent with the formation of organosulphate and nitrooxy organosulphate by uptake of isoprene oxides on ammonium sulphate particles(Surratt et al., 2007b; Surratt et al., 2007a). Moreover, the presence of C_4-C_5 molecules in CHO categories could be simply explained by the gas phase oxidation pathway of isoprene, though as with the negative mode samples, it is unclear why such small molecules partition to the particle phase. One of the possible interpretations is that weakly bound large molecules fragment during LC-Orbitrap MS analysis.

c) *o*-cresol

Fig.5c shows that approximately 20% of the signal is in the CHON category in the single VOC *o*-cresol system. The majority (18.3%) of signal from confidently attributable molecules found in all repeat experiments in this CHON category contain 6 to 8 carbon atoms. Signal in the CHO, and CHOS categories is similarly dominated by compounds containing 6 to 8 carbon atoms with fractional contributions of 5.4%, and 1.7% respectively. Specifically, the C_7 compounds has fractional signal contributions 3.8%, which is approximate 3 times higher than C_6 (1.1%) and about 12 times higher than C_8 molecules (0.3%) in CHO categories. In the CHOS categories, C_6 organic species (1.3%) made the dominant contribution compared to C_7 (0.3%) and C_8 (0.05%) species. The CHONS category in this system almost entirely comprised molecules that were not found in all repeat experiments so are considered inconclusive in this analysis.

Compounds found in all repeat experiments with between 11 and 15 carbon atoms in the CHON category account for 1.6 % of the signal (with C_{14} 1.5% and $C_{11\text{-}12}$ 0.1%). It is likely that the majority of of C_{11} to C_{15} signal is attributed to C_7 dimers.

$C_{6\text{-}8}$ CHON compounds are likely to be second-generation *o*-cresol oxidation products such as dihydroxy nitrotoluene which are also detected in negative ionization mode as a result of being both protonated and deprotonated. The CHO compound present in this study might have some contribution from multi-generation products generated from decomposition of bicyclic intermediate compounds formed from OH oxidation of o-cresol, as reported by (Schwantes et al., 2017), but are probably mainly dihydroxy toluene compounds, which have been reported with a

70% yield from *o*-cresol oxidation (Olariu et al., 2002). Decomposition of bicyclic intermediate compounds leading to formation of unsaturated carbonyl molecules could form oligomeric species resulting in formation of the C_{11-15} molecules in the CHO, and CHON groups.

d) binary α-pinene / isoprene mixture

The elemental categories in the binary α-pinene/isoprene samples shown in Fig.5(d) indicate a high similarity to the single VOC α-pinene system (Fig.5 (a)), with CHO compounds dominating the total signal and predominantly containing 9 to 10 carbon atoms, but with some fragmentation to C_6-C_8. The signal intensity of CHOS compounds reduced by 0.7% of the total signal in the binary system (Fig 5. (d)) compared to the single VOC α-pinene system (Fig 5.(a)), mostly in the C_6-C_8 signal. In contrast, the signal intensity of CHON components is 19.7% of the total in the binary system, 5.1% higher than in the single VOC α-pinene system, with the enhancement in molecules with carbon number >16.

The similarity in the elemental categorisation between single VOC α-pinene and binary α-pinene / isoprene system again supports the contention that α-pinene components dominate the total signal in the binary system. However, the enhancement of CHON compounds intensity in binary system possible implies an increase in the RO_2/NO_2 or RO_2/NO termination pathways leading to stronger organic nitrate formation. A large fraction of the signal from molecules with carbon number greater than 16 in this binary system might be attributed to dimerization of gas-phase nitrated highly oxidized molecules.

e) binary systems containing o-cresol

The distribution of SOA products from α-pinene / *o*-cresol (Fig.5(e)) and isoprene / *o*-cresol binary systems (Fig 5(f)) show obvious differences compared to the corresponding single precursor systems. In the α-pinene / cresol binary system, the dominant signal intensity was contributed by CHON compounds, and they mainly comprise molecules with more than 16 carbon atoms. The rest of the signal was found in the CHO (9.0%), CHOS (1.6%), and CHONS (3.3%), categories, while compound with nC>=9 made up a significant proportion. In the isoprene/*o*-cresol system, most of the compounds were in the CHON category (17.2%), and the majority of them were composed of 6 to 10 carbon atoms. C_9-C_{15} molecules also made a non-negligible contribution in

CHON compounds (7.4%). The remainder of the signal was found in the CHO (12.9%), CHONS (1.3%) and CHOS (5.8%) categories, again concentrated at C_{6-8}.

Lack of similarities between *o*-cresol containing binary systems and the corresponding sole precursor systems in the positive ionisation mode, suggests a significant contribution to the signal from the unique compounds shown in Figure 3 exerting some control over the elemental composition of SOA in binary systems. For instance, cross-products from α-pinene and *o*-cresol gas or particle-phase oxidation probably contribute to the high carbon number compounds in binary system. In the isoprene/*o*-cresol system, high C_6-C_8 contributions in all categories were likely from *o*-cresol, though the other contributions were dissimilar to the individual precursor systems.

f) ternary α-pinene / isoprene / o-cresol mixture

The distribution of SOA products in ternary system (Fig.5(g)) was very similar to the single precursor α-pinene experiments (Fig.5(a)). The dominant compounds were found in the CHO categories with signal intensity of 21.1%, most of them with 6 to 10 carbon atoms. The 17.5% signal contribution of molecules with carbon number greater than C_{16} in CHON is 7.2% higher than signal intensity of CHON molecules with carbon number >16 in the single precursor α-pinene system (10.3%).

The most notable difference between the positive mode signal in the ternary system and the single precursor systems was the high contribution of molecules with nC > 21 in the CHON category. As an indication of the relative contribution of accretion products to the SOA particle mass in each system, table.S2 shows that the signal-attributed mass concentration of molecules (nC>21) in the single VOC isoprene system, at 0.016 μgm^{-3}, is significant lower than in the α-pinene/o-Cresol binary (2.85 μgm^{-3}) , and is about 8 times less than in the isoprene / *o*-cresol binary (0.14 μgm^{-3}) and 70 times less than the ternary (1.10 μgm^{-3}) systems, which is comparable to the single precursor α-pinene system (1.34 μgm^{-3}). The SOA particle products of the ternary system are mainly attributable to α-pinene oxidation, and accretion reactions, possibly across different precursor products, leading to high carbon number nitrogen-containing compounds.

3.2.2.4. Positive Ionisation Aggregate Particle Component Properties

Table 4 shows the intensity weighted average values for compounds detected in positive ionisation mode in all repeat experiments of individual SOA systems. All properties were normalised to the total detected compounds abundance. Clearly, the nC values in all three single VOCs systems were higher than their precursor's carbon number. For example, the nC values in isoprene SOA is 11.73, which is 2 times higher than carbon number of isoprene (C_5). In the binary α -pinene/Isoprene system, the nC (11.90) slightly higher than in single α -pinene system (11.55), and in single isoprene system, suggesting a contribution from each. The OSc values seem comparable in both single systems and binary α -pinene/isoprene system. The average value of nC in binary α -pinene/*o*-cresol system (17.88) was significantly higher than the single VOC α -pinene (11.55) and *o*-Cresol systems (7.61). The O/C values in binary α -pinene/*o*-cresol system was approximately 0.15 lower than sole α -pinene and *o*-cresol system, while the H/C values in binary α -pinene/*o*-cresol system is comparable to single α -pinene, and about ~0.4 higher than sole o-cresol system. The average value of nC in the binary isoprene/*o*-cresol system (8.43) was lower than sole isoprene systems (nC=15.8), but higher than single o-cresol system (nC=7.61). The signal intensity weighted values for all chemical parameters in the ternary mixture shown no obvious similarity to those in any sole precursor system with the exception of DBE/C parameter.

It is apparent in the positive mode that accretion reactions occurred, and its products play an essential role in single isoprene system, the binary α -pinene-containing systems and the ternary system. Moreover, although some of the chemical parameters in the binary system show similar values compared to single precursor systems, the significant differences between mixed systems and those of the individual precursors imply that categories of components in the mixed systems were controlled by the compounds that were unique to the mixture and not found in the single precursor systems.

Table 4: Intensity Weighted Average Values obtained from positive ionization mode LC-Orbitrap MS for O/C, H/C, OSc, DBE, and the number of carbons (nC) present for SOA filters extracts from single and mixed precursor's experiment.

Chemical parameters	**α-pinene**	**Isoprene**	**o-Cresol**	**α-pinene/ Isoprene**	**Isoprene/ o-Cresol**	**α-pinene/ o-Cresol**	**α-pinene/ Isoprene/ o-Cresol**
nC	11.55	11.73	7.61	11.90	8.43	17.88	13.69
H/C	1.56	1.65	1.09	1.54	1.25	1.55	1.52
O/C	0.32	0.36	0.36	0.29	0.46	0.17	0.23
$\overline{\mathbf{OS}}$**c**	-0.95	-1.00	-0.66	-1.03	-0.50	-1.38	-1.17
DBE/C	0.32	0.32	0.64	0.33	0.54	0.31	0.33
DBE	3.72	3.15	4.82	3.86	4.28	5.49	4.55

5555

3.2.2.5. Insights from the combination of positive and negative mode elemental categorisation of signal contribution

Considering the results of both negative and positive ionization modes, the α-pinene derived compounds unsurprisingly dominate the elemental categorisation of binary α-pinene /isoprene
5560 binary system, since the α-pinene produced a much greater mass concentration than isoprene. The average carbon number in positive ionization mode (Table 3 and 4) shows that SOA formation in the binary α -pinene / isoprene binary system involves similar accretion products as found in the single VOC α-pinene system. Whilst *o*-cresol generated appreciable SOA particle mass concentration, this was still significantly lower than in the single α-pinene system. However, the negative mode analysis
5565 suggests that *o*-cresol oxidation products can make a more significant contribution than α-pinene products, notwithstanding the particularly high sensitivity to aromatic nitro-compounds, which make a high contribution to the *o*-cresol CHON category. The positive mode, being sensitive to a different subset of the compounds, differs to the observations in negative ionisation mode. The observation in positive mode reveals that SOA elemental composition in binary *o*-cresol/ α-pinene
5570 system is not driven by any single precursor's oxidation products but by the new compounds that appear to be *o*-cresol / α-pinene large molecular cross-products. Approximately half of number of compounds were unique in the binary *o*-cresol/ α-pinene system in both positive and negative modes (Fig. 2(b) and Fig 3(b)). In the *o*-cresol/isoprene system, it may be expected that the elemental composition was driven by the *o*-cresol since the isoprene oxidation produced very little
5575 particulate mass compared to that of *o*-cresol. Negative ionization results were consistent with this, though positive mode indicated an additional significant contribution from *o*-cresol / isoprene large

molecular cross-products. Overall SOA particle formation in binary systems can be seen to be mainly dependent on the high yield precursors, but also influenced by the interaction between products of the individual precursors, with the unique compounds making a greater contribution than any sole precursor's products in positive ionization mode of the *o*-cresol/ α-pinene system. In the ternary system, the elemental composition shares striking resemblance of single α-pinene system in positive ionization mode but in negative ionization mode there was little similarity with any single precursor fsystem, with all three precursors contributing. On the other hand, the elemental grouping results clearly shown that the compounds that were not present in all repeat experiments and hence inconclusively attributable in all precursor system made non-negligible contributions in both modes (especially in positive ionization), suggesting the repeatability of SOA chemical composition in each system is not ideal. This may be an artefact of operating process during chamber experiment and / or filter offline analysis. It should not affect the analysis of SOA chemical characterization between single and mixture precursor systems, since only the confidently attributable compounds between repeat experiments were employed for comparison.

3.2.3. Molecular Characterization of Particulates Organics

3.2.3.1. Negative Ionization Mode

This section aims to investigate whether the components in mixtures were also present at significant fractional abundance in particles or absent from any of the single VOC photo-oxidation system. The absence in the single VOC systems of those components making a substantial contribution to the mixtures may be indicative of interactions during the photochemistry and multiphase processing giving rise to tracers of the combinations of VOC precursors in multicomponent particles that may be of use in SOA source attribution in future ambient studies. The normalized peak area of 15 selected compounds in binary mixed system and 20 selected compounds ternary mixed system are shown in Figure 6. In all mixed systems, the five compounds with the highest signal fraction that were also present in each corresponding single precursor systems are shown alongside the top five compounds uniquely found in the mixture but absent from any single precursor system.

Only compounds found in all repeat experiments in each system were chosen for this analysis, so there is confidence in the component identification.

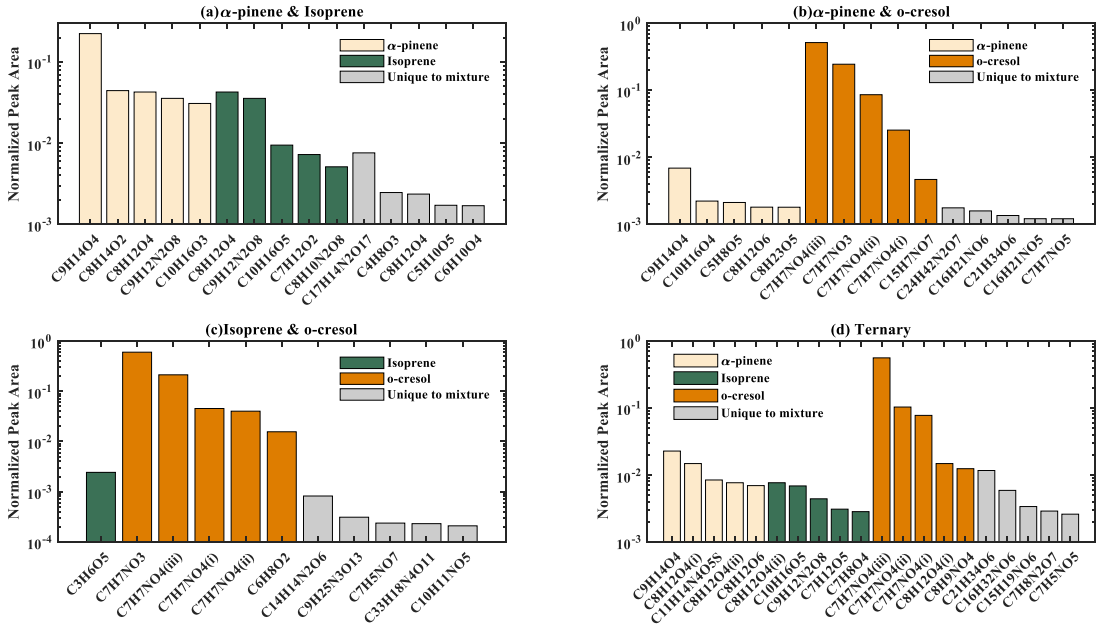

Figure 6：The dominant 15 compounds in terms of their normalized peak area in the mixed VOC systems shown in the bars: (a) binary α-pinene / Isoprene system; (b) binary α-pinene / **o**-cresol; (c) binary Isoprene / **o**-cresol; (d) ternary system respectively. The normalized peak area of these selected 10 compounds in a mixed precursor's system are also presented if they existed in corresponding single precursor's system (yellow: single **α**-pinene, green: isoprene, orange: o-cresol) . The compounds are considered identical in the mixed system and single VOC systems if they have the same empirical formula and a retention time difference of <0.1min in negative ionization mode.

a) the binary α-pinene / isoprene system

The components in binary mixture system that were also found in the single precursor α-pinene system were found to have a larger signal fraction than those found in the single isoprene system and the unique compounds. In particular, it was found that $C_9H_{14}O_4$ made the greatest signal contribution (Fig6(a)). This is also the case in the single precursor α-pinene system, and is likely to be pinic acid. $C_8H_{14}O_2$ and $C_9H_{12}N_2O_8$ made a non-negligible contribution in the binary mixture system with normalized molecular abundance 4.4% and 3.4% and were also found conserved in both single precursors systems. Compounds that were only present in the binary mixture and in neither individual VOC system had relatively low abundance, with the highest contribution from $C_{17}H_{14}N_2O_{17}$ with only 0.7% of total signal fraction. Clearly the SOA particle composition in the binary α-pinene / isoprene system was dominated by α-pinene components and partially contributed by isoprene, but not those from cross-products from their interaction.

b) binary α-pinene / *o*-cresol system

As shown in (Fig.6 (b)), the most four abundant peaks (three $C_7H_7NO_4$ isomers (i to iii) and $C_7H_7NO_3$) in the mixture were found to be present in the single precursor *o*-cresol system. $C_7H_7NO_4$ isomers in the binary mixture had signal contributions of 51.7% (iii), 8.6%(ii) and 2.5% (i) respectively, with the $C_7H_7NO_3$ contribution 24.3%. $C_9H_{14}O_4$ is present in both the single VOC α-pinene system and mixed system, with relatively high (0.68%) signal contribution in the mixed system compared to the other four compounds common to the mixture and α-pinene alone. The top five unique compounds in binary mixture system had small normalized signal fraction to total sample abundance in a range of 0.12% to 0.17%.

The four dominant compounds in the binary mixture are all nitro-aromatic compounds formed in the oxidation of *o*-cresol (Schwantes et al., 2017; Kitanovski et al., 2012). $C_7H_7NO_4$ are multiple isomers of methyl-nitrocatechol with the methyl and nitro groups at various positions on the aromatic rings. $C_7H_7NO_3$ was identified as methyl-nitrophenol. (Details of deprotonated species of $C_7H_7NO_4$ and $C_7H_7NO_3$ in table S1). As with the group categorisation, care must be taken with the interpretation of the molecular contributions to the signal owing to the enhanced sensitivity of electrospray ionisation.

c) binary isoprene / *o*-cresol system

Fig. 6(c) shows that only one compounds in the binary isoprene / *o*-cresol system was unequivocally observed in all repeat experiments the single isoprene precursor system. Components present in single *o*-cresol system make higher contribution in binary mixture system than isoprene derived compounds and those unique to the mixture, with one $C_7H_7NO_3$ and three $C_7H_7NO_4$ isomers making the most significant contribution. According to the deprotonated molecular species fragmentation (table S1), three $C_7H_7NO_4$ isomers were found at retention time 9.14, 4.52 and 7.53. These three $C_7H_7NO_4$ have similar fragmentation ions that relate to loss of NO ion (m/z=138) and NOH ion (m/z=137). The five compounds that were unique to the mixture were found to make negligible contribution to total sample abundance (between 0.05% to 0.2%).

As in the α-pinene / o-cresol binary mixture, the compounds found in the *o*-cresol system dominate the SOA particles in the binary isoprene / *o*-cresol system. Isoprene-derived compounds were found to make a negligible contribution; all of dominant compounds in the binary system were

found in the single VOC *o*-cresol system, and only one compounds in the single VOC isoprene system. There is no evidence to suggest that a compound has high enough contribution to act as tracer for the binary mixture. The three dominant compounds ($C_7H_7NO_4$ isomers) were uniquely identified as *o*-cresol oxidation products (methyl-nitrocatechol isomers) with similar retention time and fragmentation ions as the $C_7H_7NO_4$ compounds that were found in the binary α-pinene / *o*-cresol system. As with the group categorisation the consideration of enhanced sensitivity of electrospray ionization must be borne in mind in the isoprene/o-cresol and α-pinene / *o*-cresol mixtures.

d) the ternary mixture

In the ternary system (Fig.6 (d)), the top 3 largest contributing signal ($C_7H_7NO_4$ isomers) are an *o*-cresol oxidation product, the other two o-cresol compounds has comparable normalized peak area (~1.2%). Also, the α-pinene SOA also make non- negligible contribution in a range of 0.7% to 2.2% in the ternary mixture system though significantly lower than o-cresol derived compounds. Five isoprene derived compounds (0.28% to 0.76%) make comparable signal contribution to the five unique compounds (0.25% to 1.1%).

o-cresol SOA and α-pinene SOA clearly significantly influenced the chemical composition in the ternary system, while the isoprene SOA and unique compound contributions are modest. A unique potential tracer compounds ($C_{21}H_{34}O_6$) was only observed in this ternary mixture of α-pinene, *o*-cresol and isoprene with a 1.1% contribution and was found in all repeat experiments.

3.2.3.2. Positive Ionization Mode

Figure 7 compares the normalized peak area of selected compounds in mixed and single precursor systems in Positive Ionization Mode. As the negative ionization mode, figure 7 shows 15 selected compounds in each binary mixed system and 20 compounds in ternary mixed system, following the same selection criteria.

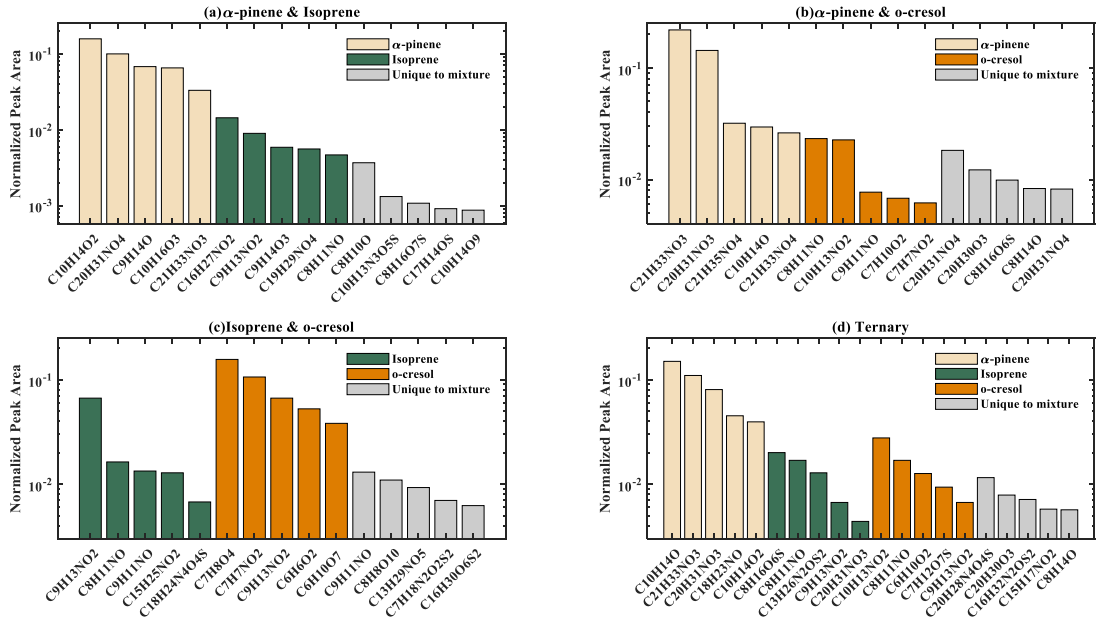

Figure 7：The dominant 15 compounds in terms of their normalized peak area in the mixed VOC systems shown in the bars: (a) binary α-pinene / Isoprene system; (b) binary α-pinene / **o**-cresol; (c) binary Isoprene / **o**-cresol; (d) ternary system respectively. The normalized peak area of these selected 10 compounds in a mixed precursor's system are also presented if they existed in corresponding single precursor's system (yellow: single **α**-pinene, green: isoprene, orange:o-cresol) . The compounds are considered identical in the mixed system and single VOC systems if they have the same empirical formula and a retention time difference of <0.1min in positive ionization mode.

a) the binary α-pinene / Isoprene system

Fig.7(a) indicates that α-pinene derived compounds dominated the binary α-pinene / isoprene system, $C_{10}H_{14}O_2$ with the highest normalized peak area of 15.5% followed by $C_{20}H_{31}NO_4$ at 8.6%. The contribution of isoprene derived compounds (0.5%-1.4%) is lower than that of those derived from α-pinene, but higher than compounds unique to the mixture, the highest farctional abundance of which was 0.32% ($C_8H_{10}O$).

The particle components in the binary α-pinene/isoprene system was substantially driven by the α-pinene components as found in negative ionization mode, likely resulting from the low SOA yield of isoprene oxidation under the conditions of our experiment. The isoprene components had little influence on the composition in this system. There is insufficient information to suggest that a compound has high enough contribution to act as tracer for the binary mixture, but compounds

unique to this mixture with seed particles under moderate NOx conditions were found to be sulphur-containing.

b) binary α-pinene / *o*-cresol system

Two α-pinene derived compounds dominated this system ($C_{21}N_{33}NO_3$ and $C_{20}H_{31}NO_3$) in positive ionisation mode (Fig.7 (b)). The other three α-pinene derived compounds were found at comparable levels to the top two derived from o-cresol ($C_8H_{11}NO$ and $C_{10}H_{13}NO_2$) at approximately 2.5% of total molecular signal. The contribution of compounds unique to the mixture were lower than all five α-pinene derived compounds, but higher than most of o-cresol SOA. The highest contribution from these unique compounds was $C_{21}H_{33}NO_4$ with 1.8% signal intensity.

Although both α-pinene and *o*-cresol oxidation products contributed to this system, the most abundant peaks ($C_{21}H_{33}NO_3$ and $C_{20}H_{31}NO_3$) were only found in the single precursor α-pinene system but not in the single precursor *o*-cresol system. The nitrated tracers ($C_{21}H_{33}NO_4$) might act as tracer compound for binary system, which is possibly driven by further oxidation of $C_{21}H_{33}NO_3$ compound.

c) binary isoprene / *o*-cresol system

Fig 7(c) shows *o*-cresol derived compounds controlled the particulate chemical compositon in this system.The fractional contribution of $C_7H_8O_4$ and $C_7H_7NO_2$ from the *o*-cresol system were 15.5% and 10.5% respectively in the binary mixture. One isoprene derived compound ($C_9H_{13}NO_2$) made considerable contribution (6.6%) in the binary mixture system. Compounds unique to the mixture were $C_9H_{11}NO$ (1.3%), $C_8H_8O_{10}$(1.0%), $C_{13}H_{29}NO_5$ (0.9%), $C_7H_{18}N_2O_2S_2$ (0.7%), and $C_{16}H_{30}O_6S_2$ (0.6%).

The higher yield *o*-cresol made a much more significant contribution to the SOA components than the lower yield isoprene. The significant abundance of two unique compounds ($C_9H_{11}NO$, and $C_8H_8O_{10}$) may result from interactions in the mixture and their exploration for use as tracers of the mixed system might prove useful.

d) The ternary mixture

From Fig. 7(d), the dominant compounds of the ternary system in positive ionisation mode were derived from α-pinene with fractional contribution range of 0.39% to 14.9%. The highest peak was $C_{10}H_{14}O$ with signal intensity 14.9%. The top *o*-cresol derived compounds were $C_{10}H_{13}NO_2$, $C_8H_{11}NO$ and $C_6H_{10}O_2$ with 2.7%, 1.6% and 1.2% signal intensity respectively. The top three isoprene derived compounds were $C_8H_{16}O_6S$ (2.0%), $C_{13}H_{26}N_2OS_2$ (1.6%)and $C_{13}H_{26}N_2OS_2$ (1.2%) respectively. $C_{20}H_{28}N_4O_4S$ was unique to the ternary mixture with a fractional contribution approximately ~1.1%, which could be the products from dimerization of α-pinene products or from interactions in the mixture.

The highest SOA yield α-pinene clearly dominated the product distribution of the ternary mixture in positive ionization mode. Isoprene and *o*-cresol derived and unique-to-the-mixture components made little contribution.

4. Conclusion

In this study, the SOA chemical composition formed from the photooxidation of α-pinene, isoprene, *o*-cresol and their binary and ternary mixtures in the presence of NOx and ammonium sulphate seed particles was determined by LC-Orbitrap MS. SOA particle mass from isoprene was almost negligible under our experimental conditions, *o*-cresol generated more and α-pinene the highest, and exhibited the highest yield in our experiments.

The number of detected SOA compounds and their molecular composition indicated that α-pinene oxidation products have a dominant influence on the SOA particle composition in the binary α-pinene/isoprene system, which can involve oligomerization/accretion reactions forming products such as $C_{20}H_{31}NO_4$. The major products in this system shows that SOA composition is clearly driven by the high α-pinene yield with isoprene oxidation products observed to make a minor contribution. The nitrogen containing compound $C_{17}H_{14}N_2O_7$ might be a potential tracter in binary α-pinene/ isoprene system in the presence of ammonium sulphate seed.

The compositional analysis in negative ionization mode reveals that *o*-cresol products dominate SOA particle composition in the α-pinene/*o*-cresol system, with major contributions from methyl-nitrocatechol isomers ($C_7H_7NO_4$) and methyl-nitrophenol ($C_7H_7NO_3$), though this will be influenced by the high sensitivity in the employed electrospray ionization method. There is a

relatively high contribution to the elemental composition from unique- to- mixture products in positive ionization mode, indicating the significant prevalence of interactions between the oxidation products in this system. The molecular analysis in both ionization modes also indicated that both α-pinene and *o*-cresol influenced the product distribution in their binary mixture.

Similarly, *o*-cresol oxidation heavily influenced SOA particle composition in the binary isoprene/*o*-cresol system in negative ionization mode, but unique-to-mixture products had made considerable contribution in the positive ionization mode. The molecular analysis in both modes suggested that higher yield *o*-cresol products were present in greater abundance than those from isoprene. Two unique compounds ($C_9H_{11}NO$, and $C_8H_8O_{10}$) in positive mode were identified that could behave as tracers in this system.

SOA composition in binary mixtures was therefore generally strongly determined by the oxidation products of the higher yield precursors, but interactions leading to cross-product formation also play an important role, especially in *o*-cresol containing systems.

In the ternary system, the elemental category composition analysis presented in positive ionization mode suggested that the chemical composition of SOA strongly depends on the sole α-pinene oxidation, with products from the oxidation of α-pinene and o-cresol identified as important in negative ionization mode. The molecular analysis shows that products from both α-pinene and *o*-cresol strongly influence the composition of SOA particles with very few isoprene oxidation products making a major contribution, indicating a limited role for isoprene oxidation. Moreover, cross-products $C_{21}H_{34}O_6$ and $C_{20}H_{28}N_4O_4S$ identified as a potential tracer in ternary system.

Data availability

All the data used in this work can be accessed on the open database of the EUROCHAMP programme (https://data.eurochamp.org/data-access/chamber-experiments/).

Competing interests

The authors declare that they have no conflict of interest.

Author contributions

GM, MRA, AV, YW and YS conceived the study. AV, YW, YS and MD conducted the experiments. KP provided on-site LC-Orbitrap MS training for filter analysis and and provided the

automated non-targeted method for LC-Orbitrap MS analysis. YS conducted the data analysis and wrote the manuscript with contribution from all co-authors.

Acknowledgements

The Manchester Aerosol Chamber acknowledges the funding support from the European Union's Horizon 2020 research and innovation programme under grant agreement no. 730997, which supports the EUROCHAMP2020 research programme. Instrumentational support was funded by the NERC Atmospheric Measurement and Observational Facility (AMOF). Y.W. acknowledges the joint scholarship of The University of Manchester and Chinese Scholarship Council. M.R.A. acknowledges funding support by UK National Centre for Atmospheric Sciences (NACS). A.V. acknowledges the funding support by Natural Environment Research Council (NERC) EAO Doctoral Training Partnership.

References

Ahlberg, E., Falk, J., Eriksson, A., Holst, T., Brune, W. H., Kristensson, A., Roldin, P., and Svenningsson, B.: Secondary organic aerosol from VOC mixtures in an oxidation flow reactor, Atmospheric Environment, 161, 210-220, https://doi.org/10.1016/j.atmosenv.2017.05.005, 2017.

Andreae, M. O. and Crutzen, P. J.: Atmospheric aerosols: Biogeochemical sources and role in atmospheric chemistry, Science, 276, 1052-1058, 1997.

Atkinson, R.: Gas-phase tropospheric chemistry of volatile organic compounds: 1. Alkanes and alkenes, Journal of Physical and Chemical Reference Data, 26, 215-290, 1997.

Atkinson, R.: Atmospheric chemistry of VOCs and NOx, Atmospheric Environment, 34, 2063-2101, https://doi.org/10.1016/S1352-2310(99)00460-4, 2000.

Atkinson, R. and Arey, J.: Gas-phase tropospheric chemistry of biogenic volatile organic compounds: a review, Atmospheric Environment, 37, 197-219, 2003.

Atkinson, R. and Aschmann, S. M.: Products of the gas-phase reactions of aromatic hydrocarbons: Effect of NO2 concentration, International Journal of Chemical Kinetics, 26, 929-944, 10.1002/kin.550260907, 1994.

Atkinson, R. B., D. L. Cox, R. A.Crowley, J. N.Hampson, R. F.Hynes, R. G.Jenkin, M. E.Rossi, M. J.Troe, J.: Evaluated kinetic and photochemical data for atmospheric chemistry: Volume I - gas phase reactions of Ox, HOx, NOxand SOxspecies, Atmos. Chem. Phys., 4, 1738, 10.5194/acp-4-1461-2004, 2004.

Berndt, T., Hyttinen, N., Herrmann, H., and Hansel, A.: First oxidation products from the reaction of hydroxyl radicals with isoprene for pristine environmental conditions, Communications Chemistry, 2, 21, 10.1038/s42004-019-0120-9, 2019.

Berndt, T., Scholz, W., Mentler, B., Fischer, L., Herrmann, H., Kulmala, M., and Hansel, A.: Accretion Product Formation from Self- and Cross-Reactions of RO2 Radicals in the Atmosphere, Angewandte Chemie International Edition, 57, 3820-3824, https://doi.org/10.1002/anie.201710989, 2018.

Bianchi, F., Kurtén, T., Riva, M., Mohr, C., Rissanen, M. P., Roldin, P., Berndt, T., Crounse, J. D., Wennberg, P. O., Mentel, T. F., Wildt, J., Junninen, H., Jokinen, T., Kulmala, M., Worsnop, D. R., Thornton, J. A., Donahue, N., Kjaergaard, H. G., and Ehn, M.: Highly Oxygenated Organic Molecules (HOM) from Gas-Phase Autoxidation Involving Peroxy Radicals: A Key Contributor

to Atmospheric Aerosol, Chemical Reviews, 119, 3472-3509, 10.1021/acs.chemrev.8b00395, 2019.

Bravo-Linares, C., Mudge, S., and Loyola-Sepulveda, R.: Production of volatile organic compounds (VOCs) by temperate macroalgae. The use of Solid Phase Microextraction (SPME) coupled to GC-MS as method of analysis, Journal of the Chilean Chemical Society, 55, 227-232, 10.4067/S0717-97072010000200018, 2010.

Buiarelli, F., Di Filippo, P., Pomata, D., Riccardi, C., and Bartocci, M.: A liquid chromatography tandem mass spectrometry method for simultaneous analysis of 46 atmospheric particulate-phase persistent organic pollutants and comparison with gas chromatography/mass spectrometry, International Journal of Environmental Analytical Chemistry, 97, 797-818, 10.1080/03067319.2017.1369535, 2017.

Burnett, R., Pope, C., Ezzati, M., Olives, C., Lim, S., Mehta, S., Shin, H., Singh, G., Hubbell, B., Brauer, M., Anderson, H., Smith, K., Balmes, J., Bruce, N., Kan, H., Laden, F., Prüss-Ustün, A., Turner, M., Gapstur, S., and Cohen, A.: An Integrated Risk Function for Estimating the Global Burden of Disease Attributable to Ambient Fine Particulate Matter Exposure, Environmental health perspectives, 122, 10.1289/ehp.1307049, 2014.

Camredon, M., Hamilton, J. F., Alam, M. S., Wyche, K. P., Carr, T., White, I. R., Monks, P. S., Rickard, A. R., and Bloss, W. J.: Distribution of gaseous and particulate organic composition during dark α-pinene ozonolysis, Atmos. Chem. Phys., 10, 2893-2917, 10.5194/acp-10-2893-2010, 2010.

Canagaratna, M. R., Jayne Jt Fau - Jimenez, J. L., Jimenez Jl Fau - Allan, J. D., Allan Jd Fau - Alfarra, M. R., Alfarra Mr Fau - Zhang, Q., Zhang Q Fau - Onasch, T. B., Onasch Tb Fau - Drewnick, F., Drewnick F Fau - Coe, H., Coe H Fau - Middlebrook, A., Middlebrook A Fau - Delia, A., Delia A Fau - Williams, L. R., Williams Lr Fau - Trimborn, A. M., Trimborn Am Fau - Northway, M. J., Northway Mj Fau - DeCarlo, P. F., DeCarlo Pf Fau - Kolb, C. E., Kolb Ce Fau - Davidovits, P., Davidovits P Fau - Worsnop, D. R., and Worsnop, D. R.: Chemical and microphysical characterization of ambient aerosols with the aerodyne aerosol mass spectrometer, 2007.

Carlton, A. G., Wiedinmyer, C., and Kroll, J. H.: A review of Secondary Organic Aerosol (SOA) formation from isoprene, Atmos. Chem. Phys., 9, 4987-5005, 10.5194/acp-9-4987-2009, 2009.

Coscollà, C., Yusa, V., Marti Requena, P., and Pastor, A.: Analysis of currently used pesticides in fine airborne particulate matter (PM 2.5) by pressurized liquid extraction and liquid chromatography-tandem mass spectrometry, Journal of chromatography. A, 1200, 100-107, 10.1016/j.chroma.2008.05.075, 2008.

Cropper, P. M., Eatough, D. J., Overson, D. K., Hansen, J. C., Caka, F., and Cary, R. A.: Use of a gas chromatography–mass spectrometry organic aerosol monitor for in-field detection of fine particulate organic compounds in source apportionment, Journal of the Air & Waste Management Association, 68, 390-402, 10.1080/10962247.2017.1363095, 2018.

Crounse, J. D., Nielsen, L. B., Jørgensen, S., Kjaergaard, H. G., and Wennberg, P. O.: Autoxidation of Organic Compounds in the Atmosphere, The Journal of Physical Chemistry Letters, 4, 3513-3520, 10.1021/jz4019207, 2013.

Danadurai, K. S. K., Chellam, S., Lee, C.-T., and Fraser, M. P.: Trace elemental analysis of airborne particulate matter using dynamic reaction cell inductively coupled plasma – mass spectrometry: Application to monitoring episodic industrial emission events, Analytica Chimica Acta, 686, 40-49, https://doi.org/10.1016/j.aca.2010.11.037, 2011.

Daumit, K. E., Kessler, S. H., and Kroll, J. H.: Average chemical properties and potential formation pathways of highly oxidized organic aerosol, Faraday Discuss, 165, 181-202, 10.1039/c3fd00045a, 2013.

DeCarlo, P. F., Kimmel, J. R., Trimborn, A., Northway, M. J., Jayne, J. T., Aiken, A. C., Gonin, M., Fuhrer, K., Horvath, T., Docherty, K. S., Worsnop, D. R., and Jimenez, J. L.: Field-Deployable, High-Resolution, Time-of-Flight Aerosol Mass Spectrometer, Analytical Chemistry, 78, 8281-8289, 10.1021/ac061249n, 2006.

Dommen, J., Metzger, A., Duplissy, J., Kalberer, M., Alfarra, M., Gascho, A., Weingartner, E., Prevot, A., Verheggen, B., and Baltensperger, U.: Laboratory observation of oligomers in the aerosol from isoprene/NOx photooxidation, Geophysical Research Letters, 33, 2006.

Donahue, N. M., Epstein, S. A., Pandis, S. N., and Robinson, A. L.: A two-dimensional volatility basis set: 1. organic-aerosol mixing thermodynamics, Atmos. Chem. Phys., 11, 3303-3318, 10.5194/acp-11-3303-2011, 2011.

Eddingsaas, N. C., Loza, C. L., Yee, L. D., Chan, M., Schilling, K. A., Chhabra, P. S., Seinfeld, J. H., and Wennberg, P. O.: α-pinene photooxidation under controlled chemical conditions –

Part 2: SOA yield and composition in low- and high-NO_x environments, Atmos. Chem. Phys., 12, 7413-7427, 10.5194/acp-12-7413-2012, 2012.

Fiore, A. M., Naik, V., Spracklen, D. V., Steiner, A., Unger, N., Prather, M., Bergmann, D., Cameron-Smith, P. J., Cionni, I., Collins, W. J., Dalsøren, S., Eyring, V., Folberth, G. A., Ginoux, P., Horowitz, L. W., Josse, B., Lamarque, J.-F., MacKenzie, I. A., Nagashima, T., O'Connor, F. M., Righi, M., Rumbold, S. T., Shindell, D. T., Skeie, R. B., Sudo, K., Szopa, S., Takemura, T., and Zeng, G.: Global air quality and climate, Chemical Society Reviews, 41, 6663-6683, 10.1039/C2CS35095E, 2012.

Gao, S., Keywood, M., Ng, N. L., Surratt, J., Varutbangkul, V., Bahreini, R., Flagan, R. C., and Seinfeld, J. H.: Low-Molecular-Weight and Oligomeric Components in Secondary Organic Aerosol from the Ozonolysis of Cycloalkenes and α-Pinene, The Journal of Physical Chemistry A, 108, 10147-10164, 10.1021/jp047466e, 2004a.

Gao, S., Ng, N. L., Keywood, M., Varutbangkul, V., Bahreini, R., Nenes, A., He, J., Yoo, K. Y., Beauchamp, J. L., Hodyss, R. P., Flagan, R. C., and Seinfeld, J. H.: Particle Phase Acidity and Oligomer Formation in Secondary Organic Aerosol, Environmental Science & Technology, 38, 6582-6589, 10.1021/es049125k, 2004b.

Glasius, M., Duane, M., and Larsen, B. R.: Determination of polar terpene oxidation products in aerosols by liquid chromatography-ion trap mass spectrometry, J Chromatogr A, 833, 121-135, 1999.

Hallquist, M., Wenger, J., Baltensperger, U., Rudich, Y., Simpson, D., Claeys, M., Dommen, J., Donahue, N., George, C., and Goldstein, A.: The formation, properties and impact of secondary organic aerosol: current and emerging issues, Atmospheric chemistry and physics, 9, 5155-5236, 2009.

Hamilton, J. F., Bryant, D. J., Edwards, P. M., Ouyang, B., Bannan, T. J., Mehra, A., Mayhew, A. W., Hopkins, J. R., Dunmore, R. E., Squires, F. A., Lee, J. D., Newland, M. J., Worrall, S. D., Bacak, A., Coe, H., Percival, C., Whalley, L. K., Heard, D. E., Slater, E. J., Jones, R. L., Cui, T., Surratt, J. D., Reeves, C. E., Mills, G. P., Grimmond, S., Sun, Y., Xu, W., Shi, Z., and Rickard, A. R.: Key Role of NO3 Radicals in the Production of Isoprene Nitrates and Nitrooxyorganosulfates in Beijing, Environmental Science & Technology, 55, 842-853, 10.1021/acs.est.0c05689, 2021.

Henry, K. M., Lohaus, T., and Donahue, N. M.: Organic Aerosol Yields from α-Pinene Oxidation: Bridging the Gap between First-Generation Yields and Aging Chemistry, Environmental Science & Technology, 46, 12347-12354, 10.1021/es302060y, 2012.

Hoffmann, T., Odum, J. R., Bowman, F., Collins, D., Klockow, D., Flagan, R. C., and Seinfeld, J. H.: Formation of Organic Aerosols from the Oxidation of Biogenic Hydrocarbons, Journal of Atmospheric Chemistry, 26, 189-222, 10.1023/A:1005734301837, 1997.

Iinuma, Y., Böge, O., Kahnt, A., and Herrmann, H.: Laboratory chamber studies on the formation of organosulfates from reactive uptake of monoterpene oxides, Physical Chemistry Chemical Physics, 11, 7985-7997, 10.1039/B904025K, 2009.

Jimenez, J. L., Canagaratna, M. R., Donahue, N. M., Prevot, A. S. H., Zhang, Q., Kroll, J. H., DeCarlo, P. F., Allan, J. D., Coe, H., Ng, N. L., Aiken, A. C., Docherty, K. S., Ulbrich, I. M., Grieshop, A. P., Robinson, A. L., Duplissy, J., Smith, J. D., Wilson, K. R., Lanz, V. A., Hueglin, C., Sun, Y. L., Tian, J., Laaksonen, A., Raatikainen, T., Rautiainen, J., Vaattovaara, P., Ehn, M., Kulmala, M., Tomlinson, J. M., Collins, D. R., Cubison, M. J., Dunlea, J., Huffman, J. A., Onasch, T. B., Alfarra, M. R., Williams, P. I., Bower, K., Kondo, Y., Schneider, J., Drewnick, F., Borrmann, S., Weimer, S., Demerjian, K., Salcedo, D., Cottrell, L., Griffin, R., Takami, A., Miyoshi, T., Hatakeyama, S., Shimono, A., Sun, J. Y., Zhang, Y. M., Dzepina, K., Kimmel, J. R., Sueper, D., Jayne, J. T., Herndon, S. C., Trimborn, A. M., Williams, L. R., Wood, E. C., Middlebrook, A. M., Kolb, C. E., Baltensperger, U., and Worsnop, D. R.: Evolution of Organic Aerosols in the Atmosphere, Science, 326, 1525, 10.1126/science.1180353, 2009.

Jokinen, T., Sipilä, M., Richters, S., Kerminen, V.-M., Paasonen, P., Stratmann, F., Worsnop, D., Kulmala, M., Ehn, M., Herrmann, H., and Berndt, T.: Rapid Autoxidation Forms Highly Oxidized RO2 Radicals in the Atmosphere, Angewandte Chemie International Edition, 53, 14596-14600, https://doi.org/10.1002/anie.201408566, 2014.

Kahnt, A., Iinuma, Y., Blockhuys, F., Mutzel, A., Vermeylen, R., Kleindienst, T. E., Jaoui, M., Offenberg, J. H., Lewandowski, M., Böge, O., Herrmann, H., Maenhaut, W., and Claeys, M.: 2-Hydroxyterpenylic Acid: An Oxygenated Marker Compound for α-Pinene Secondary Organic Aerosol in Ambient Fine Aerosol, Environmental Science & Technology, 48, 4901-4908, 10.1021/es500377d, 2014.

Kiendler-Scharr, A., Wildt, J., Maso, M. D., Hohaus, T., Kleist, E., Mentel, T. F., Tillmann, R., Uerlings, R., Schurr, U., and Wahner, A.: New particle formation in forests inhibited by isoprene emissions, Nature, 461, 381-384, 10.1038/nature08292, 2009.

Kiendler-Scharr, A., Andres, S., Bachner, M., Behnke, K., Broch, S., Hofzumahaus, A., Holland, F., Kleist, E., Mentel, T. F., Rubach, F., Springer, M., Steitz, B., Tillmann, R., Wahner, A., Schnitzler, J. P., and Wildt, J.: Isoprene in poplar emissions: effects on new particle formation and OH concentrations, Atmos. Chem. Phys., 12, 1021-1030, 10.5194/acp-12-1021-2012, 2012.

Kiontke, A., Oliveira-Birkmeier, A., Opitz, A., and Birkemeyer, C.: Electrospray Ionization Efficiency Is Dependent on Different Molecular Descriptors with Respect to Solvent pH and Instrumental Configuration, PLOS ONE, 11, e0167502, 10.1371/journal.pone.0167502, 2016.

Kitanovski, Z., Grgić, I., Yasmeen, F., Claeys, M., and Čusak, A.: Development of a liquid chromatographic method based on ultraviolet–visible and electrospray ionization mass spectrometric detection for the identification of nitrocatechols and related tracers in biomass burning atmospheric organic aerosol, Rapid Communications in Mass Spectrometry, 26, 793-804, https://doi.org/10.1002/rcm.6170, 2012.

Koch, B. P. and Dittmar, T.: From mass to structure: an aromaticity index for high-resolution mass data of natural organic matter, Rapid Communications in Mass Spectrometry, 20, 926-932, https://doi.org/10.1002/rcm.2386, 2006.

Kroll, J. H., Ng, N. L., Murphy, S. M., Flagan, R. C., and Seinfeld, J. H.: Secondary organic aerosol formation from isoprene photooxidation under high-NOx conditions, Geophysical Research Letters, 32, https://doi.org/10.1029/2005GL023637, 2005a.

Kroll, J. H., Ng, N. L., Murphy, S. M., Flagan, R. C., and Seinfeld, J. H.: Secondary organic aerosol formation from isoprene photooxidation, Environmental science & technology, 40, 1869-1877, 2006.

Kroll, J. H., Ng, N. L., Murphy, S. M., Varutbangkul, V., Flagan, R. C., and Seinfeld, J. H.: Chamber studies of secondary organic aerosol growth by reactive uptake of simple carbonyl compounds, Journal of Geophysical Research: Atmospheres, 110, https://doi.org/10.1029/2005JD006004, 2005b.

Kroll, J. H., Donahue, N. M., Jimenez, J. L., Kessler, S. H., Canagaratna, M. R., Wilson, K. R., Altieri, K. E., Mazzoleni, L. R., Wozniak, A. S., Bluhm, H., Mysak, E. R., Smith, J. D., Kolb, C.

E., and Worsnop, D. R.: Carbon oxidation state as a metric for describing the chemistry of atmospheric organic aerosol, Nature Chemistry, 3, 133-139, 10.1038/nchem.948, 2011.

Kulkarni, P., Chellam, S., Flanagan, J. B., and Jayanty, R. K. M.: Microwave digestion—ICP-MS for elemental analysis in ambient airborne fine particulate matter: Rare earth elements and validation using a filter borne fine particle certified reference material, Analytica Chimica Acta, 599, 170-176, https://doi.org/10.1016/j.aca.2007.08.014, 2007.

Li, N., He, Q., Greenberg, J., Guenther, A., Li, J., Cao, J., Wang, J., Liao, H., Wang, Q., and Zhang, Q.: Impacts of biogenic and anthropogenic emissions on summertime ozone formation in the Guanzhong Basin, China, Atmos. Chem. Phys., 18, 7489-7507, 10.5194/acp-18-7489-2018, 2018.

Lim, Y. B. and Ziemann, P. J.: Effects of molecular structure on aerosol yields from OH radical-initiated reactions of linear, branched, and cyclic alkanes in the presence of NO x, Environmental science & technology, 43, 2328-2334, 2009.

Liu, L.-b., Liu, Y., Lin, J.-m., Tang, N., Hayakawa, K., and Maeda, T.: Development of analytical methods for polycyclic aromatic hydrocarbons (PAHs) in airborne particulates: A review, Journal of Environmental Sciences, 19, 1-11, https://doi.org/10.1016/S1001-0742(07)60001-1, 2007.

Lopez-Hilfiker, F. D., Mohr, C., Ehn, M., Rubach, F., Kleist, E., Wildt, J., Mentel, T. F., Lutz, A., Hallquist, M., Worsnop, D., and Thornton, J. A.: A novel method for online analysis of gas and particle composition: description and evaluation of a Filter Inlet for Gases and AEROsols (FIGAERO), Atmos. Meas. Tech., 7, 983-1001, 10.5194/amt-7-983-2014, 2014.

McFiggans, G., Mentel, T. F., Wildt, J., Pullinen, I., Kang, S., Kleist, E., Schmitt, S., Springer, M., Tillmann, R., and Wu, C.: Secondary organic aerosol reduced by mixture of atmospheric vapours, Nature, 565, 587, 2019.

McFiggans, G., Artaxo, P., Baltensperger, U., Coe, H., Facchini, M. C., Feingold, G., Fuzzi, S., Gysel, M., Laaksonen, A., Lohmann, U., Mentel, T. F., Murphy, D. M., O'Dowd, C. D., Snider, J. R., and Weingartner, E.: The effect of physical and chemical aerosol properties on warm cloud droplet activation, Atmos. Chem. Phys., 6, 2593-2649, 10.5194/acp-6-2593-2006, 2006.

McLuckey, S. A. and Wells, J. M.: Mass Analysis at the Advent of the 21st Century, Chemical Reviews, 101, 571-606, 10.1021/cr990087a, 2001.

McNeill, V. F.: Aqueous Organic Chemistry in the Atmosphere: Sources and Chemical Processing of Organic Aerosols, Environmental Science & Technology, 49, 1237-1244, 10.1021/es5043707, 2015.

McVay, R. C., Zhang, X., Aumont, B., Valorso, R., Camredon, M., La, Y. S., Wennberg, P. O., and Seinfeld, J. H.: SOA formation from the photooxidation of α-pinene: systematic exploration of the simulation of chamber data, Atmos. Chem. Phys., 16, 2785-2802, 10.5194/acp-16-2785-2016, 2016.

Mehra, A., Bannan, T., Worrall, S., Bacak, A., Priestley, M., Liu, D., Zhao, J., Xu, W., Sun, Y., Hamilton, J., Squires, F., Lee, J., Bryant, D., Hopkins, J., Elzein, A., Budisulistiorini, S., Cheng, X., Qi, C., and Coe, H.: Using highly time-resolved online mass spectrometry to examine biogenic and anthropogenic contributions to organic aerosol in Beijing, Faraday Discussions, 226, 10.1039/D0FD00080A, 2021.

Mentel, T. F., Springer, M., Ehn, M., Kleist, E., Pullinen, I., Kurtén, T., Rissanen, M., Wahner, A., and Wildt, J.: Formation of highly oxidized multifunctional compounds: autoxidation of peroxy radicals formed in the ozonolysis of alkenes – deduced from structure–product relationships, Atmos. Chem. Phys., 15, 6745-6765, 10.5194/acp-15-6745-2015, 2015.

Minaeian, J. K.: Development and Deployment of an Airborne Gas Chromatography/Mass Spectrometer to Measure Tropospheric Volatile Organic Compounds, PhD, University of York, 2017.

Mutzel, A., Rodigast, M., Iinuma, Y., Böge, O., and Herrmann, H.: Monoterpene SOA – Contribution of first-generation oxidation products to formation and chemical composition, Atmospheric Environment, 130, 136-144, https://doi.org/10.1016/j.atmosenv.2015.10.080, 2016.

Nestorowicz, K., Jaoui, M., Rudzinski, K. J., Lewandowski, M., Kleindienst, T. E., Spólnik, G., Danikiewicz, W., and Szmigielski, R.: Chemical composition of isoprene SOA under acidic and non-acidic conditions: effect of relative humidity, Atmos. Chem. Phys., 18, 18101-18121, 10.5194/acp-18-18101-2018, 2018.

Ng, N., Kwan, A., Surratt, J., Chan, A., Chhabra, P., Sorooshian, A., Pye, H. O., Crounse, J., Wennberg, P., and Flagan, R.: Secondary organic aerosol (SOA) formation from reaction of isoprene with nitrate radicals (NO 3), Atmospheric Chemistry and Physics, 8, 4117-4140, 2008.

Ng, N. L., Chhabra, P. S., Chan, A. W. H., Surratt, J. D., Kroll, J. H., Kwan, A. J., McCabe, D. C., Wennberg, P. O., Sorooshian, A., Murphy, S. M., Dalleska, N. F., Flagan, R. C., and Seinfeld, J. H.: Effect of NO_x level on secondary organic aerosol (SOA) formation from the photooxidation of terpenes, Atmos. Chem. Phys., 7, 5159-5174, 10.5194/acp-7-5159-2007, 2007.

Novakov, T. and Penner, J.: Large contribution of organic aerosols to cloud-condensation-nuclei concentrations, Nature, 365, 823, 1993.

Odum, J. R., Hoffmann, T., Bowman, F., Collins, D., Flagan, R. C., and Seinfeld, J. H.: Gas/particle partitioning and secondary organic aerosol yields, Environmental Science & Technology, 30, 2580-2585, 1996.

Olariu, R. I., Klotz, B., Barnes, I., Becker, K. H., and Mocanu, R.: FT–IR study of the ring-retaining products from the reaction of OH radicals with phenol, o-, m-, and p-cresol, Atmospheric Environment, 36, 3685-3697, https://doi.org/10.1016/S1352-2310(02)00202-9, 2002.

Ono-Ogasawara, M., Myojo T Fau - Smith, T. J., and Smith, T. J.: A simple direct injection method for GC/MS analysis of PAHs in particulate matter, 2008.

Pandis, S. N., Paulson, S. E., Seinfeld, J. H., and Flagan, R. C.: Aerosol formation in the photooxidation of isoprene and β-pinene, Atmospheric Environment. Part A. General Topics, 25, 997-1008, https://doi.org/10.1016/0960-1686(91)90141-S, 1991.

Pereira, K., Ward, M., Wilkinson, J., Sallach, J., Bryant, D., Dixon, W., Hamilton, J., and Lewis, A.: An Automated Methodology for Non-targeted Compositional Analysis of Small Molecules in High Complexity Environmental Matrices Using Coupled Ultra Performance Liquid Chromatography Orbitrap Mass Spectrometry, Environmental Science & Technology, XXXX, 10.1021/acs.est.0c08208, 2021.

Pereira, K. L., Hamilton, J. F., Rickard, A. R., Bloss, W. J., Alam, M. S., Camredon, M., Muñoz, A., Vázquez, M., Borrás, E., and Ródenas, M.: Secondary organic aerosol formation and composition from the photo-oxidation of methyl chavicol (estragole), Atmos. Chem. Phys., 14, 5349-5368, 10.5194/acp-14-5349-2014, 2014.

Pereira, K. L., Hamilton, J. F., Rickard, A. R., Bloss, W. J., Alam, M. S., Camredon, M., Ward, M. W., Wyche, K. P., Muñoz, A., Vera, T., Vázquez, M., Borrás, E., and Ródenas, M.: Insights into the Formation and Evolution of Individual Compounds in the Particulate Phase during Aromatic Photo-Oxidation, Environmental Science & Technology, 49, 13168-13178, 10.1021/acs.est.5b03377, 2015.

Pullinen, I., Schmitt, S., Kang, S., Sarrafzadeh, M., Schlag, P., Andres, S., Kleist, E., Mentel, T. F., Rohrer, F., Springer, M., Tillmann, R., Wildt, J., Wu, C., Zhao, D., Wahner, A., and Kiendler-Scharr, A.: Impact of NOx on secondary organic aerosol (SOA) formation from α-pinene and β-

pinene photooxidation: the role of highly oxygenated organic nitrates, Atmos. Chem. Phys., 20, 10125-10147, 10.5194/acp-20-10125-2020, 2020.

Romonosky, D. E., Laskin, A., Laskin, J., and Nizkorodov, S. A.: High-Resolution Mass Spectrometry and Molecular Characterization of Aqueous Photochemistry Products of Common Types of Secondary Organic Aerosols, The Journal of Physical Chemistry A, 119, 2594-2606, 10.1021/jp509476r, 2015.

Safieddine, S. A. and Heald, C. L.: A Global Assessment of Dissolved Organic Carbon in Precipitation, Geophysical Research Letters, 44, 11,672-611,681, https://doi.org/10.1002/2017GL075270, 2017.

Saldarriaga-Noreña, H., López-Márquez, R., Murillo Tovar, M. A., Arias-Montoya, M., Guerrero-Álvarez, J., and Vergara, J.: Recent Advances for Polycyclic Aromatic Analysis in Airborne Particulate Matter, in, 10.5772/intechopen.79714, 2018.

Schervish, M. and Donahue, N. M.: Peroxy radical chemistry and the volatility basis set, Atmos. Chem. Phys., 20, 1183-1199, 10.5194/acp-20-1183-2020, 2020.

Schwantes, R. H., Schilling, K. A., McVay, R. C., Lignell, H., Coggon, M. M., Zhang, X., Wennberg, P. O., and Seinfeld, J. H.: Formation of highly oxygenated low-volatility products from cresol oxidation, Atmos. Chem. Phys., 17, 3453-3474, 10.5194/acp-17-3453-2017, 2017.

Shilling, J. E., Zawadowicz, M. A., Liu, J., Zaveri, R. A., and Zelenyuk, A.: Photochemical Aging Alters Secondary Organic Aerosol Partitioning Behavior, ACS Earth and Space Chemistry, 3, 2704-2716, 10.1021/acsearthspacechem.9b00248, 2019.

Shilling, J. E., Zaveri, R. A., Fast, J. D., Kleinman, L., Alexander, M. L., Canagaratna, M. R., Fortner, E., Hubbe, J. M., Jayne, J. T., Sedlacek, A., Setyan, A., Springston, S., Worsnop, D. R., and Zhang, Q.: Enhanced SOA formation from mixed anthropogenic and biogenic emissions during the CARES campaign, Atmos. Chem. Phys., 13, 2091-2113, 10.5194/acp-13-2091-2013, 2013.

Shrivastava, M., Cappa, C. D., Fan, J., Goldstein, A. H., Guenther, A. B., Jimenez, J. L., Kuang, C., Laskin, A., Martin, S. T., Ng, N. L., Petaja, T., Pierce, J. R., Rasch, P. J., Roldin, P., Seinfeld, J. H., Shilling, J., Smith, J. N., Thornton, J. A., Volkamer, R., Wang, J., Worsnop, D. R., Zaveri, R. A., Zelenyuk, A., and Zhang, Q.: Recent advances in understanding secondary organic aerosol: Implications for global climate forcing, Reviews of Geophysics, 55, 509-559, https://doi.org/10.1002/2016RG000540, 2017.

Singh, D. P., Gadi, R., and Mandal, T. K.: Characterization of particulate-bound polycyclic aromatic hydrocarbons and trace metals composition of urban air in Delhi, India, Atmospheric Environment, 45, 7653-7663, https://doi.org/10.1016/j.atmosenv.2011.02.058, 2011.

Steckel, A. and Schlosser, G.: An Organic Chemist's Guide to Electrospray Mass Spectrometric Structure Elucidation, Molecules, 24, 10.3390/molecules24030611, 2019.

Stroud, C. A., Roberts, J. M., Goldan, P. D., Kuster, W. C., Murphy, P. C., Williams, E. J., Hereid, D., Parrish, D., Sueper, D., Trainer, M., Fehsenfeld, F. C., Apel, E. C., Riemer, D., Wert, B., Henry, B., Fried, A., Martinez-Harder, M., Harder, H., Brune, W. H., Li, G., Xie, H., and Young, V. L.: Isoprene and its oxidation products, methacrolein and methylvinyl ketone, at an urban forested site during the 1999 Southern Oxidants Study, Journal of Geophysical Research: Atmospheres, 106, 8035-8046, https://doi.org/10.1029/2000JD900628, 2001.

Surratt, J. D., Lewandowski, M., Offenberg, J. H., Jaoui, M., Kleindienst, T. E., Edney, E. O., and Seinfeld, J. H.: Effect of Acidity on Secondary Organic Aerosol Formation from Isoprene, Environmental Science & Technology, 41, 5363-5369, 10.1021/es0704176, 2007a.

Surratt, J. D., Chan, A. W. H., Eddingsaas, N. C., Chan, M., Loza, C. L., Kwan, A. J., Hersey, S. P., Flagan, R. C., Wennberg, P. O., and Seinfeld, J. H.: Reactive intermediates revealed in secondary organic aerosol formation from isoprene, Proceedings of the National Academy of Sciences, 107, 6640, 10.1073/pnas.0911114107, 2010.

Surratt, J. D., Kroll, J. H., Kleindienst, T. E., Edney, E. O., Claeys, M., Sorooshian, A., Ng, N. L., Offenberg, J. H., Lewandowski, M., Jaoui, M., Flagan, R. C., and Seinfeld, J. H.: Evidence for Organosulfates in Secondary Organic Aerosol, Environmental Science & Technology, 41, 517-527, 10.1021/es062081q, 2007b.

Surratt, J. D., Murphy, S. M., Kroll, J. H., Ng, N. L., Hildebrandt, L., Sorooshian, A., Szmigielski, R., Vermeylen, R., Maenhaut, W., Claeys, M., Flagan, R. C., and Seinfeld, J. H.: Chemical Composition of Secondary Organic Aerosol Formed from the Photooxidation of Isoprene, The Journal of Physical Chemistry A, 110, 9665-9690, 10.1021/jp061734m, 2006.

Tomaz, S., Wang, D., Zabalegui, N., Li, D., Lamkaddam, H., Bachmeier, F., Vogel, A., Monge, M. E., Perrier, S., Baltensperger, U., George, C., Rissanen, M., Ehn, M., El Haddad, I., and Riva, M.: Structures and reactivity of peroxy radicals and dimeric products revealed by online tandem mass spectrometry, Nature Communications, 12, 300, 10.1038/s41467-020-20532-2, 2021.

Wennberg, P. O., Bates, K. H., Crounse, J. D., Dodson, L. G., McVay, R. C., Mertens, L. A., Nguyen, T. B., Praske, E., Schwantes, R. H., Smarte, M. D., St Clair, J. M., Teng, A. P., Zhang, X., and Seinfeld, J. H.: Gas-Phase Reactions of Isoprene and Its Major Oxidation Products, Chemical Reviews, 118, 3337-3390, 10.1021/acs.chemrev.7b00439, 2018.

Winterhalter, R., Van Dingenen, R., Larsen, B. R., Jensen, N. R., and Hjorth, J.: LC-MS analysis of aerosol particles from the oxidation of α-pinene by ozone and OH-radicals, Atmos. Chem. Phys. Discuss., 2003, 1-39, 10.5194/acpd-3-1-2003, 2003.

Xu, Z. N., Nie, W., Liu, Y. L., Sun, P., Huang, D. D., Yan, C., Krechmer, J., Ye, P. L., Xu, Z., Qi, X. M., Zhu, C. J., Li, Y. Y., Wang, T. Y., Wang, L., Huang, X., Tang, R. Z., Guo, S., Xiu, G. L., Fu, Q. Y., Worsnop, D., Chi, X. G., and Ding, A. J.: Multifunctional Products of Isoprene Oxidation in Polluted Atmosphere and Their Contribution to SOA, Geophysical Research Letters, 48, e2020GL089276, https://doi.org/10.1029/2020GL089276, 2021.

Yasmeen, F., Vermeylen, D., Maurin, N., Perraudin, E., Doussin, J.-F., and Claeys, M.: Characterisation of tracers for aging of a-pinene secondary organic aerosol using liquid chromatography/negative ion electrospray ionisation mass spectrometry, Environmental Chemistry, 9, 236–246, 10.1071/EN11148, 2012.

Zhang, Q., Jimenez, J. L., Canagaratna, M. R., Ulbrich, I. M., Ng, N. L., Worsnop, D. R., and Sun, Y.: Understanding atmospheric organic aerosols via factor analysis of aerosol mass spectrometry: a review, Analytical and Bioanalytical Chemistry, 401, 3045-3067, 2011.

Zhao, Y., Thornton, J. A., and Pye, H. O. T.: Quantitative constraints on autoxidation and dimer formation from direct probing of monoterpene-derived peroxy radical chemistry, Proc Natl Acad Sci U S A, 115, 12142-12147, 10.1073/pnas.1812147115, 2018.

Ziemann, P. J. and Atkinson, R.: Kinetics, products, and mechanisms of secondary organic aerosol formation, Chemical Society Reviews, 41, 6582-6605, 10.1039/C2CS35122F, 2012.

[BLANK PAGE]

Paper 4: The evolution of carbon oxidation state during secondary organic aerosol formation from individual and mixed organic precursors

This paper is going to be submitted in the journal of "Atmopsheric Chemistry and Physics" within 2022

Yunqi Shao[1], Aristeidis Voliotis[1], Mao Du[1], Yu Wang[1], Kelly Pereira[3], Jacqueline Hamilton[3], M. Rami Alfarra[1,2 ‡], Gordon McFiggans[1]

[1]School of Earth and Environmental Science, University of Manchester, Manchester, M13, 9PL, UK
[2]National Centre for Atmospheric Science
[3] Wolfson Atmospheric Chemistry Laboratories, Department of Chemistry, University of York, York, YO105DD, UK
‡ now at Environment & Sustainability Center, Qatar Environment & Energy Research Institute, Doha, Qatar

Correspondence to: Yunqi.Shao (Yunqi.Shao@Mancheste.ac.uk)

Abstract

This study reports the average carbon oxidation state ($\overline{OSc}$) of SOA particles formed from the photo-oxidation of *o*-cresol, α- pinene, isoprene and their mixtures, representative anthropogenic and biogenic precursors, in the Manchester Aerosol Chamber. Three independent mass spectrometric techniques, including two online instruments, HR-ToF-AMS and FIGAREO-CIMS, and one offline technique, LC-Orbitrap MS, were employed to characterise molar atomic ratios (e.g. O/C, H/C and N/C) leading to estimation of the SOA particle average carbon oxidation state in mixtures of α-pinene/isoprene, o-cresol/isoprene, α-pinene/o-cresol and α-pinene/o-cresol/isoprene systems. Single precursor experiments at various initial concentrations were used as reference. The oxidation state of nitrogen ($\overline{OS_N}$) for CHON compounds was shown to non-negligibly influence the average $\overline{OSc}$ in single α-pinene and o-cresol system in FIGAERO-CIMS and LC-Orbitrap MS measurement. As might be expected, the average $\overline{OSc}$ accounting for $\overline{OS_N}$ is lower than when it is considered. SOA particle average oxidation state excluding consideration of $\overline{OS_N}$ obtained by the three techniques showed substantial discrepancies. That obtained from FIGAERO-CIMS was always found to be higher than from the other techniques, likely resulting from the high sensitivity of the FIGAERO-CIMS toward highly oxygenated compounds. Quantification of the SOA particle average $\overline{OSc}$ was challenging, but all three techniques showed similar trends across systems. In the single precursor system, the initial concentration of precursors influences the average $\overline{OSc}$ in the single α-pinene system, but not in the single *o*-cresol system, which is potentially attributed by the O_3 reaction with precursor. In binary precursor systems, the injected isoprene affected the average $\overline{OSc}$ in the presence of α-pinene but the influence was more modest in the presence of *o*-cresol. The $\overline{OSc}$ in the α-pinene/isoprene system was lower than in the α-pinene system although they have a similar trend in average $\overline{OSc}$ with SOA mass

concentration. This suggests that the isoprene has the potential to decrease the average $\overline{OSc}$ by forming high volatility and less oxygenated products, followed by partitioning into particulate matter in a mixed system. The $\overline{OSc}$ in the α-pinene/o-cresol system was between those measured in the single precursor systems, where that in the α-pinene system was lower than in the o-cresol system, suggesting contributions to the $\overline{OSc}$ from both precursors. In the ternary mixture, the $\overline{OSc}$ was not dominated by any single precursor, with substantial contributions from products uniquely found in the mixture. These results present the first detailed observations of particle average carbon oxidation state during SOA formation in mixed anthropogenic and biogenic systems.

1.Introduction

Organic aerosol (OA) particles are an important component of ambient aerosol particles (accounting for ~ 50% of mass in fine particulate mass)(Kanakidou et al., 2005) (Zhang et al., 2007) and are involved in multiple atmospheric processes, such as affecting the radiative forcing, heterogeneous reactions by gas species (e.g., OH radicals, O_3 and NO_3 radicals), loss of visibility and negative effects on human health (Thompson, 1995) (Griggs and Noguer, 2002; Seinfeld and Pankow, 2003; Kroll et al., 2015). Organic aerosol can be classified as primary organic aerosol (POA), which is emitted to the ambient atmosphere directly by natural environmental processes (e.g., desert dust storms and volcanic eruptions) or human activities (e.g. Industry and transportation system), and secondary organic aerosol (SOA) that is formed from ageing of POA (Robinson et al., 2007), and gas-phase oxidation of anthropogenic/biogenic volatile organic precursors (VOCs) followed by nucleation or condensation on existing particles.

Organic aerosols in the ambient atmosphere contain a variety of organic species, including hydrocarbons, alcohol, aldehydes and carboxylic acids, while a small fraction of these organic species can be detected by current techniques and characterized at molecular level (~10-30%) (Hoffmann et al., 2011). Moreover, the chemical complexity of OA increases if there are multiple OA sources (both anthropogenic and biogenic sources) that contribute to OA formation. A current lack of detailed chemical characterisation of these organic species makes it difficult to track the OA sources, understand their atmospheric processes and mitigate their adverse impacts. Jimenez et al. (2009) indicated the 30-90% of OA is contributed by SOA, the loadings and oxidation state of which, current models find difficult to predict. The majority of ambient SOA is generated by oxidation of VOCs with the dominant prevailing oxidants, hydroxyl radicals (OH) and ozone (O_3) during the day and nitrate radicals (NO_3) at nighttime, forming low volatility products and subsequently partition to condense phase (Atkinson, 2004). SOA particles increasingly contain multi-generational products as they age, a process widely studied in chambers (Lee et al., 2011; Winterhalter et al., 2003; Pandis et al., 1991; Hoffmann et al., 1997; Eddingsaas et al., 2012; Kroll et al., 2005a; Ahlberg et al., 2017; Pullinen et al., 2020; Kroll et al., 2005b). Although some chamber experiments have focused on investigating the evolution of SOA from different VOCs, most have focused on individual precursors. A number of chamber studies of SOA formation from

photo-oxidation of biogenic precursors, such as α-pinene and isoprene in the presence of NOx have been conducted (Ng et al., 2007; Pullinen et al., 2020; Kroll et al., 2005a; Kroll et al., 2006; Surratt et al., 2006). Other studies have focused on anthropogenically-emitted VOCs, such as those using aromatic hydrocarbons (Luo et al., 2021; Henry et al., 2008). However, recent laboratories had attempted to explore the SOA formation in the presence of multiple precursors under controlled conditions in view of a complex mixture of anthropogenic and biogenic VOCs in the ambient atmosphere. Using chamber studies to investigate SOA formation in mixtures of anthropogenic VOCs (1,3,5-trimethyl benzene (1,3,5-TMB), toluene, o-xylene and octane), García Vivanco and Santiago (2010) observed that 1,3,5-TMB products dominated the SOA composition, though with some difficulty in characterisation owing to analytical constraints. Looking at the biogenic α-pinene / isoprene mixture, Mcfiggans et al. (2019) demonstrated that a reduction of SOA mass and yield with isoprene acting as a scavenger toward OH radicals and its radical's products might contribute to scavenging the highly oxygenated α-pinene products results in increasing the overall volatility of the products from mixture oxidation. This paper also pointed out the importance of the mechanistic interaction between the products of oxidized precursor's molecules impacts on SOA formation, which is necessary to understanding the mechanism of SOA formation in the presence of multiple VOCs.

Understanding the oxidation chemistry leading to SOA formation in terms of characterized individual organic species presents major ongoing challenges, owing to the complexity of SOA mixtures in both the laboratory work and the ambient atmosphere. Kroll et al. (2011) highlighted that the oxidation state of the particle-phase carbon is a key property that can usefully describe the oxidation chemistry of organics in mixtures since the average carbon oxidation state will always increase with the degree of oxidation. According to the valence rule, a simplified approach to calculate the average carbon oxidation state ($\overline{OSc}$) of organic mixtures relate to the molar oxygen to carbon (O/C) and hydrogen to carbon (H/C) ratios respectively (Equation 1).

$$\overline{OSc} = 2 * \frac{O}{C} - \frac{H}{C} \qquad (1)$$

Changes in carbon oxidation state provide a valuable insight into the oxidation dynamics associated with the formation and evolution of ensemble SOA. For example, the $\overline{OSc}$ generally increases by functionalization, which can frequently occur in VOC oxidation leading to C-O bonds, for example, replacing C-H or unsaturated C-C bonds. In contrast, the average $\overline{OSc}$ remains unchanged by oligomerization, which may occur after functionalization and fragmentation reaction (Kroll et al., 2015). On the other hand, the alteration of average $\overline{OSc}$ of particulate organic molecules is also associated with the their volatility since this is a key determinant of gas-particle partitioning results in change in the ensemble chemical composition and enhancement of OA mass concentration. In general, the overall volatility will decrease with more functionalized molecules and increase with fragmentation (Daumit et al., 2013). Changes in OSc and atomic ratios (H:C and O:C ratios) upon SOA mass loading can therefore be useful tools in identifying the key process in the atmospheric ageing of SOA.

In our chamber studies of SOA formation in mixtures of α-pinene, isoprene and o-cresol, we have reported the chemical composition of SOA offline technique orbitrap liquid chromatography mass spectrometer (Shao et al., 2022). Oxidation products from the high yield precursor, α-pinene, dominated SOA inits mixtures whilst isoprene derived compounds made a negligible contribution. Interactions in the oxidation of mixed precursors were found to lead to products uniquely found in the mixtures. In this study, we expand the investigation to report online measurements from the high resolution time-of-flight Aerodyne Aerosol Mass Spectrometers (HR-TOF-AMS) and Filter Inlet for Gases and AEROsols coupled to an Iodide high-resolution time of flight chemical ionization mass spectrometer (FIGAERO-CIMS; Lee et al. (2014)) to measure the near real-time atomic ratios and derive the oxidation state of SOA during these same experiments. The HR-TOF-AMS technique had been widely used for analyzing the non-refractory aerosol chemical composition (Aiken et al., 2008; Shilling et al., 2009; Presto et al., 2009; Chhabra et al., 2010; Docherty et al., 2018) and can provide sensitive and online measurements of SOA elemental composition. The FIGAERO-CIMS were used to provide measurements of both gas-phase and particle-phase chemical constituents of organic aerosols in real time. Both instruments have limitations precluding molecular identification (elctron impact ionization in the AMS leads to extensive fragmentation in the AMS and the CIMS cannot resolve structural isomers or isobaric

compounds (Lee et al., 2014)). Nevertheless, both online instruments can provide the time profile of atomic ratios of the SOA and derived average carbon oxidation state to add interpretation of the evolution of organic compounds to the offline measurement by LC-Orbitrap MS.

The present study aims to investigate the differences in $\overline{OSc}$ in SOA formed from the photooxidation of single precursors and their mixtures. This is achieved by considering
i) the chemical mapping of identified SOA in FIGAERO-CIMS measurement and HR-TOF-AMS measurement;
ii) the relationship between precursors' initial concentration and extent of oxidation in SOA evolution in single precursors system,
iii) the dependence of the atomic ratios (O:C ratios, H:C ratios and N:C ratios) and extent of oxidation on with SOA particle mass loading in single and mixture precursor systems, and
iv) the relative contributions to $\overline{OSc}$ from the oxidation products of each precursor and whether any individual precursor controlled the average $\overline{OSc}$ of SOA in mixed systems.

A series of photochemical oxidation experiments were designed and conducted to produce SOA from the selected VOCs (α-pinene, isoprene and o-cresol) and their mixtures in the presence of neutral seed particles (ammonium sulphate) and NOx. The experimental program thereby included three single precursor systems, three binary precursor mixtures and one ternary mixture of precursors. For studying the effect of the initial VOC concentration on the particle composition and carbon oxidation state of SOA evolution, here we also conduct single precursor experiments at ½ and ⅓ initial reactivity. However, experiments with *o*-cresol at ⅓ reactivity and isoprene at ½ reactivity are not reported as a result of technical difficulties. The HR-ToF-AMS and FIGAERO-I^--CIMS continuously sampled and measured the SOA particles throughout the experiment and the entire chamber contents were flushed through a filter for collection of the aerosol at the end of the experiment for subsequent offline analysis by LC-Orbitrap MS.

2. Materials and Methods

2.1.Manchester Aerosol Chamber

All experiments were conducted in the Manchester Aerosol Chamber (MAC; Shao et al. (2021). In short, the MAC operates as a batch reactor and consists of 18m^3 volume Teflon FEP bag suspended by three rectangular extruded aluminium frames, housed in an air-conditioned enclosure. The enclosure is covered by reflective "space blanket" material and is illuminated with two 6 kW Xenon arc lamps (XBO 6000 W/HSLA OFR, Osram) and a bank of halogen lamps (Solux 50 W/4700 K, Solux MR16, USA) with an intensity corresponding to a photolysis rate of NO_2 (JNO_2) around $1.83x10^{-3}s^{-1}$ through the entire experimental campaign. Conditioned air was introduced between the bag and the enclosure to maintain a constant chamber temperature throughout the experiment. Additionally, active water was used to cooling of the mounting bars of the halogen lamps and of the filter in front of the arc lamps to remove the unwanted heat from the lamps. Relative humidity (RH) and temperature (T) are controlled by the humidifier and by the air conditioning that couple with the chamber. RH and T were continuously monitored by the dewpoint hygrometer and several thermocouples and resistance probes during the experiment. Liquid VOCs (α-pinene, isoprene and o-cresol; Sigma Aldrich, GC grade ≥99.99% purity) were introduced into chamber through injection into a heated glass bulb for vaporization and subsequently flushed into the chamber with purified N_2 (electronic capture device-grade nitrogen stream; purity ≥99.998%). A custom-made cylinder (10% v/v) containing NOx was used for NO_2 injection into the MAC in ECD N_2 as carrier gas. A Topaz model ATM 230 aerosol generator were used to produce ammonium sulphate seed particles by atomization from ammonium sulphate solution (Puratonic, 99.999% purity).

2.2. Experimental Procedure

The concept of iso-reactivity towards OH radicals was used to select the initial VOC concentrations in each experiment to enable comparable initial turnover of VOCs in the mixture with respect to OH radicals, such that the oxidation products from each VOCs would make comparable contributions at the chosen concentration and experimental conditions at the beginning of experiment. The VOCs precursors only taking account its reactivity towards OH radicals (Atkinson, 2004) when calculating the injected mass, since the consumption of VOCs by other

oxidants (e.g., O_3) was excluded. Thirteen experimental conditions were planned, covering the α-pinene, isoprene and *o*-cresol single precursor systems (each at full, ½ and ⅓ reactivity) respectively, binary α-pinene / isoprene, α-pinene / *o*-cresol and *o*-cresol / isoprene mixtures and their ternary mixture. Initial concentrations of each VOC in the binary and ternary mixtures were the same as the initial concentration in the ½ and ⅓ reactivity individual VOC experiments respectively, ensuring comparable initial reactivity toward OH in all systems.

As described in Shao et al. (2021), a "pre-experiment' program and a "post-experiment" were conducted prior to and after each experiment. These two procedures consist of multiple auto fill/flush cycle with high flow rate (~ 3 m^3 min^{-1}) with purified air to condition and remove the unwanted contaminants in the chamber bag. A water condensation particle counter (WCPC; TSI 3786), O_3 analyser, (Thermo Electron Corporation model 49C), NO-NO_2-NOx analyser (Thermo Electron Corporation model 42i) were used to monitor residual gas and particles in the chamber during the "pre-experiment", to ensure their concentrations were close to zero in the bag prior to chamber background procedure (approximately 1 hour), which aims to establish the clean chamber baseline concentration. An "experimental background" procedure was conducted in the next stage to gain the baseline of initial experimental conditions before initiation of any VOC oxidation. This comprised continuous measurement after injecting VOC(s), NOx, and seed particles sequentially and leaving the chamber to stabilise for an hour under dark condition. The baseline of clean background and the experimental background were used to correct experimental data. Actinometry and off-gasing experiments were performed regularly during our campaign to monitor the condition and cleanliness of the chamber bag.

The duration of each experiment was nominally 6 hours after initial illumination, under similar controlled environmental conditions (RH:50±5% and T:24±2 ^oC). The summary of the initial conditions of the reported experiments were presented in table 1 (noting the lack of ⅓ reactivity *o*-cresol and ½ reactivity isoprene owing to technical difficulties). The particulate products were collected at the end of each experiment, flushing the entire chamber contents through a pre-fired quartz filter (heating in a furnace at 550℃ for 5.5 hours), which was subsequently wrapped in foil and refridgerated at -18 degrees.

Table 1: Summary of the initial conditions of experiments.

Exp. no.	Exp. Type	Precursors Reactivity	VOC	NOx (ppb)	VOC (ppb)	VOC/NOx	Seed ($\mu g\ m^{-3}$)
a	Single	Full	α-pinene	40	309	7.7	72.6
b		Half	α-pinene	26	155	6.0	45.7
c		Third	α-pinene	18	103	5.7	51.0
d		Full	o-cresol	44	400	9.1	47.8
e		Half	o-cresol	40	200	5.0	51.3
f		Full	isoprene	23	164	7.1	-
g	Binary	Full	o-cresol/isoprene	34	282 (200/82)	8.3	49.6
h		Full	α-pinene/o-cresol	30	355 (155/200)	11.8	57
i		Full	α-pinene/isoprene	39	237 (155/82)	6.1	62.0
j	Ternary	Full	α-pinene/o-cresol/isoprene	78	291 (103/133/55)	3.7	45.8

2.3. Instrumentation

2.3.1. Online Measurement

The NO-NO_2-NOx and O_3 analysers were used to measure the NO_2 and O_3 gas concentration throughout the experiments. A semi-continuous gas chromatograph (6850 Agilent) coupled to a mass spectrometer (5975C Agilent; hereafter GC-MS) with a thermal desorption unit (Markes TT-24/7) was employed to monitor the time profile of VOC precursor decay. An Aerodyne high-resolution time-of-flight aerosol mass spectrometer (HR-ToF-AMS, Aerodyne Research Inc., USA) was used to measure organic mass loading and characterize the composition of non-refractory organic particles. The AMS instrument was calibrated by using monodisperse (350nm) ammonium nitrate and ammonium sulphate particle prior to and after to the experimental program, referring to the standard protocol in Jayne et al. (2000) and Jimenez et al. (2003). The instrument operated in "V mode" during experiments and ran in mass spectra (MS) and particle-time-of-flight (PToF) sub-modes for equal time periods (30s each section). The HR-ToF-AMS data were processed in Igor Pro 7.08 (Wavemeterics.Inc.) using the standard ToF-AMS analysis toolkit (version 1.21) for both unit mass resolution (UMR) and and high resolution (HR) analyses. The average ionization efficiency of nitrate (IE=9.38 x 10^8), the specific relative ionization efficiencies (RIE) for NH_4^+ (3.57 ± 0.02) and SO_4^{2-} (1.28 ± 0.01) from calibration, and the default RIE from

Alfarra et al. (2004) of all organic compounds (RIE=1.4) were all applied in the UMR and HR analysis. HR mass spectra was fitted using the method of Decarlo et al. (2006) and analysed using the ToF-AMS analysis software that reported in D. Sueper et al. (2020). The ion fitting process for high resolution mass spectra in our analysis refers to the supporting information in Hildebrandt et al. (2011), since this is critical in the determination of the atomic ratio (O:C), and (H:C) of non-refractory organic material.

The operation of the time-of-fight chemical ionisation mass spectrometer with iodide ionisation coupled with a filter inlet for gases and aerosols (FIGAERO-I^--CIMS; Lopez-Hilfiker et al. (2014) was described in (Voliotis et al., 2021). Briefly, the particles were sampled by using PTFE filter (Zefluor, 2.0 μm pore size) at 1 sL min^{-1}, following by 15 mins thermal desorption (ambient temperature ramp to 200°C) with ultra-high purity N_2 as carrier gas. The instrument was run in negative-ion mode by producing I^- regent ion generated using polonium-210 ionisation source to ionize methyl iodide (CH_3I). The I^- reagent ions enter the ion molecule reaction region (IMR) with N_2 (ultra-high purity) as carrier gas. An "instrument background" procedure for the particle phase measurements was conducted in all the experiments for subtraction from the measurements. The FIGAERO-I^--CIMS data were processed by using the Tofware package in Igor Pro (version. 3.2.1., Wavemetrics©) (Stark et al., 2015) for peak identification. A data set of assigned molecular formula of detected compounds were produced, allowing subsequent determination of the H:C and O:C ratios.

2.3.2. Offline Measurement

Ultra-performance liquid chromatography ultra-high resolution mass spectrometry (Dionex 3000, Orbitrap QExactive, ThermoFisher Scientific) was employed for analysing the filter sampled particulate. Detail description of the instruments, experimental set-up and data processing methodology can be found on Shao et al., (2022) and Pereira et al. (2021). Briefly, the preparation of sample solution is as follows:

1) filter samples were dissolved in 4 ml LCMS optimal Methanol solvent followed by extraction in sonication (Fisher Scientific FB15051) after the sample solution had settle for 2 hours to ambient temperature;

2) 0.22 μm pore size PDVF filter (Fisher Scientific) and BD PlasticPak syringe (Fisher Scientific) were used for filtering the sample solution, subsequent by adding further 1 ml methanol on the dry filter for the second extraction of samples with the same method;
3) The extracted solution was evaporated to dryness using a solvent evaporator (Biotage) under specified temperature (36 ^{o}C) and pressure (8 mbar) conditions;
4) The dryness residual was re-dissolved in 1 ml solvent that consists of LCMS optimal grade water and methanol in a ratio of 9:1.

Once the sample solutions were prepared, they were injected into the LC-Orbitrap MS 0.3 ml/min with 2 μl volume by autosampler held at 4 ^{o}C. The mass spectrometer was mass calibrated using ESI positive and negative ion calibration solutions (Pierce, Thermo Scientific) prior to sample analysis. The sample solution was passed through a reverse-phase C18 column (Accucore, Thermo Fisher Scientific) 100 mm long × 2.1 mm wide and with 2.6 μm particle size, with temperature held at 40^{o}C. The mobile phase was composed of (a) LCMS optimal grade water with 0.1%(v/v) formic acid (Sigma Aldrich) and (b) methanol (LC-MS Optimal grade, Fisher Scientific). The elution gradient changed between (a) and (b), with starting 90% of (a) with a 1-minute post-injection hold, subsequent decline to 10 % over 26mins, back to initial mobile phase and re-equilibrium the column at total 30mins. In this instrument, electrospray ionization (ESI, 35 eV) was performed for both positive and negative mode to charge the organic compounds in a range of m/z 80 to m/z 750. High-energy collisional dissociation from tandem mass spectrometry (MS^2) was used to generate ion fragments for subsequent mass analyser detection. These ion fragments contributed to the fragmental ion spectrum, to inform the compound's structural characterisation and isomer identification. Analysis of extracted solvent (water: methanol = 9:1) and pre-conditioned bank filter was also performed with the same procedure for subtraction from the measurements to ensure exclusion of baseline noise and artefacts from sample preparation.
The mass chromatogram data was processed by an automated methodology for non-targeted composition of small molecules (Pereira et al. (2021). This approach guided the peak identification and offer molecular formula assignment for detected compounds enabling calculation of the signal weighted OSc, O:C and H:C for each system.

2.3.4. Estimation of average carbon oxidation state ($\overline{OSc}$)

For compounds that contain only carbon, hydrogen and oxygen (designated "CHO" compounds), the average $\overline{OSc}$ was straightforwardly determined using atomic ratios O:C and H:C via equation 1 ($\overline{OSc}$= 2*O/C-H/C) in analysis of data from all MS techniques.

For compounds that additionally contain nitrogen ("CHON" compounds), it is assumed that the nitrogen would exist as nitrate with $\overline{OS_N}$ = +5 if there are 3 or more oxygen atoms in the molecule and as nitrite with $\overline{OS_N}$ = +3 if there are fewer than 3 oxygen atoms. For CHON compounds, the $\overline{OSc}$ is therefore calculated using equation (2) where the H, C, O and N are determined from the FIGAERO-CIMS and LC-Orbitrap MS signal.

$$\overline{OSc} = 2 * \frac{O}{C} - \frac{H}{C} - (\overline{OS_N} * \frac{N}{C}) \qquad (2)$$

Where N:C corresponding to nitrogen-to-carbon ratios, $\overline{OS_N}$= 3 if nO < 3; or $\overline{OS_N}$ = 5 if nO ≥ 3. The signal-weighted average $\overline{OSc}$ determined by equation (2) will be presented in section 3 and referred to as "accounting for $\overline{OS_N}$". The HR-ToF-MS is unable to provide molecular information, but provides total particle ensemble C, H and O from the HR mass defect. However, retrieval of mass defect with sufficient accuracy to attribute the N-containing compounds at the resolution of the instrument is too challenging to be considered robust. The calculated $\overline{OSc}$ from AMS data uses only C, H and O and uses equation 1 (i.e. implicitly not accounting for organic nitrogen in any CHON compounds present). For comparison with the AMS-calculated $\overline{OSc}$, the average $\overline{OSc}$ for CHON compounds measured by the FIGAERO-CIMS and LC-Orbitrap MS technique has also been calculated ignoring the N and using equation (1), and this referred to as "not accounting for $\overline{OS_N}$". in section 3

Strictly, the estimation of average carbon oxidation state would account for the oxidation state of sulfur ($\overline{OSs}$) in any sulphur-containing compounds (CHOS and CHONS compounds) in the particles. Given the challenges associated with the quantification of S-containing compounds in FIGAERO-CIMS technique (Xu et al., 2016; D'ambro et al., 2019), this study does not consider the contribution of $\overline{OSs}$ in $\overline{OSc}$ calculation. It was also shown by Du et al. (2021) that the influence

of heteroatom S or NS on $\overline{OSc}$ calculation would be negligible as a result of their low fractional abundance the in LC-Orbitrap MS measurements (see also Shao et al. 2022).

3. Results

3.1. $\overline{OSc}$ of Particles in Single VOC system at various reactivity levels

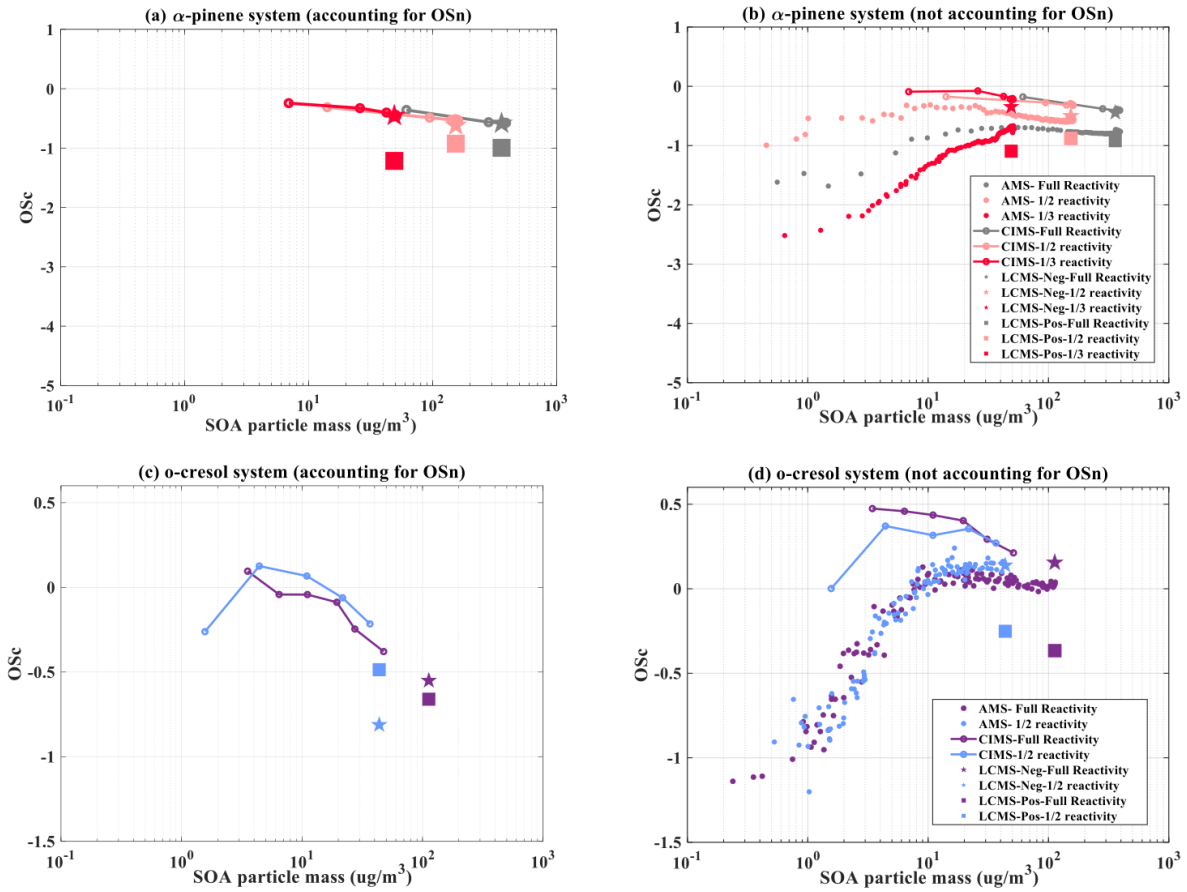

Figure 1: Average carbon oxidation state as function of SOA mass concentration of products detected by the HR-ToF-AMS, FIGAERO CIMS, and LC-Orbitrap MS (Negative Ionization Mode (Neg) and Positive ionization mode (Pos)) in the single precursor α-pinene and *o*-cresol systems. a) and c) accounting for $\overline{OS_N}$. b) and d) not accounting for $\overline{OS_N}$.

Figure 1 shows the average carbon oxidation state of SOA against SOA mass concentration from the single precursor VOC experiments (α-pinene (panel a and b) and *o*-cresol (panel c and d)) conducted at different initial reactivity level. Panels (a) and (c) show the average $\overline{OSc}$ of SOA

accounting for $\overline{OS_N}$, and (b) and (d) without accounting for $\overline{OS_N}$ of SOA detected by different MS techniques.

In the single α-pinene experiments, the average $\overline{OSc}$ accounting for $\overline{OS_N}$ as function of mass loading showed small differences between the three initial concentration experiments in FIGAERO-CIMS data ($\overline{OSc}$ in the ⅓ reactivity α-pinene system decreased from -0.24 to -0.46 across the 6-hour experimental period and was very slightly higher than in the ½ reactivity ($\overline{OSc}$ = -0.31 to -0.51) and full reactivity single α-pinene system ($\overline{OSc}$=-0.35 to -0.57) (Fig. 1a). Very comparably, the average $\overline{OSc}$ in the ⅓ reactivity α-pinene systems was -0.45 in negative ionization mode in LC-Orbitrap MS, which is slightly higher than ½ reactivity ($\overline{OSc}$ = -0.61) and full reactivity single system ($\overline{OSc}$ = -0.58). In contrast, in positive ionization mode, the average $\overline{OSc}$ in the ½ reactivity system is comparable to full reactivity system ($\overline{OSc}$ ≈-0.95) and is approximately 0.26 higher than $\overline{OSc}$ in ⅓ reactivity systems (Fig.1a).

Fig.1b shows the average $\overline{OSc}$ not accounting for $\overline{OS_N}$ against particle mass concentration enabling comparison against the AMS data in the α-pinene experiments. The HR-ToF-AMS derived average $\overline{OSc}$ showed significant differences between three initial reactivity experiments. Fig 1b shows that the AMS is able to produce $\overline{OSc}$ estimates at lower total particle mass than the other two techniques, during the rapid early growth phase of the experiments, before the first FIGAERO sample is collected. First, it is clear that the total SOA mass concentration trajectory is markedly different for the various initial α-pinene concentration (Fig.1b). Also, the ½ reactivity system has the highest average $\overline{OSc}$ from -0.99 to -0.31 compared to full reactivity ($\overline{OSc}$ = -1.68 to -0.39) and ⅓ reactivity ($\overline{OSc}$ = -2.51 to -0.66) system as function of SOA mass concentration. The average $\overline{OSc}$ of both full and ½ reactivity systems showed upward trend first, followed by reduction during SOA evolution, nevertheless, the average $\overline{OSc}$ was increasing continuously in ⅓ reactivity system and was still doing so at the end of the experiment. The FIGAERO-CIMS derived average $\overline{OSc}$ values in Fig.1b each show higher values than those from the HR-ToF-AMS. The FIGAERO-CIMS $\overline{OSc}$ is comparable between full reactivity ($\overline{OSc}$ =-0.17 to -0.40) and ½ reactivity systems ($\overline{OSc}$ =-0.17 to -0.32), which both are slightly lower than the ⅓ reactivity

system ($\overline{OSc}$ =-0.07 to -0.22), contrary to the AMS trend. The LC-Orbitrap MS derived average $\overline{OSc}$ not accounting for $\overline{OS_N}$ from the ⅓ reactivity experiment is slightly higher (-0.34) in negative ionization mode, and lower (-0.19) in positive ionization mode than that from the other two experiments, with the negative ionisation values all comparable to those from the FIGAERO-CIMS. As must be the case given the presence of N in the spectra, the average $\overline{OSc}$ accounting for $\overline{OS_N}$ is lower value than when not accounting for $\overline{OS_N}$ derived from both FIGAERO-CIMS and LC-Orbitrap MS (Fig.1a and 1b).

For single precursor *o*-cresol experiments, the FIGAERO-CIMS-derived average $\overline{OSc}$ accounting for $\overline{OS_N}$ in both full and ½ reactivity experiments reduced with increasing SOA mass concentration with the lower concentration experiment having a higher $\overline{OSc}$ (0.12 to -0.26 compared to 0.09 to -0.37), as shown in Fig.1c. The higher concentration experiment showed a higher LC-Orbitrap MS -derived $\overline{OSc}$ (-0.55) than the lower concentration experiment (-0.81) in negative ionization mode, but with an opposite trend in positive ionization mode (Fig.1c).

When not accounting for $\overline{OS_N}$, the HR-ToF-MS-derived $\overline{OSc}$ shows a similar increasing trend with SOA particle mass at each initial concentration, with comparable values ranging from -1.20 to 0.24 as shown in Fig 1d), with the only difference being that the full reactivity system showed slight decrease in $\overline{OSc}$ after SOA mass concentration reached its peak at around 10 μgm-^{3}.

As with the α-pinene experiments, the FIGAERO-CIMS-derived average $\overline{OSc}$ were comparable between initial concentration *o*-cresol experiments and higher than the HR-ToF-AMS-derived $\overline{OSc}$. The $\overline{OSc}$ reduced with increasing particulate mass concentration from (~0.4 to 0). Negative ionization mode average $\overline{OSc}$ from LC-Orbitrap MS measurements at both initial concentrations were comparable at ~0.14 (Fig.1d). In positive mode, the average $\overline{OSc}$ at the higher concentration was -0.36, 0.11 lower than the lower concentration value.

It should be noted that the values of the FIGAERO-CIMS average $\overline{OSc}$ were higher than the AMS values in experiments with both single precursors, as were those from the negative mode LC-Orbitrap MS value, but the positive mode LC-Orbitrap MS values were lower. This is consistent with the AMS being able to detect all material that would be seen by both ionization modes of the

offline filter analysis, but the FIGAERO only being sensitive to an oxygenated subset that can be ionized by I^- chemical ionization.

The SOA particle mass yield (and hence particle mass loading) in the single VOC isoprene experiment was too low to provide insightful measurements of the evolution in composition (see Voliotis et al., 2021 and Voliotis et al., 2022).

3.2. $\overline{OSc}$, O:C and H:C ratios of SOA Particles in mixtures accounting for $\overline{OS_N}$

This section compares the average carbon oxidation state and atomic ratios of particles derived from FIGAERO-CIMS and LC-Orbitrap MS data from mixed precursors systems with reference to their corresponding single precursors systems. The average carbon oxidation state presented in this section accounts for the nitrogen present in all systems (though not the sulphur) see section 2.4, and excludes AMS data, owing to the challenges with accounting for $\overline{OS_N}$.

(a) α-pinene & isoprene binary system

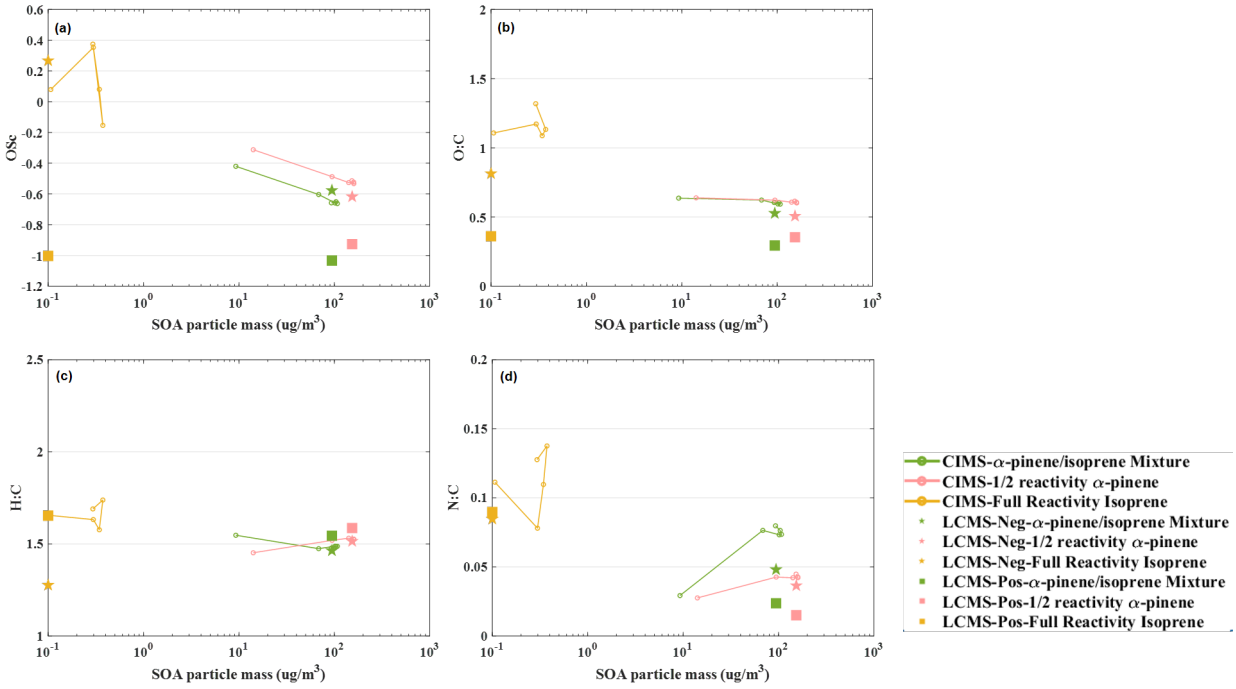

Figure 2: Evolution of SOA particle composition evolution in terms of a) average carbon oxidation state ($\overline{OSc}$), b) O:C ,c) H:C and d) N:C atomic ratios as function of SOA mass concentration from FIGAERO-CIMS and LC-Obitrap-MS measurements (-ve Ionization Mode (Neg) and +ve

ionization mode (Pos)) in binary α-pinene /isoprene mixture, ½ reactivity individual α-pinene and full reactivity individual isoprene experiments.

Figure 2 shows the atomic ratios (O:C, H:C and N:C) and average carbon oxidation state $\overline{OSc}$ of the evolving SOA particles in binary α-pinene/isoprene mixture, individual ½ reactivity α-pinene and full reactivity isoprene experiments (noting the unavailability of data for lower concentration isoprene experiments). As might be expected from its very low (near negligible) mass contribution, whilst the particle produced in the isoprene system appear quite highly oxidized in comparison to those from α-pinene, the isoprene products appear to have a minor effect on the carbon oxidation state and atomic ratios in binary α-pinene / isoprene experiments.

Panel a) shows the FIGAERO-CIMS average $\overline{OSc}$ in ½ reactivity α-pinene experiments have a similar declining trend (from -0.31 to -0.51 through the experiment) as that in the binary mixture (from -0.42 to -0.65), though being slightly more oxidised. As shown in panels b) and c), the mixture and individual α-pinene experiments showed comparable O:C (~0.63 and 0.60) and H:C ratios (H:C ~ 1.45 to 1.55). The N:C ratios increased as function of SOA mass concentration in both experiments, with more N in the mixture (N:C increasing from 0.03 to 0.08) than in the individual α-pinene experiment (N:C = 0.03 to 0.04) (panel d)).

The LC-Orbitrap MS $\overline{OSc}$ and element atomic ratios (O:C, H:C and N:C) are comparable in negative ionization modes in the mixture and individual α-pinene experiment (and similar to the FIGAERO-CIMS average $\overline{OSc}$. $\overline{OSc}$ in the individual α-pinene experiment in positive ionization mode is slightly (0.1) higher (-0.92) than in the mixture (Fig.2a), reflecting a higher O:C and lower N:C. The values from the last FIGAERO-CIMS measurements are similar to those from the LC-Orbitrap MS negative ionization measurements, but higher than those from positive ionization mode.

(b) o-cresol & isoprene binary system

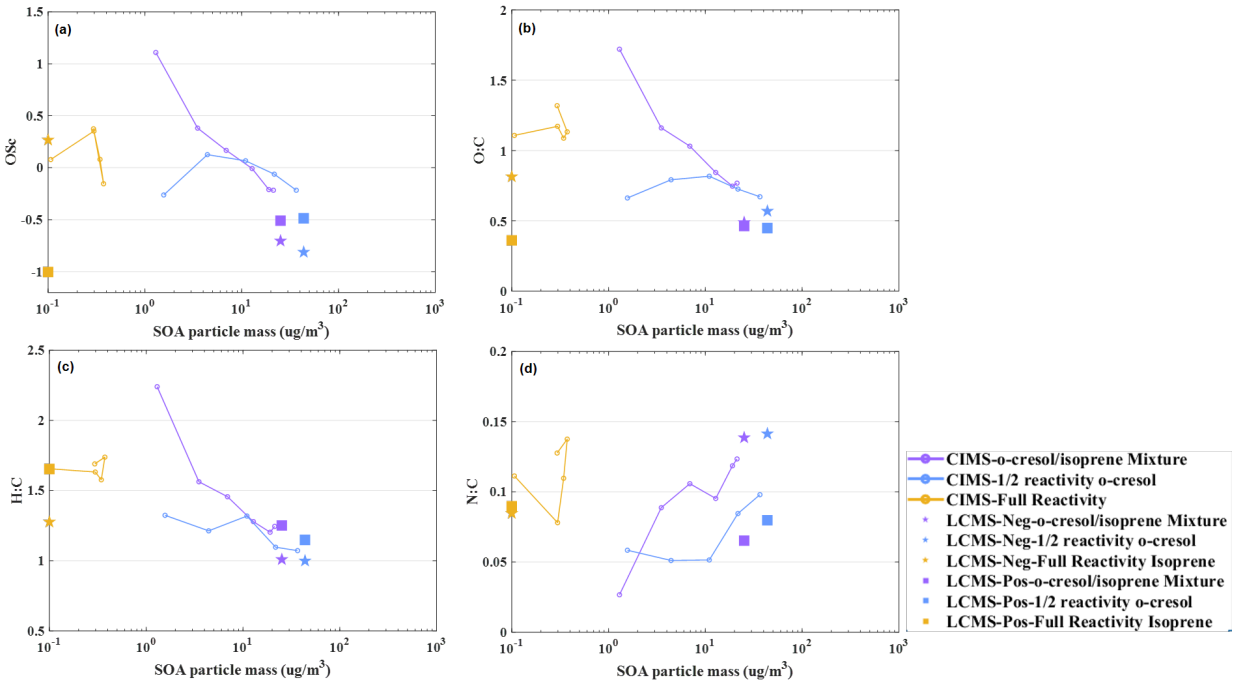

Figure 3: Evolution of SOA particle composition evolution in terms of a) average carbon oxidation state ($\overline{OSc}$), b) O:C ,c) H:C and d) N:C atomic ratios as function of SOA mass concentration from FIGAERO-CIMS and LC-Obitrap-MS measurements (-ve Ionization Mode (Neg) and +ve ionization mode (Pos)) in binary *o*-cresol /isoprene mixture, ½ reactivity individual *o*-cresol and full reactivity individual isoprene experiments.

Figure 3 shows the $\overline{OSc}$, O:C, H:C and N:C ratio of SOA particles derived from the FIGAERO-CIMS and LC-Orbitrap MS in the binary o-cresol / isoprene mixture, individual ½ reactivity *o*-cresol and full reactivity isoprene experiments respectively. Again, owing to their minor mass contribution in the individual system, it might be expected that the $\overline{OSc}$, O:C, H:C and N:C ratio of SOA products from isoprene make a minor contribution in the binary *o*-cresol / isoprene system. Nevertheless, there are some significant differences between the individual VOC and mixture experiments.

The FIGAERO-CIMS $\overline{OSc}$ in the individual *o*-cresol system and the mixture both reduce with increasing particle mass, beyond 3µg/m^3 (though the compounds in the particles are initially significantly more oxidised in the experiment on the mixture, so $\overline{OSc}$ is initially higher, driven by a high O:C). The FIGAERO-CIMS $\overline{OSc}$ in the mixture decreased from 0.38 at 3µg/m^3 mass

concentration to -0.21, while the $\overline{OSc}$ in the individual o-cresol experiment showed a more modest decrease from 0.12 to -0.26 (Fig.3a). The FIGAERO-CIMS O:C and H:C in the mixture are higher than in the individual *o*-cresol experiment (Fig.3b and 3c). In particular the O:C behaved differently between the systems, in the mixture decreasing from 1.72 to 0.76 and in the individual *o*-cresol system, slightly increasing from an initial value of around ~0.66 to a peak of 0.78 then falling towards the end of the experiment with increasing SOA mass concentration (Fig.3b). The H:C ratios simultaneously showed significantly decrease from 2.24 to 1.24 in the mixture experiment with a much smaller decrease from 1.32 to 1.09 in the individual *o*-cresol system (Fig.3c). It should be noted that this discrepancy in $\overline{OSc}$ between the systems is not seen in the AMS data, which monotonically increased with SOA mass in the individual VOC and mixture experiments as shown in Figure 6 c), though of course this does not account for any nitrogen in the particles. Figure 3 d) shows that the FIGAERO-CIMS N:C ratio in both experiments increased with mass. This was more pronounced (from 0.02 to 0.12) in the mixture than in the individual o-cresol experiment (0.05 to 0.1).

$\overline{OSc}$ and O:C ratio from positive ionization LC-Orbitrap MS in the mixture and individual *o*-cresol experiments were of a comparable magnitude (roughly -0.5 and 0.45 respectively in both systems) though the H:C ratio is slightly higher in the mixture and N:C slightly lower (Fig.3c and 3d). From negative ionization measurements, Fig3c and 3d show that the mixture and individual *o*-cresol oxidation produces similar H:C and N:C ratios. Particles formed in the individual o-cresol experiment are marginally less oxidised ($\overline{OSc}$ = -0.81), than in the mixture experiment (-0.70), though overall the low degree of oxidation is driven by the high organic N-content of the particles.

(c) α-pinene & o-cresol Binary System

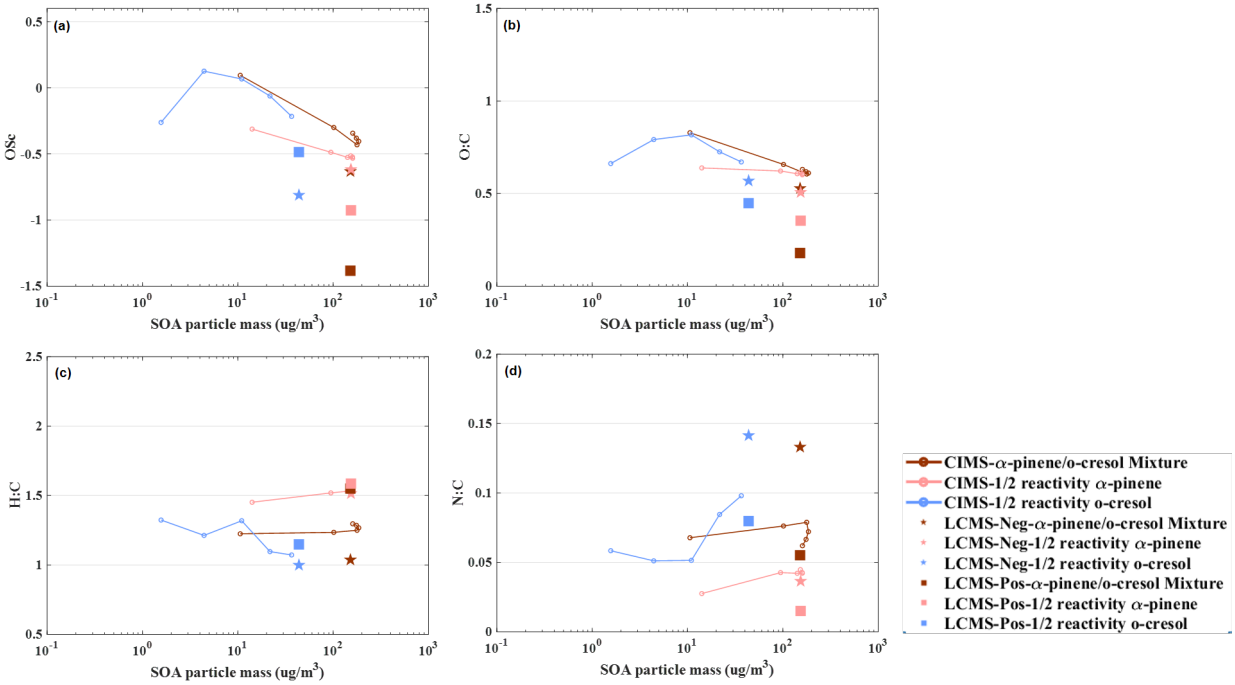

Figure 4: Evolution of SOA particle composition evolution in terms of a) average carbon oxidation state ($\overline{OSc}$), b) O:C ,c) H:C and d) N:C atomic ratios as function of SOA mass concentration from FIGAERO-CIMS and LC-Obitrap-MS measurements (-ve Ionization Mode (Neg) and +ve ionization mode (Pos)) in binary α-pinene / o-cresol mixture, ½ reactivity individual α-pinene and ½ reactivity individual *o*-cresol experiments.

Figure 4 shows the changes in $\overline{OSc}$, and atomic ratios (O:C, H:C and N:C) of SOA particles derived from FIGAERO-CIMS and LC-Orbitrap MS in the binary α-pinene / *o*-cresol mixture and the individual ½ reactivity precursor experiments. Panel a) shows that FIGAERO-CIMS average $\overline{OSc}$ decreases with SOA mass concentration above 3μg/m^3 mass concentration in all experiments, though the $\overline{OSc}$ is initially lower in the *o*-cresol experiment, driven by the low O:C. $\overline{OSc}$ in the mixture drop from 0.09 to -0.34 with increasing mass; a greater decrease than in the individual o-cresol ($\overline{OSc}$ = 0.12 to -0.26) and α-pinene ($\overline{OSc}$ = -0.31 to -0.51) experiments – overall the gradient in the mixture experiment is similar to the α-pinene experiment, but with an increase in the average degree of oxidation, though somewhat raised towards the *o*-cresol average $\overline{OSc}$ by an increase in O:C . The O:C, H:C and N:C in the mixture experiments exhibit similar trends to the α-pinene experiment (Fig.4b.4c and 4d) with absolute values in the mixture midway

between the α-pinene and *o*-cresol experiments (O:C falling from 0.82 to 0.63, N:C rising from 0.02 to 0.12, H:C modestly from 1.22 to 1.29).

The LC-Orbitrap MS negative ionization average $\overline{OSc}$ and O:C ratio for the mixture were -0.63 and 0.52 respectively, comparable to those in the α-pinene experiment. Positive ionization mixture $\overline{OSc}$ and O:C ratio values were both lower than the two single precursor values (Fig.4a and 4b). H:C and N:C ratios of the mixture in positive ionization mode were similar to the *o*-cresol experiment (H:C=1.55, and N:C = 0.55),

(d) the ternary system

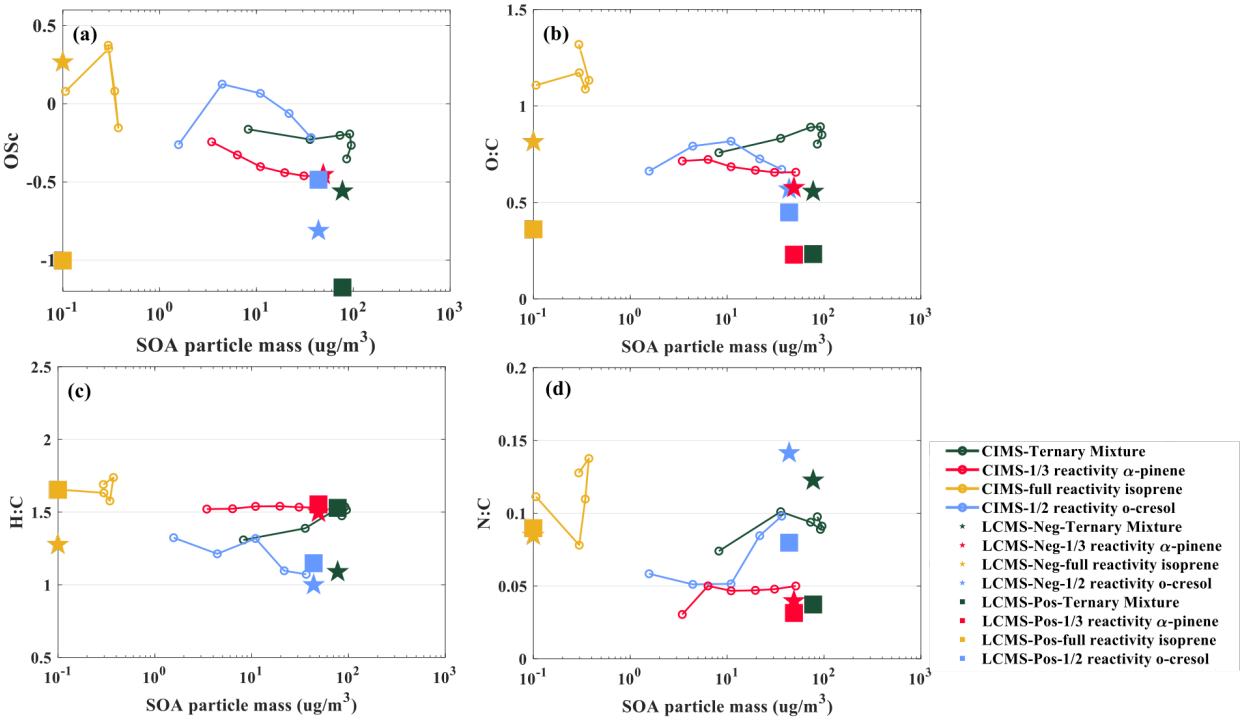

Figure 5: Evolution of SOA particle composition evolution in terms of a) average carbon oxidation state ($\overline{OSc}$), b) O:C ,c) H:C and d) N:C atomic ratios as function of SOA mass concentration from FIGAERO-CIMS and LC-Obitrap-MS measurements (-ve Ionization Mode (Neg) and +ve ionization mode (Pos)) in ternary α-pinene / *o*-cresol / isoprene mixture, ⅓ reactivity individual α-pinene and ½ reactivity individual *o*-cresol experiments.

Figure 5 shows the change in average atomic ratios (O:C, H:C and N:C) and $\overline{OSc}$ during SOA evolution in the ternary mixture experiment, along with ⅓ reactivity α-pinene, and ½ reactivity o-cresol experiments from FIGAERO-CIMS and LC-Orbitrap MS measurements. The ⅓ reactivity

o-cresol data were not available owing to instrumental failure. Fig.1c shows that the $\overline{OSc}$ and atomic ratios are comparable between full reactivity and ½ reactivity *o*-cresol experiments and it is plausible to expect similar molecular concentrations and hence aggregate properties in particles formed in the ½ and ⅓ reactivity individual *o*-cresol experiments.

Panel a) shows FIGAREO-CIMS average $\overline{OSc}$ in the ternary mixture (decreasing in degree of oxidation from -0.16 to -0.35) is between that in the α-pinene and *o*-cresol experiments, suggesting an influence from both precursors. Similarly, the mixture exhibits an average H:C ratio between the α-pinene *o*-cresol system, increasing from 1.30 to 1.47 (Fig.5c). The O:C and N:C ratios in the ternary mixture increased with mass (O/C: 0.75 to 0.80, N/C: 0.07 to 0.09) and were higher than those in the α-pinene and *o*-cresol experiments (Fig.5b and 5d).

LC-Orbitrap MS average $\overline{OSc}$ and O:C ratios were similar to those in the α-pinene experiments in both ionization modes. However, the H:C and N:C ratio in the ternary mixture (H/C=1.52, N/C=0.03) was comparable to the α-pinene experiment in positive ionization modes. (Fig.5c and 5d), but closer to the *o*-cresol in negative.

3.3. Additional insight into $\overline{OSc}$ including AMS data

This section presents a comparison of the average carbon oxidation state of SOA particles detected by HR-ToF-AMS, FIGAERO-CIMS and LC-Orbitrap MS techniques from mixed precursors systems and their corresponding single precursors systems. Owing to the inability to reliably discern the N:C using the AMS, the average carbon oxidation state presented in this section does not account for $\overline{OS_N}$ calculated from measurements from any of the instruments. This enables comparison of the compositional properties as determined by the three instruments but not directly comparable to those in section 3.2 and with $\overline{OSc}$ obviously always higher.

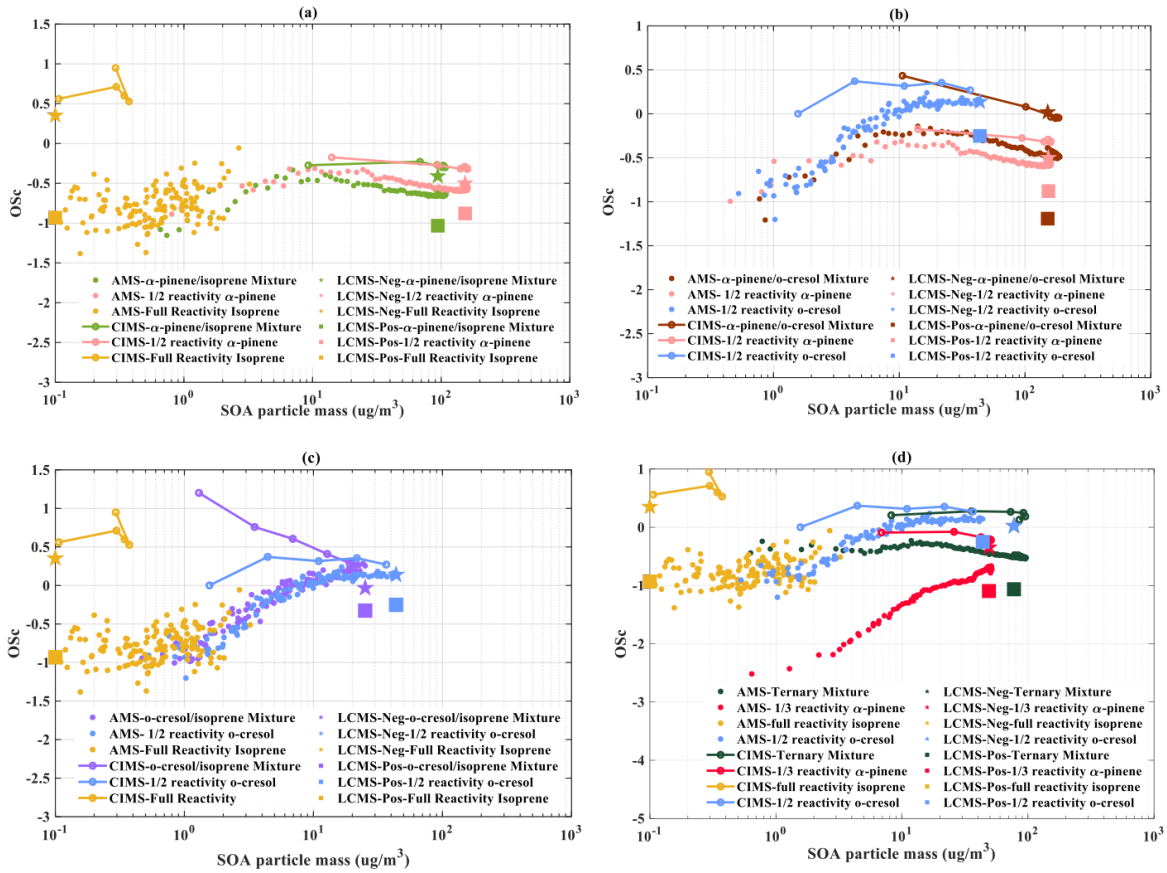

Figure 6: $\overline{OSc}$ plotted as a function of SOA particle mass concentration in mixed precursor systems, a) binary α-pinene /isoprene system; b) binary α-pinene /cresol system; c) isoprene/o-cresol system, d) Ternary mixture precursor system from HR-ToF-AMS, FIGAERO-CIMS and LC-Orbitrap-MS measurements (Negative Ionization Mode (Neg) and Positive ionization mode (Pos)).

Fig.6a suggests that the average $\overline{OSc}$ of isoprene-derived compounds has only a modest influence on the carbon oxidation state in the binary α-pinene/isoprene experiment when calculated from all MS measurements. HR-ToF-AMS derived OSc in the mixture is comparable to the individual α-pinene experiment at all particle mass concentrations and lower than the isoprene experiment (when only low particle mass was formed). Both systems exhibit an increase with SOA particle mass concentration up to ~10 μgm^{-3}, followed by reduction in the degree of oxidation as more mass was formed. The absolute values in the mixture (-0.33 to -1.15) were slightly lower than the individual α-pinene values (-0.31 to -0.99). The FIGAERO-CIMS $\overline{OSc}$ in the mixture were also close to the α-pinene in trend and absolute values (-0.26 to -0.27) as were the LC-Orbitrap MS

average $\overline{OSc}$ in both ionization modes with the negative ionization value close to those from the final HR-ToF-AMS measurement and slightly lower than from the FIGAERO-CIMS.
HR-ToF-AMS measurements in Fig.6b show $\overline{OSc}$ of SOA formed in the *o*-cresol / α-pinene binary mixture falls between that of the SOA in the individual VOC systems, indicating influence of oxidation products from both precursors. $\overline{OSc}$ in the mixture initially increases (from -1.13 to -0.30) before falling to -0.5 once the mass concentration had reached 10.8 μgm^{-3}. A similar trend was seen in the ½ reactivity α-pinene experiment at a lower $\overline{OSc}$ value. The FIGAERO-CIMS $\overline{OSc}$ in all systems was higher than the HR-ToF-AMS $\overline{OSc}$, in the mixture ($\overline{OSc}$ = 0.43 to -0.03) and α-pinene experiments ($\overline{OSc}$ = -0.17 to -0.29) following the same reducing trend, whilst the *o*-cresol $\overline{OSc}$ increased to a plateau in both AMS and CIMS analyses. The LC-Orbitrap MS $\overline{OSc}$ of SOA in the mixture was -1.19 in positive ionization mode, lower than both the α-pinene ($\overline{OSc}$ = -0.87), and *o*-cresol ($\overline{OSc}$ =-0.25) experiments. Negative mode $\overline{OSc}$ in the mixture was 0.02; 0.11 lower than for *o*-cresol and 0.52 higher than for α-pinene (Fig.6b).

Fig.6c shows that the average $\overline{OSc}$ of isoprene-derived compounds also only exert a modest influence on that of the binary *o*-cresol/isoprene binary mixture in measurements from all MS techniques. The HR-ToF-AMS measured $\overline{OSc}$ in the mixture is comparable to that in the ½ reactivity *o*-cresol experiment, both increasing from -1.2 to 0.3 at ~15μgm^{-3} thereafter slightly increasing in the mixture (Fig.6c). The FIGAERO-CIMS $\overline{OSc}$ in the mixture decreased from 1.2 to 0.2 with mass concentration increasing from 1.3 μgm^{-3} to 21.2μgm^{-3}, whilst the single VOC *o*-cresol $\overline{OSc}$ increased from 0 to 0.27 across the same range of mass concentration, all values being higher than the HR-ToF-AMS $\overline{OSc}$ until the highest mass concentrations. The $\overline{OSc}$ in the mixture is comparable though slightly lower than that in the single VOC *o*-cresol system after 6-hours in both ionization mode of LC-Orbitrap MS measurements.

Fig.6d the average $\overline{OSc}$ in the ternary mixture from HR-ToF-AMS increased marginally from -0.44 to a maximum of -0.22 with a mass concentration of 11.84 μgm^{-3}, followed by a gradual decrease to -0.52. The single VOC ⅓ reactivity α-pinene experiment showed a strong increase in $\overline{OSc}$ from -2.51 to -0.66 and the ½ reactivity *o*-cresol experiment more gradually increasing from -1.2 to a plateau of 0.3 at ~15μgm^{-3}. The FIGAERO-CIMS average $\overline{OSc}$ were more constant with

particle mass concentration and always higher than the HR-ToF-AMS values. The oxidation state in the ternary mixture (ranging from 0.13 to 0.2) sat between that in the individual α-pinene and *o*-cresol values, though closer to the latter (which ranged from 0 to 0.2). Negative ionization mode LC-Orbitrap MS measurements showed the average ternary system $\overline{OSc}$ to be similar to that in the *o*-cresol experiment, but positive mode was more comparable to that in the α-pinene system.

4. Discussion

4.1. The application of multiple mass spectrometric techniques to the average oxidation state of carbon in SOA particles

In this study, the average carbon oxidation state of SOA from different precursor systems was estimated by three mass spectrometry techniques. The combination of online and offline mass spectrometric techniques has not been widely employed in estimating average $\overline{\mathrm{OSc}}$ of complex organic mixtures, and never previously in SOA components from the oxidation of mixed precursors in atmospheric simulation chamber studies. Each technique has its own strengths and limitations. The electrospray ionisation method used in the LC-Orbitrap MS extraction can provide exact elemental ratios of individual compounds within organic mixtures using small sample volume. The FIGAERO-CIMS can provide molecular information for hundreds of compounds at hourly timescale throughout a chamber experiment, with the low instrument backgrounds enabling detection limits in the picogram m^{-3} range for particle phase organic species (Lopez-Hilfiker et al., 2014). The average $\overline{\mathrm{OSc}}$ from FIGAERO-CIMS was derived from 6 measurements corresponding to the six FIGAERO desorption cycles phases throughout each experiment whilst the LC-Orbitrap MS values were derived from analyses of filters taken at the end of each experiment. Both the LC-Orbitrap MS and FIGAREO-CIMS techniques are selective ionization technique, with different response factor toward widely various components that may bias the average $\overline{\mathrm{OSc}}$ estimation. For instance, the negative ionisation mode in LC-Orbitrap MS technique exhibits high sensitivity towards nitro-aromatic compounds (Shao et al., 2022). Low-volatility molecules may experience thermal decomposition in the FIGAERO-CIMS leading to fragmentation, influencing the average $\overline{\mathrm{OSc}}$ estimation (Du et al., 2021). The HR-ToF-AMS allows entire ensemble of SOA particles to be detected, fully fragmenting the flash vapourised particles by electron impact ionisation and measuring the elemental ratios in real time (Nash et al., 2006). The accuracy of the retrieved

elemental ratios is, however, affected by uncertain empirical corrections in the analysis. Probably more importantly, the average $\overline{OSc}$ estimation obtained from our HR-ToF-AMS measurement cannot account for $\overline{OS_N}$ given the limited resolution of the instrument calibrations. Farmer et al. (2010) reported the potential for overestimation of N and underestimation of O in the ambient measurements by HR-ToF-AMS, highlighting the need for high-quality m/z calibrations and peak width/shape parameters when attempting to quantify nitrogen-containing compounds in AMS spectra.

There are significant differences between carbon oxidation state (not accounting for $\overline{OS_N}$) derived from the FIGAERO-CIMS measurements and those from HR-ToF-AMS under the same SOA mass concentration in all single (Fig.1b and 1d) and mixed precursor systems (Fig.6a, 6b, 6c,6d) (Fig.1). The carbon oxidation state in FIGAERO-CIMS estimation is substantially higher than the HR-ToF-AMS measurement. The FIGAERO-CIMS employed in this work used iodine as reagent ion, with an inherently higher sensitivity toward to the oxygenated organic compounds, biasing the measurements towards oxidized organic species (Lee et al., 2014). Moreover, the possibility of forming thermal decomposition fragments from the larger organic molecules during the filter thermal desorption in the FIGAERO-CIMS that can potentially result in higher $\overline{OSc}$ than their parent molecules. The average carbon oxidation state from FIGAERO-CIMS will depend on a subset of compounds biased towards higher oxidation state and consequently will be higher than that derived from HR-ToF-AMS and LC-Orbitrap MS measurements. On the other hand, the average $\overline{OSc}$ in the binary o-cresol/isoprene precursor system was rarely high at the early stage of experiment (Fig.6c), which may be due to the FIGAREO filter loading being low (less than 4μgm^{-3}) at the start of the experiment. The magnitude of average $\overline{OSc}$ obtained from HR-ToF-AMS measurement was found in between the two ionization modes of LC-Orbitrap MS analysis in the single α-pinene system (Fig 1b), and binary α-pinene /isoprene precursors system (Fig.6a). This is likely due to the ionization modes in the LC-Orbitrap MS having various sensitivities toward different organic compounds. The average $\overline{OSc}$ of SOA particles in negative ionization mode shared a similar magnitude with the HR-ToF-AMS measurement in single o-cresol precursors systems (Fig.1d) although previous work in Shao et al., (2022) observed the negative ionization mode exhibits high sensitivity towards certain nitrogen-containing compounds.

There is a substantial difference of average carbon oxidation state in the single VOC isoprene experiments (Fig.6a and 6c), likely resulting from potential artefacts in the instruments and filter background since there was an insufficient amount of SOA particle mass produced.

As stated, the average $\overline{\mathrm{OSc}}$ comparisons with the HR-ToF-AMS discussed above do not account for the oxidation state of nitrogen ($\overline{\mathrm{OS_N}}$) and sulfur ($\overline{\mathrm{OSs}}$) in their calculation. Organosulfate (CHONS and CHOS) and organonitrate (CHON and CHONS) have been reported in chamber experiments with NOx and ammonium sulphate (Surratt et al., 2007; Surratt et al., 2008; Bruns et al., 2010; Fry et al., 2009). The heteroatom-containing groups will clearly impact on the derived $\overline{\mathrm{OSc}}$ which should therefore be determined from 2O/C-H/C-xN/C-yS/C, where x and y refer to the oxidation states of nitrogen ($\overline{\mathrm{OS_N}}$) and sulphur ($\overline{\mathrm{OSs}}$) (Kroll et al., 2011). The uncertainty in HR-ToF-AMS $\overline{\mathrm{OSc}}$ determination associated with S-containing groups is likely to be minimal since the S atom in weakly-bound species, such as organosulphates, tend not to be measured using thermal methods. This is not the case with nitrogen-containing compounds which may affect $\overline{\mathrm{OSc}}$ determination, but unambiguous attribution of N is challenging at the limited resolution of the technique.

The $\overline{\mathrm{OS_N}}$ of CHON compounds in FIGAERO-CIMS measurements clearly influenced the signal weighted average $\overline{\mathrm{OSc}}$, consequently reducing the average $\overline{\mathrm{OSc}}$. The LC-Orbitrap MS derived $\overline{\mathrm{OSc}}$ is similarly influenced, particularly in o-cresol containing systems in negative ionization mode (owing to an enhanced sensitivity to specific CHON species, dominated by nitro-aromatics as reported in Shao et al., 2022) and the average $\overline{\mathrm{OSc}}$ is significantly lower when accounting for $\overline{\mathrm{OS_N}}$)."

4.2. Comparison of SOA average Carbon Oxidation State in various Precursors' Concentration

The calculated carbon oxidation state of particles in the single precursor systems that generated significant mass (α-pinene and *o*-cresol) with their initial concentrationwere compared. The initial "full" isoreactive (accounting for their reactivity towards OH) concentration of the α-pinene and o-cresol were 309 and 400 ppb. Experiments with half- and third- of these initial concentrations

were also conducted to enable total initial isoreactivity in the binary and ternary mixtures. Further details can be found in Voliotis et al. (2022)

FIGAERO-CIMS average $\overline{OSc}$ from the α-pinene experiments accounting and not accounting for $\overline{OS_N}$ is shown in Fig.1a and 1b, showing comparable values at all mass concentrations. In the HR-ToF-AMS the initial ½ reactivity α-pinene experiment showed a higher average $\overline{OSc}$ than full initial reactivity α-pinene experiment, which was in turn higher than that from the ⅓ reactivity experiment (Fig.1b). It should be noted that the NOx concentration was reduced along with reduction of VOC initial concentration in half-reactivity experiment in order to maintain a comparable VOC/NOx ratio across the system. This will influence the oxidant conditions, though it is unclear precisely why the oxidation state is so divergent at the lower particle mass concentrations with in initial VOC concentration. α-pinene also has appreciable reactivity toward O_3 (Atkinson et al., 2004) and the O_3 is slightly higher for all SOA mass concentrations in the ½ reactivity α-pinene experiment compared with the full reactivity α-pinene experiment (Fig.S1). Ozonolysis of α-pinene efficiently yields low volatile highly oxygenated organic molecules (HOMs) by autoxidation on sub-second timescales (Molteni et al., 2019; Pullinen et al., 2020; Iyer et al., 2021), which may play a role in elevating $\overline{OSc}$ in the ½ reactivity α-pinene experiment.}

Unlike the α-pinene precursor, the average $\overline{OSc}$ in the single precursor *o*-cresol system seems independent of initial precursors concentration in both HR-TOF-AMS and FIGAERO-CIMS measurement, whether or not $\overline{OS_N}$ is considered (Fig.1b and 1d). The degrees of oxidation of organic species appear comparable irrespective of initial *o*-cresol and NOx concentration. This might be due to the negligible reactivity of o-cresol towards O_3 (Atkinson, 2004). It should be noted that there is difficulty in reporting the O_3 direct measurement by UV absorption in the single precursor *o*-cresol experiment in this study owing to the UV absorption by *o*-cresol and its oxidation products.

4.3. Comparison of SOA average Carbon Oxidation State accounting for $\overline{OS_N}$ in mixtures

The average $\overline{OSc}$ taking into account the $\overline{OS_N}$, H:C, O:C and N:C ratios in the mixtures (three binary and the ternary precursor system) and the corresponding single precursor systems were compared using the FIGAERO-CIMS and LC-Orbitrap MS data.

(a) α-pinene /isoprene binary mixture system

The ½ reactivity single precursor α-pinene experiment was used as reference experiment for binary mixtures containing α-pinene, since it made a half contribution to the VOC reactivity. Average $\overline{OSc}$ in the α-pinene /isoprene mixture system was comparable to that in the ½ reactivity α-pinene experiments, whilst the isoprene has no discernable influence on the mixture oxidation state, suggesting that the dominant control by α-pinene oxidation products. This is unsurprising given the high established α-pinene particle mass yield from OH oxidation in the presence of seed particles (Ahlberg et al., 2017; Eddingsaas et al., 2012; Henry et al., 2012). Isoprene is known to form C_4 and C_5 compounds with high vapour pressure (e.g. methacrolein (C4) and C5-hydroxycarbonyls) on OH oxidation, with low potential to form SOA particle mass (Wennberg et al., 2018; Stroud et al., 2001; Carlton et al., 2009).

The difference in N:C ratios between ½ reactivity α-pinene experiment and the binary mixture contributed to the difference in average $\overline{OSc}$ and the H:C and O:C ratios were similar (Fig.2b and 2c), with N:C increasing with SOA particle mass in both systems. This suggests an increasing contribution of CHON compounds in both systems, with an increased contribution in the presence of isoprene.

(b) o-cresol/Isoprene binary mixture system

The FIGAERO-CIMS $\overline{OSc}$ in the binary *o*-cresol/isoprene mixture shared a broadly similar trend with, though at a generally higher magnitude than, the ½ reactivity single precursor *o*-cresol system apart from the measurement in the first half-hour of the experiment, with little similarity to the isoprene experiment $\overline{OSc}$ (Fig.3a), suggesting a strong dependence on the *o*-cresol oxidation products. The difference of average $\overline{OSc}$ between two systems are controlled by all three atomic

ratios, H:C, O:C and N:C. The observation of difference in average O:C, H:C and N:C ratios between two systems are little, that likely a consequence of the cross interacts between the two precursors oxidized products. Isoprene will scavenge OH scavenged when mixed with another VOCs (Jaoui et al., 2008; Ahlberg et al., 2017). The presence of isoprene likely forms high volatility products during oxidation, that could partition to particulate matters resultant in a higher average O:C ratio in products of binary o-cresol/isoprene system. The study of Shao et al (2022) reports interactions during oxidation in mixtures leading to leading to compounds uniquely found in mixtures, that are not found in the oxidation of the individual precursors.

(c) α-pinene /o-cresol binary mixture system

The average FIGAERO-CIMS $\overline{OSc}$ in the binary α-pinene / *o*-cresol system exhibited a similar trend to that in the ½ reactivity α-pinene experiment at a higher magnitude, more comparable to that of the ½ reactivity *o*-cresol experiment (Fig.4a). Both α-pinene and *o*-cresol contribute non-negligibly to the average $\overline{OSc}$ in the mixture. All average O:C, H:C, N:C ratios contributed to the difference in $\overline{OSc}$ (Fig.4b,4c and 4d). Once significant particle mass had been produced, the O:C reduced with SOA particle mass, and the H:C ratios reaches a plateau at a mass concentration of 10μgm^{-3} in binary precursor system and α-pinene system, which implying there is oxygen atoms loss process (e.g. RO_2+R'O_2 termination reactions) during SOA formation. This reaction is likely occurred in α-pinene driven SOA and/or interactions between oxygenated products formed from o-cresol and α-pinene individual precursor leading to form new products that contribute to lower H:C ratios and higher O:C ratios in binary precursors system compared to single α-pinene system. Voliotis et al. (2021) reported an abundance of products uniquely found in the α-pinene /o-cresol mixture, and the majority of these unique-to-mixture compounds with nC=5-10 and nC>10 was obtained from the FIGAERO-CIMS measurement. LC-Orbitrap MS measurements reported in Shao et al., (2022) also showed that high carbon number compounds contribute significantly in positive ionization mode, likely the cross-products from α-pinene and o-cresol oxidation in either gas or particle-phase.

(d) The ternary mixture

The FIGAERO-CIMS average $\overline{OSc}$ in the ternary mixture do not obviously follow a similar trend to either the single VOC ⅓ reactivity α-pinene or ½ reactivity o-cresol systems (Fig.5a). Meanwhile, the $\overline{OSc}$ in the ternary mixture was higher than the in the α-pinene, but lower than o-cresol experiment, and the average $\overline{OSc}$ is likely not controlled by any single precursor. The trends in average atomic ratios (O:C, H:C and N:C) also have little similarity to those in the individual systems (Fig.5b,5c and 5d), implying contributions from each of them. Oxidation in the the ternary mixture involves multiple and complex reactions, and may include cross-interaction between radicals from the three individual precursors, or alterations in the oxidation pathways of the individual precursors. The LC-Orbitrap MS measurements in both ionisation modes further support the contention that each VOC contributes to the chemical composition in the ternary mixture, influencing the average carbon oxidation state, in addition to products uniquely found in the mixture (Fig.S2).

4.4. Comparison of average Carbon Oxidation State ignoring $\overline{OS_N}$ in the mixtures

This section assesses the influence of individual precursors on $\overline{OSc}$ in mixtures without accounting for $\overline{OS_N}$ using HR-ToF-AMS, FIGAERO-CIMS and LC-Orbitrap MS measurements.

In binary isoprene-containing mixtures, the $\overline{OSc}$ from all three instruments showed no clear similarity compared to full reactivity isoprene system (Fig.6a and 6c), in agreement with the values accounting for $\overline{OS_N}$ (Fig .2a and 3a). α-pinene and o-cresol products controlled $\overline{OSc}$ in their respective mixtures with isoprene. The trend in HR-ToF-AMS $\overline{OSc}$ in the α-pinene / *o*-cresol binary mixture most closely followed that of the α-pinene experiment, but increased slightly towards that of *o*-cresol (Fig.6b). Both *o*-cresol and α-pinene products likely contributed to the average $\overline{OSc}$ in their binary mixture, but possibly more from α-pinene. The FIGAERO-CIMS $\overline{OSc}$ presents a contrary picture, with the trend following that of α-pinene, but absolute value closer to that of *o*-cresol. $\overline{OSc}$ in the ternary was similarly not dominated by any single precursors, with the oxidation state in the mixture exhibiting a similar general pattern to the α-pinene / *o*-cresol

binary mixture in all 3 instruments, the values being between those of the α-pinene and *o*-cresol (Fig.6d).

In this work, we further aim to assess the relationship between average carbon oxidations state with SOA mass loading in mixture precursors systems obtained from HR-ToF-AMS measurement. The average $\overline{OSc}$ had increased at the early period of irradiation in binary α-pinene /isoprene system, binary α-pinene /o-cresol system and the ternary system in HR-TOF-AMS measurements (Fig.6a,6b and 6d). The average $\overline{OSc}$ rise along with SOA mass concertation in these mixture systems might associate with two effects, i) semi-volatile organic species formed from functionalized of VOCs could partition particle-phase upon SOA mass concertation increases regard to gas-partitioning theory, ii) further oxidized the existing organic species while the molecules do not fragment(Kroll et al., 2015; Donahue et al., 2012). However, the average $\overline{OSc}$ had significant reduced after the SOA mass loading reached to 10μgm^{-3} in the aforementioned mixture systems, which might involve condensation of less oxidized organic species and/or fragmentation of organic compounds after they further oxidized by OH radicals. The new components formed from the fragmentation of organic compounds could reduce the average $\overline{OSc}$ of SOA since these compounds have smaller size and higher volatility than the parent components, leading to evaporate from the SOA(Hildebrandt Ruiz et al., 2015; Surratt et al., 2006).

4.5. Drivers for carbon oxidation state behaviors

Knowing the oxidation pathway of precursors provides a description of the chemical behavior of the mixed systems controlling average carbon oxidation state during SOA formation and evolution. The oxidant regime (OH and O_3) during the experiments can differ between the mixture and individual precursor experiments despite our best attempts to maintain similar conditions through initial "iso-reactivity" as explained in Voliotis et al. (2022). The ozone production and hence OH profile may not be the same in the mixture as in the individual precursor experiments and the reactivity towards the available oxidants will not remain equal. This, in turn, will lead to changes in the timescale of product formation from each of the reactants. Both α-pinene and isoprene are readily oxidized by both OH and O_3, while the o-cresol is unreactive towards O_3 owing to its stable

aromatic ring and lack of double bond. This section discusses the drivers causing different carbon oxidation state between single and mixture precursors system with reference to the various classes of potential reactions (e.g. functionalization oligomerization, and fragmentation).

The FIGAREO-CIMS derived carbon oxidation state profile is higher in the single α-pinene system compared to its mixture with isoprene (Fig.2a) if $\overline{\mathrm{OS}}$N is considered, but the two systems have similar carbon oxidation state profiles if not accounting for $\overline{\mathrm{OS}}$N (Fig.6a). Fig 6a also indicated that the HR-TOF-AMS average carbon oxidation state in the mixture is lower than in the individual α-pinene system. Voliotis et al. (2022) indicated that the binary α-pinene/isoprene system has lower mass yield than the sole α-pinene system. This may suggest that the competition for oxidants when isoprene is added to the reacting α-pinene system results in formation of high volatility products from isoprene, suppressing formation of lower volatility α-pinene oxidation products. This change in products could be responsible for the lower average $\overline{\mathrm{OSc}}$ and SOA level in mixture compared to the individual α-pinene system.

In the isoprene / o-cresol system, the average $\overline{\mathrm{OSc}}$ derived from both online and offline mass spectrometry were comparable to that obtained in the individual o-cresol system, apart from the early state derived from the FIGAERO-CIMS measurement, as discussed in section 4.1 (Fig.3a and 6c). The wall-loss corrected particle mass in the mixture was lower than in the o-cresol system (as reported by Voliotis et al. (2022). This may be a result of the isoprene scavenging the available OH oxidants in the binary precursor system or reacting with O_3 which would otherwise have been available to form OH, both effects leading to reducing the SOA particle mass concentration form from o-cresol oxidation. However, the ozone production in the mixture was greater than in the individual cresol experiment. A similar average $\overline{\mathrm{OSc}}$ was observed between the two systems, which is reasonable since the chemical composition of SOA formed from binary isoprene / o-cresol shows strong resemblance to the single o-cresol system, with the dominance of CHON compounds with seven carbon atoms ($C_7H_7NO_3$, and $C_7H_7NO_4$ compounds) as identified by FIGAREO-CIMS and LC-Orbitrap-MS (Voliotis et al., 2021; Shao et al., 2022). Alternatively, it could imply that the presence of isoprene could have induced the oligomerization reaction of o-cresol oxidation products that could maintain the average $\overline{\mathrm{OSc}}$ (Kroll et al., 2011) similar to that in the individual o-cresol system.

In the binary α-pinene / o-cresol system, the FIGAERO-CIMS and HR-ToF-AMS carbon oxidation states have a similar trend to the individual α-pinene system though the absolute value in the mixture was between the o-cresol and α-pinene values whether accounting for $\overline{OS_N}$ or not in all instruments (Fig.4a and Fig.6b). Generally, o-cresol derived products will require further oxidation steps (more oxygen numbers) to be able partition to the particulate phase, compared to the α-pinene precursor owing to differences in carbon number (volatility generally increasing with decreasing carbon number) at the same absorptive mass. Thus, mixing o-cresol with α-pinene will increase the degree of oxidation at any given mass loading and enhancing the average $\overline{OSc}$ compared to single α-pinene system. These products may be partially attributed to formation of gaseous cross-product formation from α-pinene and o-cresol followed by condensation in the mixed system. More molecular information about the cross-products formation and potential mechanistic differences between the mixtures and individual precursor systems leading to compounds uniquely found in the binary α-pinene/o-cresol mixture have been reported by Voliotis et al. (2021) and Shao et al. (2022).

In the ternary mixture, the absolute magnitude of the average carbon oxidation state was between the individual o-cresol and α-pinene experiments, but not influenced by isoprene products. The average $\overline{OSc}$ of the ternary system is similar to the binary o-cresol/ α-pinene system, but the trend with SOA particle mass concentration was the not the same as in any individual precursor system (Fig.5, and Fig.6d). This may be attributed by the highly complex chemistry in ternary system. Both o-cresol and α-pinene derived products contributed to the chemical composition as Shao, et al, (2022) reported, with negligible contribution of isoprene driven products. This would lead to the average $\overline{OSc}$ in ternary mixture being higher than that in the individual α-pinene system with more oxygenated compounds being o-cresol oxidation products. Meanwhile, the significantly higher SOA particle mass in the ternary mixture compared to compared to any single precursor systems might be partially attributed to the formation of gaseous cross-products that subsequently condense. This is consistent with both Voliotis et al. (2021) and Shao et al. (2022) who reported that compounds uniquely found in the mixture made a non-negligible contribution in the ternary system. This cross-interaction between molecules might include RO_2+$R'O_2$ termination reactions

(oxygen atoms loss process as mentioned in 4.3) leading to an increase in less oxygenated organic species, reducing average $\overline{\mathrm{OSc}}$ during particulate matter formation

5. Summary

In this study, the average carbon oxidation state and atomic ratios (H:C,O:C and N:C) of SOA formed from photooxidation of α-pinene, isoprene, o-cresol and their binary and ternary mixtures in the presence of NOx and ammonium sulphate seed particles was determined by HR-TOF-AMS, FIGAERO-CIMS and LC-Orbitrap MS. We investigate the potential factors that affect the average $\overline{OSc}$ during SOA evolution in mixture precursor system by combining the online and offline mass spectrometer measurement.

The average $\overline{OSc}$ obtained from FIGAERO-CIMS and LC-Orbitrap MS were classified into two sections (i) accounting for $\overline{OS_N}$ and (ii) not accounting for $\overline{OS_N}$. The HR-TOF-AMS measurement only estimated average $\overline{OSc}$ that is average $\overline{OSc}$ due to its limited resolution. The average $\overline{OSc}$ that is not accounting for $\overline{OS_N}$ showed substantial difference between the FIGAERO-CIMS measurement, HR-TOF-AMS measurement and LC-Orbitrap MS measurement, likely due to the FIGAERO-CIMS and LC-Orbitrap MS only measuring a subset of compounds. In addition, the FIGAERO-CIMS has higher sensitivity toward more oxygenate compounds, and LC-Orbitrap MS has a particularly high sensitivity to aromatic nitro-compounds in negative ionization mode.

The average carbon oxidation state was influenced by the initial concentration of precursor in the single α-pinene system. The ½ reactivity of α-pinene has higher $\overline{OSc}$ (not accounting for $\overline{OS_N}$) during SOA evolution than full reactivity α-pinene, that might be due to an enhanced contribution of α-pinene ozonolysis leading to an increase in highly oxygenated compounds formed by autoxidation. In contrast, the average $\overline{OSc}$ (not accounting for $\overline{OS_N}$) in single precursor *o*-cresol system was not dependent on the initial concentration of precursor, since the o-cresol barely react with O_3 results in the oxidant regime in the single o-cresol system always concentrated in OH radicals. CHON compounds have a significant influence on average $\overline{OSc}$ of SOA in both the

single VOC α-pinene and *o*-cresol systems, since the average $\overline{OSc}$ (accounting for $\overline{OS_N}$) has lower value than $\overline{OSc}$ (not accounting for $\overline{OS_N}$).

In the binary mixtures, the isoprene negligibly influenced the average carbon oxidation state, with the isoprene full reactivity experiment generating insignificant SOA particle mass (<1μgm^{-3}). For instance, the average $\overline{OSc}$ of SOA in the *o*-cresol/isoprene binary mixture is almost identical in trend and magnitude with the single precursor *o*-cresol system. In contrast, the oxidation state decreased on addition of isoprene to α-pinene, with the average $\overline{OSc}$ in the α-pinene / isoprene lower than the α-pinene value, which is likely due to the isoprene act as OH scavenger in gas-phase reaction resultant of high vapour pressure products that partitioning to the particulate matte or might be associated with the RO_2+RO_2 oxygen loss termination. The degree of oxidation in the α-pinene / o-cresol system was complex since both precursors generated considerable SOA mass, and the average $\overline{OSc}$ was affected by both precursors. The α-pinene and *o*-cresol products both impacted on the oxidation state in their binary mixture. The average $\overline{OSc}$ shared similar trend with the α-pinene system, with an increase in absolute value towards that of *o*-cresol. Compounds uniquely found in the mixture likely contributed to this behaviour. In the ternary precursor system, no single precursor dominated the oxidation state, though the general pattern was similar to that in the α-pinene / *o*-cresol mixture. Whilst the current study makes some important first steps in its investigation, the oxidation state in mixtures of SOA precursors requires further work.

Data availability

All the data used in this work can be accessed on the open database of the EUROCHAMP programme (https://data.eurochamp.org/data-access/chamber-experiments/).

Competing interests

The authors declare that they have no conflict of interest.

Author contributions

GM, MRA, AV, YW and YS conceived the study. AV, YW, YS and MD conducted the experiments. KP provided on-site LC-Orbitrap MS training for filter analysis and provided the automated non-targeted method for LC-Orbitrap MS analysis. YS conducted the data analysis and wrote the manuscript with contribution from all co-authors.

Acknowledgements

The Manchester Aerosol Chamber acknowledges the funding support from the European Union's Horizon 2020 research and innovation programme under grant agreement no. 730997, which supports the EUROCHAMP2020 research programme. Instrumentational support was funded by the NERC Atmospheric Measurement and Observational Facility (AMOF). Y.W. acknowledges the joint scholarship of The University of Manchester and Chinese Scholarship Council. M.R.A. acknowledges funding support by UK National Centre for Atmospheric Sciences (NACS). A.V. acknowledges the funding support by Natural Environment Research Council (NERC) EAO Doctoral Training Partnership.

Reference

Ahlberg, E., Falk, J., Eriksson, A., Holst, T., Brune, W. H., Kristensson, A., Roldin, P., and Svenningsson, B.: Secondary organic aerosol from VOC mixtures in an oxidation flow reactor, Atmospheric Environment, 161, 210-220, https://doi.org/10.1016/j.atmosenv.2017.05.005, 2017.

Aiken, A. C., DeCarlo, P. F., Kroll, J. H., Worsnop, D. R., Huffman, J. A., Docherty, K. S., Ulbrich, I. M., Mohr, C., Kimmel, J. R., Sueper, D., Sun, Y., Zhang, Q., Trimborn, A., Northway, M., Ziemann, P. J., Canagaratna, M. R., Onasch, T. B., Alfarra, M. R., Prevot, A. S. H., Dommen, J., Duplissy, J., Metzger, A., Baltensperger, U., and Jimenez, J. L.: O/C and OM/OC Ratios of Primary, Secondary, and Ambient Organic Aerosols with High-Resolution Time-of-Flight Aerosol Mass Spectrometry, Environmental Science & Technology, 42, 4478-4485, 10.1021/es703009q, 2008.

Alfarra, M. R., Coe, H., Allan, J. D., Bower, K. N., Boudries, H., Canagaratna, M. R., Jimenez, J. L., Jayne, J. T., Garforth, A. A., Li, S.-M., and Worsnop, D. R.: Characterization of urban and rural organic particulate in the Lower Fraser Valley using two Aerodyne Aerosol Mass Spectrometers, Atmospheric Environment, 38, 5745-5758, https://doi.org/10.1016/j.atmosenv.2004.01.054, 2004.

Atkinson, R., Baulch, D. L., Cox, R. A., Crowley, J. N., Hampson, R. F., Hynes, R. G., Jenkin, M. E., Rossi, M. J., and Troe, J.: Evaluated kinetic and photochemical data for atmospheric chemistry: Volume I - gas phase reactions of O_x, HO_x, NO_x and SO_x species, Atmos. Chem. Phys., 4, 1461-1738, 10.5194/acp-4-1461-2004, 2004.

Atkinson, R. B., D. L. Cox, R. A.Crowley, J. N.Hampson, R. F.Hynes, R. G.Jenkin, M. E.Rossi, M. J.Troe, J.: Evaluated kinetic and photochemical data for atmospheric chemistry: Volume I - gas phase reactions of Ox, HOx, NOxand SOxspecies, Atmos. Chem. Phys., 4, 1738, 10.5194/acp-4-1461-2004, 2004.

Bruns, E. A., Perraud, V., Zelenyuk, A., Ezell, M. J., Johnson, S. N., Yu, Y., Imre, D., Finlayson-Pitts, B. J., and Alexander, M. L.: Comparison of FTIR and Particle Mass Spectrometry for the Measurement of Particulate Organic Nitrates, Environmental Science & Technology, 44, 1056-1061, 10.1021/es9029864, 2010.

Carlton, A. G., Wiedinmyer, C., and Kroll, J. H.: A review of Secondary Organic Aerosol (SOA) formation from isoprene, Atmos. Chem. Phys., 9, 4987-5005, 10.5194/acp-9-4987-2009, 2009.

Chhabra, P. S., Flagan, R. C., and Seinfeld, J. H.: Elemental analysis of chamber organic aerosol using an aerodyne high-resolution aerosol mass spectrometer, Atmos. Chem. Phys., 10, 4111-4131, 10.5194/acp-10-4111-2010, 2010.

D'Ambro, E. L., Schobesberger, S., Gaston, C. J., Lopez-Hilfiker, F. D., Lee, B. H., Liu, J., Zelenyuk, A., Bell, D., Cappa, C. D., Helgestad, T., Li, Z., Guenther, A., Wang, J., Wise, M., Caylor, R., Surratt, J. D., Riedel, T., Hyttinen, N., Salo, V. T., Hasan, G., Kurtén, T., Shilling, J. E., and Thornton, J. A.: Chamber-based insights into the factors controlling epoxydiol (IEPOX) secondary organic aerosol (SOA) yield, composition, and volatility, Atmos. Chem. Phys., 19, 11253-11265, 10.5194/acp-19-11253-2019, 2019.

Daumit, K. E., Kessler, S. H., and Kroll, J. H.: Average chemical properties and potential formation pathways of highly oxidized organic aerosol, Faraday Discuss, 165, 181-202, 10.1039/c3fd00045a, 2013.
DeCarlo, P. F., Kimmel, J. R., Trimborn, A., Northway, M. J., Jayne, J. T., Aiken, A. C., Gonin, M., Fuhrer, K., Horvath, T., Docherty, K. S., Worsnop, D. R., and Jimenez, J. L.: Field-Deployable, High-Resolution, Time-of-Flight Aerosol Mass Spectrometer, Analytical Chemistry, 78, 8281-8289, 10.1021/ac061249n, 2006.
Docherty, K. S., Corse, E. W., Jaoui, M., Offenberg, J. H., Kleindienst, T. E., Krug, J. D., Riedel, T. P., and Lewandowski, M.: Trends in the oxidation and relative volatility of chamber-generated secondary organic aerosol, Aerosol Science and Technology, 52, 992-1004, 10.1080/02786826.2018.1500014, 2018.
Donahue, N. M., Kroll, J. H., Pandis, S. N., and Robinson, A. L.: A two-dimensional volatility basis set – Part 2: Diagnostics of organic-aerosol evolution, Atmos. Chem. Phys., 12, 615-634, 10.5194/acp-12-615-2012, 2012.
Du, M., Voliotis, A., Shao, Y., Wang, Y., Bannan, T. J., Pereira, K. L., Hamilton, J. F., Percival, C. J., Alfarra, M. R., and McFiggans, G.: Combined application of Online FIGAERO-CIMS and Offline LC-Orbitrap MS to Characterize the Chemical Composition of SOA in Smog Chamber Studies, Atmos. Meas. Tech. Discuss., 2021, 1-42, 10.5194/amt-2021-420, 2021.
Eddingsaas, N. C., Loza, C. L., Yee, L. D., Chan, M., Schilling, K. A., Chhabra, P. S., Seinfeld, J. H., and Wennberg, P. O.: α-pinene photooxidation under controlled chemical conditions – Part 2: SOA yield and composition in low- and high-NO_x environments, Atmos. Chem. Phys., 12, 7413-7427, 10.5194/acp-12-7413-2012, 2012.
Farmer, D. K., Matsunaga, A., Docherty, K. S., Surratt, J. D., Seinfeld, J. H., Ziemann, P. J., and Jimenez, J. L.: Response of an aerosol mass spectrometer to organonitrates and organosulfates and implications for atmospheric chemistry, Proceedings of the National Academy of Sciences, 107, 6670, 10.1073/pnas.0912340107, 2010.
Fry, J. L., Kiendler-Scharr, A., Rollins, A. W., Wooldridge, P. J., Brown, S. S., Fuchs, H., Dubé, W., Mensah, A., dal Maso, M., Tillmann, R., Dorn, H. P., Brauers, T., and Cohen, R. C.: Organic nitrate and secondary organic aerosol yield from NO₃ oxidation of β-pinene evaluated using a gas-phase kinetics/aerosol partitioning model, Atmos. Chem. Phys., 9, 1431-1449, 10.5194/acp-9-1431-2009, 2009.
García Vivanco, M. and Santiago, M.: Secondary Organic Aerosol Formation from the Oxidation of a Mixture of Organic Gases in a Chamber, in, 265-282, 10.5772/9761, 2010.
Griggs, D. J. and Noguer, M.: Climate change 2001: The scientific basis. Contribution of Working Group I to the Third Assessment Report of the Intergovernmental Panel on Climate Change, Weather, 57, 267-269, https://doi.org/10.1256/004316502320517344, 2002.
Henry, F., Coeur-Tourneur, C., Ledoux, F., Tomas, A., and Menu, D.: Secondary organic aerosol formation from the gas phase reaction of hydroxyl radicals with m-, o- and p-cresol, Atmospheric Environment, 42, 3035-3045, https://doi.org/10.1016/j.atmosenv.2007.12.043, 2008.

Henry, K. M., Lohaus, T., and Donahue, N. M.: Organic Aerosol Yields from α-Pinene Oxidation: Bridging the Gap between First-Generation Yields and Aging Chemistry, Environmental Science & Technology, 46, 12347-12354, 10.1021/es302060y, 2012.
Hildebrandt, L., Henry, K. M., Kroll, J. H., Worsnop, D. R., Pandis, S. N., and Donahue, N. M.: Evaluating the Mixing of Organic Aerosol Components Using High-Resolution Aerosol Mass Spectrometry, Environmental Science & Technology, 45, 6329-6335, 10.1021/es200825g, 2011.
Hildebrandt Ruiz, L., Paciga, A. L., Cerully, K. M., Nenes, A., Donahue, N. M., and Pandis, S. N.: Formation and aging of secondary organic aerosol from toluene: changes in chemical composition, volatility, and hygroscopicity, Atmos. Chem. Phys., 15, 8301-8313, 10.5194/acp-15-8301-2015, 2015.
Hoffmann, T., Huang, R.-J., and Kalberer, M.: Atmospheric Analytical Chemistry, Analytical Chemistry, 83, 4649-4664, 10.1021/ac2010718, 2011.
Hoffmann, T., Odum, J. R., Bowman, F., Collins, D., Klockow, D., Flagan, R. C., and Seinfeld, J. H.: Formation of Organic Aerosols from the Oxidation of Biogenic Hydrocarbons, Journal of Atmospheric Chemistry, 26, 189-222, 10.1023/A:1005734301837, 1997.
Iyer, S., Rissanen, M. P., Valiev, R., Barua, S., Krechmer, J. E., Thornton, J., Ehn, M., and Kurtén, T.: Molecular mechanism for rapid autoxidation in α-pinene ozonolysis, Nature Communications, 12, 878, 10.1038/s41467-021-21172-w, 2021.
Jaoui, M., Edney, E. O., Kleindienst, T. E., Lewandowski, M., Offenberg, J. H., Surratt, J. D., and Seinfeld, J. H.: Formation of secondary organic aerosol from irradiated α-pinene/toluene/NOx mixtures and the effect of isoprene and sulfur dioxide, Journal of Geophysical Research: Atmospheres, 113, https://doi.org/10.1029/2007JD009426, 2008.
Jayne, J. T., Leard, D. C., Zhang, X., Davidovits, P., Smith, K. A., Kolb, C. E., and Worsnop, D. R.: Development of an aerosol mass spectrometer for size and composition analysis of submicron particles, Aerosol Science & Technology, 33, 49-70, 2000.
Jimenez, J. L., Jayne, J. T., Shi, Q., Kolb, C. E., Worsnop, D. R., Yourshaw, I., Seinfeld, J. H., Flagan, R. C., Zhang, X., Smith, K. A., Morris, J. W., and Davidovits, P.: Ambient aerosol sampling using the Aerodyne Aerosol Mass Spectrometer, Journal of Geophysical Research: Atmospheres, 108, https://doi.org/10.1029/2001JD001213, 2003.
Jimenez, J. L., Canagaratna, M. R., Donahue, N. M., Prevot, A. S. H., Zhang, Q., Kroll, J. H., DeCarlo, P. F., Allan, J. D., Coe, H., Ng, N. L., Aiken, A. C., Docherty, K. S., Ulbrich, I. M., Grieshop, A. P., Robinson, A. L., Duplissy, J., Smith, J. D., Wilson, K. R., Lanz, V. A., Hueglin, C., Sun, Y. L., Tian, J., Laaksonen, A., Raatikainen, T., Rautiainen, J., Vaattovaara, P., Ehn, M., Kulmala, M., Tomlinson, J. M., Collins, D. R., Cubison, M. J., Dunlea, J., Huffman, J. A., Onasch, T. B., Alfarra, M. R., Williams, P. I., Bower, K., Kondo, Y., Schneider, J., Drewnick, F., Borrmann, S., Weimer, S., Demerjian, K., Salcedo, D., Cottrell, L., Griffin, R., Takami, A., Miyoshi, T., Hatakeyama, S., Shimono, A., Sun, J. Y., Zhang, Y. M., Dzepina, K., Kimmel, J. R., Sueper, D., Jayne, J. T., Herndon, S. C., Trimborn, A. M., Williams, L. R., Wood, E. C., Middlebrook, A. M., Kolb, C. E., Baltensperger, U., and Worsnop, D. R.: Evolution of Organic Aerosols in the Atmosphere, Science, 326, 1525, 10.1126/science.1180353, 2009.
Kanakidou, M., Seinfeld, J. H., Pandis, S. N., Barnes, I., Dentener, F. J., Facchini, M. C., Van Dingenen, R., Ervens, B., Nenes, A., Nielsen, C. J., Swietlicki, E., Putaud, J. P., Balkanski, Y., Fuzzi,

S., Horth, J., Moortgat, G. K., Winterhalter, R., Myhre, C. E. L., Tsigaridis, K., Vignati, E., Stephanou, E. G., and Wilson, J.: Organic aerosol and global climate modelling: A review, Atmos. Chem. Phys.\, 5\, 1053\-1123\, 10.5194/acp-5-1053-2005\, 2005.
Kroll, J. H., Lim, C. Y., Kessler, S. H., and Wilson, K. R.: Heterogeneous Oxidation of Atmospheric Organic Aerosol: Kinetics of Changes to the Amount and Oxidation State of Particle-Phase Organic Carbon, The Journal of Physical Chemistry A, 119, 10767-10783, 10.1021/acs.jpca.5b06946, 2015.
Kroll, J. H., Ng, N. L., Murphy, S. M., Flagan, R. C., and Seinfeld, J. H.: Secondary organic aerosol formation from isoprene photooxidation under high-NOx conditions, Geophysical Research Letters, 32, https://doi.org/10.1029/2005GL023637, 2005a.
Kroll, J. H., Ng, N. L., Murphy, S. M., Flagan, R. C., and Seinfeld, J. H.: Secondary organic aerosol formation from isoprene photooxidation, Environmental science & technology, 40, 1869-1877, 2006.
Kroll, J. H., Ng, N. L., Murphy, S. M., Varutbangkul, V., Flagan, R. C., and Seinfeld, J. H.: Chamber studies of secondary organic aerosol growth by reactive uptake of simple carbonyl compounds, Journal of Geophysical Research: Atmospheres, 110, https://doi.org/10.1029/2005JD006004, 2005b.
Kroll, J. H., Donahue, N. M., Jimenez, J. L., Kessler, S. H., Canagaratna, M. R., Wilson, K. R., Altieri, K. E., Mazzoleni, L. R., Wozniak, A. S., Bluhm, H., Mysak, E. R., Smith, J. D., Kolb, C. E., and Worsnop, D. R.: Carbon oxidation state as a metric for describing the chemistry of atmospheric organic aerosol, Nature Chemistry, 3, 133-139, 10.1038/nchem.948, 2011.
Lee, B.-H., Pierce, J. R., Engelhart, G. J., and Pandis, S. N.: Volatility of secondary organic aerosol from the ozonolysis of monoterpenes, Atmospheric Environment, 45, 2443-2452, https://doi.org/10.1016/j.atmosenv.2011.02.004, 2011.
Lee, B. H., Lopez-Hilfiker, F. D., Mohr, C., Kurtén, T., Worsnop, D. R., and Thornton, J. A.: An Iodide-Adduct High-Resolution Time-of-Flight Chemical-Ionization Mass Spectrometer: Application to Atmospheric Inorganic and Organic Compounds, Environmental Science & Technology, 48, 6309-6317, 10.1021/es500362a, 2014.
Lopez-Hilfiker, F. D., Mohr, C., Ehn, M., Rubach, F., Kleist, E., Wildt, J., Mentel, T. F., Lutz, A., Hallquist, M., Worsnop, D., and Thornton, J. A.: A novel method for online analysis of gas and particle composition: description and evaluation of a Filter Inlet for Gases and AEROsols (FIGAERO), Atmos. Meas. Tech., 7, 983-1001, 10.5194/amt-7-983-2014, 2014.
Luo, H., Chen, J., Li, G., and An, T.: Formation kinetics and mechanisms of ozone and secondary organic aerosols from photochemical oxidation of different aromatic hydrocarbons: dependence on NOx and organic substituents, Atmos. Chem. Phys., 21, 7567-7578, 10.5194/acp-21-7567-2021, 2021.
McFiggans, G., Mentel, T. F., Wildt, J., Pullinen, I., Kang, S., Kleist, E., Schmitt, S., Springer, M., Tillmann, R., and Wu, C.: Secondary organic aerosol reduced by mixture of atmospheric vapours, Nature, 565, 587, 2019.
Molteni, U., Simon, M., Heinritzi, M., Hoyle, C. R., Bernhammer, A.-K., Bianchi, F., Breitenlechner, M., Brilke, S., Dias, A., Duplissy, J., Frege, C., Gordon, H., Heyn, C., Jokinen, T., Kürten, A., Lehtipalo, K., Makhmutov, V., Petäjä, T., Pieber, S. M., Praplan, A. P., Schobesberger,

S., Steiner, G., Stozhkov, Y., Tomé, A., Tröstl, J., Wagner, A. C., Wagner, R., Williamson, C., Yan, C., Baltensperger, U., Curtius, J., Donahue, N. M., Hansel, A., Kirkby, J., Kulmala, M., Worsnop, D. R., and Dommen, J.: Formation of Highly Oxygenated Organic Molecules from α-Pinene Ozonolysis: Chemical Characteristics, Mechanism, and Kinetic Model Development, ACS Earth and Space Chemistry, 3, 873-883, 10.1021/acsearthspacechem.9b00035, 2019.
Ng, N. L., Chhabra, P. S., Chan, A. W. H., Surratt, J. D., Kroll, J. H., Kwan, A. J., McCabe, D. C., Wennberg, P. O., Sorooshian, A., Murphy, S. M., Dalleska, N. F., Flagan, R. C., and Seinfeld, J. H.: Effect of NO_x level on secondary organic aerosol (SOA) formation from the photooxidation of terpenes, Atmos. Chem. Phys., 7, 5159-5174, 10.5194/acp-7-5159-2007, 2007.
Pandis, S. N., Paulson, S. E., Seinfeld, J. H., and Flagan, R. C.: Aerosol formation in the photooxidation of isoprene and β-pinene, Atmospheric Environment. Part A. General Topics, 25, 997-1008, https://doi.org/10.1016/0960-1686(91)90141-S, 1991.
Pereira, K., Ward, M., Wilkinson, J., Sallach, J., Bryant, D., Dixon, W., Hamilton, J., and Lewis, A.: An Automated Methodology for Non-targeted Compositional Analysis of Small Molecules in High Complexity Environmental Matrices Using Coupled Ultra Performance Liquid Chromatography Orbitrap Mass Spectrometry, Environmental Science & Technology, XXXX, 10.1021/acs.est.0c08208, 2021.
Presto, A. A., Miracolo, M. A., Kroll, J. H., Worsnop, D. R., Robinson, A. L., and Donahue, N. M.: Intermediate-Volatility Organic Compounds: A Potential Source of Ambient Oxidized Organic Aerosol, Environmental Science & Technology, 43, 4744-4749, 10.1021/es803219q, 2009.
Pullinen, I., Schmitt, S., Kang, S., Sarrafzadeh, M., Schlag, P., Andres, S., Kleist, E., Mentel, T. F., Rohrer, F., Springer, M., Tillmann, R., Wildt, J., Wu, C., Zhao, D., Wahner, A., and Kiendler-Scharr, A.: Impact of NOx on secondary organic aerosol (SOA) formation from α-pinene and β-pinene photooxidation: the role of highly oxygenated organic nitrates, Atmos. Chem. Phys., 20, 10125-10147, 10.5194/acp-20-10125-2020, 2020.
Robinson, A. L., Donahue, N. M., Shrivastava, M. K., Weitkamp, E. A., Sage, A. M., Grieshop, A. P., Lane, T. E., Pierce, J. R., and Pandis, S. N.: Rethinking Organic Aerosols: Semivolatile Emissions and Photochemical Aging, Science, 315, 1259, 10.1126/science.1133061, 2007.
Seinfeld, J. H. and Pankow, J. F.: Organic Atmospheric Particulate Material, Annual Review of Physical Chemistry, 54, 121-140, 10.1146/annurev.physchem.54.011002.103756, 2003.
Shao, Y., Wang, Y., Du, M., Voliotis, A., Alfarra, M. R., Turner, S. F., and McFiggans, G.: Characterisation of the Manchester Aerosol Chamber facility, Atmos. Meas. Tech. Discuss., 2021, 1-50, 10.5194/amt-2021-147, 2021.
Shao, Y., Voliotis, A., Du, M., Wang, Y., Pereira, K., Hamilton, J., Alfarra, M. R., and McFiggans, G.: Chemical composition of secondary organic aerosol particles formed from mixtures of anthropogenic and biogenic precursors, Atmos. Chem. Phys. Discuss., 2022, 1-41, 10.5194/acp-2022-127, 2022.
Shilling, J. E., Chen, Q., King, S. M., Rosenoern, T., Kroll, J. H., Worsnop, D. R., DeCarlo, P. F., Aiken, A. C., Sueper, D., Jimenez, J. L., and Martin, S. T.: Loading-dependent elemental composition of α-pinene SOA particles, Atmos. Chem. Phys., 9, 771-782, 10.5194/acp-9-771-2009, 2009.

Stark, H., Yatavelli, R. L. N., Thompson, S. L., Kimmel, J. R., Cubison, M. J., Chhabra, P. S., Canagaratna, M. R., Jayne, J. T., Worsnop, D. R., and Jimenez, J. L.: Methods to extract molecular and bulk chemical information from series of complex mass spectra with limited mass resolution, International Journal of Mass Spectrometry, 389, 26-38, https://doi.org/10.1016/j.ijms.2015.08.011, 2015.
Stroud, C. A., Roberts, J. M., Goldan, P. D., Kuster, W. C., Murphy, P. C., Williams, E. J., Hereid, D., Parrish, D., Sueper, D., Trainer, M., Fehsenfeld, F. C., Apel, E. C., Riemer, D., Wert, B., Henry, B., Fried, A., Martinez-Harder, M., Harder, H., Brune, W. H., Li, G., Xie, H., and Young, V. L.: Isoprene and its oxidation products, methacrolein and methylvinyl ketone, at an urban forested site during the 1999 Southern Oxidants Study, Journal of Geophysical Research: Atmospheres, 106, 8035-8046, https://doi.org/10.1029/2000JD900628, 2001.
Surratt, J. D., Kroll, J. H., Kleindienst, T. E., Edney, E. O., Claeys, M., Sorooshian, A., Ng, N. L., Offenberg, J. H., Lewandowski, M., Jaoui, M., Flagan, R. C., and Seinfeld, J. H.: Evidence for Organosulfates in Secondary Organic Aerosol, Environmental Science & Technology, 41, 517-527, 10.1021/es062081q, 2007.
Surratt, J. D., Murphy, S. M., Kroll, J. H., Ng, N. L., Hildebrandt, L., Sorooshian, A., Szmigielski, R., Vermeylen, R., Maenhaut, W., Claeys, M., Flagan, R. C., and Seinfeld, J. H.: Chemical Composition of Secondary Organic Aerosol Formed from the Photooxidation of Isoprene, The Journal of Physical Chemistry A, 110, 9665-9690, 10.1021/jp061734m, 2006.
Surratt, J. D., Gómez-González, Y., Chan, A. W. H., Vermeylen, R., Shahgholi, M., Kleindienst, T. E., Edney, E. O., Offenberg, J. H., Lewandowski, M., Jaoui, M., Maenhaut, W., Claeys, M., Flagan, R. C., and Seinfeld, J. H.: Organosulfate Formation in Biogenic Secondary Organic Aerosol, The Journal of Physical Chemistry A, 112, 8345-8378, 10.1021/jp802310p, 2008.
Thompson, R. D.: The impact of atmospheric aerosols on global climate: a review, Progress in Physical Geography: Earth and Environment, 19, 336-350, 10.1177/030913339501900303, 1995.
Voliotis, A., Wang, Y., Shao, Y., Du, M., Bannan, T. J., Percival, C. J., Pandis, S. N., Alfarra, M. R., and McFiggans, G.: Exploring the composition and volatility of secondary organic aerosols in mixed anthropogenic and biogenic precursor systems, Atmos. Chem. Phys. Discuss., 2021, 1-39, 10.5194/acp-2021-215, 2021.
Voliotis, A., Du, M., Wang, Y., Shao, Y., Alfarra, M. R., Bannan, T. J., Hu, D., Pereira, K. L., Hamilton, J. F., Hallquist, M., Mentel, T. F., and McFiggans, G.: Chamber investigation of the formation and transformation of secondary organic aerosol in mixtures of biogenic and anthropogenic volatile organic compounds, Atmos. Chem. Phys. Discuss., 2022, 1-49, 10.5194/acp-2021-1080, 2022.
Wennberg, P. O., Bates, K. H., Crounse, J. D., Dodson, L. G., McVay, R. C., Mertens, L. A., Nguyen, T. B., Praske, E., Schwantes, R. H., Smarte, M. D., St Clair, J. M., Teng, A. P., Zhang, X., and Seinfeld, J. H.: Gas-Phase Reactions of Isoprene and Its Major Oxidation Products, Chemical Reviews, 118, 3337-3390, 10.1021/acs.chemrev.7b00439, 2018.
Winterhalter, R., Van Dingenen, R., Larsen, B. R., Jensen, N. R., and Hjorth, J.: LC-MS analysis of aerosol particles from the oxidation of α-pinene by ozone and OH-radicals, Atmos. Chem. Phys. Discuss., 2003, 1-39, 10.5194/acpd-3-1-2003, 2003.

Xu, L., Middlebrook, A. M., Liao, J., de Gouw, J. A., Guo, H., Weber, R. J., Nenes, A., Lopez-Hilfiker, F. D., Lee, B. H., Thornton, J. A., Brock, C. A., Neuman, J. A., Nowak, J. B., Pollack, I. B., Welti, A., Graus, M., Warneke, C., and Ng, N. L.: Enhanced formation of isoprene-derived organic aerosol in sulfur-rich power plant plumes during Southeast Nexus, Journal of Geophysical Research: Atmospheres, 121, 11,137-111,153, 10.1002/2016jd025156, 2016.
Zhang, Q., Jimenez, J. L., Canagaratna, M. R., Allan, J. D., Coe, H., Ulbrich, I., Alfarra, M. R., Takami, A., Middlebrook, A. M., Sun, Y. L., Dzepina, K., Dunlea, E., Docherty, K., DeCarlo, P. F., Salcedo, D., Onasch, T., Jayne, J. T., Miyoshi, T., Shimono, A., Hatakeyama, S., Takegawa, N., Kondo, Y., Schneider, J., Drewnick, F., Borrmann, S., Weimer, S., Demerjian, K., Williams, P., Bower, K., Bahreini, R., Cottrell, L., Griffin, R. J., Rautiainen, J., Sun, J. Y., Zhang, Y. M., and Worsnop, D. R.: Ubiquity and dominance of oxygenated species in organic aerosols in anthropogenically-influenced Northern Hemisphere midlatitudes, Geophysical Research Letters, 34, https://doi.org/10.1029/2007GL029979, 2007.

[BLANK PAGE]

Chapter 6

6. Conclusion

In this thesis, the chemical properties of Secondary Organic Aerosol (SOA) particles formed from a mixture of anthropogenic (o-cresol) and biogenic sources (α-pinene and isoprene) were investigated through a series of photooxidation experiments in the Manchester aerosol chamber (MAC) using synthetic mixtures of Volatile Organic Compound (VOC) precursors in the presence of NOx and ammonium sulphate seed particles. The MAC was designed to enable investigation of coupled gas phase photochemical and aerosol microphysical processes of relevance to the atmosphere and their atmospheric impacts.

Understanding the formation of SOA from the oxidation of VOCs is essential to air quality and climate on a global scale. However, there is still a lack of information regarding the chemistry of the formation pathway and chemical composition of SOA in the atmosphere owing to the complexity of the ambient VOC mixture. Historically, synthetic SOA formation studies in the laboratory have overwhelmingly focused on the oxidation of a single VOC precursors, which provide limited insight into SOA formation in the real atmosphere. This thesis aims to provide insight into multiphase atmospheric systems inaccessible to experiments using a single VOC precursor. Through investigating and evaluating the chemical properties of SOA (e.g., chemical composition, average carbon oxidation state), this thesis provides an overview of SOA formation potential in the mixed anthropogenic and biogenic precursor system.

6.1. Summary of Key Research Findings

Paper 1 comprehensively describes the characterisation of the MAC. The MAC can provide closely controlled temperature and relative humidity between 15 and 35°C and 25–80%. The MAC usage history was shown to strongly influence the chamber characteristics including light intensity, wall loss rate of gases and particle species. For instance, after extensive use, the Teflon chamber walls can provide an additional sink to adsorb the particles and gas species irreversibly, leading to a higher wall loss rate of gas and particles, requiring regular characterisation experiments to track

changes in performance. It was shown that the derived SOA yield could be biased by inappropriate application of SOA particle wall-loss correction methods. Suggestions for the development of simple and standardised experiments generally applicable to chambers were made.

Paper 2 used the MAC to investigate SOA formation and transformation in mixtures of biogenic and anthropogenic VOCs. Specifically, it investigated the formation of SOA particulate mass driven from the chamber photooxidation of anthropogenic (*o*-cresol) and biogenic (α-pinene and isoprene) VOCs and their binary and ternary mixtures in the presence of NOx and inorganic seeds. It reported the SOA mass yield of individual components to predict the yield in the mixture when the individual components had the same mass as in the mixture or the individual components and mixture had masses forming at the same VOC consumption. The measured particles yields at the maximum SOA mass were found in descending order for the α-pinene (32±7%), α-pinene/o-cresol (28±9%), α-pinene at 1⁄2 initial reactivity (21±5%), α-pinene/isoprene (16±1%), α-pinene at 1⁄3 initial reactivity (15±4%), o-cresol (13±3%), α-pinene/o-cresol/isoprene (11±4%), o-cresol at 1⁄2 initial reactivity (11±3%), o-cresol/isoprene (6±2%) and isoprene systems (0±0%). The SOA mass yield clearly indicated suppression of α-pinene in its isoprene mixture and possibly showed a minor enhancement in the o-cresol/isoprene mixture. The measured yield of mixture α-pinene/o-cresol system showed enhancement compared to the predicted yield from additivity of the individual VOC yield at the same consumption. The measured SOA mass yield had a comparable value to that predicted from additivity of the component yields in the ternary system, possibly attributable to cancelling suppression or enhancement effects.

Paper 3 utilised the insights gained from paper 2 to understand the chemical composition and interactions during SOA formation in mixed VOC systems. Specifically, it characterised the particulate products produced in the photooxidation of mixed biogenic (α-pinene and isoprene) and anthropogenic (*o*-cresol) VOCs using offline liquid chromatography ultra-high resolution mass spectrometry (LC-Orbitrap-MS). It used a non-targeted accurate mass analysis not widely used in environmental applications to process LC-orbitrap-MS data and reduce data complexity and analysis time, rapidly extracting useful chemical information for the detected sample set. The

paper reported the elemental and molecular composition of SOA in the binary α-pinene/isoprene system is mainly contributed by the higher-yield precursor, α-pinene, in terms of the number of individual compounds and total contribution to the signal. Particle composition in both *o*-cresol binary systems is strongly dominated by on *o*-cresol oxidation products in negative ionisation mode, primarily attributed to methyl-nitrocatechol isomers ($C_7H_7NO_4$) and methyl-nitrophenol ($C_7H_7NO_3$) owing to their high sensitivity in electrospray ionisation. Compounds uniquely found in the mixtures made a considerable contribution to the signal in positive mode in both binary *o*-cresol containing systems, indicating significant interactions between the oxidation products in each system. In the ternary mixture, the particle composition was dominated by α-pinene oxidation products in positive ionisation mode, but both *o*-cresol and α-pinene derived compounds made considerable contributions in negative ionisation mode. Isoprene oxidation products made only minor contributions to the particle composition in all isoprene containing mixed systems, likely resulting from the high volatility of the isoprene oxidation products. It was proposed that some components could act as a potential tracer in a particular mixed system, including $C_{17}H_{14}N_2O_7$ in binary α-pinene/isoprene systems, $C_9H_{11}NO$, $C_8H_8O_{10}$ in binary *o*-cresol/isoprene systems, and $C_{21}H_{34}O_6$ and $C_{20}H_{28}N_4O_4S$ in ternary systems.

The fourth and final paper reported the average carbon oxidation state of SOA from online and offline measurements in all the binary and the ternary systems, aiming to understand the causes of carbon oxidation state ($\overline{OSc}$) differences between SOA formed from photooxidation of single and mixed organic precursors. This study used the online high-resolution time-of-flight Aerodyne aerosol mass spectrometer (HR-ToF-AMS) and Filter Inlet for Gases and Aerosols coupled to the Iodide high-resolution time of flight Chemical Ionization Mass Spectrometer (FIGAERO-CIMS) instruments in addition to the offline LC-Orbitrap-MS. It was found that the oxidation state of nitrogen (OS_N) for CHON compounds significantly lowered the average $\overline{OSc}$ in single α-pinene and o-cresol system in FIGAERO-CIMS and LC-Orbitrap MS measurement. It was also found that there were substantial differences in the average OSc between the FIGAERO-CIMS and HR-ToF-AMS and LC-Orbitrap MS. These were associated with the characteristic of each technique and their limitation. Nonetheless, all the techniques showed similar carbon oxidation state changes between systems, giving confidence in their relative assessment. Specifically, the initial

concentration of precursors influenced the average $\overline{OSc}$ of SOA particle components in the single α-pinene system, but not in the single o-cresol system. This may result from the changes in relative turnover of α-pinene with the two prevailing oxidants (OH and O_3) in the different concentration experiments in contrast to the *o*-cresol solely reacting with OH radicals. In the binary system, the average $\overline{OSc}$ in the α-pinene and o-cresol mixtures with isoprene were not substantially affected by the isoprene addition. Moreover, in binary α-pinene/isoprene system, the average $\overline{OSc}$ of SOA has lower value than single α-pinene system. It is likely that isoprene has the potential to decrease the average $\overline{OSc}$ by forming high volatility and less oxygenated products, followed by partitioning into particulate matters in a mixed system. The $\overline{OSc}$ estimated in the α-pinene system was found to be lower than that in the o-cresol system, while that of their mixture was somewhere in-between. Thus the $\overline{OSc}$ in the mixed system was substantially influenced by oxidation products of both precursors in binary α-pinene /o-cresol system since both precursors generated considerable particulate mass. The $\overline{OSc}$ in the ternary mixture was not controlled by the products of any single precursor.

The four papers presented in this thesis provide an insight into the chemical characterisation of particulate products from the photo-oxidation of mixtures of volatile precursors.

The work in this study associated with LC-Orbitrap MS data was analyzed by non-targeted screening method, which allows rapid characterization of the chemical composition of complex mixtures enabling identification of unknown compounds and classification of compounds in a given sample. This instrument could capture board information of chemical composition on the oxidation products formed from different mixed systems and the evidence of unique-to-mixed products formation, further support the volatility observation of products in mixed system in one of our companion paper (Voliotis et al., 2021). Moreover, average carbon oxidation state is a useful tool to evaluate the oxidation dynamic associated with the formation and evolution of organic aerosol from extreme chemical complexity. This study used three different mass spectrometry techniques, including both online and offline, to analyze the average carbon oxidation state of SOA in mixed precursor system compared to single systems, in order to provide comprehensive insight of overall effect about molecular interaction impacts the SOA formation and properties. This study, combined with the work in Voliotis et al. (2021) and (Du et al., 2021)

has probed the detailed mechanisms of interaction, and the properties of particles resulting from them in mixed precursor systems. This program will act as a springboard for the scientific community to study the SOA formation and evolution in mixtures of volatile precursors

6.2.Implications, recommendations, and future work

This thesis has explored the SOA formation from the mixed anthropogenic and biogenic VOCs in the presence of NO_x and ammonium sulphate seed particles. Our work could be a springboard for the mixture precursors studies for SOA formation. This section outlines recommendations for future research.

The effects of widely used chamber bags on the wall loss rate of gaseous compounds (NO_2 and O_3) and particle mass, which were corrected using various methods, were observed in this study, highlighting the importance of regularly characterising experiments to track potential changes in atmospheric simulation chamber performance. According to the findings in paper 1, the wall of the Teflon bag could act as a sink of reactive gases and aerosol particles over the usage history of the bag (e.g., "dirty" experiments), influencing the chamber performance. Moreover, paper one also indicated that different approaches or experimental datasets to conduct particle wall loss corrections might bias the SOA yields. Furthermore, the comparability of results between different atmospheric simulation chambers could be different considering that they are composed of various materials and come in different designs, sizes, and shapes, influencing their performance and behavior. Thus, to have a better interpretation and comparison of the performance of different simulation chambers, it is essential to have future research to develop a set of standardized and straightforward experiments for various simulation chambers across the globe.

The SOA formation potential was influenced by mixing the anthropogenic and molecular interaction of mixing precursors that may impact the SOA formation potential. However, the effect of mixing is system-dependent and not straightforward. This thesis explains the complexity and the challenges in experimental design and the interpretation of chamber experiments in a mixture of precursors to investigate the influence of mixing of various precursors on the SOA formation potential that can reveal features inaccessible to a single VOC experiment. Due to the impact of

various experimental conditions on reaction pathways and the broad range of experimental conditions that can be encountered in ambient air (e.g., temperature, relative humidity, and VOC/NOx ratios), future work requires a more systematic assessment of SOA formation in mixed precursor systems, towards more atmospherically representative chemical regimes, and use of total oxidant and radical proxy measurements. Moreover, using a well-mixed flow reactor for mixture experiments makes it beneficial to look at multiple steady states and examine SOA formation and properties across many chemical regimes that batch reactors could not probe. Furthermore, it is still unclear whether the substantial SOA formation potential from oxidation of mixture VOC occurs in dark conditions (nighttime conditions) and the cycling between daytime and nighttime that might significantly impact SOA properties in an ambient environment, which could be investigated in future studies.

The difference in the chemical composition of particulate products between mixed precursors systems and single precursor systems indicates the potential effect of molecular interactions on the quality of air and climate prediction. The study's results showed the formation of unique compounds in the mixed precursor's system, and some of them could act as a potential tracer for future field-work measurements in the real atmosphere. However, this thesis did not examine the molecular structure of these unique compounds. Identifying the molecular structure of unique-to-mixture components in future studies will help better understand the detailed mechanisms of interactions involved in ambient SOA formation from mixture VOC oxidations. The molecular interaction in a mixed system, which results in a change in SOA chemical composition and chemical characteristics, is likely to impact SOA optical properties, hygroscopic properties, and physical phase state, with climatic implications.

This thesis combined the online and offline mass spectrometry to examine the $\overline{\mathrm{OSc}}$ of SOA in mixed systems. The results demonstrated that $\overline{\mathrm{OSc}}$ of particulate products in mixed systems is potentially associated with formation of high vapour organic compounds For example, in the mixed precursor system, this study found that high volatility products were generated from the oxidation of isoprene that has oxidants competition with other precursors, followed by suppressing the formation of low volatility oxidation products, resulting in a change in the $\overline{\mathrm{OSc}}$. This is an essential consideration for the future development of identifying the gas phase components during the oxidation in mixed precursors studies. Moreover, this study revealed the challenge and

limitation in obtaining the average carbon oxidation state from different techniques. Future study of SOA formation from mixtures of volatile organic precursors might be improved by combining multiple advance measurement techniques

[BLANK PAGE]

Chapter 7

1) Appendices

Supplementary material for paper 1

Supplementary Material for:

Characterisation of the Manchester Aerosol Chamber facility

Yunqi Shao[1*], Yu Wang[1*], Mao Du[1*], Aristeidis Voliotis[1*], M. Rami Alfarra[1,2,‡], Simon P. O'Meara[1,2], S. Fiona Turner[1,†] and Gordon McFiggans[1]

[1] Centre for Atmospheric Science, Department of Earth and Environmental Sciences, School of Natural Sciences, University of Manchester, Manchester, M13 9PL, United Kingdom
[2] National Centre for Atmospheric Science (NCAS), University of Manchester, Manchester, M13 9PL, United Kingdom

[‡] Now at Environment & Sustainability Center, Qatar Environment & Energy Research Institute, 34110, Doha, Qatar
[†] Now at AMETEK Land, Dronfield, Derbyshire, S18 1DJ, United Kingdom
*These authors all made equal contributions to this work.

Correspondence to: Gordon McFiggans (g.mcfiggans@manchester.ac.uk)

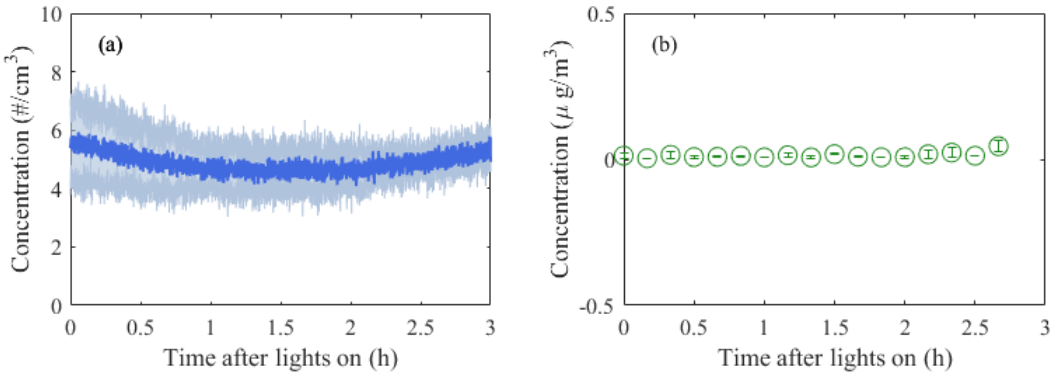

Figure S1: Time series (mean ± 1σ; n=2) of particle number (a) and mass (b) concentrations over the duration of air+lights experiments (i.e., experiments conducted by illuminating the chamber without any reactants added).

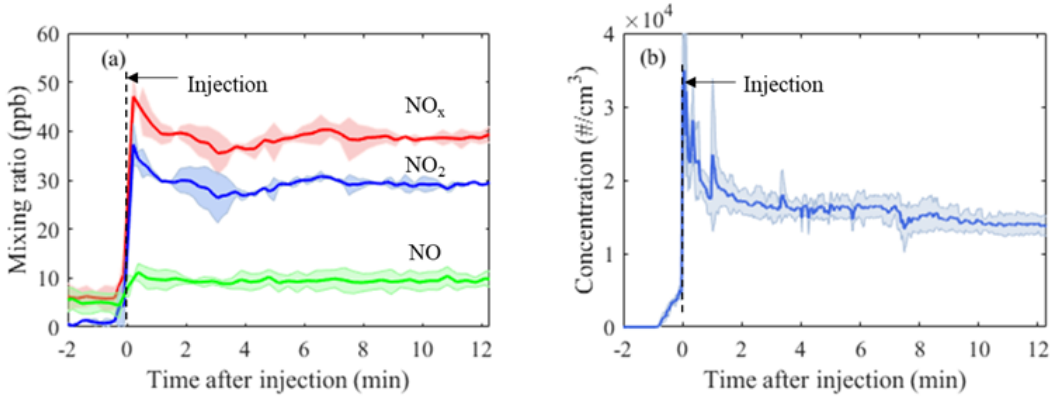

Figure S2: Mean (± 1σ; n=3) (a) gas mixing ratio of NOx (ppb) and (b) particle number concentrations (particle cm^{-3}) in three characteristic experiments as a function of their time after their injection to MAC.

[BLANK PAGE]

Supplementary material for paper 2

Supplementary Material for:

Chamber investigation of the formation and transformation of secondary organic aerosol in mixtures of biogenic and anthropogenic volatile organic compounds

Aristeidis Voliotis[1,*], Mao Du[1,*], Yu Wang[1,*], Yunqi Shao[1,*], M. Rami Alfarra[1,2,‡], Thomas J. Bannan[1], Dawei Hu[1], Kelly Pereira[3], Jaqueline F. Hamilton[3], Mattias Hallquist[4], Thomas F. Mentel[5], Gordon McFiggans[1]

[1]Centre for Atmospheric Science, Department of Earth and Environmental Sciences, School of Natural Sciences, University of Manchester, Manchester, M13 9PL, UK

[2]National Centre for Atmospheric Science (NCAS), University of Manchester, Manchester, M13 9PL, UK

[3]Wolfson Atmospheric Chemistry Laboratories, Department of Chemistry, University of York, York, YO10 5DD, UK

[4]Department of Chemistry and Molecular Biology, Atmospheric Science, University of Gothenburg, Gothenburg SE-412 96, Sweden

[5]Institut für Energie und Klimaforschung, IEK-8, Forschungszentrum Jülich, Jülich, Germany

[‡] now at Environment & Sustainability Center, Qatar Environment & Energy Research Institute, Doha, Qatar

[*] these authors all made equal contribution to the work and manuscript

Correspondence to: Gordon McFiggans (g.mcfiggans@manchester.ac.uk

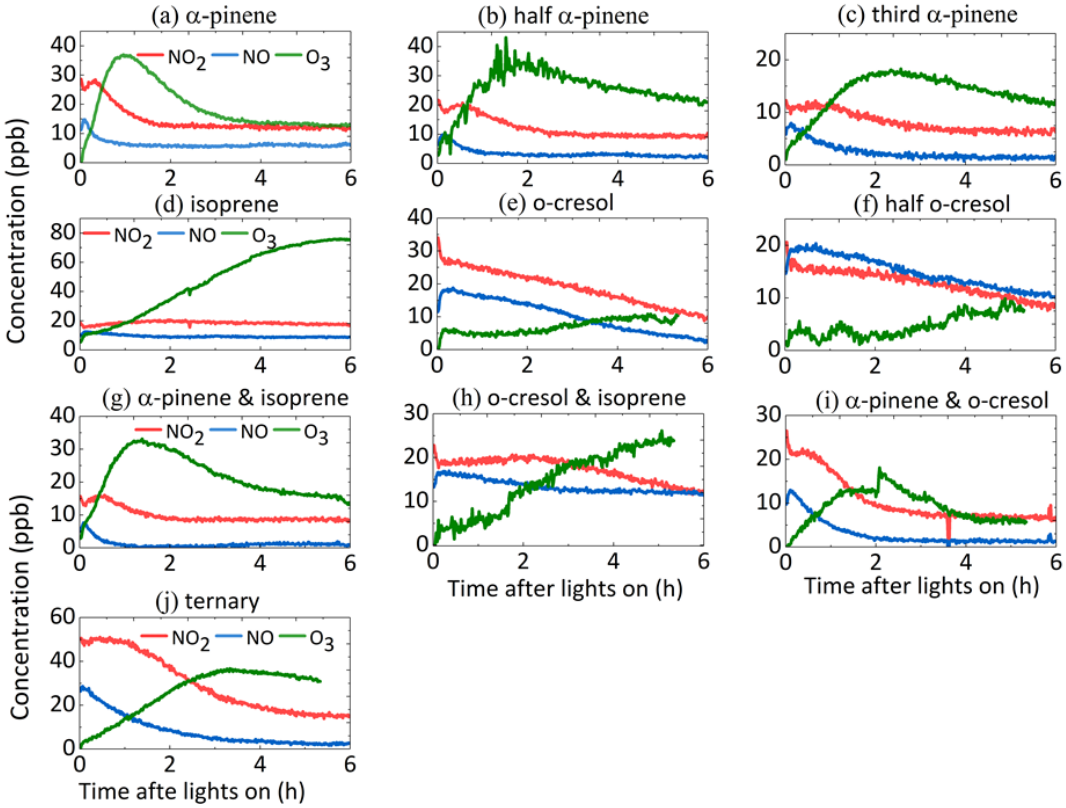

Figure S1: NO_2, NO and O_3 time series in all single and mixed VOC systems (example representative experiments)

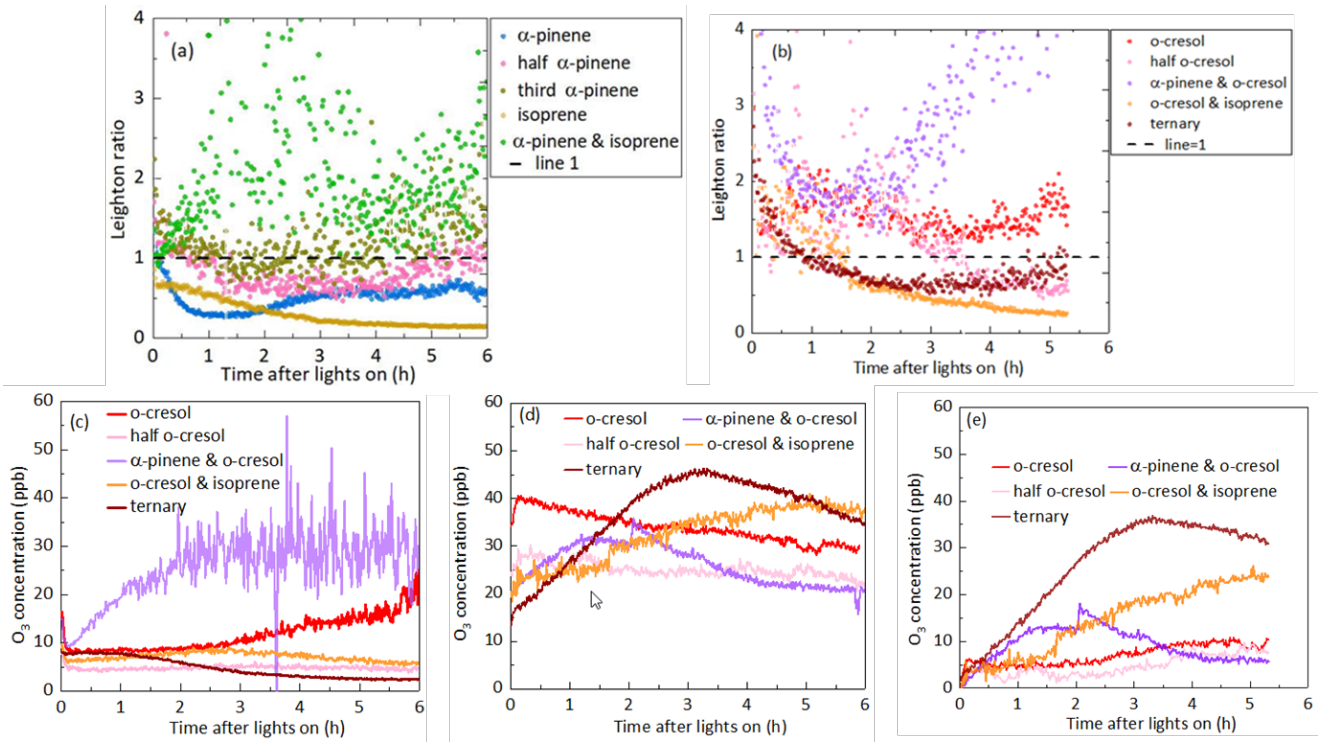

Figure S2: Leighton ratios in all systems and O_3 concentrations in all *o*-cresol containing systems. (a) Leighton ratio in all non-*o*-cresol containing systems, (b) Leighton ratio in all *o*-cresol containing systems, (c) O_3 concentrations calculated assuming PSS in the *o*-cresol containing systems, (d) measured O_3 concentrations from O_3 analyser in all *o*-cresol containing systems, (e) corrected O_3 concentrations based on CIMS *o*-cresol signal in all *o*-cresol containing systems.

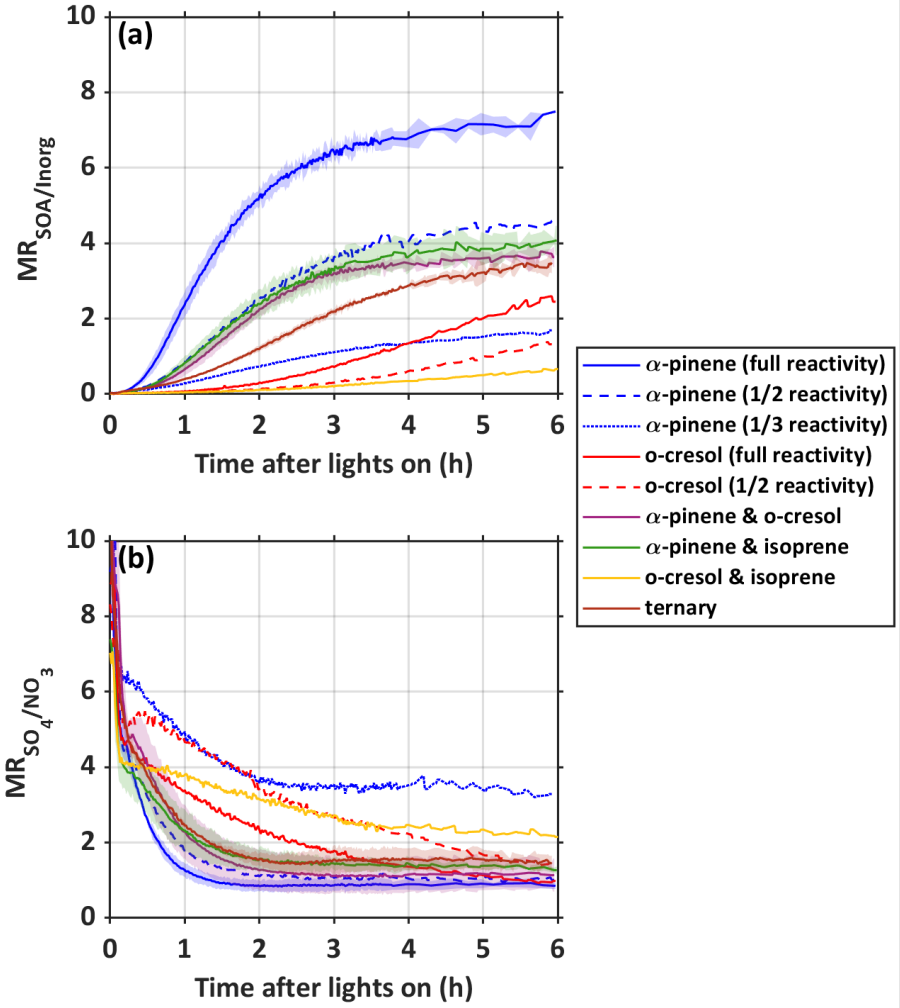

Figure S3: Total particle wall loss corrected particle component mass ratios in each system showing inorganic and organic component evolution. Panel a) shows the increase in SOA:inorg and b) shows the decrease in SO_4^{2-}: NO_3^-, throughout the experiment in each system coloured consistently with Figure 2 and 3. Note that NH_4^+ was found to ion balance the sum of NO_3^-:SO_4^{2-} in all experiments within measurement uncertainty

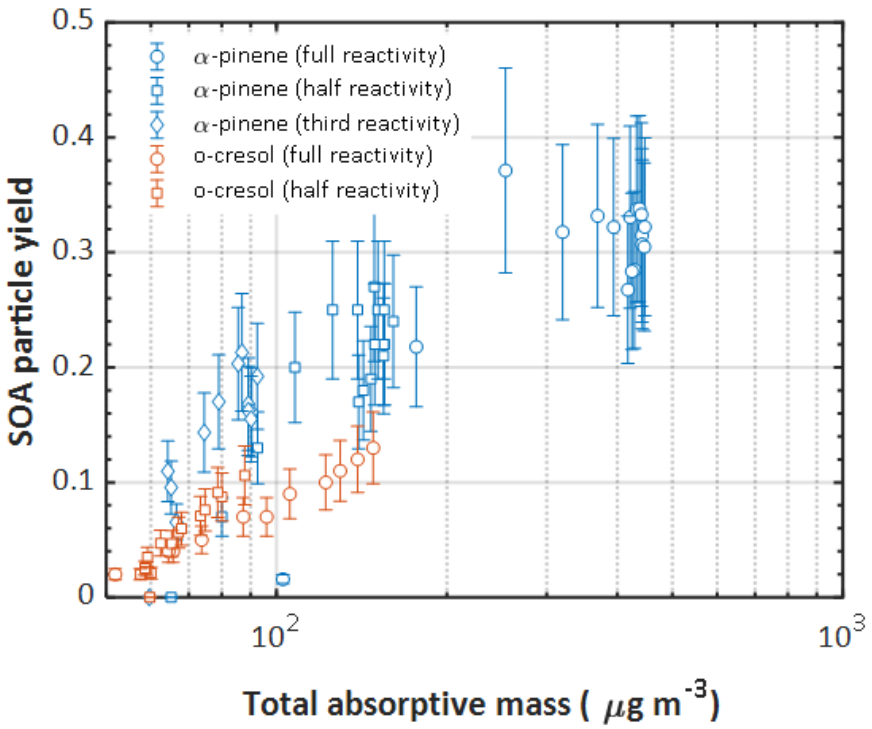

Figure S4: SOA particle mass yield as a function of total absorptive mass, including the remaining inorganic seed mass, in the single precursor □-pinene and *o*-cresol experiments at all initial concentrations. Error bars represent the propagated uncertainties in all measurements and in the particle wall loss corrections applied.

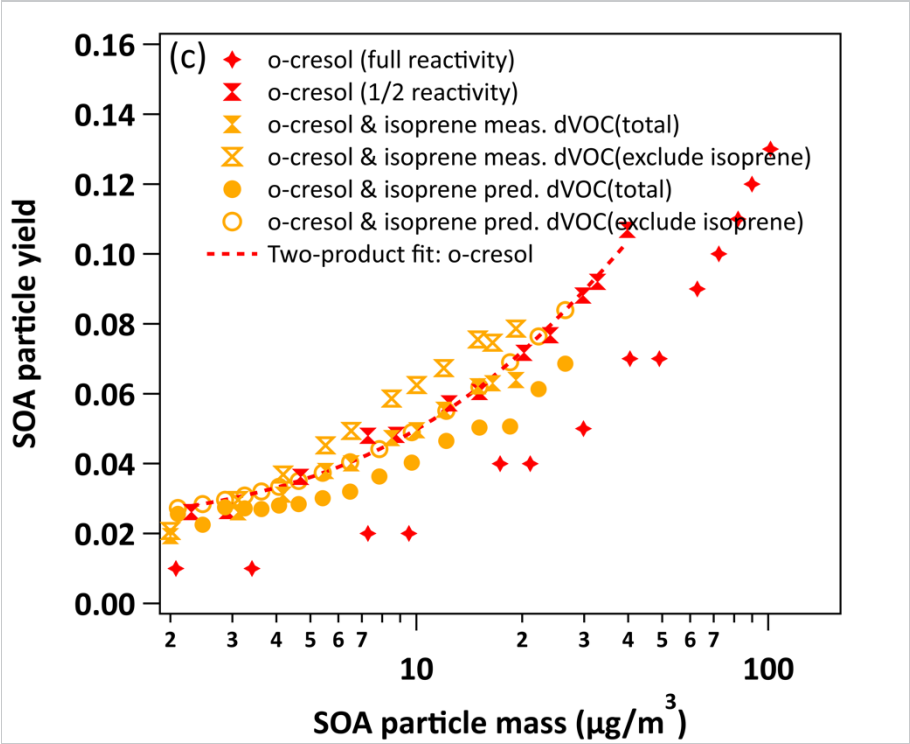

Figure S5: Expanded plot of yield data for the o-cresol / isoprene mixture (with 2-product yield curves o-cresol single VOC experiment). Yields "predicted" from the linear combination of yields from the individual VOC experiment using equation 4 are shown for the mixture.

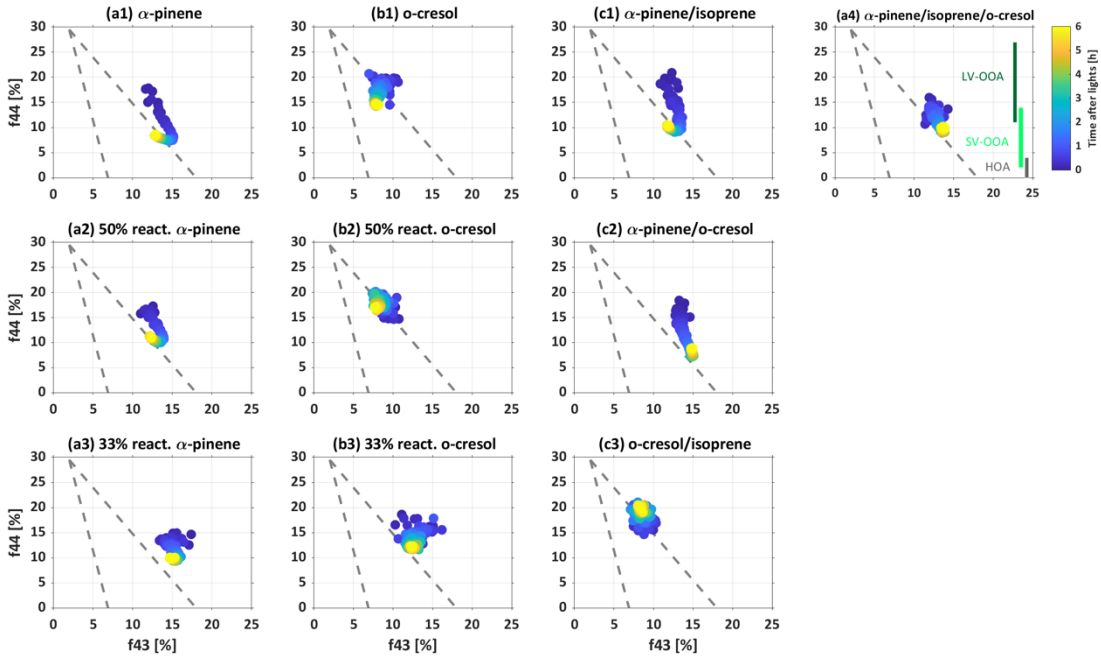

Figure S6: Trajectory of AMS f_{44} vs f_{43} in all systems

[BLANK PAGE]

Supplementary material for paper 3

Supplementary Material for:

Chemical composition of secondary organic aerosol particles formed from mixtures of anthropogenic and biogenic precursors

Yunqi Shao[1], Aristeidis Voliotis[1], Mao Du[1], Yu Wang[1], Kelly Pereira[3], Jacqueline Hamilton[3], M. Rami Alfarra[1,2], Gordon McFiggans[1]

[1]School of Earth and Environmental Science, University of Manchester, Manchester, M13, 9PL, UK
[2]National Centre for Atmospheric Science
[3] Wolfson Atmospheric Chemistry Laboratories, Department of Chemistry, University of York, York, YO105DD, UK

Correspondence to:g.mcfiggans@manchester.ac.uk;Yunqi.Shao@mancheste.ac.uk

Section 1: Supplementary figures

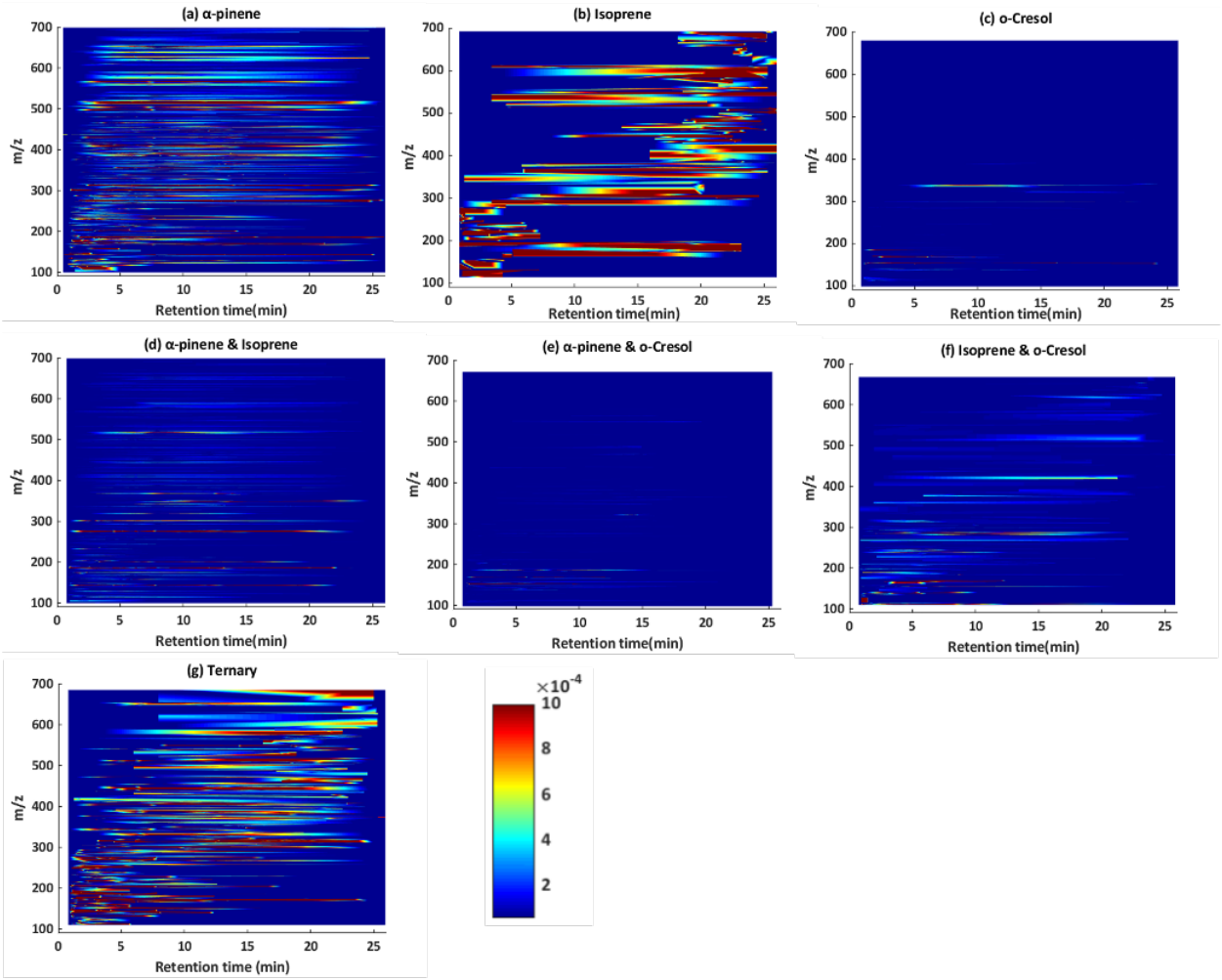

Figure S3: General Mass spectra m/z vs retention time with normalized signal intensity as colour) for compounds detected in Negative ionization mode for single and mixture experiment.

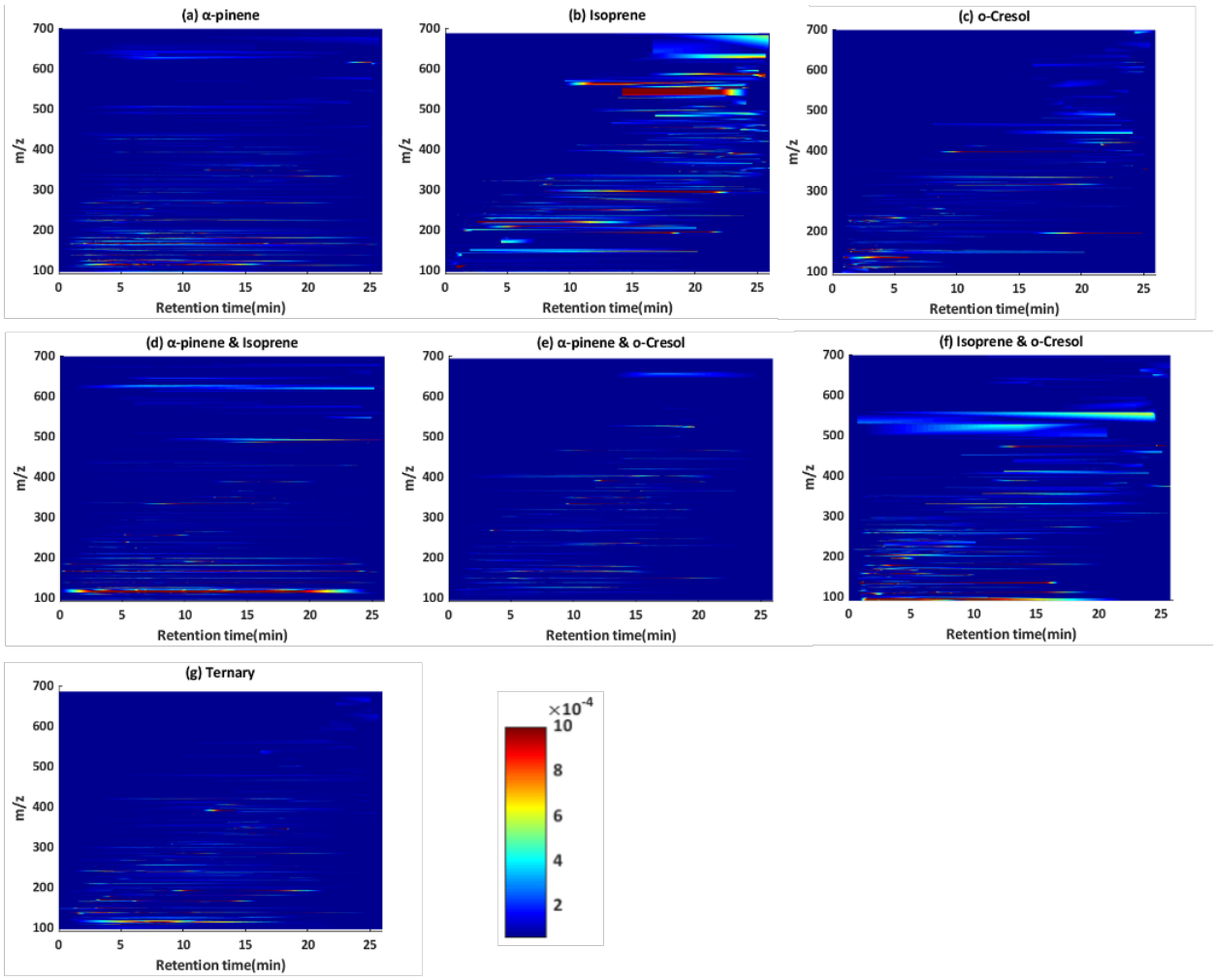

Figure S4: General Mass spectra m/z vs retention time with normalized signal intensity as colour) for compounds detected in Positive ionization mode for single and mixture experiment

Section 2: Supplementary Tables

The product ions of deprotonated species of $C_7H_7NO_4$ and $C_7H_7NO_3$ in single o-cresol system, binary α-pinene/o-cresol and Isoprene/o-cresol system will be discussed here in order to illustrate the methodology to assign SOA compound structure. For all of the $C_7H_7NO_4$ isomer, the fragment ion at m/z 138 due to neutral loss of NO group by odd electron cleavage that often happen in ring structures with nitrogen containing group (Hayen et al., 2002; Fu et al., 2006). $C_7H_7NO_4$ (i) and (III) also has the combine loss of NO and hydrogen radical (m/z=137), while the 109 m/z fragment corresponding to the combined loss of NO and CO from the deprotonated $C_7H_7NO_4$. For the $C_7H_7NO_3$ compound, the fragment ion m/z=122 has formed as a result of loss of NO from m/z 152, the loss of combined NO and hydrogen radicals resulting forming the 121m/z fragment and the combined loss of CH and NO leading to formation of 109 m/z fragment. These fragmentation ions of deprotonated molecules suggested that the $C_7H_7NO_4$ are the methyl-nitrocatechol and the $C_7H_7NO_3$ is methyl-nitrophenol(Kitanovski et al., 2012).

Table S1: Deprotonated molecular species for $C_7H_7NO_4$ isomers and $C_7H_7NO_3$, obtained from the use of the Orbitrap_LCMS in binary α-pinene/o-cresol and Isoprene/o-cresol system respectively.

Precursors System	Formula	Retention Time (min)	$[M-H]^-$	Fragment ion [m/z]	Loss [Da]	Fragment ion MF
o-cresol	$C_7H_7NO_4$ (i)	4.46	168	166	2	$C_7H_5NO_4$
				138	30	$C_7H_6O_3$
				108	60	$C_6H_4O_2$
	$C_7H_7NO_4$ (ii)	7.40	168	138	30	$C_7H_6O_3$
				137	31	$C_7H_5O_3$
				109	59	$C_6H_5O_2$
	$C_7H_7NO_4$ (iii)	8.93	168	138	30	$C_7H_6O_3$
				137	31	$C_7H_5O_3$
				109	59	$C_6H_5O_2$
α-pinene/o-cresol	$C_7H_7NO_4$ (i)	4.52	168	138	30	$C_7H_6O_3$
				108	60	$C_6H_4O_2$
	$C_7H_7NO_4$ (ii)	7.53	168	138	30	$C_7H_6O_3$
				137	31	$C_7H_5O_3$
				109	59	$C_6H_5O_2$
	$C_7H_7NO_4$ (iii)	9.08	168	138	30	$C_7H_6O_3$
				137	31	$C_7H_5O_3$
				109	59	$C_6H_5O_2$
	$C_7H_7NO_3$	10.19	152	122	30	$C_7H_6O_2$
				121	31	$C_7H_5O_2$
				109	43	$C_6H_5O_2$
Isoprene/o-cresol	$C_7H_7NO_4$ (i)	4.52	168	138	30	$C_7H_6O_3$
				137	31	$C_7H_5O_3$
				108	60	$C_6H_4O_2$
	$C_7H_7NO_4$ (iii)	9.14	168	138	30	$C_7H_6O_3$
				137	31	$C_7H_5O_3$
				109	59	$C_6H_5O_2$
	C7H7NO3	10.20	152	122	30	$C_7H_6O_2$
				121	31	$C_7H_5O_2$
				109	43	$C_6H_5O_2$

Table S1: The total normalized peak area and normalized mass concentration attributed to nC>21 molecules that were found in all repeat experiments in selected system. The normalized peak area of nC>21 molecules obtained from the both ionization mode in orbitrap-LCMS, and the particulate mass concentration of each system obtained from HR-TOF-AMS measurement. The normalized mass concentration equals the particulate mass concentration multiply the normalized peak area of nC>21 molecules.

		Negative ionization mode		**Positive ionization mode**	
	Particulate mass concentration at the end of experiment(ug/m^3)	Normalized Peak Area of nC >21 molecules	Normalized mass concentration of nC >21 molecules(ug/m^3)	Normalized Peak Area of nC >21 molecules	Normalized mass concentration of nC >21 molecules(ug/m^3)
a) α-pinene	361	0.008	3.01	0.003	1.34
b) Isoprene	0.4	0.007	0.002	0.040	0.016
d) α-pinene/isoprene	102	0.011	1.15	0.002	0.24
e) α-pinene/o-cresol	150	0.004	0.73	0.019	2.85
f) Isoprene/o-cresol	22	0.0006	0.013	0.006	0.14
g) Ternary	85	0.002	0.16	0.012	1.10

Reference:

Fu, X., Zhang, Y., Shi, S., Gao, F., Wen, D., Li, W., Liao, Y., and Liu, H.: Fragmentation study of hexanitrostilbene by ion trap multiple mass spectrometry and analysis by liquid chromatography/mass spectrometry, Rapid Communications in Mass Spectrometry, 20, 2906-2914, https://doi.org/10.1002/rcm.2683, 2006.

Hayen, H., Jachmann, N., Vogel, M., and Karst, U.: LC-Electron capture APCI-MS for the determination of nitroaromatic compouds, The Analyst, 127, 1027-1030, 10.1039/B205477A, 2002.

Kitanovski, Z., Grgić, I., Yasmeen, F., Claeys, M., and Čusak, A.: Development of a liquid chromatographic method based on ultraviolet–visible and electrospray ionization mass spectrometric detection for the identification of nitrocatechols and related tracers in biomass burning atmospheric organic aerosol, Rapid Communications in Mass Spectrometry, 26, 793-804, https://doi.org/10.1002/rcm.6170, 2012.

[BLANK PAGE]

Supplementary material for paper 4

Supplementary Material for:

Analysis of carbon oxidation state in evolution of secondary organic aerosols formed from single and mixtures organic vapors

Yunqi Shao[1], Aristeidis Voliotis[1], Mao Du[1], Yu Wang[1], Kelly Pereira[3], Jacqueline Hamilton[3], M. Rami Alfarra[1],[2], Gordon McFiggans[1]

[1]School of Earth and Environmental Science, University of Manchester, Manchester, M13, 9PL, UK

[2]National Centre for Atmospheric Science

[3] Wolfson Atmospheric Chemistry Laboratories, Department of Chemistry, University of York, York, YO105DD, UK

Correspondence to: Yunqi.Shao (Yunqi.Shao@Mancheste.ac.uk)

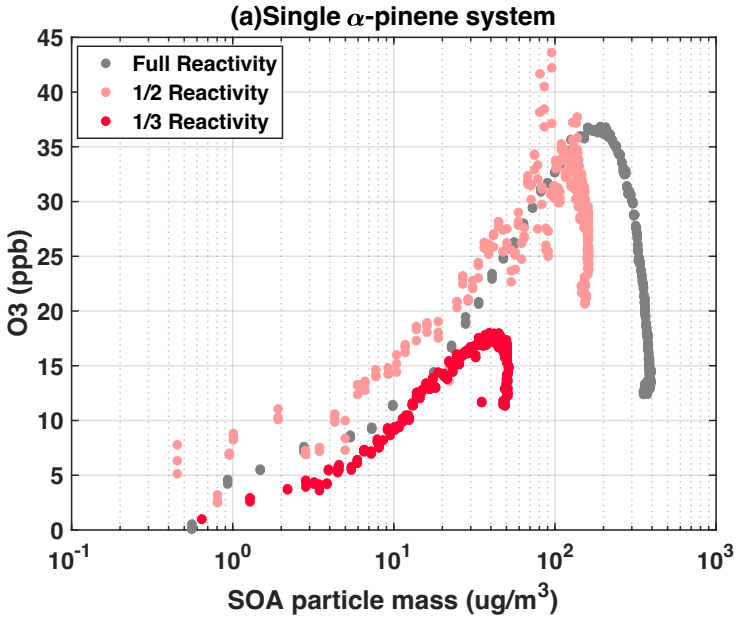

Figure S1: The O3 distribution against SOA mass concentration for single a-pinene system with full, half and third initial reactivity

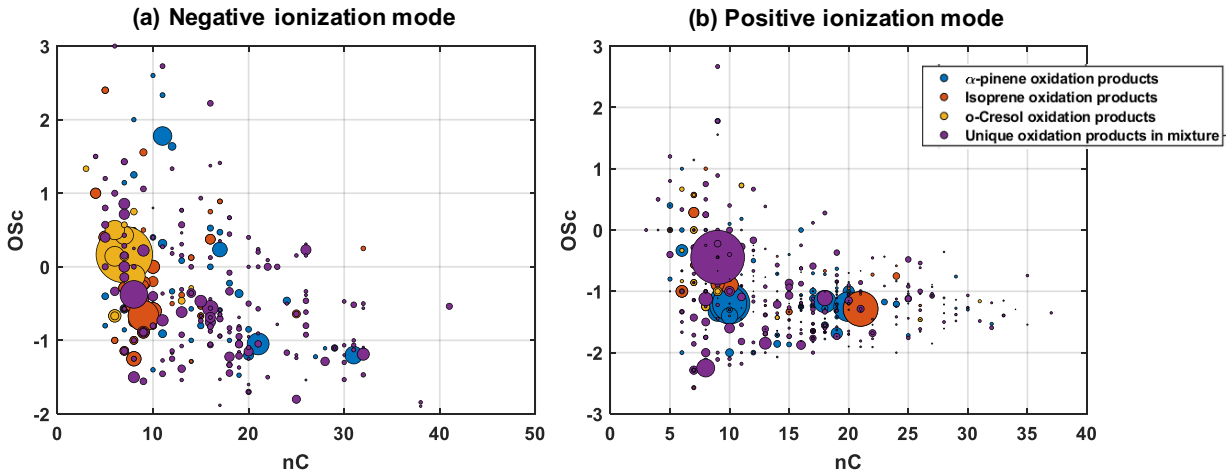

Figure S2: The OSc against nC of SOA from ternary mixture system obtain from -ve and +ve ionization modes orbitrap-LCMS. The detected compounds classified into four groups, blue: common products with a-pinene SOA, orange: common products with isoprene SOA, yellow: common products with o-Cresol, SOA, purple: the unique-to-mixture products. The size of marker represents the normalized signal contribution in total of individual compound.